STRUCTURAL AND METAMORPHIC RELATIONS BETWEEN LOW, MEDIUM AND HIGH GRADE ROCKS, MT FRANKS - MUNDI MUNDI AREA, BROKEN HILL, N.S.W.

by

Richard Arthur Glen, B.Sc.(Hons.) (Sydney)

PART I

of two parts plus Appendices

Department of Geology and Mineralogy
University of Adelaide
April, 1978.

TABLE OF CONTENTS

VOLUME I

-LIST OF ABBREVIATIONS USED IN TEXT

D_I	first deformation
D_2	second deformation
D_3	third deformation
D_4	fourth deformation
M_I	first metamorphism
M_2	second metamorphism
M_3	third metamorphism
S_o	bedding
S_I	first schistosity visible in the field and axial planar to first generation folds in bedding
S_{IP}	S_I parallel to bedding
S_{IN}	S_I non parallel to bedding
$S_o//S_I$	S_o parallel to S_I
S_IPs	S_I developed in psammite
S_IPe	S_I developed in pelite or psammopelite
S_2	second generation schistosity
S_3	third generation schistosity
S_4	fourth generation schistosity
S_{I-3}	undifferentiated S_I or S_3
S_R	retrograde schistosity occurring within retrograde schist zones
L_I	mineral/aggregate lineation in S_I
L_3	mineral lineation in S_3
L_M	mineral lineation in S_R

ABBREVIATIONS (ctd)

F_I first generation fold

F_2 second generation fold

F_3 third generation fold

F_4 fourth generation fold

F_R fold with S_R axial planar

F_{R+I} fold in S_R

XYZ maximum, intermediate and minimum axes of the strain ellipsoid

LIST OF TABLES

APPENDICES

APPENDIX I reprint of paper entitled "Tectonic Relations between the Proterozoic Gawler and Willyama Orogenic Domains, Australia" by Glen, R.A., Laing, W.P., Parker, A.J., and Rutland, R.W.R.
J. Geol. Soc. Aust., 24 (3), 125-150. 1977.

APPENDIX II reprint of paper entitled "The significance of sedimentary structures in the Willyama Complex, New South Wales" by Glen, R.A., and Laing, W.P.
Proc. Australas. Inst. Min. Metall., 256, 15-20. 1975.

APPENDIX III Geometrical analysis of Mt Franks - Mundi Mundi Area in terms of subareas.

APPENDIX IV reprint of paper entitled "Large scale early folding and tectonic levels in the northwestern part of the Willyama Complex, New South Wales" by Glen, R.A.
Geol. Surv. N.S.W. Quarterly Note 31, 4-15. 1978.

SUMMARY

Investigations in the northwestern part of the Willyama Complex centred on the Mt Franks - Mundi Mundi area have established a 4 km thick stratigraphic section of conformable metasediments containing thin horizons of basic volcanics in the lower two-thirds of the sequence. Establishment of this sequence was only possible once it was shown that the dominant lithological layering in metasediments is bedding, and that there has been no mesoscopic transposition during deformation. The metasediments represent a sequence of clay sands deposited in a distal shelf-slope or basin type of environment.

A sequence of deformational and metamorphic events established in these rocks is regarded as an expression of the Middle Proterozoic Olarian Orogeny (c. 1695 - 1520 Ma.) and except for some reactivation of shear zones, predate deposition and deformation of the unconformably overlying Adelaidean sediments.

The important D_1 deformation is a complex, progressive event with pre-S_1 static mineral growth (biotite, andalusite, sillimanite, white mica) and early minor micro-folding recognised before syn-S_1 growth and F_1 folding. An even earlier period of pre-S_1 fabric formation mainly defined by white mica, biotite and ilmenite, is not related to any visible folding and may either represent an earlier discrete event or an early phase of the D_1 event. However, as now defined, minerals outlining this pre-S_1 fabric are related to the D_1 event.

The low, medium and high grade metamorphic zones defined in the field by biotite, andalusite and sillimanite respectively are pre-S_1 in age and predate F_1 folding. The intensity of metamorphism increases with depth so that there is a broad depth control on metamorphism. Relations at the andalusite/sillimanite isograd conform to a Carmichael (1969) type model and reactions took place via an intermediate sericite phase.

The main effect of F_1 folding is the formation of the variably plunging variably oriented Kantappa - Lakes Nob Syncline of regional extent. Only the western limb of this fold is now visible over much of its length. This fold deforms existing metamorphic zones and thus controls the relationship of low, medium and high grade rocks in this part of the Willyama Complex. The orientation of this syncline changes from vertical in the low grade rocks to inclined at depth. The western limb becomes overturned at depth so that subsequent folds are downward facing. There is also a change in fold tightness with depth - from open-tight in the low grades to tight-isoclinal in the high grades, and this is accompanied by a change in S_0/S_1 relations (from core to limb area) from non parallel to parallel. These changes are coupled with a rotation of extension direction (mass transfer direction) from subvertical to inclined and may be explained by original formation and subsequent modification of upright F_1 folds. Later modifications are recorded by open folding and overturning of S_1 - this is ascribed to a final phase of the D_1 event.

Mineral growth in D_1 time resulted in the formation of S_1 varying in grade from muscovite + quartz to sillimanite. S_1 varies from homogeneous to layered, and in the latter case, consists of M + QM layers, the spacing of which is controlled by F_1 microfolding. S_1 formation involved rotation, mass transfer, and volume decrease in M layers and (re)crystallisation.

The D_2 event in this area was of only minor significance. The D_3 event developed in response to NW-SE shortening and resulted in the formation of variably plunging, vertical northeast trending folds. Where SW plunging, these folds lie subparallel to L_1. The nature of the D_3 event is controlled to a large extent by S_0/S_1 relations and folding of S_1 across unfolded S_0 occurs where S_0 lies parallel to the XY plane of the D_3 event. S_3 formed as a muscovite + quartz schistosity by rotation, recrystallisation, mass transfer and mimetic growth.

During the final stages of the D_3 event, north-east trending retrograde schist zones were formed. These were later reactivated during the folding of the Adelaidean. The final phase of the Olarian Orogeny consists of minor D_4 folding and crenulation.

This thesis contains no material which has been accepted for the award of any other degree or diploma in any University, nor does it contain, to the best of my knowledge and belief, any material published or written by any other person except where due reference and acknowledgement is made in the text.

R.A. Glen.

ACKNOWLEDGEMENTS

I gratefully acknowledge the help of Professor R.W.R. Rutland, who not only organised this project, but who also provided guidance, assistance and constructive criticism throughout the study. I would also like to thank my other supervisors - Dr. M.A. Etheridge from 1973 until 1974 when he left for Monash University, and Dr. P.R. James from 1974 onwards.

Discussions both in the field and at University with many people have helped me formulate my ideas and I would especially like to thank W.P. Laing, R.W. Marjoribanks (both fellow workers on the Broken Hill Project) and A.J. Parker. I have also had helpful discussions with J.P. Platt and N.S. Mancktelow (structure and microstructure), G.A. Chinner, A.C. Purvis and D.F. Blight (metamorphism) P.G. Haslett (sedimentary aspects), M. Bridges (computing) and D. Isles (magnetics).

For discussions about other aspects of Willyama Complex geology, I would like to thank W.P. Laing, W.F. D'Arcy, J. Thomson, K.D. Tuckwell and G. Bradley.

Discussions with other people too many to mention are also acknowledged.

Professor Rutland read and criticised the whole thesis while various sections have been read and constructively criticised by M.A. Etheridge, P.R. James, R.L. Oliver and Sisir Sen.

S. Trichzy and G. Trevellyan helped by making superb thin sections, and R. Barratt carried out photographic work at Adelaide. G. Hicks and O. Müller were responsible for the fine photographic work in Sydney and made the final plates. I would like to thank S. Wells for a magnificent typing effort, and for coping so well with all the problems caused by my move to Sydney. A. Felton and C. Baker both helped with last minute thesis compilation.

For accommodation and company in the field, and assistance in times of crisis, I would like to thank Mr. and Mrs. S.G. Langford and family

of Purnamoota.

This study was supported by a Commonwealth Postgraduate Research Award and by the Broken Hill Mining Managers Association, and was carried out while I was on study leave from the Geological Survey of New South Wales. I would like to thank its director, Dr. N.L. Markham, for general assistance and for making facilities available during final preparation.

Finally, I acknowledge the encouragement of my family throughout this study, and above all the help, understanding and forebearance of Jennifer.

CHAPTER 1 INTRODUCTION

1.1 PURPOSE OF STUDY.

This thesis discusses aspects of stratigraphy, structural geology and metamorphic geology in the northwestern part of the Lower Proterozoic Willyama Complex in the Broken Hill district of New South Wales. This study forms part of a structural project carried out between 1971 and 1977 in the Broken Hill area by the Centre of Precambrian Research at the University of Adelaide under the direction of Professor R.W.R. Rutland. This thesis study followed a reconnaissance study by Rutland (1971, 1973a), which examined structural and stratigraphic relations in a broad WNW-ESE traverse passing to the north of the rich silver-lead-zinc mine at Broken Hill itself, and was set up to investigate unexplained aspects of the geology in the northwestern part of the Willyama Complex. These were:

1. the presence of two adjoining synforms with no obvious intervening antiform or similar structure.

2. the presence of andalusite bearing rocks in the Willyama Complex which is dominated by sillimanite schist, and

3. the presence of sillimanite schist lying within the synforms and apparently structurally overlying the andalusite schist occurring "between" them. This observation raised the possibility that thrusting may have taken place early in the deformational history.

These features were investigated in this thesis by carrying out a detailed structural analysis across the northwestern part of the Willyama Complex. It was soon revealed that rocks of three, not two metamorphic zones could be distinguished - low grade (biotite), medium grade (andalusite) and high grade (sillimanite), and it also became evident that there was a major change in structural style between these zones. Since the Willyama Complex is dominated by high grade rocks, the present study was initiated with the following aims:

1. to establish the structural and metamorphic histories of the lower grade rocks and of the high grade rocks, and

2. to establish the structural and metamorphic relationship between the

lower grade rocks and the high grade rocks.

It was hoped that a study of these lower grade rocks with their different structural style would provide information on the early deformation history of the Willyama Complex.

In addition, attention has been given to metamorphic fabric development. This is of particular interest because of the recognition that metamorphic and fabric forming events preceded the first mesoscopically visible deformation, and also because the first mesoscopic schistosity shows variable development across metamorphic and structural zones. Both of these features may have important implications for the interpretation of the earliest schistosity in the high grade rocks around the Broken Hill mine area.

1.2 LOCATION OF AREA and GEOGRAPHIC BACKGROUND.

1.2.1 The Willyama Complex

Rocks of the Lower Proterozoic Willyama Complex form basement to sediments of the Upper Proterozoic Adelaidean Supergroup and occur over a large area in western New South Wales and in the adjacent parts of South Australia. (Fig. 1.1). In western New South Wales, Willyama Complex rocks outcrop over an area of about 4,600 km^2, and occur in a large triangular shaped area surrounded by Adelaidean cover and alluvium, as well as in two small inliers surrounded by Adelaidean rocks (Fig. 1.2). The Willyama Complex in New South Wales is centred on Broken Hill (population 29,000), which lies 1152 km from Sydney, but only 48 km from the South Australian border and 512 km from Adelaide.

1.2.2 The Northwestern Part of the Willyama Complex

The 'northwestern part of the Willyama Complex' is a term used to describe an area of approximately 350 km^2 which lies west of the northeast trending Apollyon Valley Retrograde Schist Zone. This retrograde zone is a major lithological, structural and metamorphic discontinuity in the Willyama Complex (Fig. 1.2). Geological relations within this area, as well as

relations between this area and the main block of Willyama Complex rocks east of the Apollyon Valley Retrograde Schist Zone (that area studied by other Adelaide University workers), are discussed below.

Results obtained from this study are based on mapping of an area of about 100 km^2 (the Mt Franks - Mundi Mundi area, (Fig. 1.2) which extends 10 km across the regional strike and 10 km along strike) and was accompanied by traversing, data collection and sample collection over a larger area extending to the Adelaidean rocks in the north.

The limits of the Mt Franks - Mundi Mundi area are shown in Figure 1.3. The western boundary is the Mundi Mundi scarp which marks the western limit of basement rocks and the eastern edge of the Mundi Mundi plain. The eastern boundary which lies east of the Apollyon Valley Retrograde Schist Zone, occurs in an area of poor outcrop, and runs irregularly along a line of hills which defines a principal watershed: creeks west of this watershed drain onto the Mundi Mundi plain and form part of the Lake Frome drainage pattern; creeks east of the watershed flow into Stephens Creek and then into the Southern Ocean via the Darling-Murray River System. The southern boundary of the Mt Franks - Mundi Mundi area coincides with the southern termination of low grade rocks just north of Lakes Nob, while the southern edge of the Gum Creek alluvial flat passing through the Black Prince Mine marks the northern limit of mapping.

Two prominent geographical features in the area are Mt Franks on the eastern side, and the old Mundi Mundi homestead on the Mundi Mundi Creek in the western part of the area. The latitude $31^{o}45'$ passes just south of Mt Franks and corresponds to National Mapping Grid line 64872 M.N., while the meridian of $141^{o}15'$ passes just east of the old Mundi Mundi homestead and corresponds to National Mapping Grid line 523500.

Access to the western part of the area is by the Broken Hill-Willangee homestead road, which is sealed as far as the Umberumberka Reservoir just north of Silverton, and which then becomes a graded road lying just west of

the Mundi Mundi Scarp. The central and eastern parts of the area can be reached by following the Nine Mile road from Broken Hill to Purnamoota homestead and then property tracks to the Black Prince, Shepherd's hut and Mt Franks areas. Just east of Mt Franks, at the boundary between Purnamoota and Acacia Vale Stations, the track from Purnamoota joins two tracks which run south to the Broken Hill-Silverton road. One of these tracks passes along Apollyon Valley, and the other passes along Lake's Grave Creek (Fig. 1.3). Most of the area lies on Purnamoota and Acacia Vale Stations, with the exception of the south western corner which lies on Belmont Station. Low grade rocks north of Purnamoota lie on Poolamacca and Willangee Stations.

The following three topographic map sheets cover the area (New South Wales Department of Lands, scale 1:25,000);

Purnamoota	7134-1-S
Lakes Creek	7134-11-N
Mundi Mundi Creek	7134-IV-S

The outcrop of early and late Proterozoic rocks in the Broken Hill area is reflected physiographically in the Barrier Range, named Stanley's Barrier Range after the Secretary for Colonies by the explorer Charles Sturt in 1844. This range consists of an asymmetrical group of hills which rises very abruptly from the Mundi Mundi Plain on the west and which decreases in height gradually to the east towards the Darling River. The highest part of the range, Mt Robe (471.8 m) lies just north of the thesis area. Mt Franks is 440 m high.

The two major creeks in the area, Mundi Mundi and Eldee, originate in the central and eastern part of the area in mature, well rounded valleys and then turn northwest across the regional strike before cutting through steep cliffs on the western side of the range to emerge on the Mundi Mundi Plain. Andrews (1922), and more recently B. Wasson (pers. comm., 1975) suggested that many of the creeks on the western side of the Barrier Range had been rejuvenated by Tertiary movements on the Mundi Mundi Fault, and they

recorded cases of creeks dissecting embankments and alluvial fans which represent earlier periods of stream activity.

Although the Broken Hill region lies in the semi-arid zone, vegetation in the area studied is more widespread than elsewhere in the district because of increased rainfall and runoff in hill areas, and also because of abnormally heavy rains from 1973 to 1976. Mulga occurs in hilly areas and on ridges, as do nightshade ('sagebush') and hops. River redgums line the big creeks while mallee, copper burr and spear grass occur on flat areas. Saltbush and blue bush, so common elsewhere in the Broken Hill area, are rare here. Animal and bird life abound.

1.3 PREVIOUS GEOLOGICAL STUDIES.

The discovery of the first of many small deposits of rich silver ores scattered throughout the Broken Hill district in 1876, and the discovery of the rich Ag-Pb-Zn lode of Broken Hill itself in 1883, have stimulated a vast amount of geological research in the New South Wales part of the Willyama Complex (in future referred to simply as the 'Willyama Complex'). Most of this research has been concerned with the nature of the ore deposits and ore genesis, and regional studies have only been of a reconnaissance nature. In particular, the northwestern part of the Willyama Complex has been generally neglected, with the exception of early work of the Geological Survey of New South Wales, a reconnaissance study by The Zinc Corporation Limited in the 1950's, and more recent university work.

Early work by the Geological Survey, the metamorphic studies of Binns (1963, 1964) and the structural and metamorphic studies of Anderson (1966, 1971) had all shown that major lithological, metamorphic and structural differences exist between the northwestern part of the Willyama Complex and areas closer to Broken Hill. Before discussing previous ideas on the geology of the northwestern part of the Willyama Complex, it is necessary to summarise geological ideas about the Willyama Complex in general, since

the development of the ideas and work in this thesis has been affected by concepts developed in other parts of the Willyama Complex. In addition, a brief discussion of lithology, structure, metamorphism, geochronology and tectonics serves to place the following study in a suitable context.

1.3.1 Lithology

1.3.1.1 Regional Studies

Early studies in the Broken Hill area by Jaquet (1894), Mawson (1907, 1912) and the Geological Sub Committee (1910) had established the presence of two major rock groups in the district: a younger, slightly metamorphosed series of slates, conglomerates and limestone (the Torrowangee Series of Mawson, 1912) and an unconformably underlying series of metamorphic and granitic rocks (Willyama Series of Mawson, 1912;, renamed Willyama Complex by Andrews, 1922). Although these early workers had recognised many of the major rock types in the Willyama Complex, a more detailed appraisal of the geology was provided by detailed mapping and petrological investigations of the Geological Survey of New South Wales between 1917 and 1922 (Andrews, 1922; Browne, 1922; Stillwell, 1922).

Andrews (ibid) suggested that rocks of the Willyama Complex could be divided into metasediments (sillimanite schist, andalusite schist, phyllite, Ettlewood 'Limestone'), meta-igneous rocks (granitic gneiss, augen gneiss, footwall (= Potosi) gneiss, amphibolite, various ages of pegmatites and late stage granite) and thin quartzites interbedded with sillimanite schist which he and Stillwell (1922) considered were sedimentary, but which Browne (1922) thought were igneous. Andrews (1922) showed that most of the Willyama Complex was dominated by sillimanite bearing schists and gneisses, but also recognized lower grade rocks in the Mt Franks area (as did Mawson, 1912), near Yanco Glen and near Bijerkerno in the Euriowie Inlier (Fig. 1.2).

1.3.1.2 Northwestern Part of the Willyama Complex

Jaquet (1894) first showed that a calc silicate unit, the Ettlewood Limestone, was restricted to this part of the Willyama Complex, and he also

established the presence of late stage granites near Mundi Mundi (Fig. 1.2). Further members of this suite within this region are now also known (King and Thomson, 1953; Vernon, 1969). Mawson (1912) first recognised the presence of andalusite schists near Mt Franks and Andrews (1922) traced this unit along strike to the northeast, and showed that it was restricted to a narrow belt flanked by sillimanite schists.

A sequence of five lithological units across these low grade schists was established by Anderson (1966, 1971). From east to west these are:

1. fine grained quartz-mica schist,
2. fine grained, grey schist, often layered,
3. chiastolite schist,
4. andalusite schist (poorly foliated) and
5. andalusite rich schist with thin layers of quartz biotite schist.

Sillimanite schists west of these units contain amphibolite horizons which Andrews (1922) and Anderson (ibid) traced around the Mt Robe Syncline further north.

In the far northern part of this area, Andrews (1922) recognised atypical Willyama Complex rocks - low grade phyllites - which were later named 'Willywangees' by King and Thomson (1953) who showed that they occurred in a narrow strip - locally known as the Kantappa 'Trough'* - which was flanked by Adelaidean sediments (Fig. 1.2). More recent studies by Tuckwell (1968), Cooper (1969), Laing (1969), Price (1969), Roberts (1969), J. Thomson (1976) and D'Arcy (pers. comm. 1975) have built up a sequence of phyllites and quartz schists in this area (see Section 7.2.1).

1.3.2 Structural Relations

1.3.2.1 Regional Studies

The earliest structural studies in the Broken Hill District were concerned with ore body/wallrock relationships although Marsh (1890)

---

* In reality the Kantappa 'Trough' is not a sedimentary trough but a doubly plunging F_1 syncline (see Section 7.2.3.1).

suggested that a regional syncline extended across the Barrier Ranges. Mawson (1912), on the other hand, suggested that the Willyama Complex occupied the core of the Torrowangee Anticlinorium. In his regional study of the Willyama Complex, Andrews (1922) recognised one period of major folding with a later period of warping and he divided the regional structure into a series of open basins separated either by tight anticlines with subvertical axial planes or by crush zones ("zones of dislocation"). Although Andrews (ibid) noted that the overlying "Torrowangee Series" was folded, he suggested that this folding postdated the main deformation in the Willyama Complex and corresponded to a period of renewed movement in crush zones.

In the Mine area, Gustafson et al. (1950) noted the presence of upright isoclinal folds as well as more open folds, and suggested that there had been more than one generation of folding. However, in their regional study, King and Thomson (1953) argued for one deformation and suggested that the isoclinal folds of Gustafson et al. (ibid) could co-exist with broad regional synclines and poorly defined anticlines. These regional folds either corresponded to original structures of Andrews (ibid) or represented subdivisions of them.

The structural studies referred to above were based on two tenets:

1. that lithological layering in the metasediments was bedding - and Thomson (1959) figured examples of graded bedding in sillimanite schist to support this - and

2. that major folds could be delineated by following marker units.

In contrast, structural studies carried out between 1966 and 1971 (Anderson 1966, 1971; Hobbs, 1966a; Hobbs and Vernon, 1968; Hobbs et al, 1968; Ransom, 1968; Williams, 1967) were based on a study of small scale structures and larger scale features were interpreted in terms of multiple deformation using modern structural analysis.

Hobbs (1966a) carried out a rigorous structural study around North Mine in association with a microstructural study by Vernon (1968), and recognised

four groups of folds, two in the 'country rock' and two in shear zones or retrograde schist zones (Vernon, 1969). Group 1 folds in the country rock were characterised by a sillimanite schistosity parallel to their axial surfaces and by a co-axial sillimanite lineation; Group 2 folds refolded this schistosity and lineation. Group 3 folds were restricted to retrograde schist zones, and had a retrograde schistosity parallel to their axial surfaces. Group 4 folds, also within these zones, folded this schistosity and its down dip mineral lineation. Hobbs (ibid) suggested that these fold groups, determined on style criteria, represented fold generations. This four-fold classification was extended to the southern part of the mine area by Ransom (1968), although he noted that Group 2 folds also had a co-axial sillimanite lineation. In the Little Broken Hill area, 13 km southeast of Broken Hill, Williams (1967) recognised two deformations which he correlated with Group 1 and Group 2 folds of Hobbs (ibid); but he also suggested that there had been an even earlier deformation. Anderson (1966, 1971) carried out structural studies in the Mt Robe district, lying in the northwest part of the Willyama Complex, and outlined two large folds which he equated with Group 3 folds of Hobbs (see below).

The fundamental differences between the early workers and this later school of thought were the interpretations placed on lithological layering and the almost ubiquitous layer parallelism between the earliest visible schistosity and layering. Before 1966, layering was regarded as bedding and the layer-parallel schistosity was regarded as a genetic bedding (apposition) fabric (e.g. Lewis et al., 1965 , and even more recently, Stanton, 1976). The second group of workers, on the other hand, described Group 1 or first generation folds in which this schistosity cut across bedding and thus argued that the schistosity was a deformational feature. They suggested that the parallelism between layering and schistosity resulted from the mesoscopic transposition of bedding during the formation of the schistosity, and consequently they argued that lithological layering could

no longer be regarded as bedding. This meant that it was not possible to describe the spatial relations between Willyama Complex rocks in terms of original stratigraphic sequences.

The third phase of structural work in the Broken Hill area began when Rutland attempted to extend the earlier structural studies of Hobbs, Ransom, Williams and Anderson to the regional scale. Hobbs et al (1968) had suggested that the regional schistosity throughout the high grade rocks was related to Group 1 folds, and Rutland (1973a) carried out a study of schistosity/layering relations in a WNW/ENE transect across the Willyama Complex from Mt Franks to the Sisters (Fig. 1.2). He recognised a major upright synform, the Parnell Synform, in the west and a complimentary antiform, the Mt Vulcan Antiform east of it, and suggested that both were Group 1 structures and related to S_1. He did point out, however, that schistosity was not strictly congruent to the Parnell Synform. In addition, Rutland (ibid) found that minor Group 1 folds and layering/S_1 intersections did not show simple relations to the major folds, and he therefore suggested that this might be due to an early period (Group 0) of recumbent folding with the formation of a schistosity sub-parallel to layering. Group 2 folds were also encountered in the transect but were considered to be of minor significance.

The results encountered in this transect led to the setting up of the Broken Hill research project from Adelaide University. Problems encountered in the western part of the Willyama Complex are the subject of this thesis. The Parnell Area was mapped by honours students and Dr. R.W. Marjoribanks, and W.P. Laing, carried out a study around North Mine. Dr. Marjoribanks also extended his mapping southeast to the Little Broken Hill area, and northwest to the Parnell Area.

The results of honours mapping projects from 1971 to 1973 are summarized by Rutland and Etheridge (1975). They showed that the regional schistosity could be sub-divided into two high grade sillimanite schistosities, S_1 and S_2, and a local retrograde schistosity, S_3, which was

generally related to S_2. Since either S_1 or S_2 could be found parallel to axial surfaces of folds, the Group 1 folds of Hobbs (1966a), which were characterised by an axial plane schistosity, could be either F_1 or F_2 in age. Rutland and Etheridge (ibid) found no macroscopic F_1 folds; most of the folds in the region were F_2 in age - the Parnell Synform, the Mt Vulcan Antiform, and the major folds around the orebody.

In contrast to the complexities in the high grade rocks outlined above, the low grade 'Willywangee' rocks are characterised by a single penetrative schistosity. These rocks in the Kantappa 'Trough' (Tuckwell, 1968; Cooper, 1969; Roberts, 1969) are characterised by an early schistosity (at an angle to bedding) which is parallel to the axial surfaces of a doubly plunging macroscopic syncline and parasitic folds in the Kantappa 'Trough'. Laing (1969) and Price (1969) showed that a regional segregation schistosity occurs in the southern part of this trough, and was overprinted by folds which were correlated with F_3 folds of Anderson (1971). Low grade rocks in the Bijerkerno area (Meares, 1969; Tuckwell, 1975) are also characterised by an early, non-parallel schistosity, and bedding lies on the dextral limb of a flat lying anticline which is refolded by an F_2 upright syncline (Tuckwell, 1975).

The relations between all these lower grade rocks and the high grade rocks, and between these structures in the lower grade rocks and those in the high grade rocks are clarified by the present study.

1.3.2.2 Northwestern part of the Willyama Complex

Structural studies in this area can be divided into a "pre-transposition" phase (Andrews, 1922; King and Thomson, 1953) and a "transposition" phase (Anderson, 1966, 1971).

In the northwestern part of the Willyama Complex, Andrews (1922) recognised two major folds (Fig. 1.4): the Great Western Fold, and east of it, the Great Western Basin. The boundary between these two was placed along the Mt Franks Valley which Andrews recognised as a "zone of shearing and

crushing." Andrews (ibid) suggested that the northern part of the Great Western Fold was dominated by the Mt Robe Basin and by a complimentary antiform lying west of it.

Although he pointed out that the Great Western Fold was a structure not fully understood, he suggested that the eastern limb of this basin could be traced southwards past Mt Franks to the Umberumberka area.

On Mt Franks itself, Andrews (1922) clearly distinguished bedding from schistosity and also presented a cross section through Mt Franks (Andrews, 1922, Fig. 11) indicating that schistosity is steeper than bedding on the east flank of the mountain but is parallel to bedding on the western side.

The regional reconstructions of King and Thomson (1953) in the northwestern part of the Willyama Complex were similar to those of Andrews (1922) although a new terminology was partially adopted. King and Thomson (ibid) used the term 'Mt Robe Syncline' to embrace the 'Great Western Fold' of Andrews and they extended this structure from Mt Robe south to Silverton where the axial trace was cut off by the Mundi Mundi Scarp (Fig. 1.4). King and Thomson (ibid) subdivided Andrews' Great Western Basin into several anticlines and synclines, and they established the presence of the Apollyon Anticline just east of the Mt. Franks Fault, and east of this fold, the Stirling Vale Syncline. The crush zone recognised by Andrews in the Mt Franks Valley was renamed the 'Mt Franks Fault', and King and Thomson extended its trace further north, under the alluvium of Gum Creek, and along the western boundary of the Kantappa 'Trough'. The low grade Willywangee rocks in the Kantappa 'Trough' were separated from the rest of Willyama Complex rocks by a northwest trending fault lying to the north of Mt Robe. (This fault was named the Kantappa Lineament by Rose in Cooper, 1975). King and Thomson further suggested that the Mundi Mundi Scarp was a fault controlled feature which was reactivated, but which was not generated (cf. Andrews, 1922), in the Tertiary. Rather, they considered that the Mundi Mundi Fault and Mt Franks Fault formed part of a set

which was initiated as a late stage feature in the main deformational episode.

In contrast to the ideas of Andrews (1922) and King and Thomson (1953) which envisaged a single deformation episode, a more recent study by Anderson (1966, 1971) suggested that rocks in the Mt Robe district had sufferred multiple deformation and he recognised two major deformational episodes. The first resulted in:

1. the formation of the regional schistosity S_1, and minor F_1 folds,

2. the almost complete transposition of bedding into schistosity, (which were, however, clearly separate in the early generation Mt Franks Fold), and

3. the formation of small second generation folds northwest of Mt Robe.

The second episode was accompanied by the emplacement of large pegmatite bodies, the formation of two major folds, and accompanying small folds. The two large folds are the Mt Robe Synform, and a complimentary antiform west of it, variously called the Western Antiform (Anderson, 1966) or the Mt Robe Antiform (Anderson, 1971), (Fig. 1.4). The area discussed in this present thesis overlaps with the southern part of the area studied by Anderson.

In contrast to Anderson's work, Rutland's 1969 traverse was mainly concerned with a reinterpretation of structures in Andrews' Great Western Basin. However, the traverse did extend across the Mt Franks Retrograde Schist Zone onto Mt Franks itself, and thus onto the east limb of the Mt Robe Synform as defined by Anderson (1966). Rutland (1971, 1973a) found no support for westerly dips in this area. He noted that layering dipped east across a steeper schistosity, and suggested that this corresponded to a position in the west limb of his Parnell Synform. On Mt Franks itself, Anderson (1966) established the presence of a first generation fold modified by F_4 effects. Rutland (ibid) re-interpreted this as a Group 1 fold, overprinted by Group 2 effects, and he also raised the possibility

of thrust faulting east of the area.

The conclusions of Rutland are at variance with those of Anderson since these authors place the same andalusite schists in oppositely dipping limbs of different synforms. The synforms themselves are dominated by sillimanite whereas lower grade rocks occur "between" them - in an area not possessing an obvious antiform.

Further north, structural studies were carried out around Mt Robe by Reynolds (1975) and in the Silver King Area east of Mt Robe by Splatt (1975). Both these workers recognised structures correlable with first and third generation features of Anderson, although they regarded lithological layering as untransposed bedding. Changes in sedimentary younging (outlined by grading) was interpreted by Splatt (ibid) in terms of first generation isoclinal folds.

1.3.3 Metamorphic Relations

1.3.3.1 Regional Studies

The first description of metamorphic features of the Willyama Complex were those of Andrews (1922) and Browne (1922). Andrews (ibid) considered that a regional metamorphic event accompanied the main deformation in the Willyama Complex, and that metamorphic grade decreased away from Broken Hill to the north, northwest and west. Browne (1922) carried out a detailed petrological study of Willyama Complex Rocks and recognised four discrete metamorphic events. These were:

1. A regional metamorphism with grade decreasing away from Broken Hill to the northwest. This resulted in the formation of sillimanite gneisses near Broken Hill, and mica schists further to the northwest.

2. A contact metamorphism associated with pegmatite intrusion. This event resulted in the formation of andalusite, tourmaline, possible sillimanite, and large muscovite.

3. A regional low grade event which produced chlorite and chloritoid and sericite.

4. A later event restricted to shear zones.

New data on the regional extent of metamorphic episodes, and on grade zonation was provided by Binns (1963, 1964), who recognised four metamorphic events, which are in broad agreement with those of Browne (1922). These are:

M_1 a high grade regional event,

M_2 a contact metasomatic event related to the intrusion of pegmatites,

M_3 a local event associated with the Mt Franks Fault which led to kinking and the growth of andalusite from sillimanite in this area, and

M_4 a dynamic event localised in shear zones and which accompanied folding of the Torrowangee Series.

In a major advance on Browne's (1922) work, Binns (1964) subdivided the products of the high grade (M_1) event into three planar, northeast trending zones, (A, B, C) which he considered represented a progressive increase in metamorphic grade fron northwest to southeast. The A/B boundary represented the outgoing of the pair sillimanite-muscovite, and the incoming of the pair sillimanite-K feldspar, but was more easily recognised in amphibolites where the colour of hornblende absorption along the Z direction changed from blue green to green brown. The Zone B/C boundary marked the beginning of the granulite facies and was marked by the appearance of two pyroxenes in the mafic rocks.

Later workers suggested modifications to Binns' (1963) scheme. Hobbs et al (1968) suggested that Binns M_1 to M_4 scheme be modified into a Willyama metamorphism (M_1) and a complex retrograde metamorphism. Vernon (1969) divided retrograde metamorphism into that occurring within shear zones, which he called "retrograde schist zones" (see also Vernon and Ransom, 1971), and "pseudomorphous retrogression" occurring outside these zones.

The recognition of two high grade schistosities by Rutland and Etheridge (1975) also had important implications for Binns' (ibid) metamorphic

scheme, since they suggested that some of the relationships used by Binns to favour a progressive grade increase could be due to separate metamorphic events at different conditions. They showed that in local areas Zone A and C amphiboles occurred in Zone B, and Zone A and B amphiboles occurred in Zone C. Rutland and Etheridge (ibid) also suggested that Binns' linear isograd traces should be folded about later F_3 structures.

In a new regional metamorphic study over the Willyama Complex, Phillips (1977) recognised four prograde metamorphic zones which he regarded as typifying peak metamorphic conditions: andalusite, sillimanite + muscovite, sillimanite + K feldspar, and granulite, all of which were then affected by a retrograde event. The isograds defining these prograde zones were large, simply folded, features, and their positions differred from those established by Binns (ibid). Although Phillips suggested that the granulite field was much larger than shown by Binns (ibid), Katz (1976a) considered that granulites were mainly restricted to the Broken Hill Basin (a large F_2 synform immediately east of the Mine Area (R. Marjoribanks, pers. comm., 1975))and to the Little Broken Hill area. He proposed a tectonic hot spot model to account for this localisation. Within the lower grade rocks in the Bijerkerno area, Meares (1969), and more recently Tuckwell (1975), showed that isograds defined by the incoming of andalusite and sillimanite were parallel to bedding and were folded by later structures.

1.3.3.2 Northwestern Part of the Willyama Complex

Andrews (1923) first showed that a narrow strip of andalusite schists near Mt Franks was faulted against sillimanite schists to the east across Apollyon Valley. According to Browne (1922), the sillimanite schists lying west of the low grade rocks had a different appearance to sillimanite schists near the Mine Area.

Although King and Thomson (1953) had suggested that the andalusite schists were the same age as the Willyama schists, and were the product of the main regional metamorphism, the Tectonic Map of Australia (First

Edition,1960) interpreted the andalusite and Willywangee rocks as a fault sliver of Adelaidean sediments. This idea, however, had already been disproven by Leslie and White (1955) who showed that boulders of Willywangee chiastolite phyllite occur in the basal Adelaidean conglomerate and who suggested that chiastolite development occurred on a regional scale before any contact metamorphism associated with granite emplacement (cf. Browne, 1922). Binns (1963, 1964) on the other hand, suggested that andalusite growth was related to the development of the Mt Franks fault (his M_3 event) and was preceded by the formation of sillimanite + muscovite* (Zone A) in the M_1 event, and by large cross cutting muscovite laths, and by tourmaline growth (M_2 event). He did, however, suggest that rocks east of the Apollyon Valley were downfaulted Adelaidean sediments.

From work in the Mt Robe district, Anderson also devised a four-fold metamorphic subdivision:

M_1 regional high grade event, resulting in the formation of andalusite and sillimanite,

M_2 local event, associated with fault zones, resulting in the formation of quartz and mica,

M_3 local contact event associated with pegmatites, resulting in the formation of tourmaline, and

M_4 widespread retrogression resulting in the formation of sericite and large cross cutting muscovite.

In contrast to Binns' views, Anderson (1966) suggested that both andalusite and sillimanite formed during the M_1 event, and he was able to define a north/south trending isograd between andalusite in the east and sillimanite in the west. Although Anderson noted that the isograd cut through the late stage Mt Robe Synform, he suggested that the isogradic

---

* Binns did note that local K feldspar occurred in two places within his Zone A.

surface itself had a gentle easterly dip throughout the area.

The implication of this study was that sillimanite schists, occupying the core of the Mt Robe Synform, were structurally overlying the lower grade andalusite schists.

1.3.4 Geochronology

The first isotope studies in the Willyama Complex were carried out on sulphides, and showed that separation of the main lode lead occurred between 1700 and 1500 Ma (Russel et al, 1961; Russel and Farquhar, 1960), and that separation of the secondary Thackaringa deposit lead occurred about 500 Ma (Kansewich, 1962). Early K-Ar studies on silicates (Evenden and Richards, 1961) suggested a leakage age of 550-450 Ma, and were followed by other K-Ar studies (Binns and Miller, 1963; Richards and Pidgeon, 1963). Rb-Sr isotope studies on minerals and whole rocks by Pidgeon (1967) and Shaw (1968) have since dated the high grade metamorphic event at c.1690 Ma, and the emplacement of the post tectonic Mundi Mundi granite suite at c.1540 Ma.

1.3.5 Tectonics of the Willyama Complex

Tectonic interpretations of the Willyama Complex have been hampered by an incomplete knowledge of the geology, and until recently, by imprecise knowledge of the ages of the major deformational and metamorphic events. Basement/cover relations between the Willyama Complex and the Torrowangee Series were established by Jaquet (1894), Mawson (1912) and Andrews (1922). Isotope studies referred to above, have inferred a 'Nullaginian' age of sedimentation for the Willyama Complex and an Upper Proterozoic age has been established for the Torrowangee Series. Mawson (1912) first suggested that the Willyama Complex could be equated in age with rocks Olary, Mt Painter and with basement inliers near Adelaide. Comparisons between the Willyama Complex in Broken Hill (N.S.W.) and Olary (S.A.) with the Gawler Craton in Eyre Peninsula have been made by Thomson (1970, 1976), by Rutland (1973b, 1976) and more recently by Glen et al.(1977, Appendix I) who incorporated the results of recent structural mapping in all three areas. Tectonic

studies in the Willyama Complex around Broken Hill were initiated by Thomson (1954). Katz (1976a) presented a 'hot spot' model to account for metamorphic zoning in the area and Katz (1976b) presented an interpretation of satellite imagery based on movement on the Darling River Lineament (see also O'Driscoll, 1968).

1.4 ORGANISATION OF STUDY.

The field seasons of 1973 and 1974 were spent in the area, and some field work was also carried out early and late in 1975, and early in 1976. Mapping was carried out on several scales (Fig. 1.3), using aerial photographs flown for The Zinc Corporation Limited by Adastra Airways Pty. Ltd. Most of the mapping centred on the Mt Franks Area was carried out on a scale of 1:4,800 (1" = 1000'). Within the main area of mapping, areas of greater complexity were mapped at more detailed scales by tape and compass surveys (see Fig. 1.3). Data from aerial photographs were plotted onto base maps at various scales which had been enlarged from New South Wales Lands Department bases. Geological information was then compiled and the final map was then photographically reduced to a scale of 1:15,000 (see Map 1, in back pocket of Volume 2). Other maps are presented of various areas in more detail and are referred to in the text.

All structural readings referred to in the text are true, not magnetic values. Structural information was compiled onto equal area nets using the computer program described by Bridges and Etheridge (1974) which contours populations on the surface of a sphere before projecting them onto a two dimensional surface.

Microstructural and metamorphic observations were made in thin sections cut from oriented specimens; many of the thin sections were of large format to encompass significant features. The presence of K feldspar was tested for by etching with HF and staining by sodium cobaltinitrite. Thin section sketches were made on a 'Shadowmaster', using 5x, 10x and 50x objectives. No distortion was encountered in this instrument. Preferred orientation

studies on micas were either made directly on shadowmaster sketches or on tracings taken from photomicrographs.

1.5 LAYOUT OF THESIS.

This thesis is set out in two parts (Volumes I and II) which reflect the divergent aims of the study. After an initial discussion of lithology and layering (Chapter 2) and mesoscopic structures (Chapter 3), Part I concentrates on microstructural (Chapter 4) and metamorphic (Chapter 5) relations. These last two chapters discuss relations between low, medium and high grade rocks in terms of relation of mineral growth to deformation, response of minerals to deformation, mechanism of fabric formation, and possible reaction mechanisms and conditions of metamorphism.

Part II discusses macroscopic structural relations in the Mt Franks - Mundi Mundi area (Chapter 6) and extends this analysis to the northwestern part of the Willyama Complex (Chapter 7). Chapter 8 discusses the overall conclusions and implications of the study.

There is thus a progression from the mesoscopic and microscopic scales, at which data is collected and interpreted, to the macroscopic scale in which large scale geometrical relations are deduced using the evidence presented in Part I. The interpretation of macroscopic geometry is dependent upon Chapters 3 and 4, especially on conclusions regarding correlations between schistosities.

Fig. 1.1 Outcrop of Willyama Complex rocks in South Australia and New South Wales. Location of Mt Franks shown. From Glen et al, (1977).

Fig. 1.2 Proterozoic rocks in the Broken Hill Area, New South Wales. Adelaidean, Upper Proterozoic cover rocks, shown in horizontal ruling. Distribution of medium and low grade Willyama Complex rocks (basement) indicated by stipple. Boundaries of the Mt Franks - Mundi Mundi area shown by hachured margins. The Apollyon Valley Retrograde Schist Zone (a) marks the eastern edge of the northwestern part of the Willyama Complex. Late stage granitoids shown in black.

Other abbreviations - m - Mt Mundi Mundi

p - Parnell Area

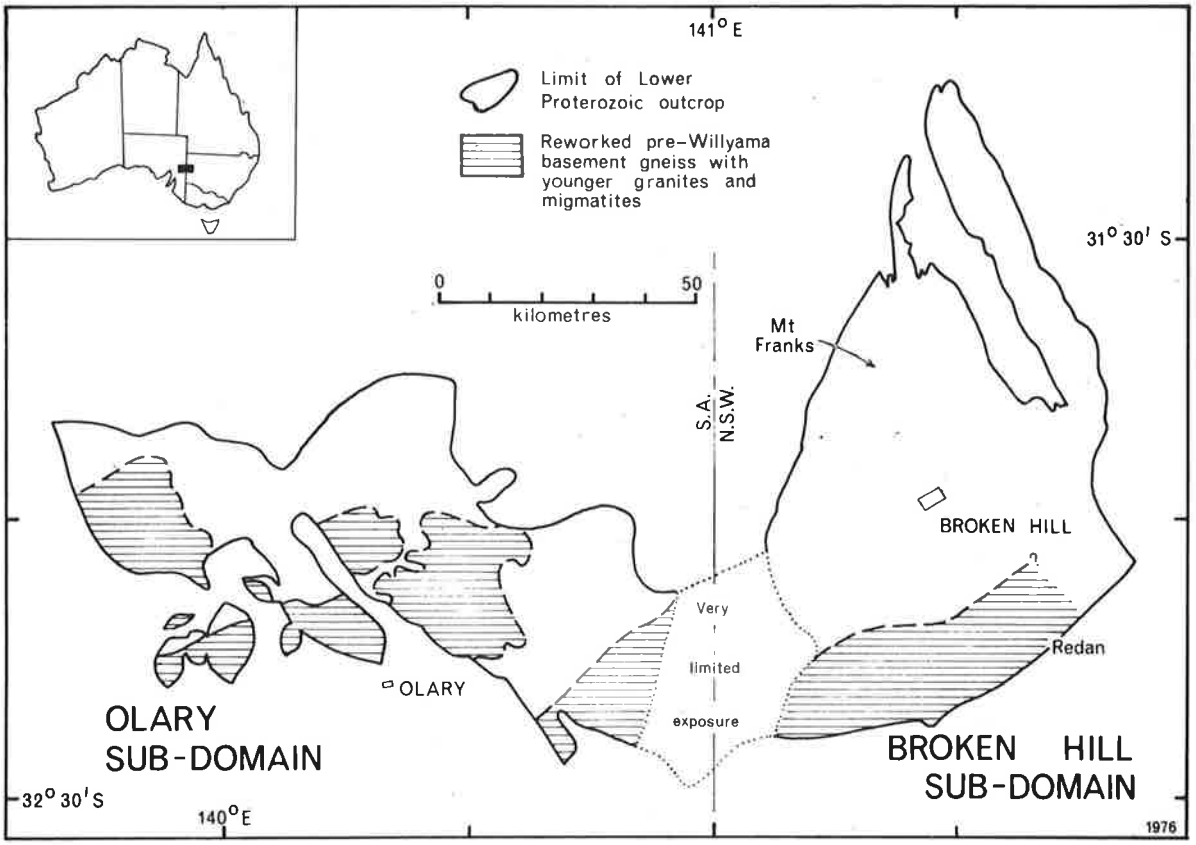
141° E
Limit of Lower Proterozoic outcrop
Reworked pre-Willyama basement gneiss with younger granites and migmatites
31° 30' S
0
50
kilometres
Mt Franks
S.A.
N.S.W.
BROKEN HILL
Very limited exposure
Redan
OLARY
OLARY SUB-DOMAIN
BROKEN HILL SUB-DOMAIN
32° 30' S
140° E
1976

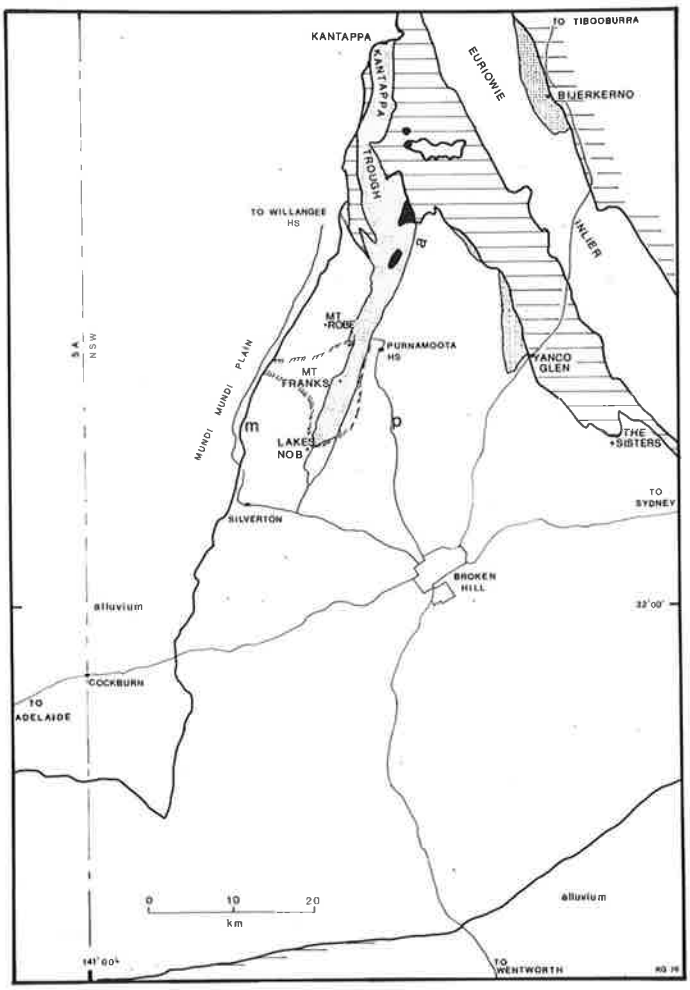
KANTAPPA
TO TIBOOBURRA
EURIOWIE
BIJERKERNO
KANTAPPA TROUGH
TO WILLANGEE HS
HILLER
MT ROSE
PURNAMOOTA HS
S.A.
N.S.W.
MT FRANKS
YANCO GLEN
MURDI MURDI PLAIN
LAKES NOB
THE SISTERS
TO SYDNEY
SILVERTON
BROKEN HILL
alluvium
32° 00'
COCKBURN
TO ADELAIDE
0
10
20
km
alluvium
141° 00'
TO WENTWORTH

Fig. 1.3 Generalised map of Mt Franks - Mundi Mundi Area and Reliability Diagram.

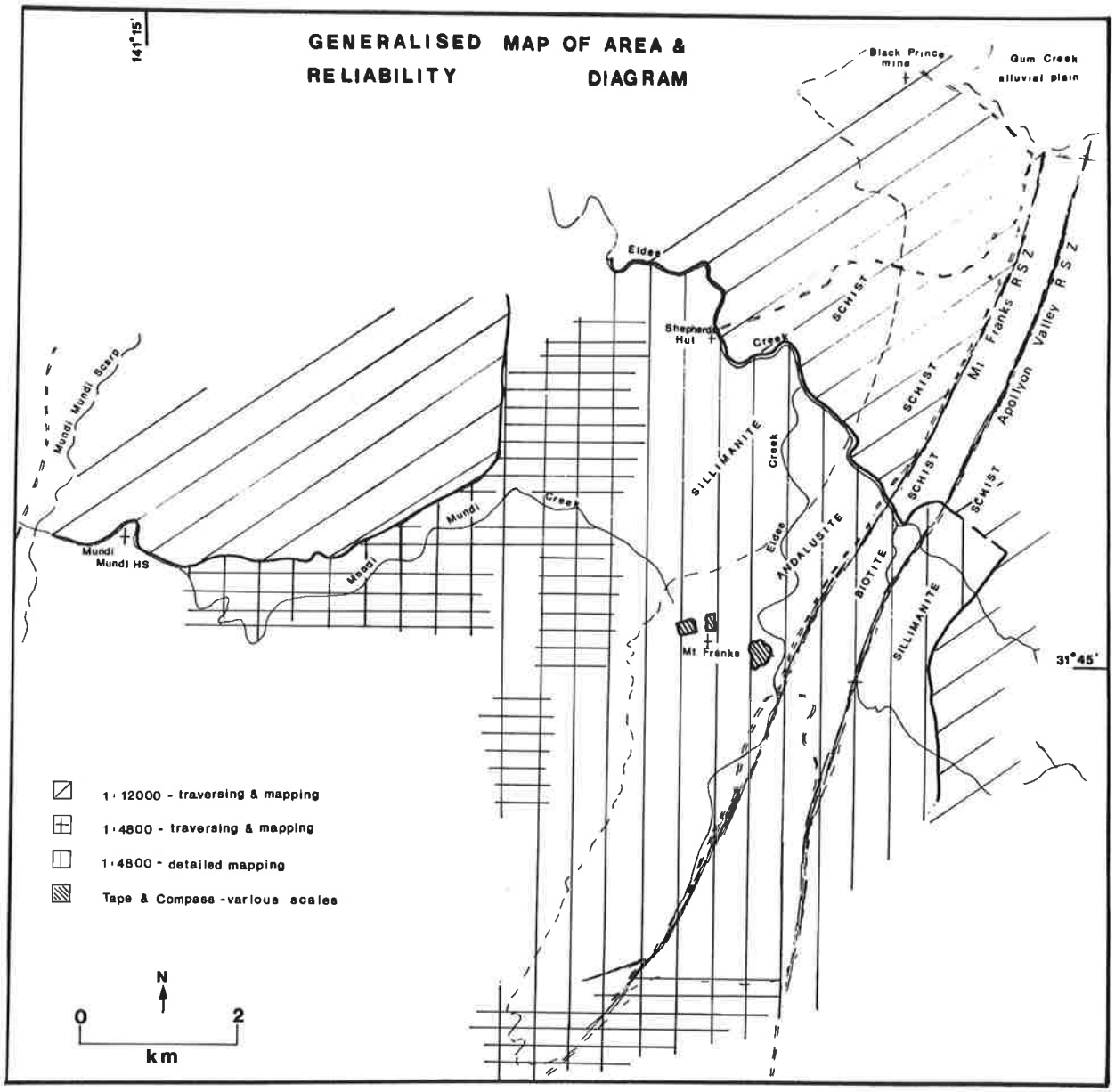
GENERALISED MAP OF AREA &
RELIABILITY DIAGRAM
141°15'
Black Prince mine
Gum Creek alluvial plain
Elder
Shepherds Hut
Creek
SCHIST
Mt Franks R S Z
Apollyon Valley R S Z
Mundi Mundi Scarp
Mundi Mundi HS
Mundi Creek
Mesas
SILLIMANITE
Creek
Elder
ANDALUSITE
BIOTITE
SILLIMANITE
Mt Franks
31°45'
1 : 12000 - traversing & mapping
1 : 4800 - traversing & mapping
1 : 4800 - detailed mapping
Tape & Compass - various scales
N
0
2
km

Fig. 1.4 Previous Interpretations of Structure in the north-western part of the Willyama Complex.

left Andrews (1922, 1923)

centre King and Thomson (1953)

right Anderson (1971), Cooper (1969), Roberts (1969), Laing (1969).

Abbreviations aa - Adelaidean sediments
p - pegmatite
(a) - amphibolite (minor)
e - Ettlewood limestone
t - granitoid
s - sillimanite
c - chiastolite
f - Mt Franks fault
k - Kantappa Lineament
R - Mt Robe
F - Mt Franks
L - Lakes Nob
M - Mundi Mundi
S - Silverton

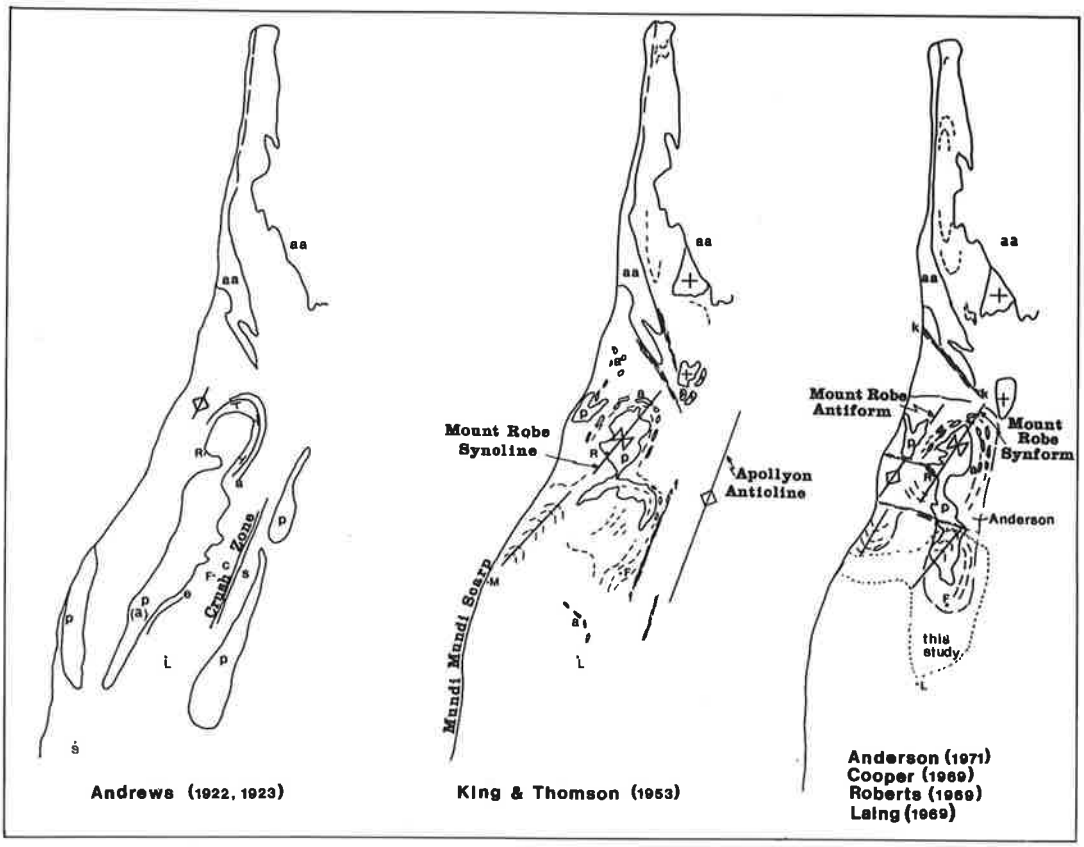
aa
aa
Cryptic Zone
Andrews (1922, 1923)
aa
aa
Mount Robe
Synoline
Apollyon
Antiline
Mundi Mundi Scarp
King & Thomson (1953)
aa
aa
Mount Robe
Antiform
Mount
Robe
Synform
Anderson
this
study.
Anderson (1971)
Cooper (1969)
Roberts (1969)
Laing (1969)

CHAPTER 2 LITHOLOGY, BEDDING AND SEDIMENTARY STRUCTURES

2.1 INTRODUCTION.

The purpose of this chapter is fourfold:

1. to provide a brief outline of the spatial relations between rock types, metamorphic zones and major structures which will serve as a background for Part I of this study. (These points will be developed further in Part II, in particular in Chapter 6, Macroscopic Relations).

2. to discuss the overall composition of lithological units recognised in the area by basic field mapping, concentrating especially on the compositional variation in the metasediments* which gives rise to a well developed layering.

3. to discuss the scale and continuity of this layering in the metasediments, and

4. to describe features along the layering interfaces which are interpreted as sedimentary structures.

Special emphasis is placed on the metasediments because the layering described in them is used to define the macroscopic geometry of the area (Chapter 6). This layering has been interpreted as bedding by early workers (Andrews, 1922; King and Thomson, 1953) but Anderson (1966) suggested that it represented transposed bedding. If this layering can be shown to be bedding, as will be argued from points 2, 3 and 4 above, then it is possible to interpret macroscopic structures in terms of bedding units and to erect stratigraphic relations between these units.

2.2 DISTRIBUTION OF LITHOLOGICAL UNITS, MAJOR STRUCTURES AND METAMORPHIC ZONES.

The Mt Franks - Mundi Mundi area is split into three by two northeast trending retrograde schist zones - the Apollyon Valley Retrograde Schist

---

* The chemical work of Edwards (1958) and Splatt (1975) has suggested that amphibolites are meta-igneous rather than metasedimentary rocks and are therefore excluded from this category.

Zone and the Mt Franks Retrograde Schist Zone (Fig. 2.1 and Map 1 in pocket at back of Part II). Rocks in the eastern block, east of the Apollyon Valley Retrograde Schist Zone, consist of retrogressed metasediments, amphibolites, pegmatites, granites and migmatites. The metamorphic rocks are called the Parnell Beds. To the east they abut against a feldspathic, poorly layered, metasediment unit recognised by G. Bradley (pers. comm., 1976). Layering in the Parnell metasediments dips to the southeast at moderate angles, and is generally defined by the small scale alternation of pelite* and psammite* layers which is characteristic of the unit. Although the Parnell Beds are highly retrogressed, relics of prograde sillimanite in the metasediments are still present.

The Apollyon Beds (Fig. 2.1) lie in the central block, west of the Apollyon Valley Retrograde Schist Zone, and also extend westwards across the Mt Franks Retrograde Schist Zone into the western block where they abut against the Robe Beds. The Apollyon Beds are characterised by mappable bands of calc silicates, units of carbonaceous schist and units of non carbonaceous quartz mica schist which is in marked contrast to the monotonous nature of the Parnell Beds to the east and the generally monotonous nature of the Robe Beds to the west. In further contrast to both these units, the Apollyon Beds do not contain amphibolites. The western boundary of the Apollyon Beds abuts against the Robe Beds and is placed at the base of the most westerly carbonaceous schist.

Between the Apollyon Valley and Mt Franks Retrograde Schist Zones, the Apollyon Beds are low grade, characterised by prograde biotite with only local chiastolite in carbonaceous lithologies. Further west across the Mt Franks Retrograde Zone, andalusite and chiastolite, as well as biotite are prevalent. Thus a metamorphic boundary running along the Mt Franks Retrograde Schist

---

* The terms 'pelite' and 'psammite' are used as in Joplin (1968, pp 23-24).

Zone separates low grade rocks from medium grade rocks. In contrast to the Parnell Beds, and much of the Robe Beds, both low and medium grade zones are characterised by only minor amounts of granitic material. Large scale folds in the Apollyon Beds are best outlined by calc silicate bands, which extend from the Mt Franks Retrograde Schist Zone across to the Apollyon Valley Retrograde Schist Zone in the east, and also by the boundary between carbonaceous and noncarbonaceous schists. In the area of these folds, the low grade, fine-grain rocks of the Apollyon Beds develop incipient ?sillimanite (now retrogressed to sericite) and give way to coarser schists and gneisses, which resemble the Robe Beds and which are characterised by sillimanite and large amounts of granitoid. Elsewhere, layering has a steep easterly dip except south of Mt Franks where steep westerly dips occur.

The Robe Beds extend from the boundary with the Apollyon Beds westwards to the Mundi Mundi Plain. They consist of metasediments, bands of amphibolite, local gneissic units, calc silicates and local carbonaceous schists in the west near the Mundi Mundi Plain. Although most of the metasediments consist of pelite with thinly layered psammite bands, thickly layered psammites and psammopelites are also present. One such occurrence, in the east of the area, has been termed a separate unit, the Mt Franks facies. Other occurrences further west are less extensive, and are shown in Map 1 (pocket of Volume 2). Bodies of amphibolite occur in several horizons outlined by layering in the surrounding metasediments. Calc silicates are restricted to the northeastern part of the Robe Beds although other bodies surrounded by metasediments and amphibolites occur to the south of the mapped area. A carbonaceous unit, the Mundi Mundi facies, occurs in the western part of the area and is surrounded by non carbonaceous pelites, psammites and psammopelites. The main body of this unit outlines a southwest plunging synform but the more easterly body has a lenticular outcrop shape.

Layering in the metasediments and distinctive marker units outline large scale folds in the Mt Franks area, in the Black Prince - Eldee Creek

Area and in the western part of the area (Fig. 2.1) and there is a marked change in the orientation of layering from east to west dipping across the area from east to west. South of Mt Franks this change occurs in the Mt Franks facies, close to the boundary with Apollyon Beds, whereas north of Mt Franks, the change occurs further to the west. Metamorphic grade in the Robe Beds increases from east to west; andalusite bearing schists in the east of the unit give way to sillimanite schist further west although the Mundi Mundi carbonaceous facies contains both sillimanite and large crystals of relict chiastolite. The boundary between the andalusite and sillimanite bearing non carbonaceous schists lies within interlayered pelites and thin psammites and is commonly parallel to layering and schistosity over large areas. Pegmatites, migmatites and granite are present especially in the northeastern part of the unit in the sillimanite schists.

Stratigraphic considerations, summarised here from a detailed discussion in Section 6.3.6, indicate that the basal units of the Apollyon Beds conformably overlie the Robe Beds. It is further suggested (Section 6.3.4) that the Mt Franks Retrograde Schist Zone is localised in a phyllitic lithology of the Apollyon Beds, and that the Apollyon Beds east of this schist zone overlie those to the west. The Parnell Beds east of the Apollyon Valley Retrograde Schist Zone have three features in common with the Robe Beds viz.,

1. the general presence of pelites alternating with thin psammites,
2. the local presence of thick psammites and psammopelites, and
3. the presence of amphibolites and granitoids,

but the relationship to the Robe Beds is unclear.

It is significant that the lowest grade metamorphics, containing biotite, occur in the highest stratigraphic unit. Medium (andalusite) grade rocks occur below the low grade rocks in the basal part of the Apollyon Beds and in the upper part of the Robe Beds and high (sillimanite) grade rocks occur in the stratigraphically lower part of the Robe Beds and in the Parnell Beds.

2.3 METASEDIMENTS.

2.3.1 Lithology and Compositional Layering

The following discussion of lithology and compositional layering in the three major lithological units is treated in the order Apollyon Beds, Robe Beds, Parnell Beds. This order was chosen since it corresponds to a sequence of increasing stratigraphic depth and metamorphic grade and illustrates not only the pre-metamorphic nature of this layering but also the change in mineral composition of layering with grade. The preservation of this layering by the restriction of different minerals to different layers, or by the change in ratios between layers suggests that the prograde metamorphic events were basically isochemical.

2.3.1.1 Apollyon Beds east of Mt Franks Retrograde Schist Zone - Low Grade Rocks

The Apollyon Beds east of the Mt Franks Retrograde Schist Zone are dominated by quartz mica schist containing bands of calc silicates and mappable units of carbonaceous schist. Outcrop is poor because these schists weather readily and retrogression is especially severe along the western edge of the Apollyon Valley Retrograde Schist Zone, and in the south of this unit.

The quartz mica schists contain small scale layering with mica-rich bands up to 2 cm wide alternating with thicker (2.5 cm) quartz rich layers (Fig. 2.2). The composition of these layers is best seen in rocks which have sufferred minimal retrogression; mica rich layers have a composition* in the range of 45-50% quartz + 20% muscovite + 20% biotite + 15-10% plagioclase + opaques + tourmaline and this contrasts with a quartz-rich layer composition of 60% quartz + 10% muscovite + 10% biotite + 15% plagioclase + opaques + tourmaline. (In the south of the Apollyon Beds, sericite

---

* This and following compositions are designed to show the ranges of mineral content rather than sum to 100%.

clots suggest the presence of ?sillimanite and ?andalusite and small sillimanite needles occur as inclusions within quartz grains).

This layering thus reflects, not the appearance or disappearance of different minerals across layer boundaries, but merely a change in proportion of a few major minerals. The nature of biotite (pale yellow to dark brown) and muscovite is similar in both layers, and plagioclase has a similar composition (An_{35}-An_{50}) in both quartz-rich and mica-rich layers. Small sub-idiomorphic crystals of pale-yellow to yellow tourmaline occur in small amounts in both layers.

Two facies variants within these quartz mica schists act as marker units. The first is a flinty grey quartzite with green knots (Fig. 3.5) which is best seen in the western part of the unit (around Loc.5321 4871). These rocks are grey in colour and either lack a layering, or possess thin (0.5-1 cm) green coloured layers defined by biotite. These knots vary in length from 2 to 6 cm, and are about 2 cm wide. They are surrounded by narrow (2-3 cm) zones poor in mica, and consist of pale-yellow to brown biotite, quartz, muscovite, feldspar and opaques. In contrast, the groundmass consists of about 40-50% quartz + 15-20% muscovite + 10-15% biotite + 10-15% plagioclase + opaques.

The second type of marker unit is also best developed in the western part of the quartz schists, such as Loc. 5320 4873 (Map 1). These rocks are characterised by the presence of small muscovite "eyes" which are oval in shape, reach a size of 4 x 1.5 mm and define both a schistosity and a shape lineation. Layering in this unit is 2-3 mm thick and is defined by variations in quartz and mica content similar to that in the undifferentiated quartz mica schists.

Carbonaceous schists within the Apollyon Beds are lenticular on map scale and some units are cut off by the Apollyon Valley and Mt Franks Retrograde Schist Zones (Fig. 2.1). Layering within these carbonaceous schists is defined by the small scale (1-5 cm) alternation of black and

lighter coloured grey bands which are graphite* rich and poor respectively (Fig. 2.3). Graphite rich layers have a groundmass composition in the range of 15-20% graphite + 20% biotite + 20% muscovite + 30% quartz + 10% plagioclase + opaques which is in contrast to the composition of graphite poor layers of 10-15% graphite + 10% biotite + 20% muscovite + 40% quartz + 10% plagioclase + opaques. It is thus apparent that the graphite-rich layers also contain more biotite and less quartz than the graphite-poor layers. In both layers, plagioclase forms part of an interlocking matrix with quartz and has a composition around An_{50-60}. Minor tourmaline may also occur in both layers. In addition to these groundmass minerals, large (3 x 1.5 mm) mineral aggregates consisting of sericite + graphite + quartz are more prevalent in graphite rich layers, and some carbonaceous schists contain large twinned plagioclase (An_{35-50}) poikiloblasts which are also more common in graphite-rich layers. The nature of the mineral aggregates is not clear. Some may be retrograde after local chiastolite while other spots have been attributed to cordierite further north (W. D'Arcy pers. comm., 1976).

Bands of calc silicate east of the Mt Franks Retrograde Schist Zone form good marker units which outline large scale folds in the southern part of the Apollyon Beds (Fig. 2.1). Layering in these rocks varies from 3-15 cm in thickness and is sharply defined by the alternation of green and grey/white coloured units (Fig. 2.4). Green coloured layers have an average content c 60-80% amphibole + smaller amounts of quartz, sphene, plagioclase (An_{30-60}), and local diopside. The white/grey layers on the other hand are dominated by diopside and plagioclase (An_{30-60}) with amphibole, quartz, local vesuvianite and sphene. Edwards (1958) reported that pargasite is elongate subparallel to

---

* The term 'graphite' is used here, and in other cases to describe fine grain granules of carbonaceous material. The original determination of carbonaceous material from this unit was made by Grieg (in Browne, 1922) and in view of the metamorphic grade of these rocks, this carbonaceous material is assumed to be graphite.

layering, and it was observed here that tremolite needles generally cut across layering and are moulded on the diopside. Diopside forms generally equant (0.1-0.4 mm) crystals and forms a polygonal aggregate with quartz and plagioclase. Sphene occurs as granules parallel to layering. Edwards (1958) gives a more detailed petrological description of these rocks, and he suggested that these rocks represent metamorphosed marls and limy rocks rather than metamorphosed igneous rocks. It is important to note that these calc silicates, often called 'Ettlewood Limestones' lie stratigraphically above the type 'Ettlewood Limestones' noted by Jaquet (1894) which occur in Robe Bed correlatives south of the area mapped. A feature of these Apollyon calc silicates is their grading along strike into psammites by a loss of calc silicate minerals.

2.3.1.2 Apollyon Beds west of Mt Franks Retrograde Schist Zone - Medium Grade Rocks

In contrast to the Apollyon Beds east of the Mt Franks Retrograde Schist Zone, these rocks are marked by the widespread occurrence of andalusite and chiastolite. North of Mt Franks and west of the retrograde zone, the Apollyon Beds consist of chiastolite schist with fault slivers of andalusite schist (i.e. non carbonaceous schist) and chiastolite carbonaceous phyllite. South of Mt Franks the Apollyon Beds west of the retrograde zone consist of two chiastolite schist units separated by an andalusite schist. The westernmost chiastolite schist is continuous with the chiastolite schist north of Mt Franks and abuts against the Robe Beds to the west.

The two chiastolite schist units west of the Mt Franks Retrograde Schist Zone are lithologically similar to each other although the more easterly unit, which is cut off by the retrograde zone, is more highly retrogressed. A third, poorly outcropping unit occurs within the retrograde zone itself. Within these units, layering is defined by the alternation of thin (0.5-3 cm) pelite layers with thicker (1-6 cm) psammite layers (Fig. 2.5). The main difference between adjacent layers is the strong concentration of

andalusite in the pelites and the strong concentration of quartz in psammite layers as can be seen in the following estimates of composition: pelite layers consist of 40-35% andalusite + 20% biotite + 35% muscovite + minor -15% quartz + 10% graphite + opaques in contrast to a psammite composition of 10-15% andalusite + 10-15% biotite + 30-40% muscovite + 40-50% quartz + 5% graphite + opaques. Straw yellow to red brown biotite with inclusions of quartz, zircon and opaques is present in both pelite and psammite but is more common in the former. Chiastolites are up to 2 cm in size and are commonly zoned parallel to crystal faces with inclusion rich zones (containing biotite, graphite, quartz and opaques) alternating with inclusion free zones. Cruciform patterns are also present, as are locally developed sieve relations between chiastolite and quartz.

In the south of the area, the main chiastolite schist crosses the andalusite/sillimanite isograd and small amounts of sillimanite occur in quartz grains. There is also a gradual decrease in graphite content in this area as the rocks become bleached and lose their characteristic colouring. A further carbonaceous unit, occurring east of this chiastolite schist in a block bounded by two retrograde zones, is characterised by chiastolite and sillimanite. Its relation to the Apollyon Beds is not clear but it may represent a lithology which is faulted out further north.

The andalusite schist unit in the Apollyon Beds west of the Mt Franks Retrograde Schist Zone is best developed south of Mt Franks (see Fig. 2.1 and Map 1), although small fault slices occur north of Mt Franks (at Loc. 5323 4884 and at Loc. 5328 4891, see Map 1). This unit is dominated by psammopelites, and interlayered psammites (Fig. 2.6) range in thickness from 1 to 15 cm. The main difference between these two layers is the presence of andalusite in the psammopelite and its absence in most of the psammites. Comparison of mineral compositions of the different layers (psammopelite — 25-30% quartz + 20-35% muscovite + 20-30% biotite + 20-30% andalusite + minor garnet, feldspar and opaques; psammite —

50-60% quartz + 20-30% muscovite + 20% biotite + 0-10% andalusite + minor garnet, feldspar and opaques) shows that the psammites are andalusite poor and quartz rich with respect to psammopelites. Whereas the mica content of both layers may be similar there is a tendency for the psammopelites to be slightly richer in biotite. Plagioclase has a similar composition (An_{30-50}) in both psammite and psammopelite.

In addition to the psammopelite/psammite layering just described, two other types of layering are present. The first is defined by thin (1 cm) andalusite rich layers (80% andalusite, 20% muscovite) within psammopelites, while the other is defined by biotite rich (100% biotite) laminations within psammites (Fig. 2.7). These biotite laminations are about 1-2 mm thick and their unfolded orientation lies parallel to the larger scale psammite/psammopelite layering. The preservation of these virtually monomineralic layers demonstrates the isochemical nature of prograde metamorphism in these rocks.

Local calc silicate bands west of the Mt Franks Retrograde Schist Zone occur within chiastolite schist at Loc. 5322 4882 (Map 1). These rocks differ from those calc silicates east of the retrograde zone because they are more finely layered (2-3 cm). Because of strong retrogression, this layering is outlined by variations in retrograde rather than prograde minerals, and tremolite rich layers alternate with quartz and epidote rich layers.

2.3.1.3 Robe Beds - Medium to High Grade Rocks

The extent of the Robe Beds is shown in Fig. 2.1. It is dominated in the east by a psammopelitic unit, the Mt Franks facies, which abuts against the lowest chiastolite schist unit of the Apollyon Beds. A local pelitic unit lies west of the Mt Franks facies and further west again lies the main, undifferentiated part of the Robe Beds consisting of psammopelite, pelite, psammite, amphibolite, local gneiss and local calc silicate. In the western part of the area, a carbonaceous unit has been termed the Mundi Mundi facies.

The Mt Franks facies (medium grade) is characterised by psammopelites, which are interlayered with psammites, and which broadly correspond to the biotite-rich subunit recognised in the andalusite schists by Anderson (1966). Psammites vary in thickness from 2 cm-0.6 m and regular variations in thickness may define upward thinning cycles (Fig. 2.8). Layering is caused by a restriction of andalusite to psammopelite layers, and a dominance of quartz in the psammites. Thus psammites have an average composition of 45% quartz + 5% plagioclase + 20% biotite + 20-25% muscovite + traces of opaques and garnets, whereas psammopelites have a composition in the range of 25-30% quartz + minor plagioclase + 25-30% biotite + 25-30% muscovite + 10-20% andalusite + garnet + opaques. Biotite is similar in both layers (straw yellow to red brown) but occurs as fewer, but larger, grains in the psammopelite. Plagioclase is associated with quartz and is more common in psammites although the composition (An_{30}-An_{50}) is similar in both layers. Andalusite crystals up to 1 x 2 cm contain inclusions of quartz, biotite and elongate opaques, probably ilmenite.

In addition to the psammite versus psammopelite layering described above, layering within the Mt Franks facies is also defined by thin (1-2 mm) biotite laminations in psammite layers similar to those in the Apollyon Beds. Other biotite laminations lie at angles to layering and are regarded as cross laminations (Section 2.3.3.1). Local quartzites are also present in these rocks. They are distinguished from psammites by their thinner nature (2-3 cm), more resistant character and overwhelming quartz content.

A local feature of the Mt Franks facies is the presence of crudely elliptical epidote nodules within a psammopelitic matrix. These nodules are commonly broken by cross cutting fractures which reveal circular white and green coloured rings which, in three dimensions, form concentric shells. The white coloured shells are dominated by quartz and plagioclase (An_{40-50}) whereas the green coloured layers are rich in epidote (see extensive discussion by Anderson, 1966).

The pelitic facies lying west of the Mt Franks facies consists of interlayered psammites and andalusite bearing pelites. The composition of the psammites is similar to that just described, but the pelites have higher muscovite and andalusite and a lower quartz content than psammopelites (composition 35-40% muscovite + 20% biotite + 20% andalusite + 20% quartz + garnet, minor feldspar and opaques). Near the Black Prince Mine, local tourmaline-andalusite schists occur and are characterised by the accumulation of small idioblastic tourmaline crystals defining bedding and cross bed laminations.

The undifferentiated part of the Robe Beds consists of psammites, psammopelites, and pelites together with amphibolites, calc silicates and local gneisses. The most dominant layering in this unit is that caused by psammite/psammopelite/pelite alternations, similar to that in the Mt Franks facies and in the Apollyon andalusite schist. Psammites are generally 1-5 cm thick, although thicker layers (up to 1 m) are locally present, and have a composition in the range 45% quartz + 5-10% plagioclase + 20% biotite + 20-25% muscovite + traces of opaques, garnet (locally up to 15%), tourmaline, zircon and apatite. Andalusite and/or sillimanite may also be present, and K feldspar (generally microperthite) may occur in small amounts, and is more common in the western part of the area.

The average psammopelite composition, on the other hand, is in the range 25-35% quartz + 20-30% biotite + 30% muscovite + 10% plagioclase + 20-25% aluminosilicate + 5-10% garnet + opaques, tourmaline, zircon and apatite. Andalusite is the only aluminosilicate in the eastern part of this unit. Further west, sillimanite* and fibrolite* are dominant although andalusite may still be present. In parts of the psammopelites, K feldspar

---

* 'Sillimanite' is used to refer to the coarsely crystalline variety of that mineral whereas 'fibrolite' refers to bundles or clots of fibrous aggregates of sillimanite ('Faserkiesel') in which rational crystal faces cannot be seen. Small needles of sillimanite, such as figured by Vernon (1975), are referred to as such rather than 'fibrolite'.

may form up to 15% of the rock and muscovite is generally absent. Plagioclase has a wide range of composition in either layer (An_{30}-An_{50}) and this compares to determinations of An_{29-41} by Binns (1964).

From the mineral compositions listed above, it is suggested that there is no significant change in mineralogy across the andalusite/sillimanite isograd.

Four other types of layering were noted in the metasediments of the Robe Beds. These were defined by:

1. concentration of biotite in laminations,

2. the concentration of andalusite crystals in thin layers within psammopelites (similar to that described in the Apollyon Beds),

3. in sillimanite schists, the concentration of sillimanite-sericite aggregates in thin layers within psammopelites (Fig. 2.9), and

4. in psammopelites, the concentration of iron oxides into layers which alternate with iron oxide free layers (Fig. 2.10).

Although the shape of these opaques suggests that they might have been magnetite they now consist of hydrous iron oxides (polished section identification).

The Mundi Mundi facies is a carbonaceous lithology occurring in two closely related areas in the western part of Mt Franks - Mundi Mundi area (Fig. 2.1). The more easterly unit is lenticular, occurring in the eastern limb of the late stage synform but not in the western limb. The larger unit outlines the synformal hinge itself. These two bodies are not joined together in the area mapped and are regarded as two separate units.

In the larger unit to the west, several different rock types have been noted. These include:

1. a well- layered rock, with layering defined by the alternation of dark coloured graphite + chiastolite + large biotite (3 cm) layers with lighter coloured graphite-poor + sillimanite rich + small biotite (0.6 mm) layers (Fig. 2.11). Small amounts of fibrolite may be present in the

graphite rich layers, and untwinned K feldspar is also present. Biotite, plagioclase (An_{60}), quartz and muscovite occur in both layers, and plagioclase is especially well developed fringing andalusites.

2. a well-lineated, poorly layered rock containing graphite, elongate sillimanite and mineral aggregates of graphite, quartz, sericite and opaques probably after andalusite. Plagioclase (An_{60}), biotite, quartz, minor fibrolite and tourmaline are also present.

3. well-layered quartzites.

Calc silicates in the Robe Beds are more thinly layered than those in the Apollyon Beds and consist of alternating coloured layers 1-2 mm wide and white coloured layers 2-4 mm wide. The green coloured layers are dominated by amphibole (80%) and quartz, whereas the white coloured layers consist of quartz (60%) + plagioclase + clinopyroxene + zircon + epidote $\pm$ amphibole $\pm$ clinozoisite, the last three of which are retrograde. Amphibole varies in colour from colourless to blue/green and may be actinolite. Clinopyroxene occurs as inclusions inside epidote and is also possibly pseudomorphed by amphibole. It is probably diopside.

2.3.1.4 Parnell Beds - High Grade Rocks

The Parnell Beds consist of highly retrogressed metasediments and amphibolites east of the Apollyon Valley Retrograde Schist Zone. The metasediments are dominated by pelites, and psammites interlayered with them are generally 1-5 cm thick although some thicker (0.3-0.6 m) layers are present. This mesoscopic layering is similar to that in the Robe Beds and reflects a variation in mineral content - predominantly that of quartz, biotite, muscovite and sillimanite - which has not been obliterated by subsequent metamorphism. An average pelite composition of 30% biotite + 10-20% sillimanite + 20% muscovite + 15% quartz + 5% plagioclase + 10% garnet $\pm$ K feldspar $\pm$ andalusite contrasts with the following psammite composition: 40-50% quartz + 20% biotite + 10% muscovite + 5-10% sillimanite + 5-10% plagioclase + 10% garnet. Small amounts of tourmaline, opaques and zircon

occur in both layers. The strong biotite and sillimanite content is a distinctive feature of the pelites and these minerals commonly occur in bands. In psammites, by contrast, sillimanite occurs in smaller amounts together with biotite and it is more common as inclusions within quartz. Plagioclase and K feldspar are associated with quartz and are thus more common in the psammites. Local andalusite was only found in pelite layers.

2.3.1.5 Summary

In summary, a description of layering in the metasediments indicates the following features:

1. Psammite/psammopelite/pelite layering is generally defined by a variation in the ratio of a few major minerals (aluminosilicates, quartz, mica) between layers.

2. In carbonaceous schists, layering is defined by the alternation of carbon rich and poor units.

3. Layering in calc silicates may be defined by the restriction of calc silicate minerals to specific layers, or by a change in mineral ratios.

4. Layering within some psammites and psammopelites is defined by the presence of monomineralic layers of biotite, andalusite, sillimanite + sericite aggregates, and biotite, and also locally by iron oxide rich layers.

These features all suggest that at the scale of individual layers, there is a strong compositional control on the high grade metamorphisms. It is accordingly suggested that this layering does not represent a metamorphic differentiation effect which predates the earliest deformation but is sedimentary bedding.

The following section demonstrates that this layering lies parallel to boundaries between major lithological units, and Section 2.3.3 describes sedimentary structures which occur along the layering interface.

2.3.2 Continuity of Bedding

Anderson (1966, 1971) suggested that with the exception of the

Mt Franks area, layering throughout the area he mapped was originally bedding which had been mesoscopically transposed into a new orientation. Transposed layering is characterised by the following features (Hobbs, 1966a):

1. It is lenticular with isolated fold hinges.

2. It is generally uniformly dipping parallel to cleavage or schistosity and does not reflect the orientation of any large scale untransposed layered units.

3. It does not preserve stratigraphic order.

This section discusses the continuity of layering and its relation to large lithological units. Chapter 6 demonstrates that layering does not always lie parallel to schistosity and that stratigraphic order is preserved. These points all indicate that significant mesoscopic transposition has not taken place (Section 6.2.5).

Large scale continuity of bedding is best seen in the Robe Beds, especially on Mt Franks where individual beds can be traced around a parasitic fold for several hundred metres (Fig. 2.12). The only local exception to this is on the northern shoulder of Mt Franks where well bedded units pass along strike into a massive psammopelite in a facies change. Bedding on Mt Franks is not atypical since large scale bedding continuity can be seen further west near Shepherds Hut (Loc. 5300 4918) and also southwest of Mt Franks (Loc. 5284 4871).

In areas of less prominent outcrop, bedding continuity can only be assessed by the measurement of bedding in individual scattered outcrops. In these cases, it was found that large scale bedding surfaces so constructed lie parallel to lithological boundaries. Thus in Figure 2.1 and Map 1, bedding trends visible in the field lie parallel to major lithological boundaries.

2.3.3 Description of Sedimentary Structures

2.3.3.1 Cross Bedding*

The identification of cross bedding is based on the recognition of foreset lamellae which are inclined to bedding, and which are bounded by other foreset lamellae or by lamellae (sub)parallel to bedding. A direction of younging can be assigned to these structures where the tops of the foreset lamellae are truncated by other lamellae, and where the bottoms of the foreset lamellae become asymptotic to bedding.

With the exception of the calc silicate units, the Parnell Beds and parts of the Robe Beds (mainly the sillimanite schists), cross bedding has been found in all metasedimnnts. The best examples are found in the Mt Franks facies on Mt Franks. Here they are defined by biotite laminations in both psammites and psammopelites and occur as compound sets (Fig. 2.13) consisting of several layers of foreset beds, or as single sets (Fig. 2.14) which consist of a single layer of foreset beds between bedding parallel laminations. Other cross beds occur in the tourmaline-andalusite schists near Black Prince Mine, where they are defined by tourmaline rich laminations, and also in the Mundi Mundi facies where they are defined by biotite laminations. There is considerable variation in dip angle of all these foresets - from about 20° in Fig. 2.14 up to 90° in some of the foresets in Fig. 2.13, and it is thought that these high dips result from steepening during deformation, either penecontemporaneous or diastrophic. In all cases, foreset heights are only in the range 3-5 cm. The three dimensional shape of these cross beds is not known since all observations were restricted to traces on surfaces lying at high angles to bedding.

The cross beds from Mt Franks described above were first noted by Anderson (1966, 1971). However, he suggested that these features were

---

* a preliminary discussion of cross bedding and other sedimentary structures from this area and the significance of sedimentary structures in the Willyama Complex was published in Glen and Laing (1975), see Appendix II.

deformational since he stated (Anderson, 1966, p.12) " ... the surface contact between the two sets of laminae (foreset and planar) always seems to be parallel to S_1 and not to S (layering). This suggests that the structure is due to the bringing together of different portions of B_1 folds along glide surfaces." The present re-interpretation of these structures is based on:

1. the fact that the surface of contact is generally parallel to bedding where visible, and lies at marked angles to the S_1 of Anderson (e.g. Fig. 2.14 where trace of crenulated S_1 is visible),

2. the fact that the younging directions from over 160 of these structures are all consistent (discussed in more detail in Section 6.2), and

3. the fact that these younging directions are consistent with younging directions obtained from other sedimentary structures (see below).

2.3.3.2 Ripple Marks

The only complete set of ripple marks found in the area occurs in a psammite of the Mt Franks facies (Fig. 2.15). The ripples have an amplitude of about 3 cm and are climbing. The cross sectional shape indicates that they are generally asymmetrical, and thus suggest an origin caused by current action. The crest lines of the ripples are straight and are sharply defined. Two dimensional traces of possible ripples in biotite laminations within psammite beds can be seen in sections parallel to bedding strike along the northern slope of Mt Franks.

2.3.3.3 Flame Structures

Loading pressure just after sediment deposition results in the formation of flame-like projections of pelite into the overlying psammite (flame structures) and the sense of projection of these features can be used to assign a direction of sedimentary younging. Flame structures have been noted from rocks occurring in, and just west of, the Mt Franks facies on Mt Franks itself. They are best seen in slabs or thin sections cut

perpendicular to bedding, where they appear as irregularities in the psammite/pelite or psammite/psammopelite interface. The direction of younging obtained from flame structures agrees with that obtained from nearby cross beds.

2.3.3.4 Graded Bedding

Most of the graded bedding recognised in the field is not dependent on grain size variation, but on variation in mineral content. This is reflected in the nature of boundaries between adjacent pelitic and psammitic layers. The recognition of these features as sedimentary graded bedding is achieved by the consistent relation between younging directions obtained from these structures with younging directions obtained from cross bedding and flame structures (Fig. 2.16). A complete graded unit, shown in Fig. 2.17 and also schematically in Fig. 2.18, contains a sharp boundary at the base of a psammite, a gradational boundary into the overlying pelite, and a sharp boundary at the base of the next graded unit. The top boundary of the psammite is generally irregular and may be difficult to determine, whereas the lower boundary is often marked by a fracture.

The classical concept (e.g. Pettijohn 1957, p.170) of a graded sedimentary unit is one which shows a "gradation in grain size from coarse to fine upwards from the base to the top of the unit." In this sense, the graded beds in the Mt Franks - Mundi Mundi area are reverse graded since the grain size variation from psammite to pelite is opposite to that found in unmetamorphosed graded beds. This reverse grading is an effect of metamorphism where the clays of the pelites have recrystallised to form large aluminosilicates, whereas the psammite layers have experienced little increase in grain size. Shrock (1948, p.420 et seq.) described 'reversal' of textural gradation in metamorphic rocks with original graded bedding.

As well as gradation in the groundmass minerals, porphyroblasts also show a grading in both size and distribution between some layers. The use of metamorphic mineral distribution as younging indicators has been

cautioned by Hobbs, Means and Williams, (1976, p.148) but in the Mt Franks - Mundi Mundi area where independent younging evidence is available, it is found that they are internally consistent and consistent also with the other younging criteria. Andalusite porphyroblasts (Fig. 2.19) increase in number from the base of a psammite across a gradational boundary into the overlying pelite, concommitant with an increase in mica content.

In the Broken Hill area, reverse grading similar to that just discussed has been noted by several workers from layered sillimanite schist east of the Apollyon Valley Retrograde Schist Zone. Thomson (1959), Australian Mining and Smelting Co. (Corruga Map, 1955), Rutland (1971), Laing (1973, pers. comm., and 1977) have recognised these features in the Parnell Area while they were recognised in the Mine area itself by Laing (1975, pers. comm.), Marjoribanks (1975, pers. comm.) and by Monash University workers (1975, pers. comm.). Garnet grading was used by Burrel as younging criteria in underground workings at Broken Hill (cited in Shrock, 1948, p.422).

2.3.4 Summary

Conclusions of the last three sections of this chapter may be summarised as follows:

1. Lithological layering in the metasediments has the compositional attributes of bedding.

2. Lithological layering lies parallel to the boundaries between large metasediment units.

3. Sedimentary structures are present within this layering.

These three points thus demonstrate that lithological layering is sedimentary bedding, and it will be treated as such in ensuing discussions. The spatial significance of younging directions obtained from sedimentary structures places important restrictions on any model of macroscopic geometry and will be discussed in Section 6.2. The palaeo-environmental significance of these structures and premetamorphic nature of these rocks are outside the main metamorphic and structural thrust of this study.

2.4 OTHER ROCKS.

2.4.1 Amphibolites and Associated Gneisses

Amphibolites in the Robe and Parnell Beds are treated together here because of their similar nature and because the chemical work of Edwards (1958) and Splatt (1975) suggested that they are meta-igneous rocks. Amphibolites occur as discontinuous bodies within horizons defined by layering in the surrounding metasediments. They appear lithologically uniform both along and across individual bodies. Unlike the rocks discussed so far, amphibolites possess no well defined layering. Rather they possess an impersistent, 1 mm thick layering which lies always parallel to schistosity in the enclosing rocks and which Anderson (1966) ascribed to metamorphic differentiation. This layering is impersistent even on a microscopic scale and is defined by the alternation of chains of amphibole with quartz rich layers. Prograde minerals in these rocks consist of hornblende, plagioclase, quartz, opaques with minor biotite and garnet. Proportions of these are highly variable. Hornblende (identified by Binns, 1964) is generally pale green to green blue in colour, although some green-brown grains are present. Plagioclase compositions are variable and values in the range An_{30}-An_{60} were noted.

Local quartzofeldspathic gneisses developed along the margins of amphibolites are best seen at Loc. 5286 4837. These gneisses are marked by the millimetre thick alternation of biotite rich versus quartz + feldspar rich layers. The feldspar is generally retrogressed plagioclase, but small amounts of K feldspar, now retrogressed, may also be present. This rock type appears similar to a quartzofeldspathic gneiss mapped near Mt Robe by Reynolds (1975).

2.4.2 Granitoid Rocks

The simplicity of appearance of granitoid rocks in the low and medium

grade schists, and their small number, contrast markedly with granitoids in the adjacent sillimanite schists. In the lower grade rocks, granitoids occur as sheets parallel to layering or schistosity. They range in size from small bodies only 6 cm wide and traceable for tens of metres to larger bodies which are shown on Fig. 2.1 and which may be up to 2 m wide and 1 km long (for example around locality 31550 86000). These long narrow bodies have straight boundaries which are parallel to planar elements within the surrounding schist and usually show an even thickness. Other bodies, especially in the retrograde schist zones are not as elongate and have a more lenticular or irregular shape.

Sheets in the lower grade rocks have sharp boundaries against the adjacent schist. The country rock maintains its original texture but there may be an increase in the size of quartz and in the amount of plagioclase in narrow zones a few mm thick around the pegmatites. Although these bodies are dominantly pegmatitic, they do show variations in grain size and grade into granites. A single vein may show considerable variation in grain size across its width.

The granitoids show a simple mineralogy, consisting of quartz, feldspar (both plagioclase and K feldspar), and muscovite. Minor biotite and accessory tourmaline may also be present. The proportions and sizes of the major minerals are very variable. Muscovite can range in size from individual laths only 0.6 mm long up to books 3 mm thick. Quartz occurs as both old (2 mm) and new grains (0.2 mm or less), and may form bands parallel to the fabric in the surrounding rocks. Plagioclase grains are generally large (2 mm) and possess both albite and pericline twinning. Composite grains are present; these consist of a core of plagioclase in which albite twins are oriented differently to those in the surrounding grain. Plagioclase composition varies from An_{35} to An_{50}. K feldspar grains are usually microperthite or microcline with characteristic cross hatch twinning. Both the plagioclase and the K feldspar show varying amounts of sericitisation.

The textural arrangement of minerals in the lower grade pegmatites can be divided into three groups:

1) minerals parallel to a planar fabric in the adjacent metasediments,

2) minerals with a random orientation, and

3) minerals with an elongation at high angles to the vein walls.

1) This is the most common type of texture developed in the thinner (less than 1 m) veins. This fabric is outlined by muscovite laths or elongate quartz grains, and is parallel to a schistosity in the surrounding schists. Later deformation effects are recorded by the crenulation of mica in the pegmatites.

2) Random textures occur in the thicker pegmatites and are characterised by the development of mica books. Type 1 and type 3 pegmatites grade into this type towards the centre of the vein.

3) This type of texture is not common. It is characterised by the growth of quartz and feldspar aggregates perpendicular or at high angles to the walls of the sill; mica also has a preferred orientation of (001) planes at high angles to vein walls.

The first group of sills probably crystallised in a stress regime, associated with the production of a schistosity in the adjacent schists, which controlled the orientation of mica especially, and also that of the quartz. The random texture exhibited by the second type of pegmatite may be due either to crystallisation in the absence of a stress field, or in the case of gradations from type 1 to type 2 pegmatites, the progressive dissipation of strain towards the centre of the pegmatite. The presence of minerals perpendicular to walls in the third class of pegmatites suggests growth during extension.

In the high grade sillimanite schists, granitoids occur as large bodies and include pegmatite, granites and the leucocratic components of migmatites. Although these bodies are numerically very common, their size is generally too small to be represented on Map 1. However, they may

locally constitute up to one third of the area of sillimanite schist.

During mapping, a distinction was made between areas of migmatites and granitoid bodies with rafts of metasediments. The boundary between the two is flexible, and was selected so that granitoid bodies contained greater than 75% leucocratic component. At this stage of granite formation, early structures become obscured by homogenization. There is a close connection between these migmatites and granitoids. The large granitoid east of Terrible Dick Mine (Locality 33720 89320) consists of an outer margin of migmatite and a core of pegmatite and granite. The large pegmatite/migmatite between Black Prince Mine and Eldee Creek grades westwards into metasediments with decreasing amounts of leucocractic material. Pegmatite mainly occurs on the eastern and northern margins which have a sharp boundary against metasediments, and also as smaller bodies within andalusite schist in the east. All these bodies contain rafts of highly retrogressed metasediments, and since structural elements in these rafts have a parallel orientation to equivalent elements in the surrounding metasediments, it is suggested that during granitoid formation there was no bulk rotation of these metasediments.

Fig. 2.1 Simplified Geological Map showing lithologies, trend of bedding and metamorphic zones.

Abbreviations - Mt F. R.S.Z. - Mt Franks Retrograde Schist Zone

A.V. R.S.Z. - Apollyon Valley Retrograde Schist Zone

a - amphibolite

c - calc silicate rock

ca - carbonaceous schist

ch - chiastolite schist

g - granitoid (generally homogeneous 75% leucocratic material).

Parnell Beds - vertical ruling

Apollyon Beds - horizontal ruling

Robe Beds - diagonal ruling


migmatites
AVRSZ
MTRSZ
SILLIMANITE
ANDALUSITE
BIOTITE
SILLIMANITE
S_0 & DIP
N
0
2
km

Fig. 2.2 (left) Bedding in Apollyon quartz-mica schist defined by mica rich and poor units. Bedding outlines a tight F_1 fold pair. Scale in cms.
Locality 5326 4878.

Fig. 2.3 (right) Bedding in Apollyon carbonaceous schist defined by alternation of graphite rich (dark) and graphite poor (white) coloured layers. Bedding outlines a sinistral F_3 fold, with the orientation of S_3 approximately shown by subvertical fractures.
Locality 5323 4869.

Fig. 2.4 (left) Bedding in Apollyon calc silicate defined by dark coloured pyroxene + amphibole rich layers alternating with lighter coloured quartz + plagioclase rich layers.
Locality 5306 4838.

Fig. 2.5 (right) Horizontal bedding in Apollyon chiastolite schist defined by the alternate of pelite (vertical S_1) and psammite (inclined S_1). Refraction of S_1 demonstrates bedding clearly.
Locality 5311 4868.

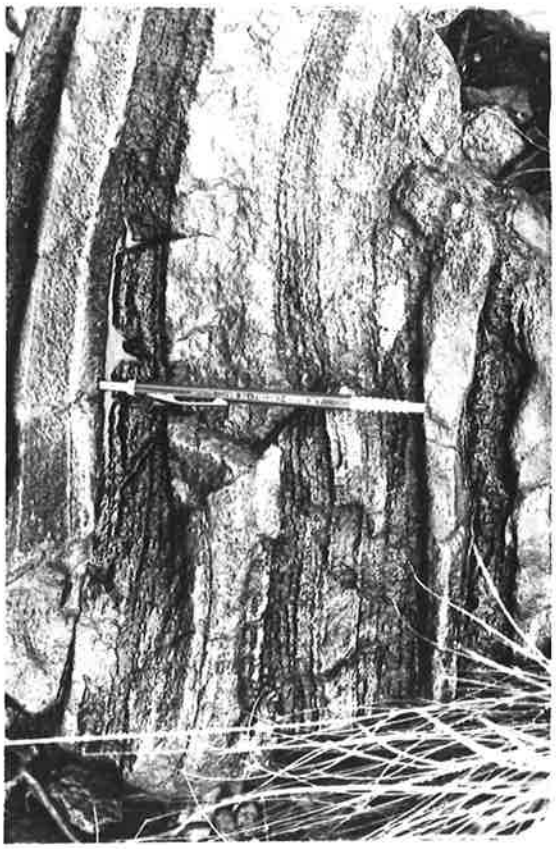

Fig. 2.6 (left) Flat lying bedding (parallel to hammer) in Apollyon andalusite schist crossed by S_1 dipping from top left to bottom right. Knobbly appearance of pelite is due to presence of andalusite. S_1 is refracted across S_0 and dips more gently in part of psammite.
Locality 5313 4869.

Fig.2.7 (right) Fine-scale bedding outlined by biotite laminations in psammite of Apollyon andalusite schist. Biotite laminations alternate with quartz rich layers defining a parasitic F_1 fold.
Locality 5313 4865.

Fig. 2.8 (left) Trace of bedding on S_3' surface. Bedding in the Mt Franks facies is defined by alternation of dark coloured psammites, lighter colour psammopelites. Note upward thinning of psammites.
Locality 5314 4879.

Fig. 2.9 (right) Bedding in Robe sillimanite schist parallel to pencil and crossed by S_1 (top left to bottom right). Bedding is defined by the concentration of sillimanite + sericite.
Locality 5299 4872.

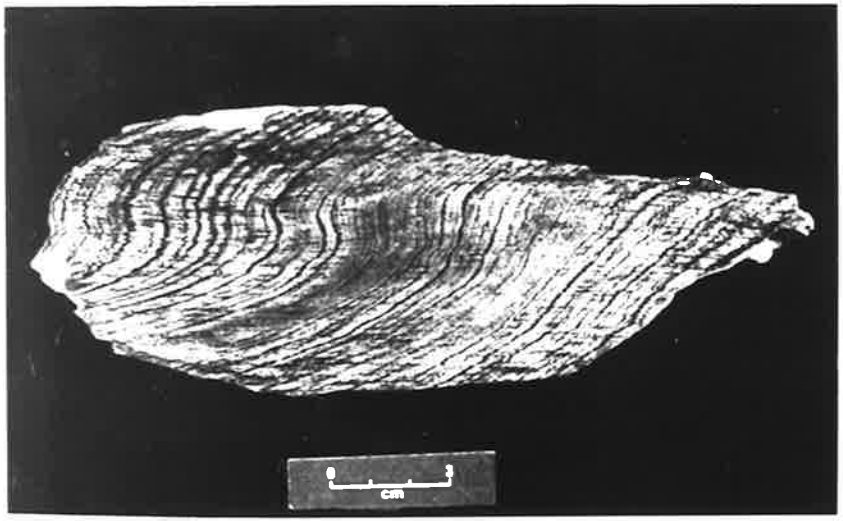
cm

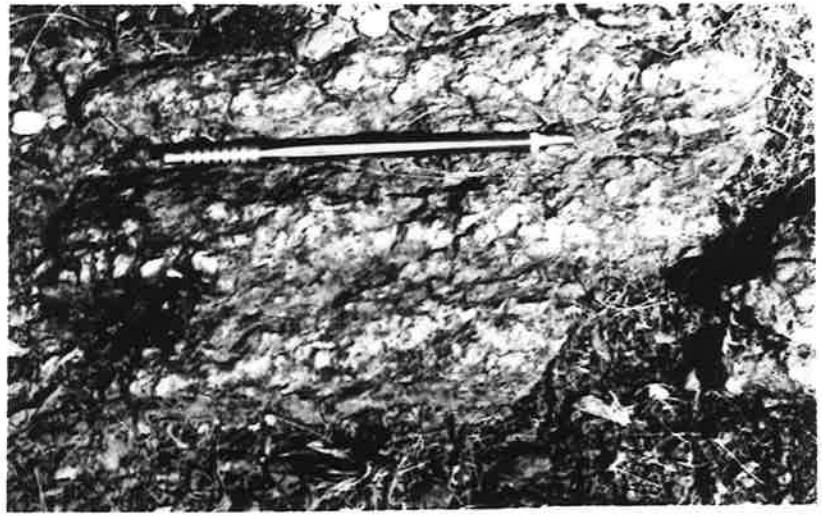

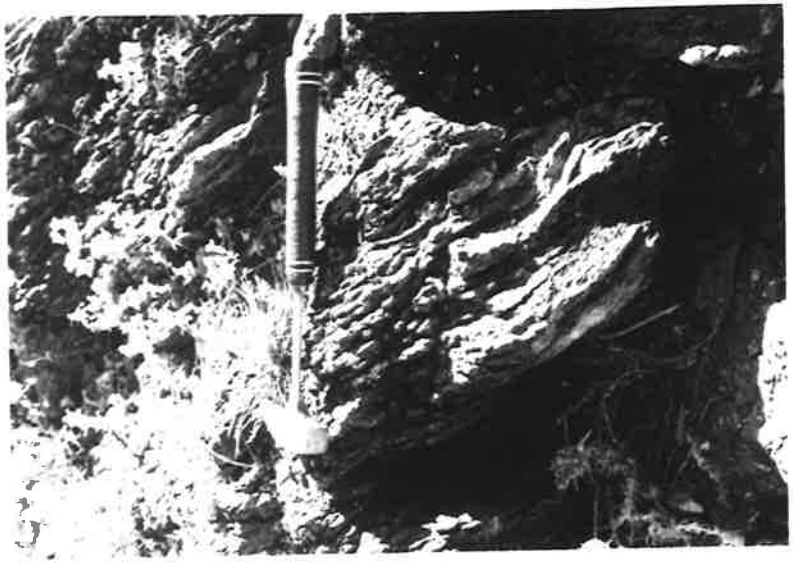

Fig. 2.10 (left) Bedding in Robe Beds defined by concentration of magnetite crystals (white squares). Darker areas consist of fine grain muscovite laths (grey), quartz (black-grey) and crosscutting muscovite plates (mottled). Grading of magnetite suggests bedding youngs to the left.
Negative print of thin section x 3.
Locality 5296 4848.

Fig. 2.11 (right) Bedding in Mundi Mundi carbonaceous facies. Central bed is graphite rich and andalusite rich. Marginal units contain sillimanite, smaller andalusites, and larger biotites.
Locality 5244 4883.

Fig. 2.12 (left) Large scale bedding continuity on short limb (facing viewer) and western limb (background) of Mt Franks fold pair. Short limb about 600 m long. Note cross cutting (left to right) S_1 terraces discussed in Fig. 6.13.
Locality 5321 4882.

Fig. 2.13 (right) Cross laminated psammite of Mt Franks facies - see especially bottom right corner. Cut surface lies parallel to axis of F_1 fold and direction of sedimentary younging is reversed around the fold.
Locality 5309 4874.

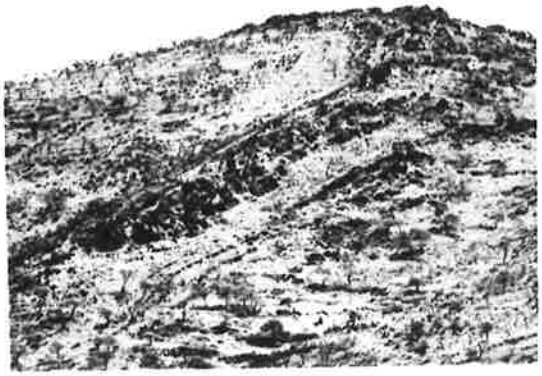


3
cm
0

Fig. 2.14 Trace on S_3' of single set of cross bedded biotite laminations in psammopelites of the Mt Franks facies. Note asymptotic relations between bottomset and foreset laminations and sharp truncation of foresets by topset laminations. Trace of S_1 marked.
Match for scale.
Locality 5313 4879.

Fig. 2.15 Climbing ripples in psammite of Mt Franks facies. Note trace of S_1 (marked) on sawn face and rippled laminations just below top surface (marked).
Locality 4880 5329.

Fig. 2.16 Psammite of Mt Franks facies grading showing increase in mica content (i.e. grading) from left to right. Sense of younging is consistent with way-upness obtained from two sets of cross beds (marked A,B) within psammite.
Locality 5309 4874.

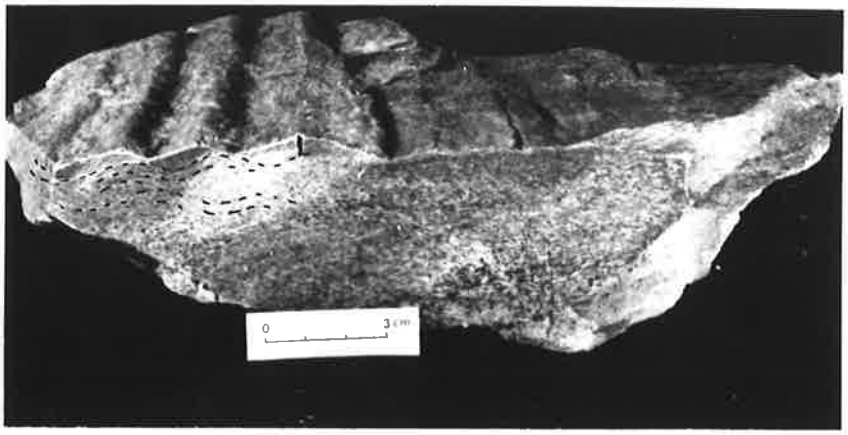
0
3 cm


B
A

Fig. 2.17 Graded psammites and psammopelites of Robe Beds (Mt Franks facies). Younging direction to top of figure. Note sharp base of psammite and irregular, gradational top. S_3 in psammopelite; crenulated S_1 in psammite.
Locality 5325 4888.

Fig. 2.18 Schematic graded unit showing concentration of biotites and alumino-silicates (in this case sillimanite) at top of pelite.

Fig. 2.19 Grading reflected by variation in number and size of andalusite crystals. Younging direction to top of figure.
Locality 5333 4906.

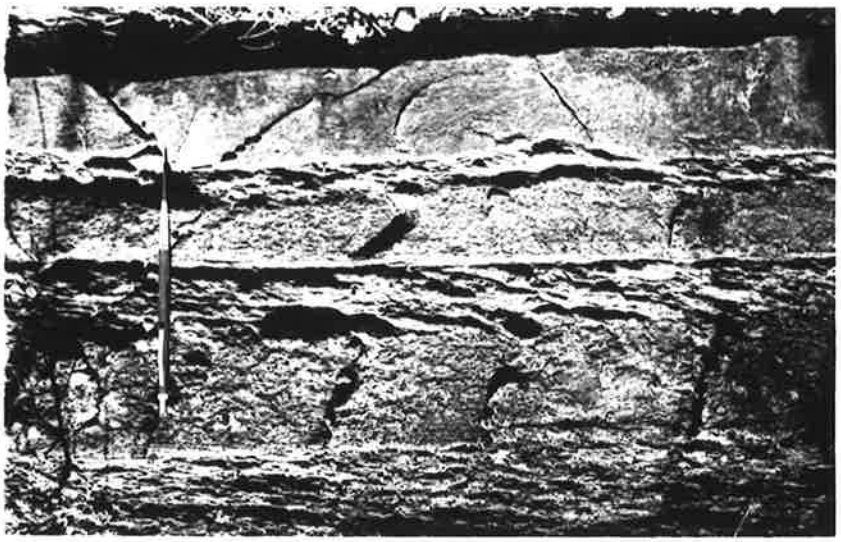

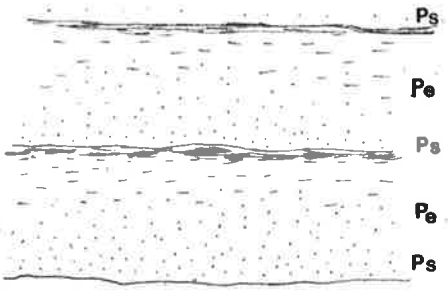
Ps
Pe
Ps
Pe
Ps

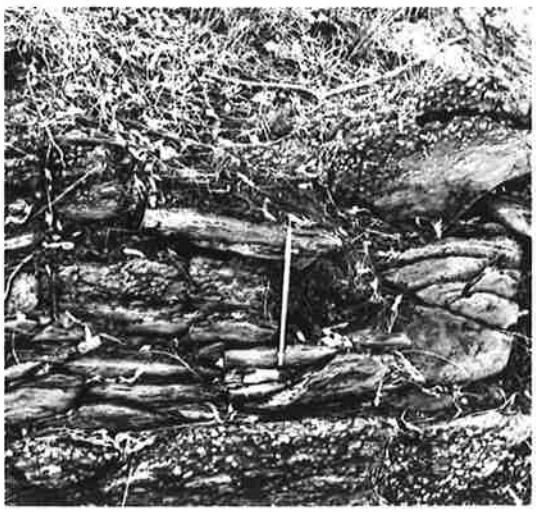

CHAPTER 3 MESOSCOPIC STRUCTURES

3.1 INTRODUCTION.

This chapter describes the different diastrophic structures found in the Mt Franks - Mundi Mundi area. This treatment is based solely on a description of geometric relations visible in outcrop scale or in hand specimen since a discussion of spatial relations between these structures belongs to a macroscopic study (Chapter 6).

Three features are emphasised in this chapter. These are:

1. The variation in morphology of the first recognisable folds and associated schistosity (F_1 and S_1 respectively) between different stratigraphic units and metamorphic zones. In particular, the change in bedding/S_1 relations from non parallel in the Apollyon and higher parts of the Robe Beds to parallel in the main part of the Robe Beds and in the Parnell Beds is discussed. A study of these relations has important implications for tectonic evolution of the Willyama Complex dominated as it is by sillimanite schists in which the first recognisable schistosity lies parallel to bedding (see Section 7.3.1.1).

2. The development of herringbone structures in which schistosity is folded about planar bedding. An understanding of the geometry and formation of this feature is critical to an understanding of macroscopic structure north of Mt Franks (Section 6.2.3.4).

3. The restricted development in psammopelites on Mt Franks of a new long limb schistosity* formed by the small scale rotation of S_1. A feature of this new fabric is that it does not necessarily lie parallel to axial planes of folds of the same generation. Discussion of this feature acts as a prelude to a microfabric treatment of schistosity formation in Chapter 4.

---

* name suggested in conversation by J.P. Platt (1974).

3.2 STRUCTURAL NOMENCLATURE and CORRELATION OF STRUCTURES BETWEEN LITHOLOGICAL UNITS.

The structural nomenclature used in this study was developed from that used by earlier workers on the Broken Hill Project, (see Rutland 1973, and Rutland and Etheridge, 1975). In the high grade schists in the Parnell and Mine areas, Rutland and Etheridge (1975) recognised the presence of two regional schistosities which they called S_1 and S_2, and a local overprinting schistosity, termed S_3. Because of the variable development and similar metamorphic grade of the first two schistosities, they also recognised that where only one schistosity was developed, it could not be classified as either S_1 or S_2, and was thus labelled S_{1-2}. Separation of all the fabric elements was possible only in folds where at least two schistosities were present and a morphological fold classification was erected to describe various fold/schistosity relations:

Group A folds: folds in layering with S_{1-2} axial plane

Group B folds: folds in layering and S_{1-2}

Group AB folds: folds in layering and S_1 with S_2 axial plane.

The early schistosity in Group AB folds was subdivided into S_{1P} (parallel to layering) and S_{1N} (nonparallel to layering). Rutland and Etheridge (1975) noted that in the Parnell and Mine area both S_{1P} and S_{1N} were high grade schistosities, but they were unsure about the relation between them.

Using this background, deformational structures in the Mt Franks - Mundi Mundi area were classified into style groups and then into generations by using overprinting and orientation criteria in key outcrops. Relations in these outcrops were then extrapolated over the rest of the area by continuous mapping. The hazards of using only style criteria to erect fold generations have been pointed out by Williams (1970) and also by Rutland and Etheridge (1975) in the Broken Hill area. In the virtual absence of mesoscopically refolded bedding, and folded lineations, overprinting criteria consist of the

TABLE 3.1

Structural Nomenclature, Characteristics of Deformational Structures[+] and Correlation of Structures in Metasediments across the Mt Franks - Mundi Mundi Area.

	APOLLYON BEDS (low and medium grade rocks)	ROBE BEDS (medium and high grade rocks)	PARNELL BEDS (high grade rocks)
First generation structures	F_1 open to close folds S_1 mica schistosity L_1 mica lineation and aggregate elongation lineation	F_1 close to tight folds S_1 mica schistosity L_1 mica or sillimanite lineation	- S_1 mica schistosity L_1 sillimanite lineation
Second generation structures	-	F_2 overturned tight folds S_2 local mica schistosity	-
Third generation structures	F_3 open to close folds S_3 mica schistosity S_3' long limb schistosity (rotated S_1) L_3 mica lineation	F_3 kink folds, open folds S_3 mica schistosity S_3' long limb schistosity (rotated S_1) L_3 mica lineation	F_3 kink folds, open folds S_3 local mica schistosity
Fourth generation structures	F_4 open folds and warps, - close folds, crenulations	F_4 open folds and warps, crenulations	F_4 open folds, or may be cusp like crenulations
Other structures	F_4' open folds and warps, cusp like folds S_4' local schistosity	F_3^* crenulations and local cusps ?related to F_3	-

+ intersection lineations not shown.

crenulation and folding of schistosities which formed as axial plane structures in an earlier deformation. In many cases, schistosity/bedding relations are used to separate schistosities of different ages.

During the mapping, it was recognised that boundaries between lithological units might represent structural discontinuities, and that adjacent rock units might have sufferred different structural histories. In order to assess this possibility, it was decided to establish sequences of deformational effects within each of the lithological units discussed in Chapter 2, and then to correlate these sequences between units. In each unit, the first recognisable folds, - those folding only bedding - were called 'First Generation Folds' (F_1). The associated schistosity, axial planar or approximately so, to these folds is called S_1 and a mineral lineation within S_1 is called L_1. Overprinting criteria were used to separate later deformational effects into second (F_2, S_2), third (F_3, S_3, L_3) and fourth (F_4, S_4) generation structures. Local structures associated with effects of the third and fourth deformations (D_3 and D_4) are also present.

Correlation of minor structures between lithologies is complicated by changes in style and orientation and by change in metamorphic grade across the area. Despite these factors, the correlation deduced between lithological (and metamorphic) zones is summarised in Table 3.1. From this table it can be noted that first, third and fourth generation structures are correlable across the whole area whereas second generation structures are restricted to the Robe Beds. This means that folds in the Apollyon and Parnell Beds which were called "second generation structures" during the mapping become "third generation structures" when placed in the wider context of the area as a whole. Structures within retrograde schist zones are also described and discussed in relation to structures in the surrounding country rock.

3.3 FIRST GENERATION STRUCTURES.

3.3.1 Apollyon Beds

3.3.1.1 F_1

F_1 folds are not common in the Apollyon Beds. East of the Mt Franks Retrograde Schist Zone they are upright or steeply overturned to the west; west of the zone they are overturned steeply to the east. In the quartz-mica schists F_1 folds are outlined by alternating 1-2 mm thick biotite and quartz layers. Both wavelength and amplitude are small and the folds vary in style from open to close, and may be characterised by an overturning of one limb (Figs. 3.1, 3.2). F_1 folds are overprinted by F_3 structures with the resultant formation of local interference patterns (Fig. 3.3) belonging to Class I of Ramsay (1967). All these folds are associated with an axial plane S_1 which is best seen in the mica layers. In many cases hinges are destroyed by the presence of axial plane fractures.

Identification of F_1 folds in calc silicates is made difficult by plunge changes and lack of axial plane surfaces other than fractures. Consequently, the recognition of F_1 folds in this unit is based on congruency to F_1 folds in surrounding schists and on orientation. These folds have a larger amplitude than those described above and are characterised by a concentric rather than similar style.

West of the Mt Franks Retrograde Schist Zone, F_1 folds are best recognised in the Apollyon andalusite schist, where they are outlined by biotite rich laminations. These folds are steeply overturned to the east and vary from open to tight (Fig. 3.4, Fig. 2.7).

3.3.1.2 S_1 and L_1.

In the quartz-mica schists, S_1 forms a fine axial plane parting which may contain a down dip mica lineation. In some quartz rich rocks, S_1 is not homogeneous and is defined by mica rich bands which weather out to form grooves, and quartz rich bands about 0.5 mm apart which weather out to form rills. In characteristic grey quartzites, S_1 is defined by the shape

orientation of green mineral aggregates which also define a down dip lineation (L_1) (Fig. 3.5a,b,c).

In many cases S_3 is morphologically similar to S_1 and where the two cannot be differentiated by schistosity/bedding relations the undifferentiated surface is called S_{1-3}.

By contrast, in both Apollyon andalusite and chiastolite schists, S_1 is a refracted schistosity (Figs. 2.5, 2.6). In psammites of the andalusite schist, S_1 occurs as a homogeneous muscovite schistosity or as a fine scale biotite streaking (Fig. 2.7). In psammopelites, S_1 is a spaced schistosity, the spacing of which is controlled by the size of andalusite crystals. S_1 in the psammite (S_1Ps) lies closer to bedding than S_1 in the psammopelite (S_1Pe); the curving of S_1Ps in Fig. 2.6 is a reflection of increasing mica content towards the top of the psammite. In chiastolite schists, S_1 is defined by splitting surfaces about 1 cm apart although S_1 is more closely spaced in detail. As described above, S_1 changes orientation across bedding and lies closer to bedding in psammitic beds than in pelitic beds. S_1 wraps around chiastolite crystals.

Ramsay (1967, pp.403-407) suggested that schistosity refraction between layers forms in response to variation in strain between layers. He argued that the more competent layers deform by tangential longitudinal strain and form convergent fans while in the less competent layers the schistosity shows divergent fans due to a large component of simple shear acting along the layering. In the Mt Franks - Mundi Mundi area, S_1 refraction patterns suggest that the pelites are more competent than the psammites. This reversal of competency is attributed to the preferred growth of andalusite in the pelitic layers before the D_1 event, and micro-structural evidence for this growth is presented in Section 4.2.2.

In addition to the high angle S_0/S_1 relations described above, two other types of relations occur in the overturned limbs of macroscopic F_1 folds. The most common situation is one in which S_1 is dipping more gently

west than S_0 and is refracted across bedding as in Figure 3.6. However, in local areas, S_1 lies precisely parallel to S_0 in both pelite and psammite.

3.3.2 Robe Beds

3.3.2.1 F_1

F_1 folds in the Robe Beds are best seen in the eastern (andalusite bearing)part which is dominated by S_{1N} relations. S_{1P} relations prevail in the sillimanite schists further west. Mesoscopic F_1 folds are overturned at moderate angles to the east, except in the south of the area where they are steeply overturned to the east or are upright.

In Chapter 2 it was shown that bedding in these rocks is outlined by:

1) biotite and andalusite laminations,

2) psammite/psammopelite/pelite alternation, and

3) quartzites,

and as a result there is considerable variation in the style of F_1 folds.

1) Folds in these laminations are the smallest amplitude folds found in the area and are parasitic rather than intrafolial. They are commonly tight although there may be considerable variation along the axial surface, (Fig. 3.7). The change in sedimentary younging direction around these F_1 folds is illustrated in Fig. 2.13. Andalusite laminations are thicker than biotite laminations, and as a consequence F_1 folds in them are more-open (Fig. 3.8). Whereas F_1 folds in biotite laminations are characterised by an axial plane mica schistosity, F_1 folds in andalusite laminations are accompanied by a set of fanning fractures.

2) Mesoscopic F_1 folds in psammite/ psammopelite/ pelite bedding are parasitic, vary in style from open to tight (Fig. 3.9a,b,c,d,e,f) and are associated with an axial plane or refracted schistosity. In some situations (Fig. 3.9c) these folds share the same axial planes as folds in biotite laminations. In the sillimanite schists to the west, F_1 folds may be flat lying and tight, with long limbs characterised by S_{1P} relations (Fig. 3.9f).

3) F_1 folds in thin quartzites vary from tight to isoclinal and may

be marked by disruption of the hinge zone (Figs. 3.10a,b). No mesoscopic S_1 is visible in these beds.

3.3.2.2 S_1 and L_1.

The main effect of the first deformation is the development of a schistosity S_1. S_1 lies at an angle to S_0 in the eastern part of the Robe Beds but generally lies parallel to bedding further west in the andalusite schists near the boundary with sillimanite schists, and in most of the sillimanite schists. S_1 overprints andalusite crystals (Fig. 3.11) and sillimanite-sericite clots (Fig. 2.9) and is itself overprinted by F_2 and F_3 effects. Except for a narrow zone just west of the Mt Franks Retrograde Schist Zone in which S_3 is developed, S_1 is the dominant schistosity in the area.

In andalusite schists, S_1 is defined by laths of muscovite and, in layer parallel situations, by trains of biotite. In sillimanite schist, S_1 is defined by laths of muscovite, crystals and needles of sillimanite and by laths or trains of biotite. S_1 forms a penetrative schistosity in pelites but a closely spaced (2 mm spacing) schistosity in psammites (Fig. 3.12). S_1 varies from a homogeneous to a spaced schistosity in pelites, and commonly occurs as a hackly fracture in psammopelites, particularly in sillimanite schists (Fig. 3.13).

S_1 is commonly refracted across bedding not only around small F_1 folds (Fig. 3.9b), but also where it is unfolded. Where the latter occurs (e.g. Fig. 3.13), the orientation of S_1 lies closer to bedding in psammites than in pelites, and may actually lie parallel to bedding. Where pelites and psammite beds form a graded unit, S_1 outlines a concave upward trace in the psammite.

Two other types of S_0/S_1 relation are present in the Robe Beds. In the first type, both S_0 and S_1 are inclined in the same direction, but S_0 dips more steeply than S_1 (Fig. 3.14a,b) - a feature which is characteristic of overturned bedding. The other type of S_0/S_1 relation occurs where S_1

lies precisely parallel to bedding in both pelite and psammite (Fig. 3.15).

Andalusite schists are dominated by an S fabric (terminology after Flinn, 1965), with only local development of a mica lineation. By contrast, parts of the Mundi Mundi facies are dominated by elongate sillimanites (L fabric), although a layer parallel spaced schistosity may be also developed. In the sillimanite schists, mica and sillimanite define a common lineation (LS fabric). The sillimanite lineation is caused by the alignment of discrete crystals (best seen in the Shepherds Hut area) and also by elongate aggregates of sillimanite, fibrolite and sericite. The difference in sillimanite habit between this area and the Mine area alluded to by Browne(1922) is caused by the prevalence of these sericite-sillimanite-fibrolite clots either wrapped around by S_1 or elongate within S_1.

The S_1 and L_1 recognised in the Robe Beds during this study correlate with S_1 and L_1 of Anderson (1966, 1971) and with the Group 1 deformation effects recorded on Mt Franks by Rutland (1971, 1973a).

3.3.3 Parnell Beds

The D_1 event in the Parnell Beds is expressed by the formation of a schistosity S_1, and by the formation of a mineral lineation, L_1, which lies within S_1 (LS fabric). As far as can be ascertained, S_1 is everywhere parallel to bedding; no F_1 folds were found.

The morphology of S_1 in these rocks is similar to that in the Robe Beds, and varies from a spaced schistosity in psammites to a penetrative, planar surface in pelites. A mineral lineation, L_1 defined by sillimanite crystals may also be present.

3.3.4 D_1 Migmatites

Migmatites have been recognised in the Parnell Beds and in the sillimanite bearing part of the Robe Beds - especially north and northwest of Mt Franks. They consist of alternating leucocratic and melanocratic layers parallel to S_1 which occur at all scales - from mesoscopic (Fig. 3.16a) up

to macroscopic. Leucocratic layers consist of quartz, plagioclase, K feldspar and mica, generally muscovite. Melanocratic layers on the other hand are dominated by biotite and sillimanite.

The parallelism between this migmatitic layering and S_1 suggests that the migmatites are D_1 in age. A sequence of granitoid formation can be recognised from these migmatites; with an increasing leucocratic component, migmatitic layering loses its strict parallelism with S_1 and outlines polyclinal folds. Late stage nebulites may cut across this layering (Fig. 3.16b) during the granitoid forming process. Consideration of migmatite formation in terms of partial melting is treated in Section 5.2.4.

3.4 SECOND GENERATION STRUCTURES.

Second generation structures are restricted in extent. They were only found in a small area of Robe sillimanite schist in the Shepherds Hut Area (see Map 1) where they consist of type B and AB folds in $S_0//S_1$. All these folds are tight in style, overturned to the east and are characterised by an inclined axial surface which dips more gently than the overturned limb. (Figs. 3.17a,b). Bedding is attenuated in overturned limbs and thickened in hinge zones. The thickening of psammites rather than psammopelites in the fold hinges, suggests that there has been a reversal of competency contrast before folding and this is attributed to the effects of previous metamorphisms. In some cases F_2 hinges in S_1 contain co-axial crenulations. F_2 folds can also be recognised with migmatite complexes where they fold melanocratic and leucocratic layers and may be characterised by broad hinge zones (Fig. 3.17c).

The B_2 folds reported by Anderson (1966, p.29-30; 1971, pp.1848-1849) northwest of Mt Robe have a similar style and orientation to the folds just described and are regarded as belonging to the D_2 event recognised in this study.

The synformal hinge in Fig. 3.17b is marked by the development of crenulations in S_1Pe and by the formation of a new axial plane schistosity

in the adjacent psammite where it is defined by mica bands (Fig. 3.17d).

3.5 THIRD GENERATION STRUCTURES.

3.5.1 Apollyon Beds

3.5.1.1 F_3

F_3 folds outlined by biotite laminations in the quartz-mica schists are generally close to open in style with a small amplitude (Fig. 3.18). They are generally accompanied by an axial plane fabric (S_3), and can only be distinguished from F_1 folds where a crenulated S_1 is visible (AB type folds). F_3 folds in bedding plunge to the northeast and are upright with a consistent northeast trend. Overprinting of F_1 folds leads to the formation of Class I interference patterns of Ramsay (1967), (Fig. 3.3). B type F_3 folds in S_1 are also upright, northeast trending but may plunge to the southwest. They are more open than folds in S_0 and hinge zones generally contain co-axial crenulations. Fractures parallel to S_3 may be present.

In andalusite and chiastolite schists, mesoscopic F_3 folds are outlined by biotite laminations (Fig. 3.19) and may be accompanied by the formation of an axial plane schistosity (S_3). More commonly, however, D_3 effects are manifested by asymmetrical crenulations in S_1 (B type folds) which are not related to the presence of mesoscopic folds.

3.5.1.2 S_3, L_3 and S_3'

In quartz-mica schists, S_3 is a vertical or steeply east dipping mica schistosity axial plane to F_3 folds. It is morphologically similar to S_1 and can only be differentiated

a) in fold hinges,

b) with reference to S_3/S_0 relations, and

c) by its consistent NNE-NE orientation.

Where bedding is absent or where S_1 also has a northeasterly trend, the undifferentiated schistosity is labelled S_{1-3}.

In more massive quartzites, S_3 is a mesoscopically discontinuous unrefracted surface defined by mica "eyes" which also define L_3 (Fig. 3.20). Locally, (Loc. 5316 4865) it can be seen that these eyes overprint S_1 and occur in the

short limbs of sinistral folds in S_1 (Fig. 3.21). Similar S_3 eyes are developed in some carbonaceous schists where they consist of small aggregates of sericite + graphite.

In Apollyon andalusite and chiastolite schists S_3 reaches maximum development just west of the Mt Franks Retrograde Schist Zone where it occurs as a northeast trending, steeply east dipping surface. S_3 varies from a strongly segregated schistosity consisting of mica and quartz rich domains to a more homogeneous mica schistosity. A local mica lineation, L_3, may be developed down dip within S_3. Further west from the retrograde zone, S_3 does not develop. Rather a strong NNE-NE trending, vertical or steeply west dipping splitting surface, S_3' occurs. S_3' in contrast to S_3 is not a recrystallisation feature but consists of long limbs of asymmetrical crenulations in S_1. A complete discussion of S_3' and its relation to S_3 is presented in Section 3.5.2.2.

3.5.2 Robe Beds

D_3 structures in the Robe Beds overprint D_1 and D_2 structures. Although overprinting of S_1 is seen in most outcrops, evidence for the overprinting of F_2 is best seen on a macroscopic scale (Section 6.2.3.3).

The development of different D_3 structures in the Robe Beds is controlled by bedding/schistosity relations formed in the first deformation. Three types of S_0/S_1 relations are recognised, each restricted to a particular geographic area. These are:

1. areas in which S_1 lies parallel to S_0 ($S_0//S_1$, S_{1P} relations),
2. areas in which S_1 lies at an angle to S_0 (S_{1N} relations), and
3. areas transitional between the two.

D_3 effects in these areas will now be discussed.

3.5.2.1 D_3 Effects in $S_0//S_1$ Rocks

D_3 effects in these areas resulted in the development of macroscopic parasitic folds in $S_0//S_1$, and in the formation of mesoscopic, upright, variably plunging, NNE-NE trending F_3 folds in hinge and limb areas. Folds outlined by psammites are open and concentric (Fig. 3.22), and contrast with kink folds developed in pelites. F_3 folds are commonly associated with

irregular axial plane fractures rather than schistosity development (Fig. 3.23) and in tight cusp like folds, bedding continuity may be lost across the axial surface. F_3 crenulations are preferentially developed in pelites or psammopelites especially in hinge zones of large folds. They are characterised by regularly spaced axial surfaces in profile (Fig. 3.24) and by a well developed intersection lineation on S_1 (Fig. 3.25).

F_3 folds can also be recognised in areas of migmatisation in the northeastern part of the Robe Beds where they fold melanocratic and leucocratic layers (Fig. 3.16a).

The development of S_3 in this terrain is generally restricted to fold hinges, and there is a strong tendency for S_3 to form preferentially in pelites rather than in psammites. However, the reverse situation may occur (Fig. 3.26). S_3 is a NNE-NE trending subvertical schistosity which varies from a homogeneous mica surface to a segregated schistosity which consists of light coloured quartz-rich and dark coloured mica-rich layers parallel to S_3. Relict S_1 may be visible within these layers and the transition from crenulated S_1 to segregated S_3 may be seen in one outcrop (Fig. 3.27a,b,c). Granitoid veins may also show an S_3 fabric (Fig. 3.28) which is outlined by the orientation of muscovite and elongate quartz aggregates.

3.5.2.2 D_3 Effects in S_{1N} Rocks

The main D_3 effects in S_{1N} rocks are the folding and crenulation of S_1. Small folds in bedding or in quartz veins parallel to bedding are uncommon. Lithology exerts a strong influence on the development of D_3 structures, and tighter, more intense, folds generally occur in pelites and psammopelites. The development of different D_3 effects in adjacent lithologies leads to the recognition of three types of herringbone effect, and these will now be discussed.

Type I Herringbone Structures

These occur when the wavelengths of F_3 folds are about half as long as the thickness of individual beds. As a result, parasitic folds may be

developed within one bed (Fig. 3.12). Strong lithological control on folds of this type is best seen in Fig. 3.29 where S_1Ps is unfolded whereas S_1Pe outlines a parasitic F_3 synform/antiform pair. The axial surfaces of these folds do not cross the bedding interface because the orientation of bedding after the first deformation lies subparallel to S_3. The herringbone nature of this type of structure is seen on a horizontal face: bedding has a dextral relationship with the trace of S_1Ps, but a sinistral relationship with the trace of the S_1/S_3 intersection lineation which is dominant in the pelite (Fig. 3.30).

Type II Herringbone Structures

This type of herringbone structure occurs in the western limb of a macroscopic F_3 synform defined by a change in orientation in S_1Ps (Section 6.2.3.4). On the mesoscopic scale, the orientation of S_1Ps reflects the orientation of this western, southeast dipping limb whereas S_1Pe has undergone only small scale crenulation, the enveloping surface of which reflects the orientation of the eastern, south-west dipping limb.

This type of herringbone structure is shown in Fig. 3.31 (two layer system) and Fig. 3.32 (multilayer system). In both cases, there is an abrupt change in S_1 orientation at the bedding interface, and in the multi-layer system, changes in schistosity orientation outline folds which are lithologically controlled, since the wavelength of the fold is controlled by the thickness of the psammite/psammopelite pair. Bedding acts as kink planes to these F_3 folds and S_1 is unfolded, and because of the re-orientation of S_1Ps, S_0/S_1 relations change from layer to layer. S_0/S_1 relations are dextral, southwest plunging in pelites, but are sinistral, southwest plunging in psammopelites. S_1Ps also dips to the southeast at a more gentle angle than S_0 (Fig. 3.32) - a situation normally indicative of overturning on S_1.

A detailed examination of type II herringbone structures was carried out from the specimen in the top part of Fig. 3.32 by cutting serial sections perpendicular to the S_0/S_1 intersection. These sections (Fig. 3.33)

show that S_0 surfaces do not act as discontinuities, and that S_1 is continuous from psammite to psammopelite. These sections also show that the kink surfaces to folds in S_1 lie parallel to the general orientation of bedding and lie on the bedding interface except where minor bedding irregularities (flame structures and load markings) are present.

Type II herringbone structures are caused by a re-orientation of S_1Ps. They are not caused by refraction because:

(1) F_3 fold hinges "move off" the bedding interface and are located wholly within one lithology where bedding plane irregularities are present, and

(2) these relations are restricted to the rotated limb of a macroscopic F_3 synform outlined by S_1Ps.

It is thought that type II herringbone structures occurred by flexural slip along S_1 planes with the resultant displacement of particles parallel to S_3 resulting in the formation of kink folds. The constraints imposed by the lithology lying parallel to S_3 only permit the rotated limb of these kink folds to develop in psammite beds.

That kink folding was the dominant mechanism of re-orientation is suggested by the following lines of evidence:

(1) The intersection lineation of S_1Ps/S_1Pe pairs plotted on an equal area net lie parallel to the F_3 crenulation lineation developed in S_1 in pelites (Fig. 3.34).

(2) The orientation of 94 sets of S_0, S_1Pe and S_1Ps readings were plotted on an equal area net. This plot shows that poles to bedding lie at 90° measured along a great circle from S_1Pe/S_1Ps intersections (Fig. 3.35). This situation is only fulfilled when the fold axes lie in the bedding plane. This fact, coupled with relations in Fig. 3.32, indicate that S_0 lies parallel to S_3. Measured deviations from 90° in Fig. 3.35 are most probably due to the difficulty in accurately measuring the orientation of a crenulated schistosity which wraps around andalusite crystals.

(3) On a macroscopic scale, type II herringbone relations are restricted to areas in which S_0 lies parallel to S_3 (Section 6.2.3.4).

It is thus suggested that the non folding of S_0 during D_3 is fortuitous, and type III herringbone structures only occur in situations where the orientation of S_0 after the first deformation is closely parallel to the orientation of axial surfaces developed during the refolding. Where this particular situation does not occur, S_0 may be folded by F_3 together with S_1 (Fig. 3.36).

The non folding of S_0 indicates that the direction of maximum shortening during the D_3 event was oriented perpendicular to S_0 in this area - this means that it was oriented NW-SE.

The difference in response between S_1Pe and S_1Ps is probably explained by the higher degree of anisotropy and greater ease of slip on micas in pelites (resulting in intense, small scale crenulation) and the higher quartz content and presence of quartz rich layers in psammites which control the wavelength of folding (Section 4.5.2.2).

Type III Herringbone Structures - Formation of long limb schistosity S_3'

Type III herringbone structures are best seen along the northern slope of Mt Franks (Loc. 5310-5314 4880). Here, the strong lithological control on the D_3 deformation has resulted in the formation of a vertical fabric in psammopelites and an inclined fabric in interbedded psammites (Fig. 3.37). Anderson (1966) suggested that the vertical surface in the psammopelites formed by bulk rotation of S_1, which is preserved in its original orientation in the psammites, and thus regarded this paired feature as a late stage fold. However, detailed inspection indicates that the vertical fabric in the psammopelites represents the long limbs of small scale asymmetrical crenulations in S_1Pe and is therefore not a bulk rotated orientation of S_1 but is actually a new surface developed during D_3 and here labelled S_3'. S_3' surfaces are approximately planar and are penetrative in the psammopelites. They form a strong splitting surface which contains the trace of bedding

(Fig. 2.8). The presence of an inclined S_1 in psammites and a subvertical S_3' in psammopelites leads to the recognition of herringbone structures.

The sequence of formation of S_3' from S_1 in the psammopelites will now be discussed on a mesoscopic scale with reference to a representative number of samples (Figs. 3.38-3.42). This serves as a prelude to Section 4.5.2.4 which discusses the mechanisms of S_3' formation on a microscopic scale.

Fig. 3.38 illustrates incipient crenulation of S_1Pe which contrasts with the unfolded nature of S_1Ps. Two types of crenulation are shown in S_1Pe. The first type consists of small amplitude symmetrical (Area A) or asymmetrical (Area B) crenulations, the enveloping surfaces of which approximate to the original attitude of S_1Pe. The second type of crenulation (Area C) is characterised by the formation of long limbs and is markedly asymmetrical; enveloping surfaces to these crenulations do not reflect the original orientation of S_1Pe. Despite the change in long limb orientation between these two types of crenulation (which results in a style variation), there is a common orientation of S_3 as defined by axial surfaces.

Figure 3.39 illustrates the large scale development of asymmetrical crenulations in S_1Pe (especially around area A), the enveloping surface of which has been rotated from a pre-F_3 orientation. Crenulations in the main part of the psammopelite have assumed a regular wavelength and amplitude (unlike in Fig. 3.38) but those near the bedding interface are more symmetrical and have a smaller amplitude.

In Figure 3.40, strongly asymmetrical crenulations are developed which are characterised by a consistently oriented long limb. The formation of a vertical fabric by the alignment of these long limbs is evident, and several short limbs may merge into one long limb (area A). Short limbs are characterised by the development of small scale crenulations which are absent from the long limbs. Axial surfaces drawn through these small crenulations have variable angular relations with the long limbs; most dip more steeply east (to the left) but some are parallel.

Figure 3.41 shows the development of S_3' as a splitting surface (area A) which lies parallel to the long limbs of asymmetric crenulations (area B). S_3' does not necessarily lie parallel to axial surfaces of these crenulations (S_3) and is thus a long limb, rather than an axial plane schistosity.

Maximum development of S_3' is shown in Fig. 3.42, but even here relict short limbs are still present (area A). Unrotated S_1 is only visible in psammitic beds running diagonally across this Figure.

The above descriptions suggest that S_3' develops by the formation of asymmetrical crenulations in S_1Pe, and by the rotation of these long limbs into a new orientation. Concomittant with this is the destruction of short limbs, and the merging of several short limbs into long limbs. These processes will be discussed on a microscopic scale in Section 4.5.2.4.

S_3' is a penetrative schistosity which extends from the northern slope of Mt Franks eastwards to the Mt Franks Retrograde Schist Zone. Adjacent to this zone, a new schistosity lies parallel to F_3 axial planes and it is now known whether this presents S_3' rotated into S_3, or a new recrystallised schistosity S_3. S_3 commonly contains a steep mica lineation. The zone of S_3' formation is generally restricted to the northern slope of Mt Franks. Further west, S_3 may locally occur, or west dipping S_1 is crenulated about steeply east dipping axial surfaces (Fig. 3.43).

3.5.2.3 D_3 Effects in Areas Transitional between S_{1P} and S_{1N}

Just northwest of Mt Franks, about Loc. 4299 4862, S_0/S_1 relations as seen in mesoscopic outcrop vary from parallel to non parallel. F_3 refolding relations in this area may thus be complex and some examples are shown in Figs. 3.36, 3.44, 3.45, 3.46. The presence of both S_{1N} and S_{1P} relations on a mesoscopic scale in a small area may suggest that the macroscopic domains characterised by S_{1N} and S_{1P} relations merely represents a larger scale variation in bedding schistosity angles, and that S_1 parallel to bedding is equivalent to S_1 non parallel to bedding. This correlation is treated in more detail on a microscopic scale in Section 4.3.6.

3.6 STRUCTURES RELATED TO F_3.

Folds occurring in various parts of the Robe Beds especially around Loc. 4299 4862 both overprint, and are overprinted by, F_3 structures, and are labelled F_3*.

The following points suggest that these two fold types are broadly synchronous:

1. F_3 folds overprint S_1 and earlier F_3* crenulations (Fig. 3.46)
2. F_3* folds cause a change in plunge of F_3 crenulations and overprint F_3 crenulations (Fig. 3.47)
3. F_3 and F_3* folds form a Class I interference pattern of Ramsay (1967) (Fig. 3.48).

Crenulations assigned to F_3* are also present around Mt Franks where they are smaller in amplitude than, and occur on the limbs of, F_3 crenulations (Fig. 3.49). In the absence of clear overprinting relations between structures in this area, it is not known whether they are broadly synchronous with, or postdate, F_3. They are similar, however, to secondary kinks developed experimentally by Paterson and Weiss (1966) within one progressive deformation, and may thus be part of the D_3 deformation.

3.7 FOURTH GENERATION STRUCTURES.

In addition to the first, second and third generation structures just discussed above, another group of folds is present in the area. These folds are only minor significance, however. Since some of these folds overprint D_3 effects, they are regarded as D_4 in age. Most of them occur in S_1 and although clear evidence of age relationships is lacking, they have a consistent ESE-WNW trend and differ both in orientation and style from D_2 and D_3 folds.

Four types of D_4 structures were noted:

1. kink bands in segregated S_3 in Apollyon chiastolite schist (Fig. 3.50),
2. crenulations in F_3-kinked S_1 in both the Parnell and Robe Beds (Figs. 3.51, 3.52), and
3. open folds or cusp-like folds in S_1 in the Apollyon, Robe and Parnell Beds (Fig. 3.53, 3.54). These folds may be accompanied by the presence of axial plane pegmatites, and axial surfaces may be steeply north dipping.

3.8 OTHER STRUCTURES.

The Apollyon Beds near Loc. 5322 4871 are characterised by the formation of open to tight, steep ENE plunging type A folds (Fig. 2.3 and Fig. 3.55) outlined by thin bedding. These folds are consistently sinistral. They are congruent to F_3 folds in S_0 in this area in style and plunge, but have a more easterly orientation (axial plane schistosity trends 060° cf. S_3 trend of 040°). These folds and schistosity are labelled F_4' and S_4' respectively. They may represent a fanning S_3 structure or may represent F_4 folds which have been tightened. No other folds of this type were found in other areas although a fracture with an 060° orientation occurs in other parts of the Apollyon Beds.

3.9 STRUCTURES WITHIN RETROGRADE SCHIST ZONES.

The Apollyon Valley and Mt Franks Retrograde Schist Zones are dominated by a vertical, northeast trending schistosity (S_R) which is dominated by mica

together with local graphite. S_R contains a steeply plunging, down dip mica (mineral) lineation (L_M), and is crenulated around open ESE-WNW trending F_{R+1} folds. Rare F_R folds in these zones are tight to isoclinal and characterised by an axial plane S_R.

The characteristics of these structures are similar to those reported from retrograde zones near Broken Hill by Hobbs (1966a) and Vernon and Ransom (1971). Both Hobbs and Vernon (1968) and Vernon and Ransom (1971) noted a similarity in fold style between Group 3 folds in retrograde zones and folds on the margins of these zones which they suggested had been mimetically retrogressed. These authors suggested that the structures in the retrograde zones postdated those in the country rock. Rutland and Etheridge (1975), on the other hand, described structures in the country rock which they suggested had a primary retrograde axial plane fabric, and they suggested that these structures were also older than those in the retrograde zones. F_R, S_R, L_M in the Mt Franks Retrograde Schist Zone are parallel to F_3, S_3 and L_3 in the adjacent Robe and Apollyon Beds. It is thus suggested that structures in the Mt Franks and Apollyon Valley Retrograde Zones are correlable with D_3 and D_4 structures in the country rock. Laing (1977) has similarly implied a correlation between structures in the retrograde zones near Broken Hill and D_3 and later events in the country rock.

F_1 STRUCTURES

Fig. 3.1 (bottom right) Profile sketch of F_1 fold outlined by biotite laminations in Apollyon quartz-mica schist.
Bar scale 1 cm.
Locality 5319 4864.

Fig. 3.2 (top right) Field sketch of overturned F_1 fold, Apollyon quartz-mica schist. Note hinge thickening and development of L_1 in S_1 lying at an angle to fold axes.
Bar scale 1 cm.
Locality 5319 4859.

Fig. 3.3 (bottom left) Basin and dome interference structures between F_1 and F_3 folds. Apollyon quartz-mica schist.
Bar scale 5 cm.
From photograph.
Locality 5325 4879.

Fig. 3.4 (top left) Profile view of F_1 folds in biotite laminations in psammite of Robe Beds.
Locality 5309 4857.

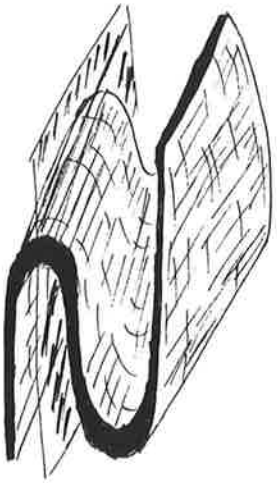

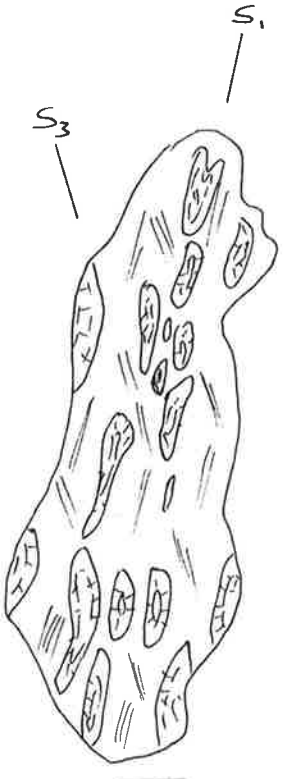
S1
S3

Fig. 3.5a (top) XY section of lineated quartz-mica schist.

Fig. 3.5b (middle) XZ section of lineated quartz-mica schist.

Fig. 3.5c (bottom) YZ section of lineated quartz-mica schist.
Bar scale 1 mm.
Apollyon quartz-mica schist.
Locality 5321 4871.

A

B

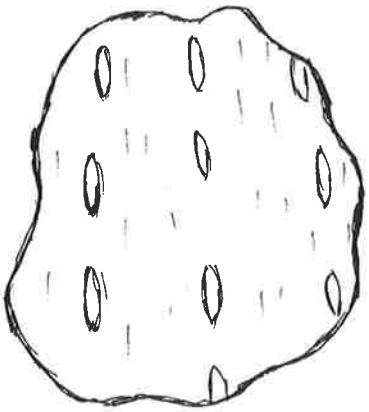

C

F_1 EFFECTS

Fig. 3.6 Field sketch looking north and showing bedding dipping west and overturned on S_1.
Bar scale 5 cm.
Locality 5311 4869.

Fig. 3.7 Profile view of F_1 folds outlined by biotite laminations in psammites of Robe Beds. Note variation of profile along axial surface. Cross bedded laminations also present (e.g. Area A).
Locality 5309 4874.

Fig. 3.8 Profile view of F_1 folds in psammite of Mt Franks facies. Folds outlined by biotite and andalusite laminations; cross bedding also present. Note fanning cracks in andalusite layer, and irregular thickness of layering.
Locality 5309 4874.


MM

F_1 FOLDS IN ROBE BEDS

Fig. 3.9a F_1 fold in south of area. Note hinge thickening of psammite and refraction of S_1 across layering. In the limb areas, S_1 in the psammites lies closer to bedding than does S_1 in the pelite.
Bar scale 10 cm.
Locality 5291 4851.

Fig. 3.9b Oblique view of F_1 fold defined by psammite bed.
Locality 5310 4874.

Fig. 3.9c F_1 folds outlined not only by psammite (Ps)/psammopelite (Pe) interface but also by biotite laminations in the psammite. Folds in biotite laminations are characterised by the overturning of one limb.
Locality 5313 4879.

Fig. 3.9d Overturned fold (profile view) outlined by psammite/pelite layering. Note development of new schistosity, S_3 in pelite.
Bar scale 10 cm.
Locality 5312 4879.

Fig. 3.9e Fold outlined by psammite (Ps)/psammopelite (Pe) interface and also by biotite laminations within psammite.
Bar scale 2 cm.
Locality 5319 4880.

Fig. 3.9f Fold outlined by psammite (Ps)/psammopelite (Pe) bedding in sillimanite schist. Note parallelism between schistosity (S_1) and bedding in limb areas, and tight-isoclinal nature of fold compared to more open other folds above.
Locality 5293 4849.


A
Ps s
Pe e
B
Pe
Ps
30 cm
C
So
Pe
Ps
2cm
D
Ps
Pe
E
Pe
Ps
F
So
Ps
Pe
cm

Fig. 3.10a (left) Tight dextral F_1 folds in quartzite bed (Robe Beds). No obvious fabric is developed in this lithology whereas S_3 is developed in surrounding units. S_3 is incongruent to these folds.
Locality 5316 4876.

Fig. 3.10b (right) F_1 fold in quartzite layer (Robe Beds). Hinge of fold is disrupted by displacement parallel to S_1 in surrounding schists.
Locality 5304 4846.

Fig. 3.11 (left) Profile view showing spaced S_1 in psammopelite deflecting around andalusite crystals.
Locality 5312 4879.

Fig. 3.12 (right) Spaced S_1 in psammite of Robe Beds. S_1 outlines F_3 fold pair which is localised wholly within psammite.
Profile view. Top of pen for scale.
Locality 5309 4857.

S_1, ROBE BEDS

Fig. 3.13 (left) Refraction of S_1 across bedding. S_1 in psammite (darker area) lies sub parallel to S_0 whereas S_1 in psammopelite occurs as a hackly surface inclined to S_1. Match for scale.
Locality 5293 4871.

Fig. 3.14a (right) Profile view looking north. S_1, best seen in psammites (grey), dips westwards more gently than S_0 - i.e. bedding is overturned.
Locality 5309 4857.

Fig. 3.14b (left) Sketch of overturned bedding showing relations between S_0 and S_1. View looking north.
Locality 5305 4874.

Fig. 3.15 (right) Parallel relations between S_0 and S_1 (S_{1P} relations). S_1 occurs as a spaced schistosity in psammite (centre of photo). Bedding is graded; psammites are defined by sharp bases or by fracture and grade into overlying psammopelite. Bedding youngs to left.
Locality 5312 4885.

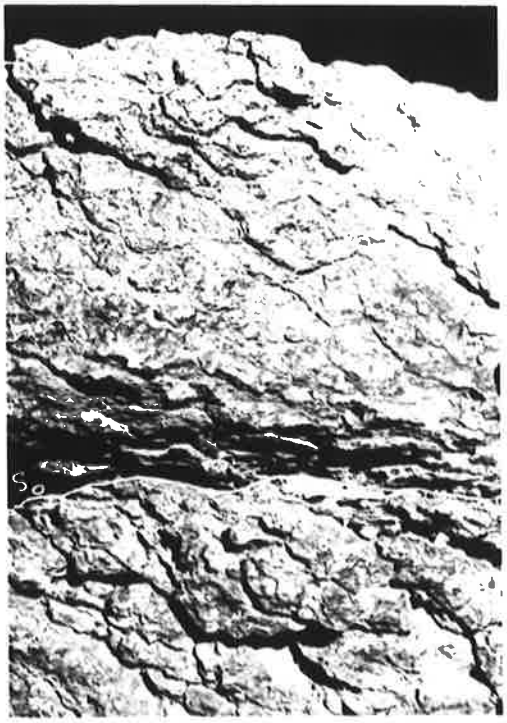
S_o

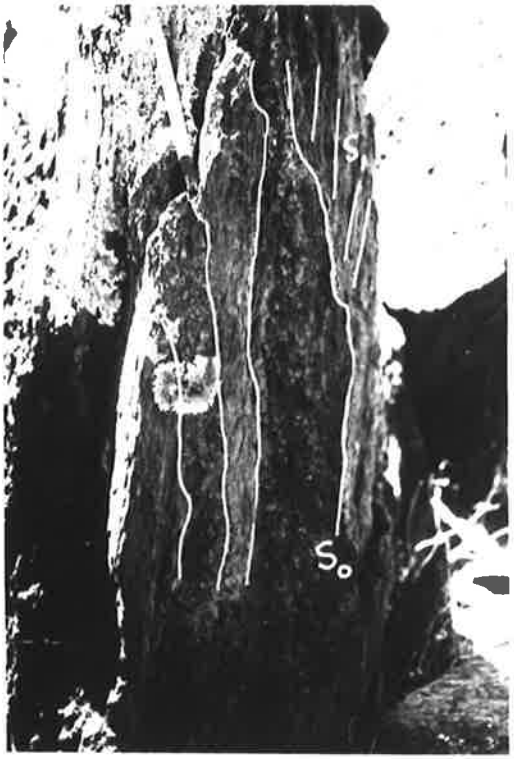
S
S_o

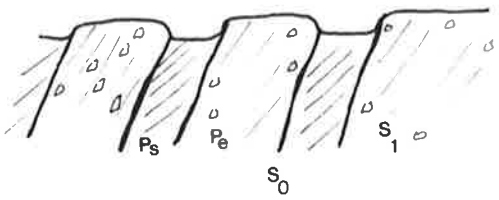
P_s
P_e
S_1
S_0


S_o

Fig. 3.16a (left) D_1 migmatite in Robe Beds defined by the alternation of leucocratic layers (quartz + feldspar) and melanocratics layer (biotite + sillimanite) parallel to S_1. This migmatitic layering is folded around F_3 folds.

Fig. 3.16b (right) Formation of nebulite cutting across folded migmatitic layering parallel to S_1.
Locality 5312 4914.

Fig. 3.17a (left) B type F_2 fold in psammopelites of the Robe Beds. Profile photo looking down plunge. Note hinge thickening.
locality 5312 4928.

Fig. 3.17b (right) AB type F_2 fold outlined by psammite bed in Robe Beds. Note characteristic hinge thickening of psammite rather than psammopelite and open nature of antiformal hinge in psammopelite.
Locality 5302 4918.

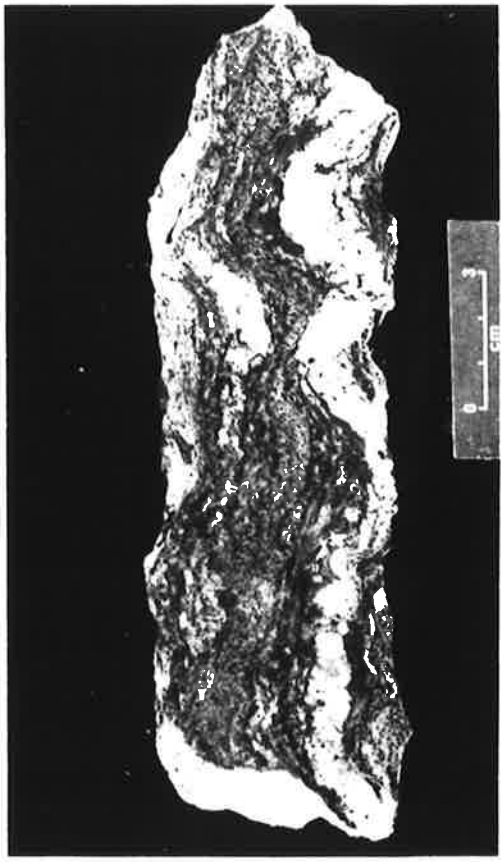

Fig. 3.17c (left) F_2 folds in migmatitic layering, with incipient development of mullions in hinge area.
Profile view.
Locality 5312 4928.

Fig. 3.17d (right) Enlargement of Fig. 3.17b, showing crenulations in S_1Pe, and development of S_2 in hinge of psammite.
Locality 5302 4918.

Fig. 3.18 (left) Profile view of F_3 folds in S_0 in Apollyon carbonaceous schist. Note thickening of bedding in hinge area.
Profile view.
Locality 5323 4869.

Fig. 3.19 (right) Asymmetrical F_3 folds in biotite laminations, Apollyon chiastolite schist. Vertical fabric in S_3; biotite grains are white.
Negative print.
Specimen 19 x 1½.

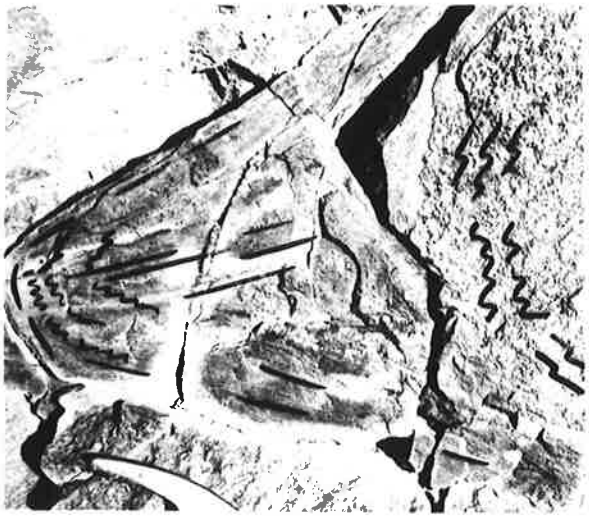

Fig. 3.20a (left) Strong S_3 mica "eye" schistosity developed oblique to bedding in Apollyon quartz-mica schist. Scale in cms. Locality 5321 4873.

Fig. 3.20b (right) Sinistral crenulations in S_1 (outlined in black) with the development of S_3 mica "eyes" axial planar to the folds in Apollyon quartz-mica schist.
Locality 5317 4865.

Fig. 3.21 (left) Open, gently plunging F_3 folds outlined by psammites in Robe Beds. Note the irregular fold geometry thinning of most prominent psammitic layer, and presence of D_3 fractures. Locality 5312 4918.

Fig. 3.22 (right) Poorly defined, irregular axial surface to F_3 folds in psammopelites of the Robe Beds. Note presence of axial surface fracture in foreground.
Locality 5340 4933.


S3
So


S2
S1

F_3 STRUCTURES, ROBE BEDS

Fig. 3.23 Profile view of F_3 crenulations in S_1 psammites. Locality 5342 4939.

Fig. 3.24 (left) Intersection lineation parallel to pen developed by intersection of S_3 on S_1. View of S_1 face. Note randomly oriented andalusites. Locality 5313 4879.

Fig. 3.25 (right) Bedding parallel to hammer. S_1 parallel to hammer in pelites (top of figure) contrasts with S_3 development in psammites below hammer. Locality 5340 4933.

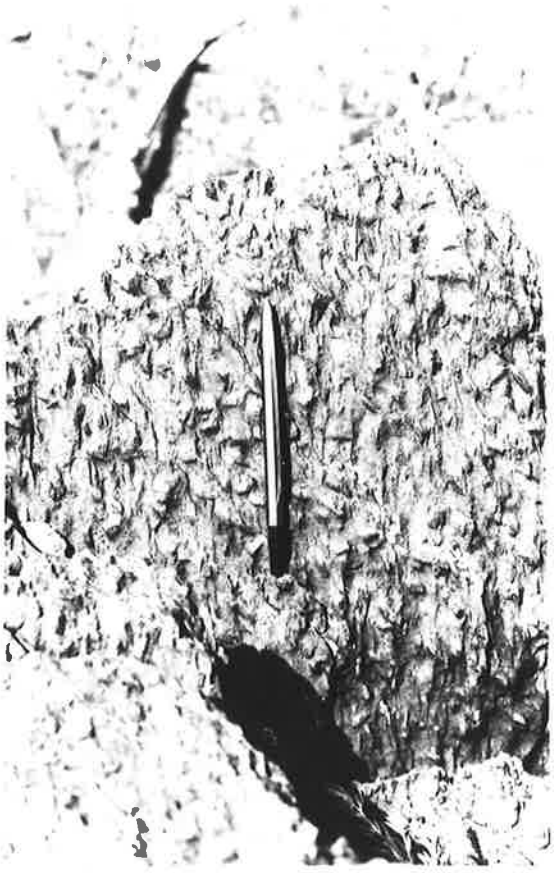

Fig. 3.27 a, b, c. Stages in the F_3 crenulation of S_1 and the development of a segregated S_3 schistosity. Photos taken from the same outcrop, and taken perpendicular to F_3. Match for scale. Robe sillimanite schist. Locality 4879 5207.

Fig. 3.28 (right) S_3 schistosity in psammite (diagonal from top left to lower right) refracted through granitoid vein where it is defined by mica and elongate quartz aggregates. Robe andalusite schist. Locality 5337 4933.

TYPE I and II HERRINGBONE STRUCTURES

Fig. 3.29 (left) Type I herringbone structure. On right of photo, S_1 in psammite dips to the right, parallel to pen. In left of photo, S_1 in psammopelite is folded and defines an F_3 synform/antiform pair. S_0 lies parallel to S_3. Profile view.
Locality 5308 4873.

Fig. 3.30 (right) Schematic view of Fig. 3.29 on horizontal face looking north showing development of herringbone structure. Dominant structure in psammite is S_1. Dominant structure in psammopelite is S_1/S_3 intersection. These two structures define a herringbone pattern about S_0.
Same locality as above.

Fig. 3.31 (left) Type II herringbone structure. Two layer system looking SW, perpendicular to S_1/S_3. S_1 in psammopelite (left of photo) dips to right whereas S_1 in psammite (right of photo) dips to left, in the same direction as, but more gently than S_0. S_1Ps has been rotated from an S_1Pe orientation. S_0 acts as kink plane.
Locality 5309 4879.

Fig. 3.32 (right) Type II herringbone structure. Multilayer system looking perpendicular to S_1/S_3. Note change in S_1 orientation at bedding interface. Psammopelites - knobbly rock; psammite - smooth rock.
Locality 5309 4879.

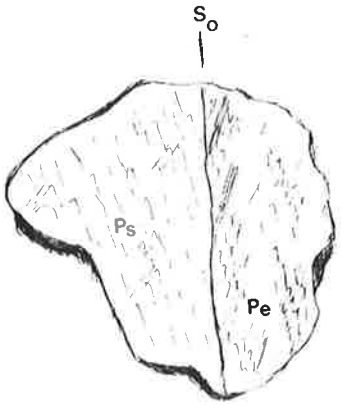
S_o
Ps
Pe

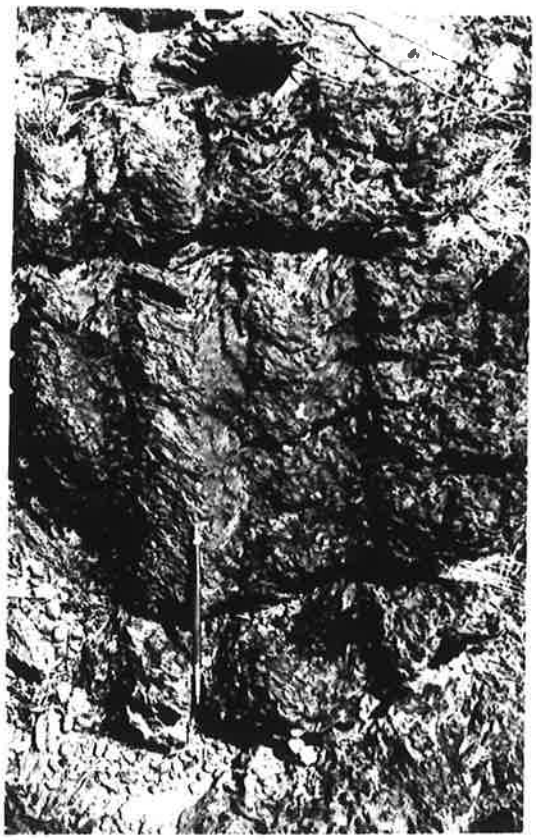

Fig. 3.33 Serial Sections taken from top part of outcrop in Fig. 3.32. Bar scale 1 mm.

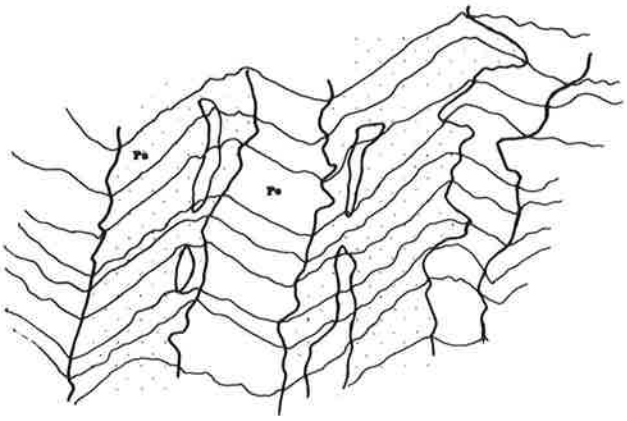

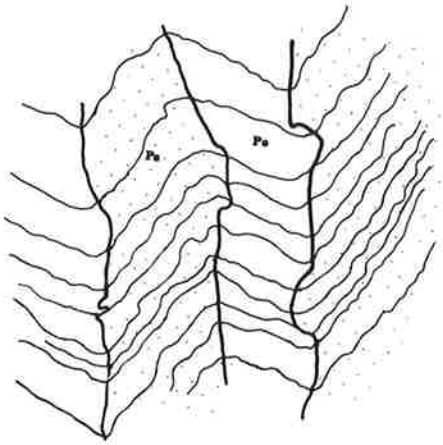

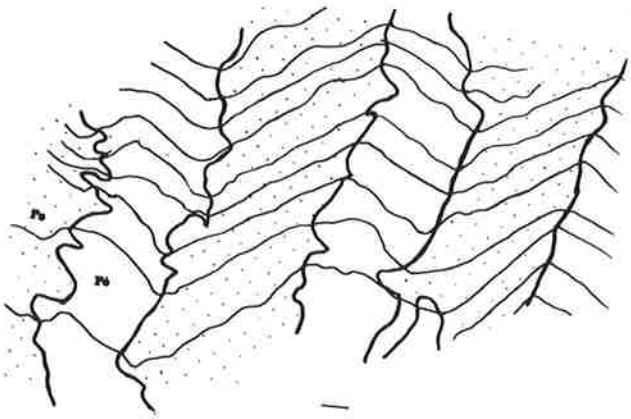

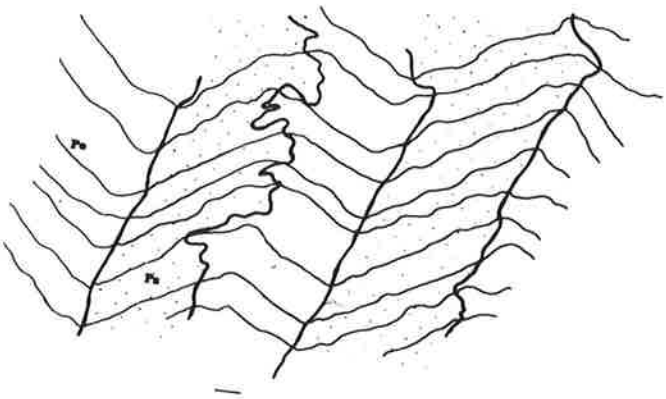

TYPE II and III HERRINGBONE STRUCTURES

Fig. 3.34 (left) Equal area plots of intersection lineation between S_1Ps and S_1Pe (crosses) and F_3 folds in S_1 (dots).
29 points S_1Ps/S_1Pe; 26 points F_3 fold.

Fig. 3.35 (right) Equal area plot of S_1Ps, S_1Pe, S_0 sets.
16 sets of readings.

Fig. 3.36 (left) F_3 folding of S_0 (dashed) and S_1.
Locality 5309 4879.

Fig. 3.37 (right) Type III herringbone structure. Vertical fabric in psammopelites is S_3'. Inclined fabric in psammites is S_1. S_0 dashed.
Locality 5313 4879.

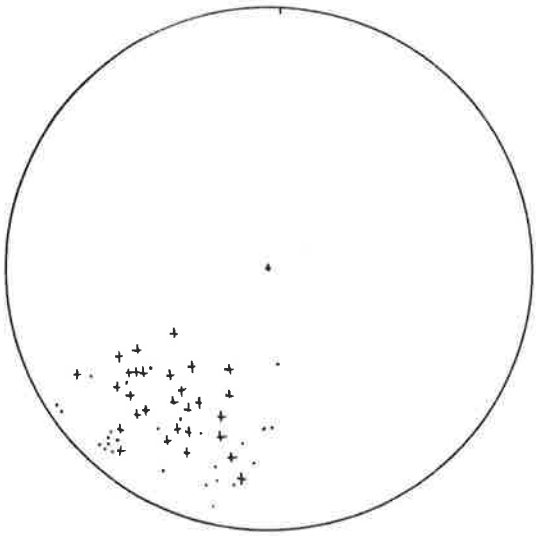

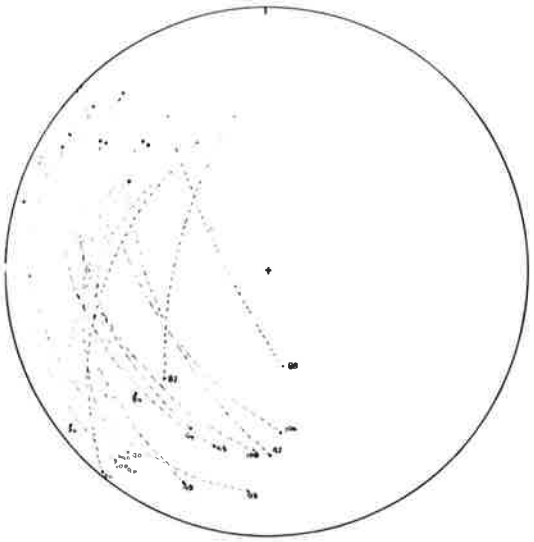

TYPE III HERRINGBONE STRUCTURES

Fig. 3.38 - Fig. 3.42. All from Locality 5314-5312, 4879 (separate plates).

Fig. 3.38 S_1Ps uncrenulated or gently crenulated at top of figure contrasts with crenulated S_1Pe in rest of figure. Note the development, in S_1Pe, of two types of crenulations - small amplitude (areas A,B) and large amplitude (area C).

Fig. 3.39 Strongly crenulated S_1Pe contrasts with undeformed or gently undeformed S_1Ps. Note change in style of crenulations from symmetrical near the bedding interface (area B) to asymmetrical (area A).

Fig. 3.40 Strongly asymmetrical crenulations in S_1Pe. Note alignment of long limbs and merging of short limbs (area A).

Fig. 3.41 Formation of splitting surface, S_3' (A) by the alignment of long limbs of asymmetrical crenulation (B).

Fig. 3.42 Development of penetrative S_3'. Relict short limbs are still present (area A). More psammitic bed marked by dashed lines is characterised by less strongly deformed S_1.

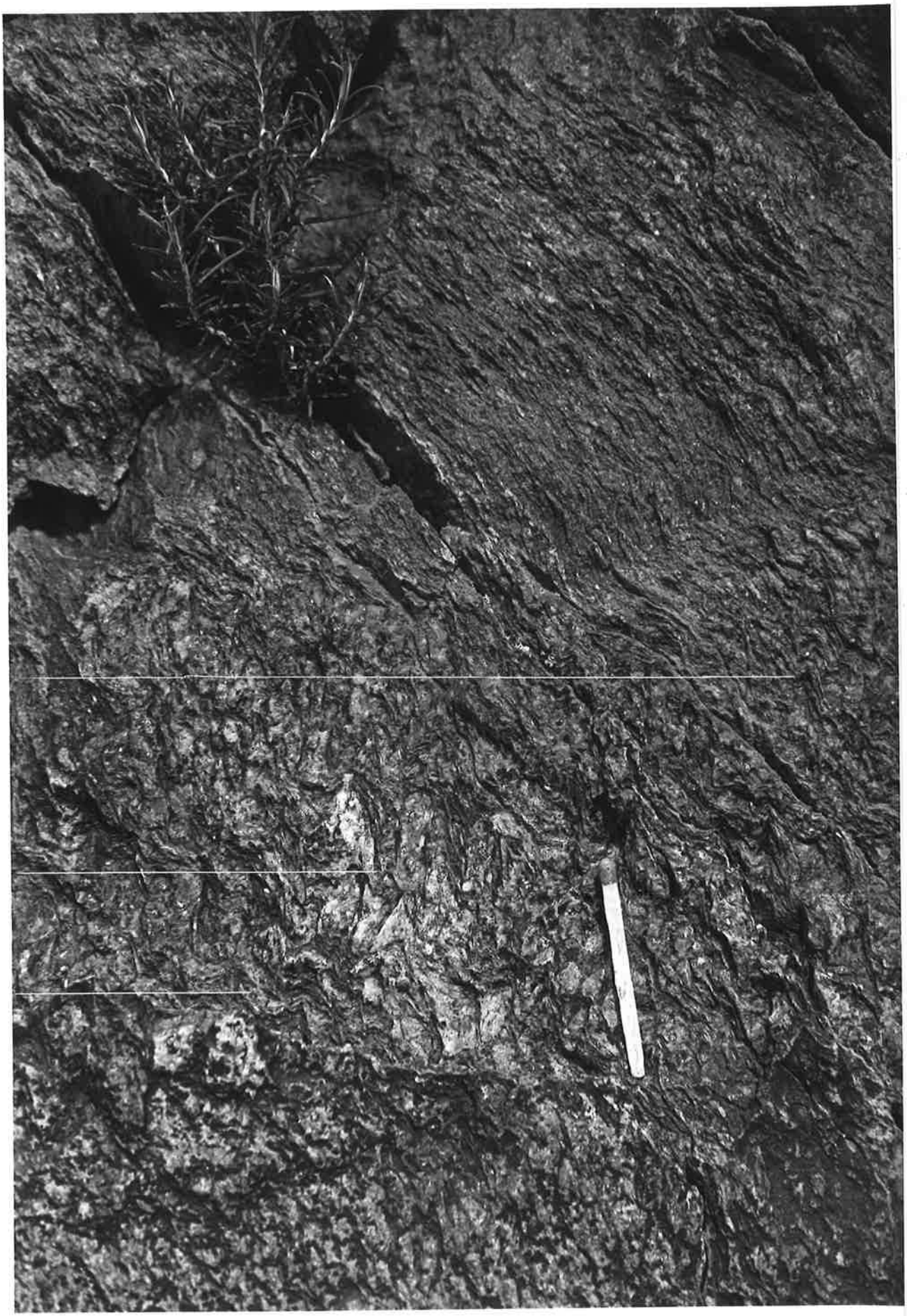

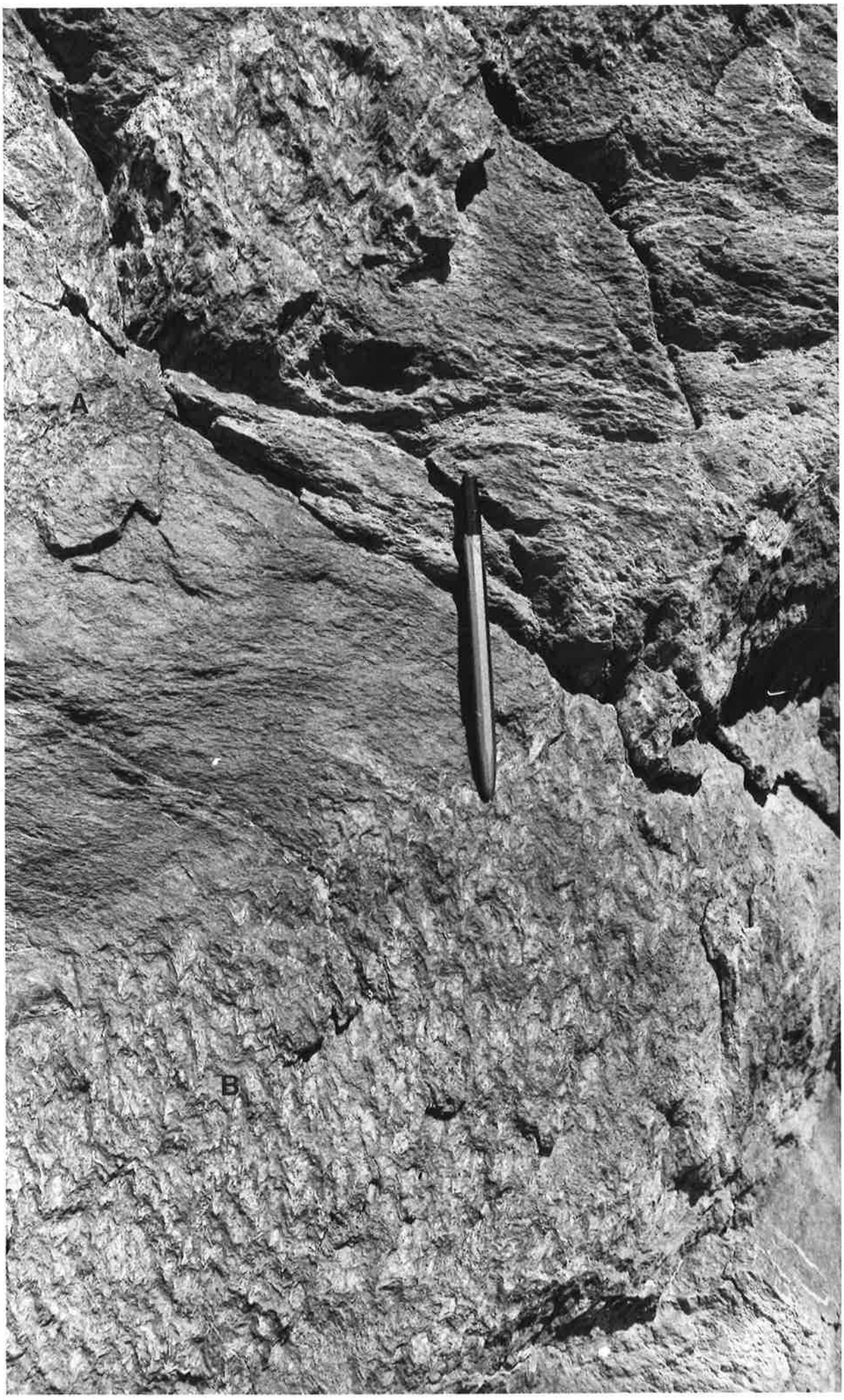
A
B


A


A

Fig. 3.43 (left) D_3 deformation in S_{1N} psammopelites of the Mt Franks facies. S_1 outlines sinistral F_3 folds, the enveloping surface of which lies parallel to match. S_3, the axial plane to the folds lies parallel to the steeply dipping fracture (top right - bottom left). Locality 5309 4877.

Fig. 3.44 (right) F_3 folds in S_0, S_1Ps (right of photo) and S_1Pe (left of photo). S_1 crosses bedding at top of figure (marked) but lies parallel to bedding at bottom of figure.
Locality 5309 4879.

Fig. 3.45 (left) Field sketch of variable S_0/S_1 relations (overprinted by F_3) in F_1 fold.
Bar scale 2 cm.
Locality 5308 4879.

Fig. 3.46 (right) Field sketch of variable S_0/S_1 relations (overprinted by F_3) in F_3 fold.
Locality 5308 4879.

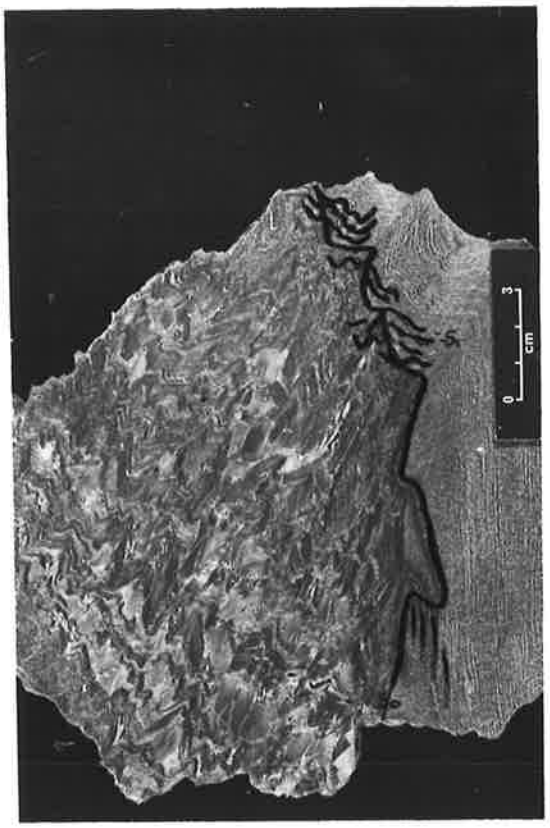
0
cm
3

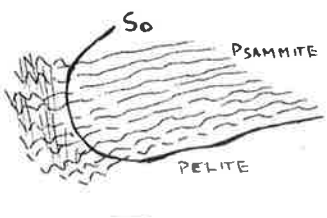
So
PSAMMITE
PELITE

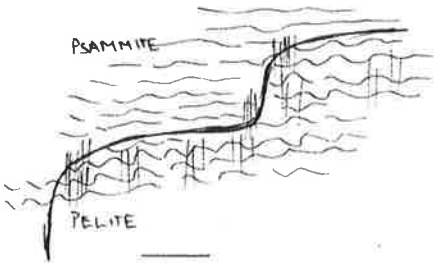
PSAMMITE
PELITE

Fig. 3.47 (right) F_3 folds in S_1 plunging out of plate overprint an early set of crenulations (F_3*). Psammopelites of Robe Beds.
Locality 5297 4858.

Fig. 3.48 (left) F_3* cusp fold parallel to hammer in S_1 refolds an earlier set of F_3 crenulations, the trace of which is outlined by parallel lines below the hammer handle.
Locality 5297 4858.

Fig. 3.49 (right) Small scale dome and basin interface pattern (Type 1 pattern of Ramsay, 1967) developed between F_3 folds (parallel to light coloured pen) and F_3* folds (parallel to pencil).
Locality 5297 4858.

Fig. 3.50 (left) F_3 kinks in S_1 (E-W) 'overprinted' by F_3^* kinks trending top right to bottom left.
Locality 5309 4881.

Fig. 3.51 (right) S_4 and F_4 kink band in segregated S_3, Apollyon chiastolite schist. Field sketch.
Locality 5326 4888.

Fig. 3.52 (left) F_4 folds in both S_1 and F_3 kinks.
Locality 5314 4878.

Fig. 3.53 (right) Major F_3 kink in S_1, Parnell Beds. F_3 crenulations trend parallel to pencil. In other limb, F_4 crenulations developed at high angles to S_3.
Locality 5344 4889.

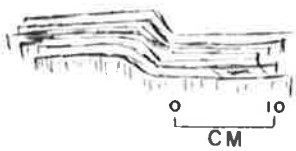
0
10
CM

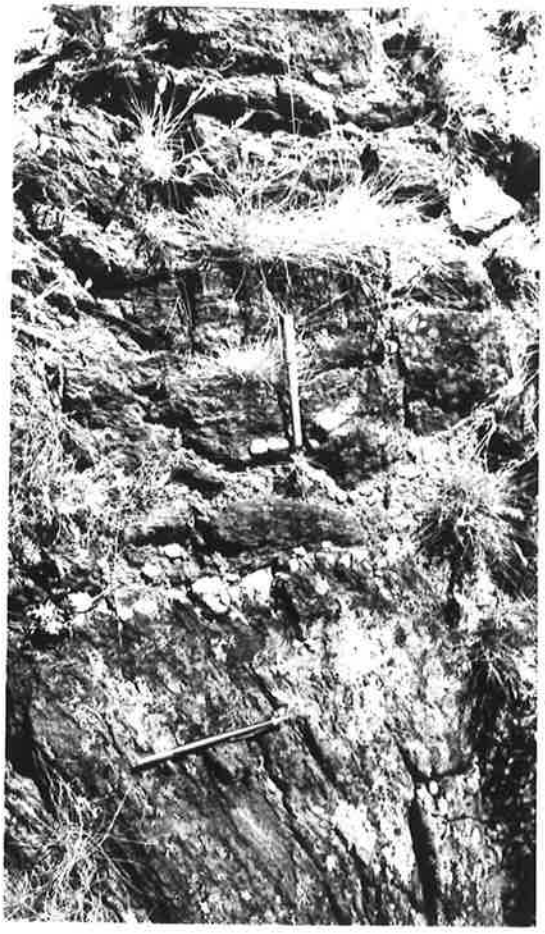

Fig. 3.54 (left) Group B, F_4 fold in S_1, Robe Beds.
Locality 5291 4831.

Fig. 3.55 (right) F_4 fold in M_1 migmatitic layering, Parnell Beds. Continuity of melanocratic layers is disrupted in core of fold.
Locality 5336 4885.

Fig. 3.56 Group A, F_4' fold in quartz-mica schist of Apollyon Beds. Bedding laminations outlined by iron oxides define a symmetrical fold pair. Finely developed S_4' is locally characterised by remobilised trains of iron oxides. Scale in cms.
Locality 5323 4869.

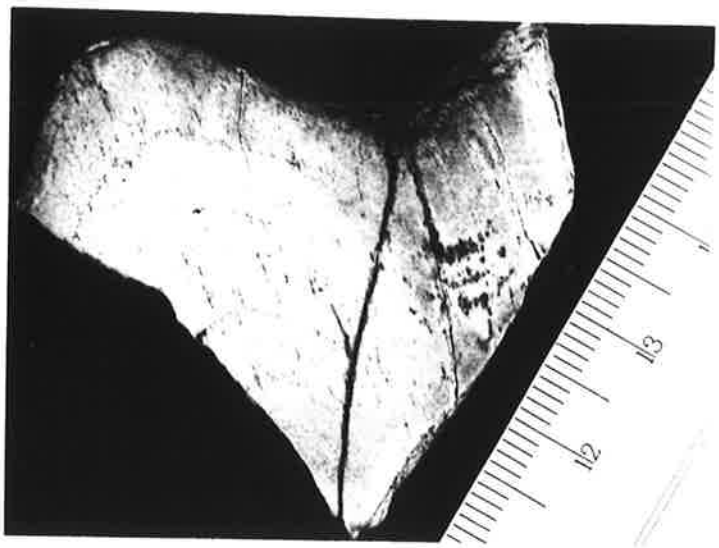
12
13

CHAPTER 4 MICROFABRIC DEVELOPMENT IN PELITIC AND PSAMMITIC METASEDIMENTS

4.1 INTRODUCTION.

In the last chapter, it was shown that by using mesoscopic criteria, three discrete schistosities could be distinguished in the area. This chapter presents a microscopic study of these schistosities and establishes microscopic criteria which can be used to distinguish between various schistosities when mesoscopic identification cannot be readily made. This chapter is thus concerned with the morphology and development of S_1, S_2 and S_3 on a microscopic scale. It is also concerned with the establishment of microstructural relations between deformation history and mineral growth. By defining groups of minerals with the same relative time relations, this chapter serves as a basis for the subsequent chapter which discusses metamorphic assemblages, mineral growth, habit and stability, possible reaction mechanisms and P-T-X conditions of metamorphism.

Zwart (1960), Rast (1965) and Spry (1969) have all provided possible criteria which can be used to establish relations between metamorphic growth and deformation episodes, and Vernon (1976) has recently cautioned against over-enthusiastic application of them.

Particular emphasis is placed on four aspects of the total microfabric*:

1. the establishment and significance of pre-S_1 oriented growth and pre-S_1 porphyroblast growth,

2. an examination of evidence which supports the mesoscopic suggestion that S_{1N} is equivalent to $S_{1P}(=S_1)$,

3. the morphological variation of S_1 with lithology, metamorphic grade, and a study of schistosity forming mechanisms, and

4. the stepwise development of F_3 microfolding and formation of different variants of S_3.

---

* used in the sense of Hobbs et al (1976).

In addition, microstructural aspects of the D_2 deformation, and of the retrograde schistosity are also discussed.

A study of pre-S_1 microstructural relations and a study of S_{1N} and S_{1P} development and morphological variation in the region covered is particularly important in deciphering the early structural history of the Willyama Complex. The reason for this is that it is only west of Apollyon Valley that the first mesoscopically visible schistosity lies at an angle to S_0 in large areas of low, medium and high grade schists, and it is only in these areas of clear S_0/S_1 relations that an insight into the early deformational history of the Willyama Complex can be gained.

The studies on S_1 and S_3 schistosity development concentrate on morphological variation, possible mechanisms of formation of mineral preferred orientation and relationships to the XY plane of the strain ellipsoid ($X > Y > Z$). These studies are carried out in the light of recent literature discussion of slaty cleavage (see reviews by Siddans, 1972; Wood, 1974; and Williams, 1976).

4.1.1 Previous Microfabric Work in the Northwestern Part of the Willyama Complex

Early microstructural works in Mt Franks - Mundi Mundi area were those of Browne (1922), Binns (1963) and Anderson (1966). Browne and Binns both discussed microstructural relations between andalusite, sillimanite and muscovite and suggested that andalusite growth postdated sillimanite. Binns also noted opaque inclusion trails within andalusite, and commented on possible sillimanite growth mechanisms and on the relationship between sillimanite and biotite. Anderson (1966) carried out a detailed microstructural study of minerals formed in his main metamorphic event and discussed microscopic characteristics of his S_1 and L_1. In contrast to Browne (1922) and Binns (1963), Anderson (1966) suggested that andalusite and sillimanite were co-eval with S_1. Rutland (1973a), on the other hand, suggested that andalusite predated the main schistosity on Mt Franks.

Further north in the Mt Robe area, Splatt (1975) described deformed early biotite (pre-S_1 in age) and oriented inclusion trails in andalusites, and Reynolds (1975) discussed aspects of S_1 in that area. In low grade rocks north of Mt Robe, characteristics of various schistosities and schistosity/porphyroblast* relations were discussed by Laing (1969), Price (1969) and Roberts (1969).

4.2 PRE-S_1 MICROFABRICS.

Application of classical overprinting criteria in rocks dominated by S_1 reveals the presence of a wide range of pre-S_1 minerals in all thin sections of all rock types. Figure 4.1 schematically illustrates the type of pre-S_1 features developed in each of the major pelitic and psammitic metasediments. Evidence for pre-S_1 mineral growth in various rock types will now be described and will be followed by a discussion on the geometrical significance of pre-S_1 growth and on the time relations to S_1 formation.

4.2.1 Apollyon Carbonaceous Schist and Quartz Mica Schist - S_{1N} Rocks - Low Grade

Graphite, biotite and mica are all overprinted by S_1 in these rocks. Graphite occurs as small spicules elongate parallel to S_0. These spicules are crenulated by F_1 microfolds and some grains have been mobilised into F_1 hinge zones to form narrow irregular zones parallel to S_1. Rare pre-S_1 biotite occurs in carbonaceous schist and quartz mica schist where it is characterised by irregular terminations, and small kinks in (001) traces. Pre-S_1 biotite also occurs within elongate knots in quartz mica schist where it defines a preferred orientation which is crenulated about S_1 (Fig. 4.2). The lack of undulose extinction in the biotites is attributed to

---

* the term 'porphyroblast' as used here covers porphyroblasts as well as poikiloblasts.

annealing. Fig. 4.2 also shows biotite has undergone alteration to muscovite laths which either lie subparallel to S_1 or which mimic biotite orientations. The presence of pre-S_1 white mica in quartz mica schists is indicated by heavily iron stained undeformed micas outlining a relict preferred orientation which is crenulated about S_1 (Fig. 4.3).

Graphite bearing mineral aggregates, now mainly retrogressed to sericite (= fine grain muscovite) or coarse muscovite laths, are present in carbonaceous schists where they are enclosed by S_1, and may thus be pre-S_1 in age. The original nature of these porphyroblasts is unknown: local elongate porphyroblasts probably represent chiastolite, others were probably twinned plagioclase and still other small 'spots' may have been cordierite.

4.2.2 Apollyon Chiastolite and Andalusite Schist and Robe Andalusite Schist — S_{1N} Rocks* - Medium Grade

Similar pre-S_1 minerals occur in both andalusite and chiastolite schists, and include andalusite (including chiastolite), quartz, opaques, biotite, sericite, graphite and zircon. Andalusite occurs as isolated porphyroblasts or as concentrations of porphyroblast defining bedding laminations. Andalusites are bordered by S_1 wrapping around crystal margins, and by pressure shadows containing polygonal quartz. D_1 deformation in andalusite is recorded by the formation of pull-apart textures with the growth of muscovite parallel to S_1 in cracks (Fig. 4.10a) and by the formation of sericite filled cracks which fan around F_1 folds (Fig. 3.9). The main response to deformation however, is the alteration of andalusite to sericite with the formation of sericite laths with a random orientation. However, in some areas, sericite outlines a preferred orientation which is crenulated about S_1 (Figs. 4.4, 4.5).

---

* S_{1P} Robe andalusite schists are treated in the next section so that a discussion of S_{1N}/S_{1P} equivalence is not pre-empted in Section 4.3.6.

Inclusions of biotite, ?ilmenite, graphite and quartz are common in andalusites. Binns (1963) first drew attention to oriented inclusion trails of ?ilmenite within andalusites from this area and suggested they were aligned parallel to S_1. However, in areas of S_{1N} relations, it can be seen these trails lie parallel to S_0, not S_1. Inclusion trails in adjacent andalusites may be continuous in orientation (Fig. 4.6a) although they locally outline open folds and shear zones (Figs.4.6b,c). The axial surfaces of these folds show variable relation to S_1. The discordance between these inclusion trails and S_1 has been destroyed in many thin sections by F_1 folding of andalusite laminations with the consequent rotation of andalusites and their inclusions.

Inclusion trails of biotite and graphite spicules in andalusites are also overprinted by S_1 and maintain their orientation despite alteration of andalusite to sericite. Graphite spicules lie parallel to bedding; biotite laths define straight trails which are commonly aligned parallel to S_0 (Figs. 4.7, 4.10b, c) but also define curved trails (Fig. 4.8). Biotites in these curved trails lie parallel to S_1 along the andalusite margins, and thus suggest either that andalusite growth occurred after initial F_1 microfolding but before S_1 consolidation, or that marginal andalusite growth occurred after microfolding but before S_1 consolidation.

The sericite preferred orientation referred to above may lie parallel to this early mineral fabric where it is unfolded, and may be controlled by it. In other areas it cuts across the early fabric.

Biotite occurs as isolated porphyroblasts, as inclusions in andalusite, and as concentrations of grains defining bedding and foreset laminations. Where laminations are not folded, biotites possess randomly oriented cleavage traces (Fig. 4.9); where laminations outline F_1 folds, biotites contain kink boundaries parallel to S_1 (Fig. 4.11) and may contain small muscovites lying

in kink boundaries*. Biotite also occurs as small laths defining an early fabric lying at angles to S_1, (Figs. 4.12, 4.10d) and as aggregates of grains outlining tight kink-like structures (interpreted as annealed kinks, see Section 4.3.7.1) parallel to S_1 in mica bands lying in S_1 (see below).

In rare cases, relicts of a white mica orientation can be seen in the groundmass of chiastolite schists (Fig. 4.10e). These white micas define an early orientation crenulated about S_1 and lie statistically parallel to graphite lamination. Elsewhere, this orientation is defined by annealed F_1 kinks in micas on the margins of biotite porphyroblasts (Fig. 4.10f) and biotite , and zircon occur as small inclusions in biotites. Graphite occurs as spicules aligned parallel to S_0 within andalusite grains, and also as trails parallel to S_0 in the groundmass.

4.2.3 Robe Andalusite Schist — S_{1P} Rocks - Medium Grade

Like most of the S_{1N} andalusite schists, S_1 in S_{1P} andalusite schists is a layered schistosity defined by M (mica) and QM (quartz + mica) domains. In contrast to S_{1N} rocks, however, M domains in S_{1P} rocks are mainly defined by biotite concentrations. Biotites in these domains are deformed with kink bands parallel to S_1, and also outline kink type structures (Fig. 4.13) with axial planes parallel to S_1. In QM domains, biotites are commonly aligned sub-parallel to S_1. However, biotites also outline a relict preferred orientation crenulated about S_1 (Fig. 4.15). Andalusites in these rocks are similar to those just discussed. S_1 bows around these crystals and inclusions of ?ilmenite and/or biotite define as an early orientation crenulated about S_1 (Fig. 4.14).

4.2.4 Robe Sillimanite Schist - S_{1P} Rocks - High Grade

It was suggested in Section 2.3.1.3 that sillimanite schists of the Robe

---

* A detailed discussion of D_1 deformation effects in these biotites is presented in Section 4.3.7.1.

Beds are lithologically similar to the andalusite schists just described. Andalusites in this rock type are wrapped around by S_1 micas and by quartz filled pressure shadows and contain inclusions of biotite and ?ilmenite. As in the andalusite schists, these andalusites are surrounded by fine grained muscovite and coarse plates of muscovite are also present as a late stage alteration product. Within andalusite muscovite aggregates, small biotites and muscovites are kinked about S_1 as described above. Fibrolite also occurs in some of these clots and some of the typical "swirls" appear to be folded about an axial plane parallel to S_1 (Fig. 4.16). Figures 4.17-4.19 suggest that in these clots there is a complete gradation from aggregates of andalusite + muscovite $\pm$ biotite to aggregates of andalusite + muscovite $\pm$ biotite $\pm$ fibrolite to aggregates of muscovite $\pm$ biotite + fibrolite or sillimanite. Andalusites are pre-S_1 in age. Sericite laths are random, or outline a pre-S_1 orientation crenulated about S_1 (Fig. 4.39) or outline an orientation parallel to S_1 (Section 4.3.3.2). Fibrolite and sillimanite are pre-S_1 in age (Fig. 4.16) or are syn-S_1 in age (Fig. 4.39) and cut across crenulated sericite. The relationship between these three minerals in terms of metamorphic reactions will be discussed in Section 5.2.3.7.

Sillimanite also occurs in these rocks as a pre-S_1 mineral in the groundmass. It is locally preserved as bent needles in hinges of tight isoclinal F_1 folds (Fig. 4.20) which have sufferred recrystallisation to S_1 sillimanite in the axial planes.

The S_1 microfabric development of these rocks is similar to that of S_{1P} andalusite schists. As a result biotites dominate M domains and are kinked parallel to S_1 and outline kink type structures parallel to S_1 (Fig. 4.21). In QM domains, biotites outline relict preferred orientations crenulated about S_1 (Figs. 4.22-4.23). These orientations are commonly preserved on the margins of andalusites or within S_1 K feldspars (Fig. 4.24).

4.2.5 Mundi Mundi Facies - S_{1P} Rocks - Medium to High Grade

An early preferred orientation in these rocks may be reflected by the development of small sericite laths at an angle to S_1 muscovite. The trend surface to these laths defines a zig zag orientation, about S_1 and may reflect folded early micas. The sericite laths themselves are undeformed and are thus late stage.

4.2.6 Parnell Beds - S_{1P} Rocks - High Grade

Pre-S_1 biotite in these rocks occurs as isolated porphyroblasts or as kinked aggregates in laminations parallel to $S_0//S_1$. Andalusite is only rarely developed in this rock type and has only been found in rocks dominated by S_3, not S_1 microstructure. However, analogy with other rocks described above suggests a pre-S_1 origin.

4.2.7 Discussion

4.2.7.1 Time Relations between Pre-S_1 Mineral Growth and S_1

Microstructural observations based on the strict application of classical overprinting criteria suggest that pre-S_1 growth occurred of andalusite, biotite, sillimanite (including fibrolite), graphite, zircon, quartz and white mica. Recent thought (Vernon, 1977; M.A. Etheridge, pers. comm., 1977) has veered away from the rigid compartmentalising of mineral growth and has attempted to explain mineral/deformation relations in terms of single assemblages formed in complex, progressive events.

In applying these ideas to the microstructural relations just discussed, it is suggested that "pre-S_1 criteria" merely implies the cessation of growth of the above minerals before final cessation of growth of S_1- forming minerals. Since schistosity formation is a progressive event, the "freezing" of some minerals before final consolidation of S_1, such as by incorporation in a porphyroblast, will preserve a pre-S_1 feature. Similarly, porphyroblast inclusions need not represent an earlier period of growth than that represented by the porphyroblast (Vernon, 1977, p.443). Thus it is suggested

that the formation of andalusite and biotite porphyroblasts occurred very early in the formation of S_1 and locally continued into S_1 time. This is supported by the overlap of biotite into S_1 in quartz mica schists and part of the Robe sillimanite schists, and by the presence within some andalusites of curved biotite inclusion trails which are continuous with groundmass biotites. The formation of laths of sericite fringing andalusite and bent about S_1 suggests that andalusite breakdown had commenced already in the early part of this D_1 event. The presence of sericite laths parallel to S_1 could be due to later mimetic growth, but is interpreted as a continuation of andalusite alteration in S_1 time, and also as recrystallisation products of early sericite. Folded and planar bundles of fibrolite associated with andalusite and sericite are interpreted as ceasing growth before and during S_1 formation. In Section 5.2.3.7 it is suggested that fibrolite forms by andalusite breakdown via an intermediate sericite phase. The establishment of an early D_1 age for andalusite and sillimanite differs from the findings of Browne (1922), Binns (1963) and Anderson (1966).

Relicts of biotite, ?ilmenite and white mica indicate that there was some mineral preferred orientation before the final formation of S_1. The presence of biotite and ilmenite oriented inclusions within andalusites may not necessarily indicate an earlier period of metamorphism. Rather it may indicate the formation of greater numbers of biotite and ?ilmenite nuclei and their cessation of growth before the cessation of andalusite growth (cf. Vernon, 1977) - that is they represent early D_1 growth. This view is supported by the presence of random biotite inclusions in andalusite and also by optically similar biotite occurring as early D_1 porphyroblasts and as S_1 minerals. Similarly biotite and white mica outlining early preferred orientations in the groundmass probably represent early growth stages of D_1, before later F_1 modification and S_1 growth. This now raises the question as to the significance of this early preferred mineral growth.

4.2.7.2 Geometrical Significance of Early Mineral Preferred Orientation

In S_{1N} andalusite and chiastolite schists, the early mineral preferred orientation varies from parallel to non-parallel to bedding. Relationships between this fabric and bedding cannot be ascertained in the quartz mica schists, but in S_{1P} andalusite and sillimanite schists, this early mineral preferred orientation cannot lie precisely parallel to bedding. The orientation of this early fabric in these S_{1P} rocks is difficult to reconstruct from crenulated relicts, but its non parallelism to bedding means it cannot be a sedimentary deposition or compaction fabric.

An understanding of the geometrical significance of this early fabric is also hampered by lack of information on its penetrative nature. Although relicts of this early fabric were found in all thin sections, it is not known if these relicts represent the total development of the fabric or represent the development of a widespread penetrative schistosity.

If this early preferred mineral orientation is related to folding, the consistency of macroscopic younging directions throughout the whole area in relation to F_1 folds and the absence of any small scale pre-F_1 folding suggests that these folds have limb areas greater than tens of square kilometres (Section 6.3). Alternately, this fabric may simply represent a flattening fabric developed in the early part of a complex D_1 event which is unrelated to folding. This fabric is not called S_1; the term "S_1" is reserved for the first recognisable schistosity lying axial planar to mesoscopic first generation folds in bedding.

Further aspects of this mineral growth in relation to the D_1 event and sericite formation are treated in the summary to the section on S_1 development (Section 4.3.8).

4.3 MORPHOLOGY AND DEVELOPMENT OF S_1.

Development of S_1 in different lithologies and structural domains (S_{1P} and S_{1N}) must reflect the deformation undergone by the pre-S_1 mineral fabric and by the pre-S_1 porphyroblasts. A description of S_1 mineralogy

and microfabric is presented in order to assess the influence of pre-S_1 mineral growth on the development of S_1. An examination of morphological variation with metamorphic grade, lithology and structural domain (S_{1P} or S_{1N}) in relation to presence of pre-S_1 mineral growth paves the way for a discussion of schistosity forming mechanisms and deformation mechanisms. Most of this information is gained by the study of D_1 deformation effects in early S_1 biotites.

4.3.1 S_1 in Low Grade Rocks - S_{1N} Domain

4.3.1.1 Apollyon Quartz Mica Schist

In most of these schists, S_1 is a homogeneous schistosity defined by thin (0.1 x 0.03 mm) wispy or straight sided muscovite laths or by groups of laths (Fig. 4.25) which show a poor parallelism to a statistical S_1. S_1 may also be defined by the alignment of biotite laths which are stumpier than the muscovites. These biotites vary in colour from pale yellow to brown and are similar to the larger pre-S_1 biotites in the same rocks. Quartz and plagioclase grains between the micas are equant or slightly elongate (0.2 x 0.1 mm) parallel to S_1. Straight or slightly curved quartz/quartz and quartz/plagioclase boundaries generally exhibit D_3 strain effects, but 120° triple point junctions are still present.

In local areas, S_1 is domainal rather than homogeneous and is defined by the alternation of narrow, irregular iron stained M (mica) domains with wider QM (quartz + iron stained muscovite) domains in which a pre-S_1 fabric is preserved (Fig. 4.3). This domainal character thus appears to have a direct relation to the presence of a strongly developed early surface and M domains occur in limb areas of F_1 microfolds and are high strain zones. Less well developed domainal S_1 (Fig. 4.26) may also reflect the presence of an early fabric.

The variable development of S_1 might thus reflect the variable development of an earlier fabric or the degree of recrystallisation during S_1 formation.

The only other areas preserving a pre-S_1 fabric are the large "porphyroblasts" elongate parallel to L_1 (Fig. 3.5 and Fig. 4.2). These mineral aggregates now consist of biotite, quartz, opaques, feldspar and muscovite and might represent original inhomogeneities rather than retrogressed pre-S_1 porphyroblasts because of the lack of obvious retrograde minerals such as sericite and chlorite, and because of the presence of pre-S_1 biotite (Section 4.2.1).

4.3.1.2 Apollyon Carbonaceous Schist

Where relicts of a pre-S_1 fabric are present, S_1 is domainal. It is defined by the alignment of irregular, narrow zones of graphite spicules which have been mobilised out of their previous orientation parallel to S_0. This early fabric is also outlined by sericite laths; irregularly shaped quartz is also present. Where S_1 is better developed it forms a homogeneous schistosity with no sign of an earlier fabric. Thin irregular layers of graphite form anastomosing S_1 zones around elongate tightly packed quartz grains in mica poor rocks. In mica rich rocks, S_1 is defined by muscovite, together with some biotite, and resembles S_1 in quartz mica schists. Small biotites are kinked parallel to S_1.

4.3.2 S_1 in Medium Grade Rocks - S_{1N} Domain

4.3.2.1 Apollyon Chiastolite Schist

The S_1 microfabric for a typical chiastolite schist is shown as a negative print in Fig. 4.27. S_1 microstructure in the pelite beds is shown in Fig. 4.27a and b, and consists of bands of interleaved muscovites and graphite spicules wrapping around older biotites (now altered to iron oxides) and altered andalusites. Areas of mismatch between the mean S_1 orientation and muscovite laths are regarded as areas in which muscovite is mimetic after biotite (Fig. 4.27b, circled).

On the scale of a thin section, S_1 microstructure in psammite beds appears homogeneous. However, local variations in the quartz/muscovite

ratio leads to the recognition of five different types of domains, the distribution of which may be a reflection of pre-S_1 mineral growth. These different domains are described in Figure 4.27 and are self explanatory. Their distribution is as follows:

Domain 1: Fig. 427c. Equant polygonal quartz $\pm$ graphite. This domain occurs as pressure shadows on pre-S_1 porphyroblasts, and more rarely as quartz-rich enclaves.

Domain 2: Fig. 4.27d. Elongate quartz + graphite occupying areas of high strain anisotropy which presumably resulted in a change of shape from early ? equant quartz grains. The lack of strong intracrystalline deformation features sgggests that shape change may have been due to diffusion processes (cf. Elliott, 1972).

Domain 3: Fig. 4.27e and f. Equant-elongate quartz (70%) + muscovite (10-25%) $\pm$ biotite $\pm$ graphite $\pm$ feldspar $\pm$ garnet. These domains are elongate parallel to S_1. Muscovite lies along quartz/quartz or quartz/feldspar boundaries and appears to be controlled by this anistropy rather than by parallelism to S_1. Muscovites lying across S_1 are stumpier than those parallel to S_1. Garnets form rounded grains with quartz inclusions. Clear evidence of their age is lacking: they may be early or late S_1 in age.

Domain 4: Fig. 4.27g and h. Equant to elongate quartz (about 50%) + muscovite (35%) + minor biotite, graphite and opaques. Muscovite forms single laths, groups of laths or thin bands, and the better alignment of muscovite in this domain is shown in the Rf/Ø* plots, taken from shadow-master sketches (Figs. 4.27f and h).

Biotites in domains 3 and 4 consist of single grains or randomly oriented aggregates. They may be kinked in S_1 or truncated by muscovite laths parallel to S_1. A feature of these biotites is their strong pseudomorphous

---

* Rf/Ø plots plot the length/width ratios of micas against their orientation (cf. Dunnet, 1969).

alteration to iron oxides ± muscovite, and the formation of iron oxide tails in S_1 (Fig. 4.28) which indicates the presence of mass transfer during schistosity formation.

Domain 5: Fig. 4.27i. Muscovite ± graphite ± biotite ± iron oxides ± minor quartz. These bands vary in persistence and width, and are best developed adjacent to pre-S_1 biotites and andalusites. This type of domain merges into type 4 domain by a dying out of mica bands. Muscovites within this domain are commonly interleaved, forming a tightly packed mat and as a result, not all of these laths lie parallel to S_1. Areas of greater mismatch are regarded as due to mimetic muscovite growth on biotite. The alternation of domain 5 with domains 2, 3 or 4 leads to the recognition of a domainal schistosity (Fig. 4.29) with M domains (about 0.1 mm wide and 0.4-0.6 mm apart) separated from QM domains. The change in shape of biotites - from elongate in M domains to ragged or stumpy in QM domains - suggests that these domains formed in response to different strain domains set up during S_1 formation (see Section 4.3.7.1).

4.3.2.2 Apollyon Andalusite Schist

The S_1 microfabric in psammopelite beds is similar to that of the Robe Andalusite Schist (see below) and will not be discussed here. S_1 in psammite beds is generally a homogeneous muscovite + quartz schistosity similar to domain 4 in chiastolite psammites. However, near folded bedding laminations defined by biotite grains (Fig. 4.30a), S_1 is also defined by elongate narrow bands of biotite, or biotite with muscovite (Fig. 4.31). The preferred orientation of muscovite in these rocks varies from extremely good in Fig. 430a to poor in Fig. 4.31. In this latter figure, muscovites occur between quartz boundaries and are also moulded on biotites.

4.3.2.3 Robe Andalusite Schist

Relations in andalusite bearing psammites and psammopelites are best summarised in Fig. 4.32. S_1 microstructure in psammitic beds varies from

homogeneous in Fig. 4.32a (domain 3 or 4 equivalent in chiastolite schist) to domainal, consisting of alternating M (muscovite + biotite $\pm$ quartz) domains, about 0.1-0.2 mm wide with QM (quartz + muscovite + biotite $\pm$ garnet) domains about 0.4-0.6 mm wide (Fig. 4.32b). M domains consist of bands of biotite or kink like biotites, overgrown by S_1 muscovite. QM domains consist of equant quartz, S_1 muscovite and ragged or stumpy biotites. The change in shape of biotite grains between QM and M domains suggests that the domainal nature of S_1 is related to varying D_1 strain history, and this is confirmed in rare cases (Fig. 4.12) where an early schistosity is outlined by the orientation of biotites in QM domains. M domains are thus regarded as limb areas and QM domains correspond to hinge zones of D_1 microfolds (Section 4.3.7.3). A similar origin is proposed for the formation of domainal S_1, even where an early fabric is not visible because of biotite rotation or corrosion in QM domains (Section 4.3.7.1). Where S_1 is more homogeneous in psammites, there may still be minor domainal development with the formation of bands of iron stained biotites or by the localisation of muscovite on annealed biotite kinks (Fig. 4.32c). Parts of some psammites contain no S_1 fabric. Rather, the networks of altered biotite grains which dominate these areas define relict cross beds.

S_1 microfabric in psammopelites is strongly domainal (Fig. 4.32). M domains anastamose and wrap around pre-S_1 andalusites and biotites, and consist dominantly of interleaved muscovite laths (Fig. 4.32d). In some M domains, biotites occur as ragged grains with a shape but not a lattice orientation parallel to S_1 (Fig. 4.32e). QM domains contain a homogeneous muscovite + quartz $\pm$ biotite fabric (corresponding to domain 3 or domain 4) but even here local muscovite/quartz variations result in the formation of muscovite rich bands (domain 5) which cut off biotites (Fig. 4.32f). The change in shape of pre-S_1 biotites between QM and M domains, and even within QM domains, suggests that the S_1 microfabric reflects local variations in strain history involved in the deformation of pre-S_1

minerals. The change in shape and preferred orientation of muscovite laths between M and QM domains is shown in Fig. 4.32g; muscovites lying across S_1 are stumpier than those lying parallel to S_1. Reference to Fig. 4.32f suggests that muscovites in QM domains lie along the boundaries of elongate to equant quartz grains.

S_1 in psammopelites in the Lakes Nob Area (Map 1) differ from those described above; S_1 here is dominated by bands of sericite alternating with quartz rich domains.

S_1 in S_{1N} pelites is similar to S_{1P} pelites discussed below.

4.3.3 S_1 in Medium Grade Rocks - S_{1P} Domain

4.3.3.1 Apollyon Chiastolite Schist

Although these chiastolite schists are dominated by S_{1N} relations, local S_{1P} relations occur in the overturned limb of a macroscopic F_1 fold (Section 6.2.3.4). The morphology of S_1 in these S_{1P} schists is similar to that in S_{1N} rocks. S_1 in pelites is defined by bands of muscovite wrapping around andalusites and elongate biotites. S_1 in psammites is defined by the orientation of muscovite laths. Local muscovite/quartz variations lead to the recognition of similar domains to those in S_{1N} chiastolite schist.

4.3.3.2 Robe Andalusite Schist

Typical relations in these S_{1P} rocks are shown in Fig. 4.33. The microstructure of the psammites is dominated by impersistent biotite + minor muscovite laminations which alternate with quartz rich layers which also contain biotite, muscovite, retrogressed feldspar and minor garnet (Fig. 4.33a).

Within biotite laminations, biotites are kinked or outline kink like shapes which are regarded as kinks which have sufferred kink boundary migration (Fig. 4.33b). Thin muscovite laths occur in these laminations either along kink boundaries in biotites or parallel to the cleavage of partially altered biotites.

Quartz rich domains are dominated by equant quartz and by individual laths or groups of intersecting laths of biotite. Some of these grains are elongate subparallel to S_1; others are kinked about S_1 or outline kink shapes. In some cases, enveloping surfaces to trains of biotite define an early crenulated schistosity (Fig. 4.15).

In these S_{1P} rocks, and in the S_{1P} sillimanite schists discussed below, the parallelism between S_1 and S_0 means that the layering parallel to S_1 is caused by a combination of two factors:

1. the presence of biotite laminations parallel to S_0, and
2. the wavelength of F_1 microfolds.

The presence of kinked biotites and kink-like biotites in biotite laminations do not necessarily define the presence of pre-S_1 preferred growth, since they may simply be results of the kinking of randomly oriented biotites concentrated in thin bands. However, the presence of biotite fabrics in QM layers also suggests that the spacing of biotite rich laminations may be controlled at least to some extent by the wavelength of F_1 microfolds.

Where bedding in psammopelites is defined by iron oxides rather than by biotite (Fig. 2.10), S_1 microstructure is dominated by the alternation of M and QM domains similar to that in S_{1N} psammopelites. Brittle deformation of these iron oxides results in the formation of pull apart structures with the alignment of biotite and muscovite in cracks parallel to S_1 (Fig. 4.33c). Where bedding is defined by biotites, M domains are dominated by biotite and QM domains also contain biotite. Biotites in M domains outline annealed kinks (Fig. 4.13); biotites in QM domains either outline an early fabric (Fig. 4.15) or lie at various angles across S_1. These relations are similar to those of the sillimanite schists discussed below.

Andalusites in these psammopelites are enveloped by S_1. They contain oriented biotite inclusions (Fig. 4.14) and together with andalusites in S_{1N} rocks, alter to sericite laths in S_1 (Fig. 4.33d).

The morphology of S_1 in a typical S_{1P} pelite is shown in Fig. 4.33 (inset). Narrow bands of anastomosing muscovite laths wrap around elongate

quartz and elongate biotites. These biotites commonly have a crystallographic preferred orientation lying at angles to S_1 and may be overprinted by muscovite.

4.3.4 S_1 in High Grade Rocks - S_{1P} Domain

The typical S_1 microfabric in high grade psammites is shown in Fig. 4.34. S_1 is defined by thin stringers of iron oxides which anastomose and wrap around quartz and feldspar grains, and which link irregularly shaped biotite aggregates. The biotites themselves form ragged grains and aggregates, outlining kinks parallel to S_1 and kink like shapes. Their original distribution is probably controlled to a significant extent by bedding as well as by the wavelength of F_1 microfolds (see above). Biotites oriented at high angles to S_1 are overprinted by biotite laths in S_1 (Fig. 4.35). In the western part of the Robe Beds, S_1 in psammites is defined by idioblastic laths of biotite but it is not known if this is a recrystallisation feature, or whether early biotite growth persisted into S_1 time in this area. Sillimanite growth in these rocks is restricted to small needles lying parallel to, or across S_1, within quartz grains (see below).

The S_1 fabric in psammopelites is dominated by biotite laminations (Fig. 4.36). Biotites in these laminations either lie parallel to S_1 or form open to tight kinks about S_1 (Fig. 4.21). Thin muscovite laths in these bands form parallel to S_1 or mimic the cleavage orientations of folded biotites. Intervening QM domains contain equant quartz, sericite clots after feldspar, and individual or groups of biotite laths. These are also kinked about S_1 but may outline a relict early fabric (Fig. 4.23).

Some psammopelites as well as some pelites contain aggregates of large idioblastic biotites which cut across S_1 and are undeformed (Fig. 4.37). They either represent biotite growth which outlasted S_1 formation, or biotite growth in S_1 time but in areas with little anisotropic diffusion (M.A. Etheridge, pers. comm., 1977).

Sillimanite is an important part of the S_1 microfabric in these rocks.

Although coarse grained sillimanite, up to 4 cm long and surrounded by sericite, lies parallel to L_1, sillimanite more commonly occurs as bands of needles parallel to S_1 between biotite rich laminations (Fig. 4.38a). Sillimanite needles themselves have well defined prism faces and square or curved terminations and may fan about S_1 in these bands. They may also be overgrown by sillimanite crosscutting S_1. Whorls of sillimanite may also be present. Needles of sillimanite also occur in quartz grains where they are regarded as part of the high grade, M_1, assemblage (cf. Vernon's 1975 fibrolite). Needles in coarse muscovite plates, however, are regarded as true inclusions and older than their host since the muscovites are part of a late stage event (Section 4.5.1.3).

Sillimanite needles also occur in biotite grains, where they generally lie parallel to biotite cleavage traces (Fig. 4.38b) but where they may also lie parallel to S_1. Where needles occur in basal sections of biotite, they outline two directions oriented at 60° to each other (Fig.4.38c). A common feature of biotite/sillimanite relations is the dirty nature of sillimanite needles and crystals where the two are in contact. The significance of these points will be discussed in Section 5.2.3.8.

Fibrolite and sillimanite also occur in sericite clots (Section 4.2.4). Fibrolite aggregates either form swirling masses, or are aligned parallel to S_1. In this case, they may overprint pre-S_1 sericite which is crenulated about S_1 (Fig. 4.39), or may lie axial planar to F_1 folds in pre-S_1 fibrolite (Fig. 4.16). Sillimanite needles within these clots lie parallel to S_1 or crosscut S_1.

K feldspar grains vary in shape from equant (not common) to elongate (very common) parallel to S_1 and are also part of the S_1 microfabric. Microperthite is the dominant phase but microcline has been recognised and the presence of orthoclase west of Apollyon Valley was verified by Binns (1964) by x-ray diffraction. K feldspar is characterised by smooth but irregular boundaries against quartz and sericite with which it generally

occurs. Inclusions of biotite either define a pre-S_1 fabric (Fig. 4.24) or define an orientation parallel to S_1 (Fig. 4.40). The relation between K feldspar and sillimanite is discussed in Section 5.2.3.12.

Some garnet is a member of the S_1 microfabric in the Parnell Beds where it occurs as elongate skeletal chains parallel to S_1. These grains have embayed boundaries against quartz and are surrounded by biotite poor zones up to 0.5 mm wide which suggests that they grew at the same time as the matrix which is depleted in Fe and Mg around it. Rounded garnets in sillimanite and andalusite schists may also be related to the S_1 event.

4.3.5 Summary of Critical Data

1. In S_{1N} rocks, there is a general trend for S_1 to vary from homogeneous in quartz-mica schist, carbonaceous schist, chiastolite schist, and in psammites of the Apollyon andalusite schist, to heterogeneous in Robe psammites and psammopelites.

2. Rare domainal S_1 occurs in quartz-mica schists, carbonaceous schists, and in psammites of the Apollyon andalusite where there is some evidence of early oriented mineral growth.

3. Domainal S_1 in the Robe Beds can be related to the deformation of an early S_1 fabric in some cases and is assumed to be related to this in all cases, even where there is no longer evidence of a pre-S_1 fabric.

4. The formation of a domainal S_1 solely by segregation in S_{1N} andalusite schist contrasts to the S_1 microfabric in biotite rich S_{1P} rocks which results not only from the segregation of early biotites but also from the spacing of bedding laminations defined by pre-S_1 biotites.

5. In biotite poor S_{1P} rocks, S_1 is similar to S_1 in S_{1N} rocks.

6. With the exception of some psammites in S_{1P} Robe Beds, S_1 is defined by the growth of muscovite in all rocks, and by the growth of muscovite and biotite in some low grade rocks. S_1 in most of the S_{1P} rocks is defined by the alignment of rotated pre-S_1 biotite. The exceptions are some sillimanite schists which are defined by S_1 biotite, and S_{1P}

chiastolite schist which is defined by muscovite.

7. Discounting mimetic muscovite growth on pre-S_1 biotite, there is an increase in shape preferred orientation of muscovite from low to high grade rocks.

8. Within one lithology, the preferred orientation of muscovite increases from QM to M domains. This is associated with a change in quartz shape from equant to elongate (with a loss of 120° triple point junctions) and with a change in shape of pre-S_1 from stumpy or ragged to elongate subparallel to S_1.

4.3.6 Equivalence of S_{1N} and S_{1P}, and S_1 Relations Transitional between S_{1N} and S_{1P}

The critical data just discussed suggests that:

1. in chiastolite schists S_{1N} and S_{1P} are morphologically similar and are probably equivalent,

2. that the main difference between the mineralogy of S_{1N} and S_{1P} in the Robe Beds is the presence of biotite laminations defining S_1 in most S_{1P} rocks. It was suggested that biotite laminations in S_{1P} rocks probably represent, in part, bedding laminations and it is suggested that the absence of widespread muscovite in this area may be due to lack of widespread biotite breakdown (see Section 4.3.7.1 for a similar effect in S_{1N} rocks). S_1 in biotite poor S_{1P} rocks is similar to S_1 in S_{1N} rocks.

S_{1P} and S_{1N} are also regarded as equivalent because they both overprint biotite and andalusite porphyroblasts and because they both overprint an early biotite schistosity. Each is in turn overprinted by D_3 effects. S_{1N} does not overprint any fabric which is not also overprinted by S_{1P}.

Direct microscopic evidence relating to the equivalence of S_{1N} and S_{1P} can be best observed just northwest of Mt Franks, in an area of herringbone development and variable mesoscopic S_0/S_1 relations (Section 3.5.2.3). Critical microscopic relations between S_0 and S_1 from this area are shown in Fig. 4.4la,b. They are self explanatory and suggest equivalence between S_{1N} and S_{1P}.

4.3.7 Deformation and Schistosity Forming Mechanisms

The formation of S_1 is associated with the deformation of pre-S_1 minerals. Examination of the response of these minerals, especially biotite, to D_1 strain yields important information about the development of S_1.

4.3.7.1 Deformation Effects in Early Biotites

CHEMICAL

During S_1 formation, biotite undergoes partial or complete alteration to muscovite and iron oxide. (see Reaction1, Section 5.2.3.1). Both of these minerals pseudomorph biotite, and in addition iron oxides occur as trails in S_1 (Section 4.3.2.1) and also as spicules along the biotite/muscovite interface (Fig. 4.42). Evidence for syn-S_1 age for some of the alteration of biotite to muscovite is established by

1) the formation of muscovite laths parallel to S_1 in F_1 kinks in biotites, and

2) the presence of deformed and bent muscovite laths in F_3 kinks in pseudomorphed biotite.

Evidence for the syn-S_1 formation of iron oxides after biotite is provided by

1. replacement of kinked biotites by iron oxide-muscovite assemblages in which the relict cleavage is outlined by undeformed muscovite,

2. formation of iron oxide tails, now consisting of hydrated iron oxides, parallel to S_1, and

3. formation of iron oxide-quartz intergrowths which are deformed by F_1 folds (Section 4.3.4.2).

DEFORMATIONAL

In rocks without visible D_3 effects, five different types of pre-S_1 biotite can be distinguished on a basis of habit and deformational effects:

1. kinked irregularly shaped grains in quartz rich domains,

2. irregularly shaped or elongate, apparently undeformed grains in quartz rich domains,

3. elongate grains in muscovite rich domains,

4. elongate aggregates of biotite and iron oxides lying parallel to S_1 in muscovite rich domains of S_{1N} rocks, and

5. bedding laminations defined by biotite.

Type 1 (Fig. 4.43)

These biotites, where present, more commonly contain large kinks than small crenulations distributed throughout the grain. Kinked biotites are characterised by planar undeformed limbs. Cleavage may be continuous across angular hinges, or may be cut off by discontinuities along the axial surfaces or by axial plane muscovite $\pm$ graphite $\pm$ iron oxide (annealed kinks). Axial surfaces themselves lie both parallel and subparallel to S_1, and vary from planar to stepped across cleavage segments, the latter suggesting kink boundary migration. Open to tight kink-like undeformed biotite aggregates are also regarded as kinks which have sufferred kink boundary migration (cf. Williams et al., 1977). Adjacent to M domains, biotites may be strained with curved cleavage traces and may be cut off by M domains.

Type 2 (Figs. 4.44, 4.45)

These biotites show no evidence of kinking. Rather, they occur as grains which have a dimensional orientation close to, or parallel to, S_1 which is not the same as their crystallographic preferred orientation - that is they are elongate across (001) traces. This type of biotite can be divided into two groups: the first is characterised by (001) traces lying at high angles (90°) to S_1; the second is characterised by (001) traces inclined at smaller angles (e.g. 40°) to S_1. Biotites of the first group are characterised by non rational, often iron stained boundaries. Biotites of the second group possess rational boundaries parallel to (001) and stepped prismatic boundaries. The steps consist of small offsets of the crystal margin across (001) and commonly persist across the grain. The width of each step corresponds to the distance between cleavage planes.

Both groups of biotite may be rimmed by quartz pressure shadows along sides at high angles to S_1 and may be rimmed by dense bands of muscovite along sides sub parallel to S_1. Many type 2 biotites terminate against M domains (Section 4.3.4.2) or are bounded or overgrown by M_1 muscovite laths.

Type 3 (Fig. 4.32e)

These biotites occur in muscovite rich domains. They are commonly surrounded by muscovite laths although some are continuous with type 2 biotites in adjacent quartz rich domains (Section 4.3.7.2). In contrast to both type 1 and 2 biotites, type 3 biotites are markedly elongate with an irregular rather than a lath-like shape and are highly altered to iron oxides and muscovite. The long boundaries of these biotites generally cut across (001) cleavage traces and lie close or parallel to S_1 in orientation. These boundaries may also be stepped owing to the presence of small offsets across (001) similar to those described for type 2 biotites. The short boundaries of these biotites are parallel to (001) cleavage planes.

Type 4 (Figs. 4.32b, 4.32c, 4.31)

These biotites and their breakdown products (iron oxides, muscovite) contribute to the formation of M domains which alternate with QM domains to produce a segregated schistosity in S_{1N} rocks. The biotites themselves consist of interconnected rather than individual grains and occur as:

1) stacks of kinked biotites with axial plane muscovite,

2) bands of biotite with variable oriented cleavage segments outlining kink type structures which are cut across by S_1 muscovites. Some of these cleavage segments lie parallel or subparallel to S_1.

3) bands of iron oxide (from biotite breakdown).

Type 5 (Figs. 4.13, 4.30a, 4.34, 4.46)

Bedding laminations defined by biotite are clearly distinguishable from S_1 in S_{1N} rocks, but form part of the S_1 microfabric in S_{1P} rocks. In S_{1P} rocks, biotites in these laminations have been deformed by F_1 kinking and and outline open to tight kinks as well as open to tight kink like shapes

which are interpreted as kinks which have sufferred kink boundary migration (cf. Williams et al, 1977).

In S_{1N} rocks, biotite laminations, partly pseudomorphed to chlorite, outline F_1 parasitic folds (Fig. 4.30a). The re-alignment of biotites into appressed kink like structures subparallel to S_1 similar to that in S_{1P} rocks is best seen in a series of shadowmaster sketches around a typical fold hinge (Fig. 4.46) - starting from the long limb (A) approaching the hinge (B), in the hinge zone (C) and in the short limb (D). Critical features of this figure are

1) the change in shape of biotite laminations from slightly irregular (A) to partially transposed and transposed (C), with the formation of isolated lenticles and partially isolated lenticles of biotite in S_1,

2) the presence of crossing biotite cleavage trends in all sections which suggest kinked and annealed biotites, and

3) the presence of some biotite cleavage traces parallel to S_1. This is interpreted as suggesting that after kinking some biotite cleavage fragments lie parallel to S_1.

4.3.7.2 Deformation Mechanisms Involved in Biotite Re-orientation

Any deformation mechanism or combination of mechanisms acting during D_1 must be compatible with the biotite data discussed above, and in particular must be able to explain:

1) the general presence of biotites with a shape elongation which cuts across (001) cleavage traces,

2) the change in shape of biotites between QM domains (domains 2, 3 and 4) and M domains (domain 5), and the presence of biotites in these latter domains which have a shape but not a crystallographic preferred orientation (sub-) parallel to S_1,

3) the stepped margins of some Type 2 biotites,

4) the general lack of optically visible deformation in Type 2

biotites, and

5) the formation of biotite bands parallel to S_1 in S_{1N} rocks.

The restriction of well defined biotite laths with (001) lying parallel to S_1 to some quartz mica schists and some sillimanite schists suggests that oriented growth mechanisms are not widely developed. The formation of biotite with a shape but not a crystal preferred orientation must therefore be due to:

1) processes that involve external rotation, or processes which involve a change of shape either by

2) slip along basal cleavage planes, or

3) addition or removal of material.

1) Mechanisms which result in external rotation of biotites include kinking and bulk rotation. Simple kink folding involving slip on basal cleavage planes leads to the production of angular kinks with planar limbs containing oppositely directed (001) traces. Each limb thus has a different crystallographic orientation to the other. Heterogeneous slip on biotite (001) planes resulting in the formation of kinks is regarded as a major D_1 deformation mechanism. It is envisaged that kinked biotites undergo annealing with the resultant formation of undeformed, oppositely oriented limbs separated by an axial plane discontinuity which may be the site of muscovite growth or deposition of graphite or iron oxides. Kink boundary migration after kinking is also regarded as a deformation mechanism which results in the formation of stepped axial surfaces and in the formation of kink-like but undeformed biotites. Tight kinking followed by kink boundary migration results in the appression of biotites so that they show an approximate parallelism with S_1. This deformation mechanism is identical to that described by Williams et al.(1977). The separation of oppositely oriented biotite grains about M domains may be due to kinking, annealing and muscovite growth with the stepped margins across (001) common in these biotites indicative of slip (see below). The suggestion

that bulk rotation of inequant particles was a contributing factor in cleavage formation was first suggested by Sorby (1853) who also carried out experiments with iron filings. More recently, Williams (1972) has described examples of detrital micas rotated into parallelism with a superimposed cleavage, and Tullis (1976) in a series of experiments was able to analyse the results in terms of rigid body rotation using the March Model and a modified Jeffery model. The theoretical basis behind these studies is that inequidimensional laths rotate so that the longest dimension assumes higher angles to the direction of shortening.

Rigid body rotation of pre-S_1 biotite laths in these rocks is probably not a major deformation mechanism since most of the biotites with a dimensional orientation parallel to S_1 do not possess a similar crystallographic orientation. It can, however, account for the shape and lattice orientation of ragged biotites which do lie parallel to S_1.

2) Homogeneous slip or glide along basal cleavage planes of mica was hinted to be a deformation mechanism by Means and Paterson (1966, p.128) who suggested that in their experimental work, "a re-orientation (was also) expected to result from the presumed gliding on the basal plane." Internal deformation accomplished by homogeneous glide on (001) planes would result in an external rotation of the grain itself and the deformed grain would possess a shape elongation lying at angles to its crystallographic orientation (e.g. Hobbs et al, 1976, Fig. 2.23). Etheridge et al.(1973) noted that basal slip occurs in three discrete directions on (001) in biotites. Although Von Mise's criterion requires the presence of five independent slip systems for strain to be taken up solely by this mechanism, this criterion does not apply to individual grains in non-monomineralic aggregates (M.A. Etheridge, 1977, pers. comm.).

The presence of stepped margins on Type 2 biotites reported above is consistent with homogeneous basal slip in these grains. Basal slip can result in the formation of elongate grains which, depending upon the

orientation of the original grain, will lie parallel to S_1. It can also explain the greater degree of elongation of grains with (001) as low angles to S_1 compared to those grains with (001) at high angles to S_1. However it cannot explain elongate biotites in muscovite rich domains which are characterised by (001) at high angles to S_1 - similar to angles in stumpy grains in the more quartz rich layers. If stepped boundaries are indicative of glide, it is tempting to suggest that grains with cleavage lying at high angles to S_1 deform by kinking whereas grains with cleavage lying at smaller angles to S_1 deform by this mechanism. Beutner (in press) has drawn attention to detrital chlorite-grains in Martinsburg Slate which are elongate across (001) parallel to cleavage. By being able to relate this orientation to the orientation of (001) in undeformed chlorites he has been able to show that there has been a relative rotation of grains away from the cleavage plane and he has interpreted this as due to rotation of bedding towards cleavage about unrotated chlorites. He then attributed a change in grain shape to corrosion. Comparable measurements to those of Beutner could not be carried out in the thesis area because the original orientation of biotite is unknown. Beutner thus suggests that grains elongated across their cleavage trace can form without rotation but simply by corrosion. While a similar corrosion process has occured in pre-S_1 biotites (see below) it is thought that the presence of stepped margins may suggest homogeneous glide. Allison and La Tour (1977), on the other hand, have demonstrated that slip on parting planes in hornblendes results in rotation of mineral fragments with the resultant formation of a shape orientation and they suggest that this is analagous to translation glide in crystals.

3) The action of processes best described as 'mass transfer mechanisms' can also play a significant role in the modification of grain shapes and sizes. Thus, for example, Sorby (1879) ascribed the solution of grains at points of high pressure (contact points) and the precipitation of material in areas of low pressure to pressure solution, and Durney (1972) and Elliott (1973) have drawn attention to changes of shape in detrital

grains and in fossils which they consider represent examples of solution effects. Durney (1972) and Elliott (1973) have also both emphasised that during deformation, solution transfer mechanisms will act so that the dimensions of a particular grain perpendicular to the maximum principal compressive stress will diminish, and the dimension parallel to this direction will increase. They have suggested that these solution changes are driven solely by differential stress, i.e. are true pressure solution effects. Durney (1972, 1974), Gray and Durney (1974), Cosgrove (1976) and Gray (1977) have all suggested that pressure solution is responsible for the formation of many types of cleavage, especially crenulation cleavage. On the other hand, Marlow and Etheridge (1977), while recognising the effect of solution transfer, consider that it is not solely induced by stress, but may be driven by strain or by chemical gradients established during metamorphic changes.

There is strong evidence that in the medium grade rocks being discussed, mass transfer processes were an integral part of the D_1 event. This evidence is:

1) the truncation of biotite grains together with their quartz inclusions by muscovite rich domains (see below),

2) the formation of zones of iron stained muscovites adjacent to truncated biotites,

3) the formation of elongate slivers of iron oxides in muscovite rich bands adjacent to truncated biotites,

4) the formation within S_1 of iron oxide tails (now hydrated) to pseudomorphed biotites,

5) the formation of bands of iron oxide (now hydrated) parallel to S_1 and along axial planes of kinked biotites, and

6) the formation of quartz pressure shadows and dense bands of muscovite around pre-S_1 biotite porphyroblasts.

It is suggested that mass transfer processes were also able to change the

dimension and shape preferred orientation of biotites. These changes would have no effect on the crystallographic preferred orientation, and would lead to a situation in which biotites would be elongate across their cleavage trace. These changes are certainly consistent with the biotites described above, especially since so many of them are not deformed. They are also capable of forming grains which are elongate parallel to or close to S_1 in orientation. Beutner (in press) has attributed the formation of chlorites elongate across (001) parallel to cleavage to a similar process of grain boundary corrosion.

As a result of these discussions, it is suggested that deformation and orientation-producing mechanisms in biotites are consistent with processes involving rotation, dominantly by kinking, mass transfer and simple glide on (001). It cannot be determined if the solution processes are driven solely by differential stress (pressure solution) or are affected by strain and metamorphic fluid concentrations. Further treatment of this topic occurs in Section 4.3.7.4.

4.3.7.3 Relationship between M Domains in S_{1N} Rocks and the XY Plane of the Finite Strain Ellipsoid

A study of biotite continuity across muscovite bands in these rocks is potentially capable of distinguishing between two documented models of cleavage formation: that in which cleavage forms parallel to the XY plane of the finite strain ellipsoid (Ramsay, 1967; Ramsay and Graham 1970; Wood, 1974) and that in which cleavage does not lie parallel to the XY plane (Williams 1975; Hobbs et al, 1974) and thus has a component of simple shear acting along it. In the first model, muscovite bands (= cleavage) lie perpendicular to the direction of maximum shortening and thus lie parallel to a principal plane of finite strain. As a consequence there is no resolvable shear strain along them. In the second model these bands would be marked by the displacement of earlier marker units. In these rocks, marker units consist of pre-S_1 laminations of biotite, and to a minor extent, andalusite. This

section describes the geometric relations across these bands and then analyses the results.

The simplest case to consider is one in which biotites are continuous across muscovite bands without displacement. No example of unequivocal continuity could be found, but continuity is implied in Fig. 4.47 where two parts of biotite aggregates on either side of a mica band are separated along the strike of their cleavage.

Continuity of Type 2 biotites (but not their quartz inclusions) into muscovite bands is indicated by trails of iron oxides lying parallel to relict cleavage traces in the biotites (Fig. 4.48, 4.49). These trails indicate that whereas Type 2 biotites are undeformed in QM domains, they are kinked both within and marginal to M domains. These opaque trails further suggest that muscovite in these bands has, at least in part, formed as an alteration product of biotite, and also that the formation of muscovite bands was associated not with displacement but with the kinking of biotite.

In some areas, there is the suggestion of apparent displacement of once continuous biotite grains across muscovite bands. The best examples of apparent displacement are seen in psammopelites in the basal part of the Mt Franks facies. Here laminations outlined by andalusite and by biotite* are truncated by a segregated schistosity which is comprised of parallel or anastomosing M and QM domains (Fig. 4.50). Relations between biotites across M domains are best seen near the centre of this figure where the apparent displacement of laminations is consistent with their dips (see also Fig. 4.51). These biotites are separated by a mica band which varies in width from 1 to 2 mm and which is heavily iron stained only between these

---

* In most cases, biotites have been pseudomorphed by iron oxides which contain inclusions of quartz. The formation of these opaques and of quartz is regarded as a D_1 effect because the shape of the quartz trails mirrors the shape of the deformed 'biotite,' and also because many of the quartz grains are vermicular and are continuous with quartz in the groundmass and are thus suggestive of intergrowths.

grains. Shadowmaster drawings of these relations show the amount of apparent offset (Fig. 4.52 and Fig. 4.53) and also show (Fig. 4.52) that the relict biotite cleavage is intensely kinked about S_1 near the muscovite band. Apparent displacements with "a sense of movement" opposite to that of the limb dip are not common in Fig. 4.50 and in one case (Fig. 4.54) close inspection shows that this apparent displacement is due to kinking across M bands.

The apparent displacement shown by many biotites in the previous section would seem to militate against the model in which S_1 lies parallel to the XY plane. However, both Hobbs et al.(1976) and Williams (1976) have pointed out that apparent displacement with the same sense as the dip of the marker unit may result from removal of material during shortening and they have shown that a strain history dominated by simple shear can only be inferred to have taken place when displacements occur in the "wrong sense" to the dip of the marker layer, or when individual grains are physically bent into the schistosity.

Since no unequivocal displacement of biotite or andalusite crystals occur across S_1 in the "wrong sense," a strain history dominated either by simple shear or by shortening is not ruled out. Strain histories dominated either by simple shear or by shortening can produce kinks in biotites. The formation of pull apart textures in andalusites and iron oxides discussed previously suggest that extension has occurred parallel to S_1. In a strain history dominated by shortening, extension may lie precisely parallel to S_1 whereas extension close to parallel to S_1 could be associated with a simple shear history.

Slight variation in orientation of M bands in these areas does not permit distinction between these two strain histories to be made. Since these thin sections were taken from the limb area of a regional F_1 syncline (Section 6.2.3.4), the strain history of this area must involve a

significant component of simple shear. Similarly, the formation of M domains in limb areas of F_1 microfolds suggests that these domains have sufferred a non co-axial strain history (at least during part of the D_1 deformation) and thus that there has been some simple shear parallel to the schistosity.

The truncation of quartz inclusions in biotites where they abut against M domains, and the concentration of iron oxides in M domains suggest that there has been a volume decrease in these zones. An estimate of volume loss can be roughly made from Figs.4.52, 4.53 if it is assumed that the shape of the biotites,as now seen result,from the removal of the centre part of a larger, uniformly dipping biotite during shortening. This leads to an estimate of volume loss of about 80% if accomplished solely by shortening. Such a figure is not reflected by the surrounding microfabric and this contradiction may be resolved by some simple shear along M domains.

In such a situation, M domains would not lie parallel to the XY plane of the finite strain ellipsoid. However, Williams (1975) has shown that material lines can track the XY plane during non co-axial strain, and Hobbs et al.(1976) have shown that at amounts of shortening of about 60%, there is little angular difference between a principal plane of strain and a plane of maximum shear strain.

4.3.7.4 Development of S_1

S_1 in most of the andalusite and sillimanite schists is domainal. In S_{1N} rocks, the presence of a relict crenulated pre-S_1 fabric shows that the spacing of M and QM domains in S_1 is related to the wavelength of F_1 microfolds, with M domains developed in limb areas or in zones of high rotational strain, and QM domains, developed in hinge areas - or in zones of lower rotational strain. In S_{1P} rocks, the kinking of biotites in M domains also suggests that these are zones of high strain compared to the intervening QM domains. However in these rocks, the spacing of S_1 domains appears to be controlled not only by F_1 microfolding of an earlier fabric, but also by the

spacing of bedding laminations. In some psammites, bedding laminations are clearly visible; in psammopelites where bedding is less obvious, the relative contribution of these two components to the S_1 microfabric is less clear.

The development of layered S_1 can best be discussed in S_{1N} rocks where S_1 lies at a high angle to S_0. Here, the concentration of strain in the M domains is indicated by

1) the general undeformed nature of biotites in QM domains except along the margins of M domains,

2) the presence of strongly kinked biotite relicts in M domains (revealed by opaque trails),

3) the presence of biotite slivers, interpreted as kink remnants, elongate parallel to S_1 in M domains, and

4) the inferred simple shear history of these M domains.

The next stage in the development of these M domains is regarded as the formation of discrete channel ways in the high strain zones. These channel ways are associated with the operation of mass transfer mechanisms which result in the removal of quartz and biotite, and the concentration of iron oxides. Volume decrease also takes place in these zones. The final stage in the formation of M domains is the growth of muscovite. Unlike muscovite laths lying along quartz/quartz boundaries in QM domains (see below), it is considered that most of the components for muscovite growth in these zones are provided by the local breakdown of biotite (Section 5.2.3.1). It is thought that the transfer and concentration of these components into these channel ways promoted the syntectonic growth of muscovite (e.g. Wood, 1974, p.398). This model differs from that of Gray (1977) who envisaged the passive concentration of muscovite and only limited recrystallisation after the formation of the cleavage discontinuity. Within M domains, muscovite laths either lie parallel to the domain boundaries, or are interleaved with each other to produce an average orientation parallel to the domain

boundaries. Local areas of mismatch are interpreted as muscovites growing mimetically on old biotites.

QM domains are characterised either by the presence of an early biotite fabric or by the rotation and corrosion of these biotites so that they approach an orientation parallel to S_1. Muscovite laths lie parallel to S_1 and appear to have nucleated and grown mainly on deformed biotites. Quartz grains vary in shape from equant to slightly elongate parallel to S_1 and the presence of 120° triple point junctions suggest that they are in microstructural equilibrium.

Where S_1 is homogeneous in S_{1N} rocks, (most of the quartz mica schists, carbonaceous schists and some andalusite bearing psammites,) S_1 is generally defined by the uniform distribution of elongate muscovite laths which lie along quartz/quartz or quartz/feldspar boundaries. S_1 is also defined by a strong muscovite alignment in the domainal psammites of chiastolite schists. In both these cases, there is some evidence (Section 4.2) to suggest that these S_1 muscovites are preceded by an early white mica fabric. Since most of the S_1 muscovites are not moulded on pre-S_1 biotites, it is suggested that the components for S_1 muscovite growth were supplied by the deformed early white micas - the limited information available (Fig. 4.10e) suggests that S_1 muscovite nucleates and grows from an early crenulated fabric.

Two schools of thought exist on the oriented growth of anisotropic grains:

1) that growth is controlled by the imposed stress (Flinn 1965) or strain (Dieterich, 1969) field and this will result in micas oriented with (001) perpendicular to σ_1 or ε_1, and

2) that growth is controlled to a large extent by the shape anisotropy of the deforming and/or crystallising medium (itself not unrelated to strain), which controls the distribution of fluids and supply of material to the growing crystal and which, when coupled to the growth anisotropy of

mica, results in a preferred orientation lying at high angles to ε_1 (Etheridge, 1971; Etheridge et al, 1974).

If the growth of muscovite is directly related to stress or strain then variations in its preferred orientation must reflect variation in the orientation of σ_1 or ε_1. On the other hand, in the Etheridge model, such variations in preferred orientation are probably to be expected from minor irregularities in the shapes of controlling grains.

In contrast to muscovite preferred orientation in M domains, muscovite in more quartz rich domains has a poor preferred orientation. The especially poor preferred orientation of muscovite in very quartz rich domains (e.g. domain 3, Section 4.3.2.1) is interpreted as a reflection of control exerted by the quartz crystal boundaries on muscovite growth. This control tends to dominate any tendency for muscovites to grow parallel to S_1, although it was noted that muscovites aligned parallel to S_1 are more elongate than those lying across S_1. In chiastolite bearing psammites a simple stress/strain model is unable to explain differences in muscovite preferred orientation between domains 3 and 4. The differences can be explained in terms of the Etheridge model by considering that the shape of the growing quartz grains controls the distribution of the fluid phase and components to the growing muscovites and thus influences their orientation. Since there are more elongate quartz grains in domain 4 than in domain 3, this suggests that the difference in preferred orientation between the domains is not a muscovite growth dependence on strain but a quartz grain shape dependence probably on strain which in turn affects the preferred orientation of muscovite.

Variation in quartz and muscovite (and graphite) content in these rocks not only results in a change in muscovite preferred orientation between mica and quartz rich domains, but also results in changes in the size of quartz grains. Thus, as summarised in Section 4.3.5, quartz grains decrease in size and increase in shape preferred orientation from quartz rich to mica rich domains. Hobbs (1966b), Wilson (1973) and Vernon (1976) have all

commented on this feature and have attributed the restriction of quartz growth to the pinning of quartz boundaries by mica flakes (inclusion inhibition of Vernon). In addition to this variation in size, quartz grains in equivalent domains are larger in andalusite schists than in chiastolite schists. This difference is attributed to the presence of graphite (see Section 5.2.5.1).

4.3.8 Summary of Pre-S_1 and S_1 Microfabrics

There is a close relationship between minerals defining the pre-S_1 fabric, pre-S_1 porphyroblasts (really interkinematic porphyroblasts) and S_1, viz.,

biotite defines a pre-S_1 fabric, occurs as interkinematic porphyroblasts and defines S_1,

andalusite occurs as interkinematic porphyroblasts which overlap into F_1 microfolding and early S_1 formation,

sillimanite defines a pre-S_1 and an S_1 fabric,

sericite defines a pre-S_1 fabric in chiastolite schists and occurs as random and oriented growth from andalusite breakdown which predates S_1,

muscovite defines S_1.

It is not known, however, whether there is a close time relationship between pre-S_1 oriented growth and S_1 growth, or whether an earlier pre-S_1 fabric is now only defined by the minerals above (which are related to S_1 minerals). The possibility cannot be ruled out that the pre-S_1 orientation is part of a complex D_1 event. The progressive nature of the D_1 event is suggested by other lines of evidence:

1) the folding and formation of shear zones in ?ilmenite inclusion trails aligned at various angles to S_1,

2) the formation of a sericite preferred orientation from andalusite breakdown,

3) the presence of pre-and syn-biotite orientations in K feldspar.

The lack of visible folds associated with the pre-S_1 fabric may suggest that it is an early part of the D_1 event which then must be characterised by rotation of strain axes.

The best evidence for pre-S_1 oriented growth is preserved by the alignment of biotite in andalusite and sillimanite schists. The orientation of this fabric is best protected from S_1 crenulation and from S_1 corrosion and rotation within porphyroblasts of andalusite and K feldspar, and in the pressure shadows around these grains.

During the D_1 deformation, the pre-S_1 biotite fabric in QM layers was destroyed by homogeneous glide on (001), heterogeneous glide on (001) leading to kinking of biotite, and by corrosion of biotite. In S_{1N} rocks, the formation of M domains is related to high strain zones - zones of shortening, simple shear and probable volume decrease. Insoluble minerals as well as muscovite laths became concentrated in these zones. QM domains on the other hand, are dominated by 'rotated' biotites, equant quartz grains and poorly oriented muscovite laths. In S_{1P} rocks, S_1 segregation effects cannot be clearly distinguished from the spacing of original biotite laminations.

4.4 MORPHOLOGY AND DEVELOPMENT OF S_2.

S_2 formation is restricted to the Shepherds Hut Area (Map 1), where it occurs in the hinge zones of mesoscopic type A and type AB F_2 folds (Section 3.4). Here, incipient S_2 development occurs in F_2 microfolds by the rotation of S_1 biotite and sillimanite (Fig. 4.55a,b). The style of these folds varies from open and rounded in quartz rich layers to tight and kink style where biotite is dominant. Kinks in biotites may be marked by axial plane discontinuities or by stepped axial surfaces similar to those in F_1 kinked, pre-S_1 biotites which are attributed to kink boundary migration (Section 4.3.7.2). Quartz deformation is restricted to minor intracrystalline deformation (undulose extinction, deformation bands, minor subgrain formation) with the formation of sutured quartz/quartz boundaries. Quartz grains

themselves may become elongate parallel to S_2 - presumably by corrosion rather than by glide. Although most of the biotite in these rocks is characterised by mimetic alteration to muscovite + opaques, or by alteration to muscovite and sericite lying in S_2 or S_3, some biotite laths lie in S_2 axial planes (Fig. 4.56) and thus form part of the S_2 microfabric. These biotites are more likely to be rotated than recrystallised.

Where S_2 is better developed, it is defined by the shape alignment of sericite, biotite, iron oxides, bands of quartz and bands of sericite (Fig. 4.57). Biotite generally occurs as tightly appressed kink like structures or as relict kink aggregates surrounded by sericite and elongate parallel to S_2 (Fig. 4.58). Some biotites have a shape and crystallographic preferred orientation parallel to S_2. Sericite aggregates aligned parallel to S_2 may contain recrystallised sericite laths aligned parallel to S_3. Evidence that sillimanite forms part of the S_2 microfabric is seen in Fig. 4.59 where folded S_1 sillimanite is truncated by rotated or recrystallised sillimanite lying parallel to S_2. S_2 is also defined by irregularly shaped iron oxide stringers within sericite bands, and these are thought to be remobilised biotite alteration products.

S_2 is thus dominated by a rotational fabric and by sericite and iron oxides formed from mineral breakdown. It can be differentiated from S_1 by:

1) its limited development,

2) its non parallel relation with bedding,

3) the lack of widespread sillimanite or biotite as part of its microfabric, and

4) the absence of equant quartz grains with 120° triple point junctions.

4.5 MORPHOLOGY AND DEVELOPMENT OF S_3.

The D_3 event is marked by three main features:

1) the crenulation of S_1,

2) the formation of a new schistosity (S_3), and

3) the adjustment of high grade minerals with their recrystallisation

or with the crystallisation of new mineral species.

Detailed thin section examination of low, medium and high grade rocks has made it possible in many cases to trace the formation of schistosity through from an early period of crenulation.*

The first part of this section discusses the response of individual minerals to D_3 strain and the microstructural relations of new minerals formed in D_3. This clears the way for a discussion of fabric forming processes which may be accompanied by recrystallisation. The second part of this section discusses the stepwise crenulation and development of four different morphological types of S_3. These are:

1. formation of S_3 by asymmetrical or symmetrical microfolding accompanied by segregation of high grade minerals into M (mica) and QM (quartz mica) domains, and the recrystallisation of some minerals (Fig. 4.60a),

2. the crenulation of S_1 in quartz rich schists and the formation of S_3 either by recrystallisation, segregation or by the formation of stylolites (Fig. 4.60b),

3. the formation of S_3 defined by a shape preferred orientation of biotite (Fig. 4.60c), and

4. the formation of S_3 via a long limb schistosity (S_3') formed by asymmetrical crenulation and long limb rotation (Fig. 4.60d).

4.5.1 Adjustment of High Grade Minerals and Growth of New Minerals

The S_3 microstructure in these rocks is determined by the adjustment and persistence of M_1 minerals, and by the formation of new, M_3, minerals. This generally involves the replacement of a medium - coarse grain assemblage by a finer grain assemblage, but unlike the high grade rocks around the Mine area (Laing, 1977) both schistosities are defined by similar mineralogies.

---

* crenulation terminology is adapted from Rickard (1961) and Williams (1972).

Quartz persists into S_3 time as deformed M_1 relicts although new quartz is also present. Biotite breaks down to chlorite or muscovite + iron oxides, and andalusite and sillimanite show further alteration to sericite. Muscovite growth is the main feature of S_3 formation although local chloritoid, staurolite and garnet growth occurs.

The response of individual M_1 minerals to the D_3 event, and the growth of new M_3 minerals will now be discussed.

4.5.1.1 Quartz

D_3 features in quartz grains are very localised. Optically undeformed quartz grains in F_3 hinges in one area contrast with recrystallisation to new grains in another.

D_3 effects on M_1 quartz grains are best seen in single quartz grains and in quartz aggregates rather than in M_1 quartz grains in mica rich domains where they tend to be elongate parallel to mica (001) traces. Three types of effects have been noted:

1) change in shape of quartz and formation of internal deformation structures,

2) modification of quartz/quartz boundaries, and

3) growth of new quartz.

1) Where S_3 lies close to S_1 in orientation, M_1 quartz merely changes shape from equant to elongate or lozenge shape (Fig. 4.61). These new grains are not as wide as the undeformed grains, but they are longer, parallel to the dominant schistosity. These lozenge shape grains form a tight interlocking network which plays the dominant part in outlining S_3. Grains show internal deformation and grain boundary adjustments (see below) but only limited recrystallisation. In some areas, large lozenge shaped quartz grains aligned parallel to S_3 occur surrounded by sericite bands, or quartz occurs within elongate ribbons also parallel to S_3.

Where S_3 lies at a higher angle to S_1, quartz grains do not undergo any obvious size change, but rather exhibit signs of intracrystalline strain.

These effects also occur in the elongate grains discussed above, and vary from gentle undulose extinction to more regularly defined zones of lattice mismatch which result in the formation of deformation bands, some of which are sharply defined (kink bands). In some quartz grains, deformation lamellae occur at high angles to deformation bands. The boundaries of the deformation bands are generally parallel and they may traverse completely through the grain or intersect with other differently oriented deformation bands. Some deformation bands are parallel to mica or opaque inclusions within the quartz and are apparently pinned by them. In many thin sections, deformation bands occur sub-parallel to S_3.

More intense intragranular deformation may result in polygonisation with the formation of subgrains, local patches differing in optical orientation from each other by only a few degrees (see Bell and Etheridge, 1976 for a definition of 'subgrain'). These sub areas are usually only vaguely defined but in some areas, well defined subgrains are present.

2) D_3 effects on quartz/quartz boundaries are best seen in quartz aggregates which show a polygonal equigranular microstructure with common triple junctions and with straight or slightly curved quartz/quartz boundaries. D_3 effects in these boundary areas are first apparent optically with the development of a shadow zone along one margin of the boundary, or by the diffuse nature of the boundary, which becomes wavy. Further development leads to sutured boundaries which may be marked by lobes of one grain projecting into the other (Fig. 4.62). Greater mobility of quartz/quartz boundaries results in more pronounced bulges and in the formation of new quartz grains defined by the closing-off of these lobate projections (Fig. 4.63).

3) The formation of new quartz is characteristic of the D_3 deformation. New grains are commonly located around old quartz/quartz boundaries (Fig. 4.64). They range in size from 0.01 to 0.02 mm and form zones, generally elongate parallel to S_3. New grains also occur within old quartz grains where they are associated with subgrains. Recrystallisation is common in

inner arcs of F_3 microfolds. New quartz grains here fringe older grains, and may totally enclose old grains. Thin sections cut parallel to S_3 and L_3 show that old quartz grains are matrix supported and contain tails of new grains aligned parallel to L_3. Within these tails, new grains vary in size from 0.02 to 0.05 mm and are themselves elongate parallel to L_3.

Widespread recrystallisation results in the formation of mosaics of fine grain (0.08 mm) equant quartz grains with polygonal boundaries and triple point junctions. In mica domains, quartz is elongate in shape and lies parallel to S_3. An important feature is the presence of gentle undulose extinction in all these new grains.

Discussion of Quartz Deformation

The sequence of changes reported above in quartz grains - the change of shape of old grains, the suturing of polygonal boundaries, the formation of deformation bands, subgrains and of new grains - all correspond with the deformation of quartz followed by recovery and recrystallisation as described by many authors from natural rocks (e.g. Wilson, 1973, Marjoribanks, 1976) and summaries, together with experimental results, by Hobbs et al. (1976) and Vernon (1976). Most of these workers suggest that the formation of elongate grains is due to the intracrystalline slip, although grain boundary sliding (Hobbs et al., 1976) or solution effects cannot be discounted in this study. Recovery features include the formation of deformation lamellae, bands and subgrain formation (polygonisation). New grains form by recrystallisation in areas of high strain and high lattice misorientations along deformation bands, grain boundaries, and subgrain boundaries. This recrystallisation is probably syntectonic since new grains are deformed, are slightly elongate and show a size variation which may be due to growth after initial nucleation.

Without any detailed orientation work on the relation between old and new grains, it is difficult to determine the exact nature of the deformation process. The features described above, however, all accord with deformation

by bulge nucleation along quartz boundaries and deformation bands, and from subgrains. Recrystallisation probably also occurs by subgrain rotation, but the extent of these two mechanisms cannot be judged.

Hobbs et al.(1976) and Vernon (1976) both discussed factors that lead to the restriction of size of new quartz grains - orientation inhibition and inclusion inhibition (impingement boundaries of Vernon 1976, p.138).

4.5.1.2 Sillimanite

Sillimanite needles and bands of fibrolite define open to tight F_3 folds (Fig. 4.74). There is no sign of sillimanite recrystallisation in the hinge area and it is thus suggested that sillimanite is unstable and breaks down to muscovite and sericite. This recrystallisation is suggested by the presence of F_3 axial plane muscovites in hinge areas, and by x-ray diffraction analysis of fibrolite which shows that it has been replaced by $2M_1$ muscovite. The timing of this pseudomorphous alteration cannot be determined. Breakdown of sillimanite + K feldspar to muscovite + quartz is discussed in Section 5.4.2.2.

4.5.1.3 Andalusite (including chiastolite), its inclusions and its alteration products

Except for the formation of pull-apart structures, andalusite does not exhibit any sign of D_3 strain. Rather, its main response to deformation is one of chemical alteration, with the pseudomorphous alteration to sericite laths lying parallel to S_3 (Fig. 4.65). It was noted in Section 4.2.2 that partial alteration of andalusite to sericite is a feature of the D_1 event, and this results in the formation of sericite-andalusite clots with sericite laths aligned parallel to S_1. During D_3, these sericite laths are crenulated about S_3 (Fig. 4.66) or recrystallise into S_3 sericite. Graphite spicules lying in S_1 may be mobilised into F_3 hinge zones (Fig. 4.66). The increasing development of sericite parallel to S_3 results in a rotation of these mineral clots which become elongate parallel to S_3.

In the western part of the Robe andalusite schists, and in the Robe sillimanite schists, sericite $\pm$ andalusite $\pm$ sillimanite clots contain, or are rimmed by, large plates of muscovite. These muscovites are generally randomly oriented (Fig. 4.67) but some lie parallel to F_3 axial planes. Most are undeformed, but minor kinks and curved cleavage traces do occur. These large crosscutting muscovite laths contain inclusions of quartz, biotite, sillimanite and local sericite. Their general undeformed nature, continuity of orientation between several grains and sharp boundaries with sericite are interpreted as evidence for growth as sericite recrystallisation products. They correspond to the M_2 muscovites of Binns (1963).

4.5.1.4 Chloritoid

The D_3 event is marked by the growth of new chloritoid within sericite clots pseudomorphing andalusite crystals (Fig. 4.68). Chloritoid occurs within these clots as multiply twinned, undeformed laths which lie both parallel to, and across, S_3. The grains are mainly in contact with sericite rather than andalusite and are commonly anchored in opaque iron oxides or biotites. Both biotites and opaque iron oxides occur as inclusions. Features of the growth of chloritoid are discussed in Section 5.4.2.6.

4.5.1.5 Biotite

Biotite undergoes alteration to chlorite or to muscovite + opaques in the D_3 event. The timing of this alteration is difficult to determine in many cases because of mimetic replacement of biotite. However, evidence for the D_3 formation of chlorite after biotite is suggested by the alignment of chlorite at small angles to S_3 (Fig. 4.69). The formation of muscovite laths in S_3 axial planes of kinked biotites (Fig. 4.70) also suggests D_3 alteration. In chiastolite schists, alteration of biotite is associated with the formation of elongate trails of opaques parallel to S_3 (Section 4.5.2.3).

4.5.1.6 M_1 Garnet

With the exception of minor irregularities around the edges of garnet grains, there is little sign of chemical breakdown of garnet. There is, however, evidence for brittle deformation. Garnet grains have been cracked and pulled apart parallel to S_3 (Fig. 4.71). There is good matching of garnet pieces across these cracks, and biotite and quartz in the cracks lie parallel to S_3.

The presence of cracks in garnets implies extension parallel to S_3 and further implies that S_3 lies close to the XY plane of the local finite strain ellipsoid. Laing (1977) has found similar features in the D_3 event in the Mine area.

4.5.1.7 Feldspar

Both plagioclase and K feldspar are unstable in D_3 time and undergo alteration to sericite without any visible deformation effects.

4.5.1.8 Muscovite and Sericite

S_3 muscovite and sericite occur in several ways. Muscovite occurs as thin laths or layers defining S_3, as biotite breakdown products, or as large stumpy laths in low and high grade rocks which either lie parallel to, or cut across S_3. Sericite occurs as alumino-silicate alteration products as described above, and as bands lying parallel to S_3 - the latter being especially prominent in the Lakes Nob area.

Muscovite laths defining S_3 possess rational (001) faces but tapered frayed prismatic terminations. They have an average size of 0.1 x 0.4 mm, although several laths may be joined end on or sideways to form larger grains or bands parallel to S_3. Muscovite laths either lie parallel to S_3 or form an anastomosing network around quartz grains (see Section 4.5.2.1).

Large muscovite laths (the M_2 event of Binns, 1963) occur within mineral clots in both low and high grade rocks. In the low grade rocks, these clots define the S_3 "eye" schistosity discussed in Section 3.5.1.2

and the clots themselves are elongate parallel to S_3. On a microscopic scale (Fig. 4.72) these clots consist of large (1.5 x 0.3 mm) plates of muscovite and small quartz grains. Muscovite laths lie both parallel and across S_3 and contrast markedly with the elongate laths defining S_3 in the groundmass. Muscovite laths associated with mineral clots in higher grade rocks were discussed in Section 4.5.1.3.

Bands of sericite lying parallel to S_3 are most common in the Lakes Nob area, where they may be associated with large laths of muscovite parallel to, and crosscutting, S_3. Zones of sericite range in width from 3-7 mm, and contain sericite laths with an average size of 0.04 x 0.01 mm as well as some large (0.4 x 0.05 mm) grains of muscovite which lie subparallel to S_3.

4.5.1.9 Staurolite and Garnet.

Staurolite and related garnet only occur in the Parnell Beds east of Apollyon Valley. Staurolite poikiloblasts occur as subidioblastic pale yellow to yellow grains rimmed by incipient sericite and containing inclusion trails of ?ilmenite (Fig. 4.72b). Since the inclusion trails outline open F_3 folds, it is apparent that staurolite growth took place after the initiation of the D_3 deformation. Although staurolite was not observed in rocks containing an S_3 microfabric, it is suggested that staurolite growth is part of the D_3 event. Similar staurolite growth in the D_3 event in the Mine area has been reported by Laing (1977).

Small idioblastic garnets in these rocks are also related to the D_3 event although no direct relation to S_3 was found. Metamorphic relations between staurolite and garnet are discussed in Section 5.4.2.7.

4.5.2 Crenulation and Schistosity Formation

4.5.2.1 Microfolding and the Development of Axial Plane Schistosity in Pelitic Schists

This section discusses the nature of F_3 crenulations and the progressive formation of an axial plane schistosity in the more pelitic metasediments.

The best examples of these D_3 effects occur in S_{1N} andalusite and chiastolite schists west of the Mt Franks Retrograde Schist Zone where F_3 crenulations and S_3 formation occur on a regional scale (see mesoscopic descriptions, Section 3.5.2.2). Further west in S_{1P} andalusite and sillimanite schists, F_3 crenulations and S_3 development are restricted to hinges or short limbs of major parasitic F_3 folds (Section 3.5.2.1).

For the purpose of the following discussion, the tightness of F_3 microfolds is regarded as an indicator of D_3 strain. Thus the open to tight microfolds found in thin section are regarded as part of a progressive sequence representative of increasing strain. In the andalusite and chiastolite schists, the crenulated surface, S_1, is a layered anastomosing schistosity which consists of M layers and QM layers. In the chiastolite schist, S_1 is a more homogeneous muscovite schistosity. In both cases, S_1 wraps around partially altered biotite and andalusite/chiastolite porphyroblasts.

DESCRIPTION OF MICROFOLDS

a) Low Strain Effects

Gentle F_3 microfolds in S_1 have interlimb angles of 90° or greater and are best defined by trains of muscovite in chiastolite schist, by the folded shape of M layers in andalusite schist (Fig. 4.73) and by sillimanite needles and biotites in sillimanite schist (Fig. 4.74). Most hinges are rounded or angular (kink) in shape although box folds and cusps may occur. Rounded hinges are characterised by bending of individual muscovite laths (Fig. 4.73) whereas kink folds are defined by abrupt changes in orientation between separate, undeformed laths, or by the bending of individual laths over narrow zones. There is no sign of muscovite recrystallisation in hinge or limb areas of these folds. Strain effects within quartz in QM layers are restricted to minor undulose extinction with some boundary shadowing effects. Axial surfaces vary from planar in M layers to irregular in both QM layers and in biotite-sillimanite layers (Fig. 4.74) and it may be

impossible to trace axial surfaces across M and QM layers. A feature of some kink folds is the "overlap" of muscovite from one limb to another so that the kink plane describes a zig zag pattern and is pinned along (001) and prism faces (Fig. 4.75). Opaques generally lie in axial surface positions.

In andalusite schist, low strain F_3 folds are sporadically developed and occur adjacent to altered porphyroblasts where they amplify the shape of deflected S_1 schistosity (Fig. 4.76).

b) *Intermediate Strain Effects*

At intermediate strains, F_3 microfolds in S_1Pe are characterised by interlimb angles in the range 90°-50°. Hinge shapes vary from sharp kinks or box type in mica rich lithologies (Fig. 4.77) to more rounded in M layers interbedded with QM layers (Fig. 4.78).

Rounded folds of this type are characterised by bending of muscovite laths over a relatively large area. Muscovite may undergo local recrystallisation in the short limb to muscovite or sericite laths, aligned parallel to S_3 (Fig. 4.78). Short limbs may also be marked by a decrease in muscovite birefringence from second order to first order grays, and by an obscuring of lath boundaries; these features are regarded as incipient recrystallisation.

The kink folds in the pelite bed of Fig. 4.79 are the tightest found in the area which are not accompanied by the formation of discontinuities or by mineral segregation. A measurement of kink angles in both antiforms and synforms indicates that limb dips are essentially statistically symmetrical about axial surfaces ($\phi^* \sim \phi^*_K \sim 30^\circ$) when large numbers of readings are taken. Interlimb angles of 60° ($\phi + \phi_K$) suggest that these

---

* ϕ, ϕ_K terminology from Paterson and Weiss (1966). Measurements were made on pairs of folds - 100 pairs in synforms and 107 pairs of antiforms.

folds conform to chevron folds rather than kink bands. Comparison with models of chevron fold development (Ramsay, 1974) suggests that axial planes are approximately normal to the direction of maximum shortening and that deformation took place by flexural slip on S_1 plane. The interlimb angles recorded above are similar to those measured mesoscopically by Anderson (1966).

Tighter folds in more thinly layered M and QM S_1 show considerable variation in profile shape and in axial surface orientation. M layers may become bulbous in shape (Fig. 4.81) and characterised by overstepping of muscovite laths and by "thrusts" with resultant mismatch of limbs (Figs. 4.81, 4.82). "Levering-off" effects, in which muscovite laths are only anchored by one prism face, are also present (Fig. 4.82, circled). As a result of all these effects, axial surfaces are variable in orientation. All these effects are consistent with flexural slip.

A feature of M layers in both Figs. 4.81 and 4.82 is the change in shape of biotites from elongate in F_3 limbs to more equant and stumpy in hinge areas. These biotites are pre-S_1 in age and have been rotated into S_1 and have sufferred partial alteration to muscovite in S_1 time (Section 4.3.7.2). There is little change in the shape of biotites in QM layers around F_3 folds (Fig. 4.81) and D_3 strain within these layers is restricted to minor undulose extinction and grain boundary suturing in quartz. Most quartz/quartz boundaries are still straight or slightly curved and relict triple point junctions can still be recognised.

Tighter F_3 folds (Figs. 4.83, 4.84) are marked by the formation of non penetrative iron stained discontinuities along hinge surfaces in M layers and by some subgrain formation in quartz grains located within hinge zones. Discontinuities along hinge zones are best defined by abrupt changes in the orientation of undeformed muscovite laths, and also by termination of biotites.

c) *High Strain Effects*

At high strains, F_3 microfolds are accompanied by the formation of an axial plane schistosity (S_3). These effects will be described after a discussion on the development of F_3 microfolds.

DEVELOPMENT OF MICROFOLDS

At low strains, F_3 folds are marked by variable axial surface orientation, low amplitudes and irregular wavelengths. The close spatial relationship between low strain folds and some porphyroblasts suggests that folds may develop or nucleate on instabilities generated during low strains (e.g. Cobbold et al, 1971); in these cases, instabilities consist of deflections of S_1 around pre-S_1 porphyroblasts.

At higher strains, F_3 folds vary in shape from symmetrical kinks (chevrons) to asymmetrical kinks and possess better defined axial surfaces and more regular wavelengths. Bulbous noses, internal thrusts and interlimb angles of about 60° of symmetrical kinks are consistent with attributes of chevron folds and thus probably formed by layer parallel shortening with axial planes lying parallel to the direction of maximum shortening (Ramsay, 1967, 1974). Asymmetrical kink folds also have interlimb angles of about 60° and have parallel axial surfaces to chevron folds. They are thus regarded not as kink bands, characterised by interlimb angles of 120° (Paterson and Weiss, 1966), but as asymmetrical chevron folds. Their climbing nature probably results from inclination of S_1 away from the direction of maximum shortening.

These asymmetrical folds are similar to those experimentally generated in a "squeeze box" by Cobbold et al (1971) who compressed an anisotropic layering inclined at 20° to the compression direction with the resultant formation of axial planes perpendicular to the maximum compression direction. The weak deformation in QM layers contrasting with muscovite deformation and recrystallisation in M layers is consistent with deformation by flexural slip at the boundaries of, and within, the more anisotropic layer (proposed

by Paterson and Weiss, 1966 and Ramsay, 1967, 1974).

The development of asymmetrical folds with well defined long and short limbs is probably accompanied by stress and strain heterogeneities. Hobbs (1972) suggested that both differential and mean stresses are likely to be higher in limb areas than in hinges of his modelled microfolds. Higher strain in limb areas of F_3 folds is supported by preferential thinning of biotites in this area as described above, and by limited data on reduction in size of quartz grains in M layers (but not in QM layers where little deformation is evident).

The different stress and strain histories of long and short limbs of asymmetric folds (Hobbs, 1972) leads to stress and strain complexities in hinge zones between limbs or along flexure zones, and it is in these areas that discontinuities develop. In hinge zones continuity of muscovite laths may be lost and muscovite and biotites may be abruptly truncated. Truncation of quartz, and formation of iron oxides and graphite in these zones suggest that removal and deposition of material accompanies passive rotation of fold limbs. The significance of these discontinuities is discussed below.

DESCRIPTION OF S_3

At high strains, F_3 microfolds are accompanied by the formation of an axial plane schistosity, S_3, which is homogeneous on a mesoscopic scale yet discontinuous and domainal on a microscopic scale. Three different morphological variants of S_3 have been found and will be discussed in turn. These different types of S_3 may be found within one thin section.

Type 1: S_3 defined by iron stained discontinuities.

These discontinuities are best seen in psammopelites of the Mt Franks facies and in the Apollyon chiastolite schist. In the psammopelites, iron oxides form narrow (0.01 mm) "stylolites" which are broadly parallel to S_3. In detail (Fig. 4.85) these "stylolites" are irregular in shape, deflecting around some quartz grains and splitting and re-joining. Biotites show maximum crenulation immediately adjacent to these zones and may even be cut

off by the "stylolites". Quartz grains may also be truncated. "Stylolites" may also contain muscovite laths aligned parallel to S_3. These laths occur where "stylolites" intersect deformed biotites and probably form by biotite recrystallisation. In addition to "stylolite" alignment, the S_3 fabric in these rocks may be defined by the formation of elongate or lozenge shaped quartz grains.

The non penetrative irregular nature of S_3 "stylolites" in chiastolite schist are best seen in Fig. 4.86. Here, "stylolites" are defined by the concentration of graphite, as well as iron oxide, into narrow zones. In addition, muscovite laths aligned parallel to S_3 may lie on the edge of these zones.

In the andalusite bearing pelites, S_3 discontinuities are developed along hinge zones of tight F_3 microfolds (where they are similar to, but more penetrative than the discontinuities discussed above) and are also associated with flexures in S_1 muscovite layers (Fig. 4.87). In both cases, they are marked by a concentration of iron oxides which may spread out into S_1.

Biotite slivers in S_1 are cut off by these narrow (0.03 mm) zones, and there is no obvious S_1 continuity across them.

Type 2: S_3 defined by zones of re-oriented muscovite.

These zones occur as asymmetrical flexures in M layers (Fig. 4.88), and on limbs of symmetrical folds or as long limbs of asymmetrical folds. As a result of this rotation, muscovite within these zones does not lie parallel to S_3 but lies in S_1 which is rotated towards S_3. In all cases, these S_3 zones are separated by microlithons containing S_1 lying at high angles to S_3. In some cases it may be possible to trace muscovite laths from microlithons into S_3 zones; elsewhere S_3 zones are bounded by iron stained discontinuities which truncate muscovite laths, and F_3 hinges. Since these S_3 zones occur within M layers, there is no change in ratio of quartz to muscovite composition.

Type 3: Differentiated S_3.

This type of schistosity is defined by the segregation of homogeneous quartz

mica schist into alternating M and QM domains which define mesoscopic S_3 and which lie parallel to the axial planes of F_3 crenulations. These segregation processes have been observed in psammopelites and pelites of the Robe Beds and the Apollyon Beds. The general nature and development of this type of S_3 will be briefly described with reference to psammopelites of the Robe andalusite schist (Fig. 4.89), the Apollyon chiastolite schist (Figs. 4.90-4.92) and the Robe sillimanite schist (Figs. 4.93, 4.94). Various aspects of the development of this segregated S_3 raised by this treatment will be further discussed with a detailed discussion of S_3 formation in pelites of the Robe andalusite schists (Figs. 4.95-4.103).

In Fig. 4.89, S_3 is marked by a poorly defined zone which occupies the steeply rotated limb of an F_3 microfold. Muscovites within this zone do not lie parallel to S_3 but still lie in S_1 which lies at a smaller angle to S_3 than S_1 in the adjacent microlithons. Muscovite grains are thus bent across domain boundaries (Fig. 4.89). Qualitative examination shows that, whereas there is a decrease in size of quartz grains in the M domain, there is no corresponding increase in size in the adjacent microlithon - i.e. the size of quartz in QM domains is similar to the size of quartz in crenulated S_1. This point will be further discussed below.

The formation of segregated S_3 in Apollyon chiastolite schist by the alternation of M and QM domains is similar to that described above (Fig. 4.90). M domains occupy steep limbs of F_3 microfolds and S_1 in these limbs lies at small but distinct angles to S_3. QM domains occupy the hinge zones of F_3 microfolds and S_1 in them lies at high angles to S_3. There is no discontinuity at M/QM domain boundaries and muscovite laths can be traced across them. M domains are narrower than QM domains, and are richer in muscovite, biotite, graphite, iron oxides than QM domains. There is a marked decrease in size of quartz grains between QM and M domains. In QM domains quartz grains display only minor internal strain and 120° triple point junctions are present. In M domains, quartz grains are elongate parallel to S_1

and are surrounded by micas.

Final development of S_3 segregation cleavage results in the obscuring of F_3 microfolds in a late stage period of quartz modification and muscovite recrystallisation. These relations are best seen in chiastolite schists, where the transition from M and QM domains preserving a relict folded S_1 schistosity to M and QM domains with muscovites parallel to S_3 can be seen. QM domains are characterised by the formation of elongate or lozenge shaped quartz grains, and by the presence of individual muscovite laths either parallel to S_3 or anastomosing around quartz grains - mica film arrangement (Figs. 4.91, 4.92). In some areas, relict F_3 crenulations may still be outlined by undeformed muscovites. M domains in these rocks are similar to those where F_3 folds are still readily recognised and consist of muscovite + graphite $\pm$ biotite $\pm$ small quartz grains. Muscovites are generally parallel to S_3 not S_1 (cf. previous description above) although areas of muscovite mismatch do occur.

Differentiated S_3 in sillimanite schist is defined by the alternation of M domains (which occupy the long limbs of asymmetrical crenulations) with QM domains (which occupy the hinges and short limbs). Figure 4.93 shows that whilst M domains are generally narrower than QM domains, there are significant exceptions. Although the boundaries between M and QM domains lie parallel to S_3, biotites in both QM and M domains lie in S_1 - at high angles to S_3 in QM domains and closer to sub parallel to S_3 in orientation in M domains. The ragged nature of biotites in M domains indicates that they do not represent new growth, and it is possible to observe bent biotites at the boundaries of M and QM domains (Fig. 4.94). There is thus no discontinuity at domain boundaries. M domains are enriched in biotite and sericite and depleted in quartz compared to QM domains.

It is suggested that there has been a decrease in quartz size, i.e. a loss of quartz, from M domains compared to the crenulated S_1 since quartz in QM domains has a similar size to quartz in crenulated S_1 and does not appear

to have been enlarged. There is no sign of quartz overgrowths or new quartz growth, and quartz in this domain still preserves 120° triple point junctions and straight or slightly curved boundaries despite the presence of internal strain. The significance of this will be discussed below.

Type 3: S_3 *A Detailed Study of Segregated Schistosity in Pelites*

The above descriptions of Type 3 S_3 suggest that M domains occupy the long limbs of tight F_3 microfolds, and are defined by rotation of mica into an orientation close to that of S_1. These descriptions also suggest that there is a change in mineral ratios between M and QM domains. A treatment of these points, and a discussion of schistosity forming processes are carried out in this section with reference to S_3 formation in Robe pelites - Figs. 4.94-4.103.

Characteristics of differentiated S_3 are best seen in muscovite pelites in sections cut perpendicular (Fig. 4.95-4.101) and parallel (Figs. 4.102-4.103) to F_3*. S_3 is defined by the alternation of light coloured QM domains with dark coloured M domains. Domains vary greatly in persistence along strike and in width, and some QM domains may be narrower than adjacent M domains (Figs. 4.95 circled, 4.98). In general, M domains occupy alternate limbs of F_3 microfolds (but see Fig. 4.96) and QM domains occupy the other limbs or the hinge areas. There is, however, considerable variation between S_3 domains and F_3 geometry because of impersistence of domains and variations in F_3 geometry.

Although domain boundaries lie parallel to S_3 on a broad scale (Fig. 4.95), they have quite variable shapes in detail and may even lie at significant angles to S_3 which is itself variable in orientation (Fig. 4.99). Muscovite zones may even project into QM domains from M domains where they define small prominences outlining F_3 folds (Fig. 4.99).

In sections perpendicular to F_3, the orientation of S_1 varies from high

---

* and perpendicular to S_3.

angle to S_3 in QM domains to close to S_3 in M domains (Fig. 4.98). The orientation of S_1 in M domains is also outlined by the shape orientation of quartz and biotite grains (Figs. 4.100, 4.101), and in many places it is possible to trace bent biotite and muscovite grains across domain boundaries (Fig. 4.99 circled). In such cases, there is no offset or discontinuity along domain boundaries. In other areas, domain boundaries separate undeformed mica laths of different orientations and iron stained discontinuities may occur along domain boundaries.

In sections parallel to F_3, (Figs. 4.102-4.103) muscovite laths and elongate biotite and quartz grains define a preferred orientation (S_1=S_3) parallel to S_3. In QM domains, on the other hand, bent biotite grains and muscovites define a crenulated S_1 orientation. Changes in shape of biotite and quartz grains in this orientation indicate that QM domains can be divided into two groups (areas A and B, Figs. 4.102-4.103). Domain A is characterised by equant quartz grains and corresponds to QM domains in sections perpendicular to F_3; domain B is characterised by quartz and biotite grains intermediate in size between domain A and M domains.

The change in biotite and quartz orientations between QM and M domains is accompanied by changes in the length to width ratios of these grains. Although biotite grains in QM domains were too irregular to measure, Figs. 4.100-4.103 show that quartz grains change in the following ways (Table 4.1):

1) in sections perpendicular to F_3, there is a minor change in the length of quartz grains from QM domains (peak at 2 mm) to M domains (peak at 0.6 mm)*

2) in sections parallel to F_3 there is a progressive decrease in the lengths of quartz grains from domain A through domain B to M domains

---

* all measurements were made on X5 shadowmaster enlargements. All length and width frequencies have been normalised to 100 points.

TABLE 4.1

Changes in Dimensions of Quartz and Biotite Grains Between QM and M Domains.

	Section $\perp F_3$		Section // F_3, S_3		
	QM	M	QM(A)	QM(B)	M
Quartz					
length (mm)	2	0.6	1.8-2	1.4	0.6-1
width (mm)	0.8	0.2	1.2	0.6	0.2
area of average grain (mm^2)	1.1	0.22	1.44	0.83	0.24
percentage of quartz in domain	24	5	36	26	6
Biotite					
area of average grain (mm^2)	.45	.32	1.1	0.4	0.2
percentage of biotite in domain	6	5	8.7	6.1	3.7
Mineral Composition					
quartz	24	5	36	26	6
biotite	6	5	8.7	6.1	3.7
muscovite	70	90	55.3	67.9	90.3

(maximum at 1.8-2 mm in domain A; maximum at 1.4 with a secondary at 2 mm in domain C; maximum from 0.6-1 mm in M domains).

3) in sections perpendicular to F_3, there is a decrease of approximately 75% in the width of quartz grains from QM domains (maximum at 0.8 mm) to M domains (maximum at 0.2 mm).

4) in sections parallel to F_3, there is a decrease in the width of quartz grains from domain A (maximum 1.2 mm) to domain B (maximum 0.6 mm) to M domain (0.2 mm) - a total decrease of about 80%.

There is thus an overall change in the length and width of quartz grains in two perpendicular orientations which amounts to a change in shape of the typical quartz grain from equant to disc-shaped lying in a folded S_1.

An estimate of the change in area of quartz grains between QM and M domains was gained by overlying 5X shadowmaster tracings on mm graph paper and counting squares. The results indicate that:

1) in sections perpendicular to F_3 the average quartz grain has decreased in area from about 1.1 mm^2 in QM domains to 0.22 mm^2 in M domains - a decrease of about 80%.

2) in sections parallel to F_3 the average quartz grain has decreased in size from 1.44 mm^2 (domain A) to 0.83 mm^2 (domain B) to 0.24 mm^2 (M domain) - a decrease of about 83%.

3) in sections perpendicular to F_3, the percentage (area) composition of quartz, normalised over uniform domain area, decreased from 24% in QM domains to 5% in M domains - a decrease of 19%.

4) in sections parallel to F_3, the percentage area composition of quartz, again normalised, decreased from 36% (domain A) to 26% (domain B) to 6% (M domains) - a total decrease of 30%.

Similar calculations can be performed on biotite grains in M and QM domains, not on any change in linear dimension because of irregular boundaries,but on area.

Thus, in sections perpendicular to F_3, the average biotite decreases

in area from 0.45 mm^2 in QM domains to 0.32 mm^2 - a decrease of 29% in M domains. There is a corresponding decrease in the normalised percentage (area) composition from 6% (QM) to 5% (M).

In sections parallel to F_3, the average biotite decreases in area from 1.1 mm^2 (domain A) to 0.4 mm^2 (domain B) to 0.2 mm^2 (M domain) - a decrease of 82%. There is a corresponding decrease in the normalised percentage (area) composition of biotite from 8.7% (domain A) to 6.1% (domain B) to 3.7% (M domain). This change in percentage composition is achieved without any new biotite growth in M domains or QM domains. Since biotite is unstable in S_3, breaking down to muscovite + opaques or to chlorite, there is no biotite recrystallisation or overgrowth.

Total percentage mineral compositions, indicating decrease in biotite and quartz and increase in muscovite are shown in Table 4.1. All these results are analysed in terms of crenulation theory in the next sections.

Discussion

The formation of a segregated S_3 is best seen as an accompaniment to tight microfolding. M and QM domains defining S_3 are generally related to long and short limbs of asymmetrical folds, or to limb and hinge zones of chevron folds respectively, although local anomalous relations do occur. The fact that muscovite laths in M domain commonly lie at small but significant angles to S_3 and the presence in some areas of bent muscovite laths between domains suggest that muscovites in M domains are merely re-oriented S_1 muscovites.

Data, summarised in Table 4.1, indicate that there is a change in the amount of quartz and biotite per unit area from QM to M domains. The recognition of a domain intermediate between the two (domain B) in sections parallel to F_3 suggests that this change is progressive. Such an area change can be achieved by:

1) a relative decrease in the amount of quartz and biotite between

domains,

2) a relative increase in the amount of muscovite between domains, or

3) a combination of 1) and 2) above.

There is compelling evidence for a decrease in the amount of quartz and biotite between QM and M domains. Compared to the average grain in QM domains, the average quartz in M domains has sufferred a decrease in area of about 80% in each of two mutually perpendicular orientations. Similarly biotite grains have been reduced in area by a maximum of 82% in sections parallel to F_3, but only 29% in sections perpendicular to F_3. The average volume of each quartz and biotite thus suffers a reduction from QM to M domains. However, the area occupied by quartz and biotite grains in each domain only decreases by 20-30% and 1-5% respectively and is not accompanied by any increase in the number of new grains per unit area.

If there is no muscovite growth concurrent with the loss in quartz and biotite, there has to be an overall volume loss in M domains compared with QM domains. This would be expressed by a reduced width of M domains compared to QM domains. Since this is not everywhere true (Fig. 4.9_5), there must be muscovite nucleation and growth during the crenulation stage. Muscovite growth parallel to a folded S_1 is also implied by the non reconciliation between changes in area of quartz and biotite which are greater than percentage area loss of quartz and biotite between QM and M domains. Without independent measurement of the amount of muscovite growth the volume change involved in the crenulation process cannot be worked out. It is possible that a combination of volume loss and muscovite nucleation and growth parallel to S_1 has taken place. Marlow and Etheridge (1977) reached a similar conclusion of muscovite nucleation and growth in crenulated rocks of the Kanmantoo Group.

We now look at where the removed material went. It is suggested that the size of quartz grains in QM domains is similar to the size of quartz in crenulated S_1, and thus that there was no diffusion of quartz from M to QM

domains. Although this idea cannot be based on a study of the same rock which is less crenulated, it is based on examination of similar lithologies in lower D_3 strain areas, and also on the development of segregated S_3 in sillimanite and chiastolite schists discussed above. All these rocks show that the size of quartz in a mildly crenulated S_1 is similar to quartz in QM domains. The preservation of straight or slightly curved quartz/quartz boundaries, the preservation of triple point junctions, the presence of only minor strain features, and the absence of quartz overgrowths all suggest that there has been no increase in the size of quartz. A similar but stronger, case can be made out for a comparison of biotite sizes since biotite is unstable in this deformation and there is clear evidence that there has been no addition to the size of biotites in QM domains.

If there is no increase in size of quartz and biotite in QM domains, then the grain size ratios discussed above relate directly to the size of quartz in a crenulated S_1. It is suggested that quartz has actually migrated out of the system to form quartz veins parallel and at angles to S_3 (cf. Hobbs et al, 1976, p.40). Biotite removal was probably achieved by formation of muscovite + opaques or of chlorite.

These ideas on the removal of quartz from the system differ from those of Rickard (1961), Cosgrove (1976), Gray (1976), Fletcher (1977) and Marlow and Etheridge (1977), all of whom suggested that there is direct migration of quartz from limb to hinge areas. Cosgrove (1976) and Fletcher (1977) attribute quartz migration to differences in stress or mean stress between different areas of the microfold. The removal of quartz from the system above may indicate that other driving forces are also present (cf. Marlow and Etheridge 1977). Williams (1972) on the other hand, noted that quartz removed from M domains is not simply redeposited in the adjacent QM domain, but must migrate over larger areas.

Strain History

The strain history of the crenulation process can be divided into

several component parts. Rotation of S_1 in M domains involves progressive simple shear parallel to domain boundaries. Components of shortening are involved in both M and QM domains. In sections perpendicular to F_3 shortening in M domains lies normal to S_1 and accounts for the dramatic change in grain widths. In sections parallel to F_3, shortening in M domains lies normal to S_3 and there is also a minor amount of shortening in QM domains (domain A to domain B) which must lie at small angles to S_1. These various components of shortening can be accounted for by shortening approximately perpendicular to domain boundaries. In addition there may be some volume reduction in M domains.

Deformation Mechanisms

The presence of bent muscovites in QM domains and the presence of muscovites bent across some M/QM domain boundaries suggest that deformation of biotite took place by heterogeneous glide on (001) with resultant rotation. Extrapolating from this, it is suggested that the presence of undeformed muscovites with different orientations in different domains - one sub parallel to S_3 in M domains and the other at high angles to S_3 in QM domains - reflects annealing and grain boundary migration of once continuous and bent muscovites. (see also Williams, 1976). The formation of axial-plane muscovites within kinked biotites and the recrystallisation of sericite to muscovite in axial regions between limbs consisting of now undeformed muscovite limbs both suggest that annealing of deformed micas has occurred.

It is tempting to regard the minimal amount of intracrystalline quartz deformation as also due to annealing, and to regard the decrease in quartz grain size from QM to M domains as a recrystallisation phenomenon. However, the evidence discussed above suggests that there has been no significant recrystallisation of quartz and no annealing of quartz. Most quartz deformation is restricted to minor grain boundary sliding and minor sub grain formation. (Some new quartz grains occur margining old grains in the

hinges of some microfolds). Small quartz grains in M domains possess similar amounts of undulose extinction to larger grains in QM domains and are not regarded as products of recrystallisation. The presence of relict triple point junctions and relict straight quartz/quartz boundaries in QM domains coupled with the presence of minor but no major deformation features (e.g. deformation bands, and subgrains) all point towards minimal intracrystalline deformation and recovery. Partially recrystallised grains are rare. Similarly, the decrease in size of biotite grains between QM and M domains is not due to recrystallisation, since biotite is unstable in S_3 time and breaks down to chlorite or muscovite + opaques (Section 4.5.1.5). Marlow and Etheridge (1977) came to a similar conclusion regarding the absence of quartz deformation in crenulation cleavages of Kanmantoo rocks.

If changes in the shapes of quartz and biotite cannot be accounted for by intracrystalline deformation or by brittle deformation, they must be due to mass transfer processes. These have been discussed by Elliott (1973) and recently summarised by Marlow and Etheridge (1977) who suggest that diffusive mass transfer may be driven by other than stress or differential stress controls. There is little evidence available from this study to comment on the driving forces of mass transfer processes. If, however, there is no direct migration of quartz from limb to hinge, as modelled by Cosgrove (1976), Fletcher (1977) and Gray (1976), driving forces other than stress are probably involved.

The final stages in the formation of a segregated S_3 are the recrystallisation of muscovite, mainly in QM domains so that relict S_1 orientations outlined by mimetic muscovites are destroyed, and the elongation of quartz in QM domains. Formation of muscovite parallel or subparallel to S_3 in QM domains involves nucleation and growth of new grains. Elongation of quartz is not a recrystallisation feature. There is little evidence of extensive intracrystalline deformation and thus shape change may be due to diffusive processes.

4.5.2.2 Microfolding and the Development of Axial Plane Schistosity in Quartz Rich Schists

In contrast to S_3 formed by segregation in the rocks just discussed, S_3 in the quartz rich rocks is defined by new S_3 muscovite or by stylolites. In quartz mica schists and carbonaceous schists, small undeformed muscovite laths outlined a crenulated S_1 orientation. At low strains, S_3 effects are best seen in sericite clots where sericite laths outline a crenulated S_1 or are aligned parallel to S_3. Spicules of graphite may also lie parallel to S_3. In the groundmass, the first sign of S_3 occurs in the concave side of F_3 fold hinges. Here in mica rich layers, muscovites occur with a bimodal orientation - parallel to S_3 or in a crenulated S_1 (Fig. 4.104). Graphite , sericite and opaques may also lie parallel to S_3. Quartz grains show undulose extinction and some grain boundary suturing but no recrystallisation effects.

Where S_3 is mesoscopically visible as an "eye" schistosity (Section 3.5.1.2), muscovite laths in the groundmass define a homogeneous S_3 fabric (Fig. 4.72). Muscovite laths are about 0.15 x 0.02 mm in size with wispy terminations and rational (001) faces and may show variable thickness. The overall orientation of these laths varies from good (parallel to S_3) to medium with muscovite anastomosing around small quartz grains.

S_3 schistosity in mica poor lithologies is best seen in psammites of the Mt Franks facies, where S_3 is defined by narrow (0.01-0.05 mm) zones of hydrated iron oxides which anastomose around equant or elongate quartz grains (Fig. 4.105). In addition to iron oxides, these bands may also contain sericite and muscovite laths, and thin wisps of altered biotite. Equant quartz grains possess relict 120° triple point junctions. Elongate grains possess smooth, curved grain boundaries. D_3 strain in quartz is recorded by deformation bands, sutured boundaries and the local development of new quartz. Where muscovite occurs in these rocks, it varies from small (0.1 x 0.02 mm) laths parallel to S_3 to narrow irregular bands also

parallel to S_3.

Since these iron oxide zones truncate biotite and quartz grains and are represented by a concentration of insoluble material, it is suggested that they represent stylolites, that is narrow zones characterised by solution of soluble material (e.g. quartz) and by concentration of insoluble iron oxides, graphite and local white mica. Removal of quartz in these zones would result in a passive concentration of white mica along these solution planes. Similar "stylolites" have been described by Williams (1972) and more recently by Gray (1977).

D_3 effects in more mica rich psammites are best seen in relation to folds in the adjacent pelite. In Fig. 4.106, the amplitude of kinks in S_1 decreases from pelite across S_0 towards psammite. At higher strains, Fig. 4.41, Fig. 4.79, folds in S_1Pe can be traced along axial surfaces into S_1Ps, albeit with a change in style from angular to rounded.

The different responses of pelite and psammite to D_3 strain is related to the morphology of S_1 in the different layers. Pelites are characterised by a well developed S_1 anisotropy consisting of alternating M and QM layers, whereas psammites are more quartz rich and any M layers developed in them are thinner and less persistent (compare pelite and psammite in Fig. 4.107). Response to layer parallel shortening depends on resistence to compression in individual layers and ease of slip between layers (e.g. Cobbold et al, 1971). The greater development of M domains in pelites presumably facilitates slip leading to the nucleation of kinks. The general lack of well defined M layers in psammites thus prevents slip. Where F_3 folds do occur in psammites - presumably at higher strains than in adjacent pelites - F_3 folds are rounded. Even where psammites contain a well developed anisotropy (Fig. 4.41) the thinness of M layers and the presence of more competent QM layers controls the shape of F_3 folds. In these rocks strains are relieved by small scale kinking of biotites and muscovites, by the deformation of quartz grains and by the recrystallisation of muscovite.

4.5.2.3 Microfolding of Biotite Laminations and Development of a Shape Orientation of Biotites Parallel to S_3

DISRUPTION OF BIOTITE LAMINATIONS

Low to Intermediate Strains

Open to tight F_3 microfolds in biotite laminations are best seen in the Apollyon chiastolite schist. Folds are generally characterised by hinge thickening and there is gradual attenuation of width of limb with distance away from hinge zones (Fig. 4.107). Where limbs lie close to S_3 in orientation, laminations are either strongly attenuated (Fig. 4.107, Area A), or are segmented into individual biotite grains (Fig. 4.107, Area B). In these areas biotites may possess a shape orientation sub parallel to S_3.

High Strains

At high strains, chiastolite schists are characterised by the general formation of individual biotites elongate parallel to S_3 (Fig. 4.108). In some cases, it is still possible to reconstruct segments of disrupted biotite laminations such as in Fig. 4.109, and it is suggested that these laminations have been disrupted by rotation of biotite grains during S_3. Relict F_3 hinge zones, outlined by both S_1 and by the shape of biotite grains, together with limb areas may still be present (Fig. 4.110). Continuity of biotite in this figure is, however, partially disrupted by remobilisation of iron oxides into S_3 and by the shape alignment of some biotites also in S_3.

DEFORMATION OF BIOTITE GRAINS

At low strains, deformation within biotite grains is restricted to the development of small kinks (sub) parallel to S_3 in stumpy grains lying at high angles to S_3. At higher strains, it is possible to divide biotites into two populations on the basis of shape and orientation of (001). Biotites with (001) lying at angles greater than about 45° to S_3 are stumpy, irregularly shaped laths or compound grains with intersecting cleavage traces. Biotites

with (001) lying at angles less than about 45° to S_3 are elongate (sub) parallel to S_3 with rational (001) traces but ragged prismatic terminations.

Stumpy biotites either contain small scale crenulations parallel to S_3 or are undeformed and are commonly characterised by step like terminations of prism traces (Fig. 4.111). The paired nature of biotites in Fig. 4.112 suggests that they may be annealed kinks.

Biotites with (001) traces lying less than 45° to S_3 are elongate generally across (001) and possess ragged terminations. Small step like offsets of (001) may be present (Fig. 4.112.). Kinking of (001) does not occur but biotites may contain small lenses of quartz lying along cleavage planes. These elongate biotites may have a close spatial relationship with more equant kinked biotites (Figs. 4.113, 4.114), and offshoots of iron oxides may occur parallel to S_3. It is the large scale development of these elongate biotites which leads to the recognition of a biotite defined schistosity in Fig. 4.109.

Deformation Mechanisms

The alteration of biotite to muscovite and iron oxides in the D_3 event indicates that biotite parallelism to S_3 is not a growth feature, but is a result of deformation. Two groups of processes can be envisaged which would result in the types of deformation discussed above. The first are mass transfer processes involving diffusion (Elliott, 1973). Simple corrosion of biotites would result in the formation of biotites elongate across (001), without any rotation of the crystal lattice. The second group of deformation processes involve the rotation of biotites, either by homogeneous glide on (001) or by heterogeneous slip (kinking). Homogeneous glide on (001) will result in the formation of biotites elongate across (001) and is supported by the presence of stepped margins on elongate biotites. Rotation of biotites by kinking can also re-orient biotite grains into an orientation close to S_3, especially when there has been annealing or kink boundary gliding. The local formation of quartz slivers along cleavage planes suggests

that there has been a phase of brittle deformation and moving apart of (001) planes.

4.5.2.4 Microfolding and the Development of a Long Limb Schistosity

The long limb schistosity, S_3', occurs just west of the Mt.Franks Retrograde Schist Zone in psammopelites of the Apollyon andalusite schist and of the Mt Franks facies of the Robe Beds. The progressive development of S_3' as a penetrative surface formed in D_3, yet inclined at an angle to S_3, defined by axial planes of F_3 folds and by alignment of sericite laths, is best seen along the northern ridge of Mt Franks itself. Mesoscopic features of this schistosity (Section 3.5.2.2) indicated that:

1) S_3' develops by the alignment of long limbs of asymmetrical crenulations and is enhanced by the coalescence of short limbs,

2) these asymmetrical crenulations probably develop from low amplitude more symmetrical crenulations, and

3) S_3' rotates towards S_3 as defined by axial surfaces to F_3 crenulations.

The progressive development of S_3', discussed below on a microscopic scale with reference to representative shadowmaster* sketches (Figs. 4.115-4.122), is equated with increasing strain as measured by the rotation of long limbs. In all cases, the crenulated surface, S_1, is a layered anastomosing schistosity which consists of M layers (dashed areas, Fig. 4.115) and QM layers (blank areas, Fig. 4.115).

Low strain, open F_3 crenulations in S_1 dominate most of Fig. 4.115, and are best defined by the shape of M layers. Crenulations are both symmetrical and gently asymmetrical in shape, and are characterised by limbs of similar length. Hinge zones are generally poorly defined and there is

---

* All figures illustrate sections looking southwest, and are cut perpendicular to $S_1 \wedge S_3$. Development of S_3' from S_1 involves rotation of S_1 from westerly dipping orientation into new (S_3') subvertical orientation.

considerable variation in the orientation of axial surfaces. Muscovite laths within M layers are bent across hinge zones. By contrast, muscovite laths in QM layers are more sporadically developed and F_3 hinges are defined by changes in orientation between discrete, undeformed laths.

F_3 crenulations in the top part of Fig. 4.115 are more asymmetrical than those just described, and are characterised by well defined long limbs. Hinges of these crenulations are better defined than those discussed above, but they may be obscured by recrystallisation of muscovite either to sericite laths in clots lying parallel to S_3(Fig. 4.123) or to large (0.4 x 0.1 mm) muscovite laths aligned parallel to S_3.

At higher strains, the microfabric of these rocks is dominated by steeply inclined or subvertical M layers which represent the long limbs of highly asymmetrical crenulations (Figs. 4.116, 4.117). These limbs impart a new penetrative fabric (S_3') to the rock on a mesoscopic scale (corresponding to Fig. 3.40), despite the fact that they lie at marked angles to S_3. Hinge zones in M layers are broad with complex crenulation effects and interlimb angles are generally high (commonly about 70-90°). In addition, there is some variation in the orientation of axial surfaces to these crenulations (Fig. 4.116). There is preferential formation of crenulations in F_3 short limbs rather than in long limbs.

Short limbs and hinge zones also form sites of incipient recrystallisation of muscovite to sericite, and of quartz sub grain formation.

Although the strong development of S_3' in Fig. 4.116 is accompanied by mica recrystallisation and formation of elongate sericite clots, the development of S_3' in Fig. 4.117 is independent of widespread (re)crystallisation. Thus there is no complete alteration of andalusite to sericite aligned parallel to S_3, and no total recrystallisation of S_1 sericite with the formation of elongate clots of sericite parallel to S_3.

Another important feature which contributes to the development of S_3' is the merging of M layers in short limb orientations into a single M layer

in a long limb orientation (Fig. 4.116 Area A, B, and see also below).

Disruption of short limb or hinge area in an M layer by recrystallisation to sericite also promotes the long limb fabric (Fig. 4.124). Sericite laths formed by this recrystallisation of M layers may be in optical continuity with sericite laths in clots after andalusite and this results in a "growth" of the clots and the truncation of M layers. The role of local recrystallisation of muscovite to sericite in short limbs is clearly seen in Fig. 4.118, area A, where it is still possible to trace the outlines of relict M layers through sericite clots. Recrystallisation in these areas is independent of the preservation of wide short limbs in other areas (areas C, D, Fig. 4.118) which are characterised by S_1 enveloping surfaces lying at high angles to S_3.

The figures discussed so far serve to illustrate one important point: the restriction of small F_3 crenulations to short limbs and hinge zones of F_3 microfolds and the absence of crenulations in long limbs.

Relations between subvertical S_3' in psammopelites and west dipping S_1 in psammites (Fig. 4.119) show that S_3' formed by the alignment of long limbs of crenulations which are highly asymmetrical in psammopelites. Microscopic relations in this figure correspond to the mesoscopically continuous S_3' in Fig. 3. 41. Although forming a new penetrative surface, long limbs in Fig. 4.119 are still inclined to S_3, defined by alignment of sericite clots. However, local variations in the attitudes of F_3 axial planes mean that some of these surfaces lie parallel to S_3' (Fig. 4.119, Area A).

Although some crenulations are marked by high interlimb angles and by short limbs containing crenulated muscovite lying at high angles to S_3 (Fig. 4.119, Area B), crenulations at the top of this figure (Areas C and D), are tighter, with more sharply defined axial surfaces. As a result, S_3' in these areas lies closer in orientation to S_3. These tight hinges are characterised by three different features:

1) the truncation of M layers in short limb orientations against M layers in long limbs (Fig. 4.119, Area E). The boundary between both limbs varies from smooth to irregular and is generally parallel to the long limb. It is commonly iron stained (Fig. 4.125). Muscovite laths are not continuous across the discontinuity.

2) multiple hinge effects (Fig. 4.119, Area D, and Fig. 4.126) caused by merging of several M layers lying within F_3 short limbs into a single M layer in the adjacent long limb. Figure 4.120 shows that one such multiple hinge consists of a normal short limb/long limb progression (top of figure) coupled with an abrupt change across an iron stained discontinuity between other short limbs and the same long limb (middle and bottom of figure). Multiple hinges may also occur with or without the formation of discontinuities. In some cases, muscovite mismatch may be evident in long limbs opposite a truncated short limb.

3) complex hinge effects (not restricted to S_3' formation, but also present in crenulations discussed in Section 4.5.2.2). Hinge shapes vary from open, characterised by smoothly curved muscovites, to kinks characterised by bending of muscovite laths over narrow zones. Kink planes vary from planar to stepped across muscovite terminations, and iron oxides may lie within kink planes. "Levering-off" effects are also common. Here, muscovites are anchored within an M layer along one prism face and are separated from that layer along (001) by quartz grains.

The ultimate development of S_3' inclined to S_3 is shown in Fig. 4.121. S_3' here is defined by the alternation of QM layers with thin (0.02-0.1 mm) M layers whereas S_3 is defined by the alignment of sericite laths and by the shape alignment of sericite clots. Short limbs of F_3 folds are still present in some areas (Areas A, B, C, D); presumably others have been destroyed by the recrystallisation of muscovite to sericite as outlined above. Those short limbs still present are characterised by a high interlimb angle.

Investigation of S_3' in Section 3 indicates that S_3' becomes mesoscopically parallel to, and indistinguishable from, S_3. Microscopic investigations of this relationship (Fig. 4.122) show that S_3' is defined by anastomosing M layers which in some cases lie parallel or subparallel to S_3 defined by sericite clots. That these M layers form long limbs of asymmetrical F_3 crenulations is confirmed by the presence of relict short limbs (Fig. 4.122, Areas A, B, C), lying at high angles to S_3. Other short limbs (Fig. 4.122, Area D) show partial recrystallisation to sericite. Partial recrystallisation of quartz in QM layers occurs in short limbs.

Mechanism of Formation of S_3'.

F_3 crenulations described above are asymmetrical, consistently sinistral, kink folds rather than symmetrical kink folds (chevron folds) or kink bands. There is no evidence of their formation from intersecting conjugate kink bands (e.g. Paterson and Weiss, 1966), and they are probably best understood as forming by slip along S_1 with consequent formation of axial surfaces perpendicular to shortening direction (cf. Ramsay, 1967). The development of asymmetrical folds suggests that shortening was not layer parallel.

Qualitative inspection of Figs. 4.116-4.122 indicates that the angle between F_3 long limbs and S_3 decreases with the development of S_3'. In contrast, a high angle between F_3 short limbs and S_3 is maintained even where S_3' is well developed and lies locally parallel to S_3. Since recrystallisation phenomena are restricted to short limbs and hinge zones, changes in the angles between long limbs and S_3 must be either due to a rotation of the long limbs, or a rotation of S_3. With the exception of local variation in the orientation of S_3, large scale rotation of S_3 is invalidated by:

a) the common orientation of axial surfaces to symmetrical and asymmetrical crenulations in Fig. 4.115,

b) the absence of any tracking of S_3 rotation by sericite laths, and

c) absence of any consistent change in width of short limb with

development of S_3'. If axial planes rotate, short limbs would be expected to widen as more and more material underwent a change in orientation.

On the other hand, it is possible to observe a mesoscopic (Section 3.5.2.2) rotation of long limbs from west dipping to subvertical about a constant S_3. Thus formation of S_3' by development of long limbs, and their rotation is envisaged. Weiss (1968) noted that long limbs of his experimentally kinked cards also rotated towards perpendicularity to the compression direction while short limbs possessed a constant orientation.

Rotation of, and lack of crenulation within, long limbs contrasts with crenulate deformation in short limbs and hinge zones, and suggest that different fold limbs possess different D_3 deformation histories: long limbs probably undergo thinning by slip on (001) mica planes and undergo bulk rotation; short limbs undergo shortening by crenulation, which forms sites for new quartz growth and muscovite recrystallisation. Kink boundary sliding in this area might account for truncation of limbs in kinked muscovites.

Since strain histories are likely to have been different in different limbs, it follows that complex strain effects occur at hinge zones between them. It is in these areas that transfer of mineral components - as evidenced by truncation of fold limbs, formation of discontinuities and loss of quartz occur. These features together with formation of iron oxides within discontinuities suggests that there has been removal and deposition of material, and this is attributed to mass transfer effects.

It is thus envisaged that the formation of S_3' develops largely by the crenulation of S_1, and the bulk rotation of long limbs into perpendicularity to the shortening direction and parallelism to S_3. This rotation is aided by limited recrystallisation of muscovite and quartz in short limbs and by mass transfer of components away from hinge zones and short limbs.

Fig. 4.1 Schematic illustration of S_1/pre-S_1 relations in different rock types (S_1 everywhere vertical).

A. Apollyon quartz-mica schist.
Homogeneous to layered S_1. Crenulates early schistosity and wraps around early porphyroblast preserving early mineral fabric.

B. Apollyon carbonaceous schist.
Homogeneous to layered S_1 which wraps around porphyroblasts and kinked early biotites. Graphite laths define laminations parallel to S_0.

C. Apollyon chiastolite schist.
S_1 refracted across S_0. In central pelite, a homogeneous S_1 wraps around porphyroblasts with internal structures and is axial planar to kinked biotites. In psammites, S_1 wraps around porphyroblasts with internal fabrics and contains irregularly shaped biotites.

D. Robe andalusite schist - S_{1N} rocks.
S_1 is layered, consisting of mica (M) and quartz-mica (QM) domains. S_1 wraps around earlier porphyroblast with internal fabrics, crenulates an earlier fabric and lies axial planar to kinked biotites.

E. Robe andalusite schist - S_{1P} rocks.
Similar to above, except that M domains are dominated by kinked biotites and biotite aggregates rotated or corroded into S_1.

F. Robe sillimanite schist - S_{1P} rocks.
Similar to E. Porphyroblasts preserve an early fabric, a crenulated early fabric is visible in QM domains and M domains consist of strongly deformed early biotite. Early fibrolite is also deformed.

A

B

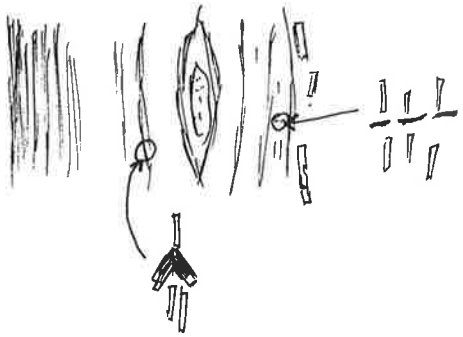

C

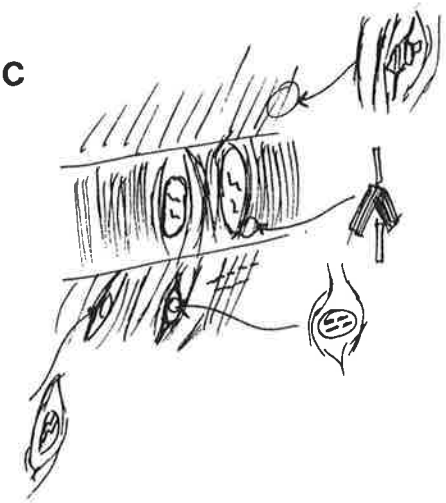

D

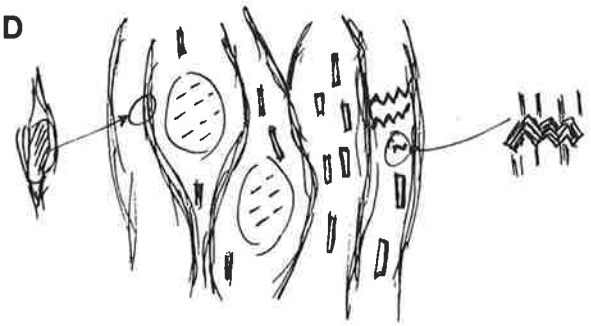

E

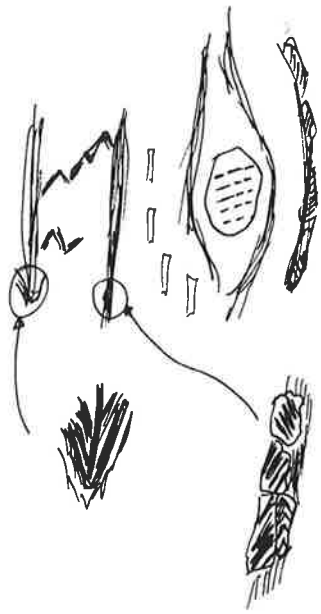

F

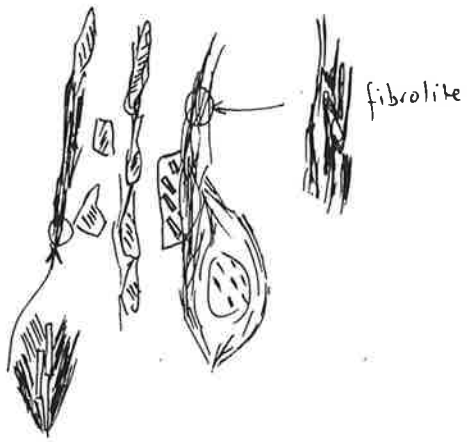

PRE-S_1 FABRICS

Fig. 4.2 (left) Part of green lineated mineral aggregate in Apollyon quartz-mica schist. A vertical early pre-S_1 fabric, outlined by kinked biotites is crenulated about an horizontal S_1. Muscovite laths define S_1 and are also mimetic after biotite.
Specimen 882, normal to S_1 and L_1.
PPL, length of side 0.9 mm.

Fig. 4.3 (right) Segregated S_1 (vertical) defined by heavily iron stained M domains. QM domains consist of thin stringers of anastomosing mica parallel to S_1 and an early crenulated pre-S_1 fabric defined by mica laths.
Specimen 1075, normal to S_1.
PPL, base of figure 0.6 mm.

Fig. 4.4 (left) S_1 (horizontal) and domainal overprints crenulated sericite (vertical) which defines an early fabric. Sericite pseudomorphous after andalusite. Black minerals are ?ilmenites.
Specimen 753.
PPL, base of figure 0.6 mm.

Fig. 4.5 (left) Sericite clot after andalusite showing early fabric crenulated about S_1.
Specimen 3591.
Sketch from photo.


S_1


S_1

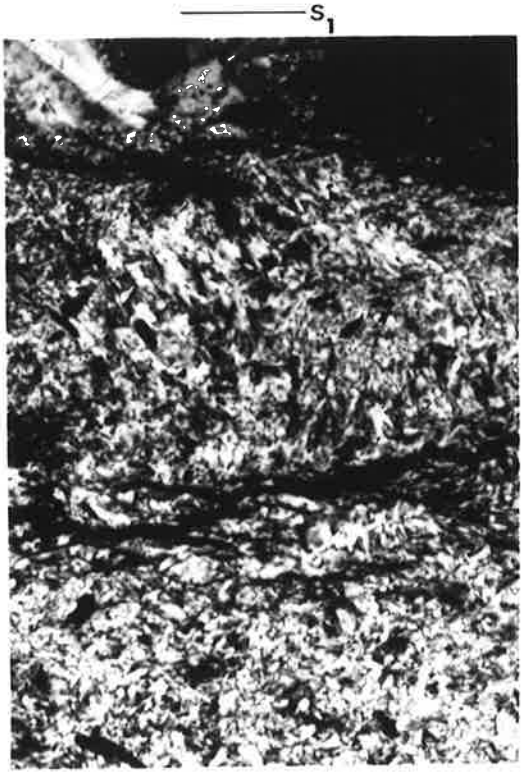
S_1


S_1
0·1 mm

PRE-S_1 MICROFABRICS

Fig. 4.6a (left) Shadowmaster sketch of bedding defined by accumulation of andalusite crystals. Within these crystals ?ilmenite trails define an internal fabric, the orientation of which lies parallel to S_0.
Bar scale 2 mm.
Specimen 1667.

Fig. 4.6b (right) Detail of andalusite, showing fold in ?ilmenite fabric aligned to S_1.
Bar scale 2 mm.
Specimen 1667.

Fig. 4.6c (right) Detail of andalusite, showing a shear zone within a crystal defined by ?ilmenite rods.
Bar scale 1 mm.
Specimen 1667.

Fig. 4.7 (left) Retrogressed andalusite porphyroblast with internal fabric aligned parallel to S_0 graphite lamination and defined by wispy biotite laths (dark grey). Pressure shadows flank porphroblast.
Specimen 843, normal to S_1.
PPL, length of side 1.4 mm.

Fig. 4.8 (right) Shadowmaster sketch of retrogressed porphyroblast showing rotated biotites (black). Marginal biotites lie parallel to biotites (blank in groundmass). Note quartz pressure shadows and domainal S_1 (left hand side) with muscovites in QM domain aligned to muscovites in M domain.
Specimen 843, normal to S_1.
Bar scale 1 mm.

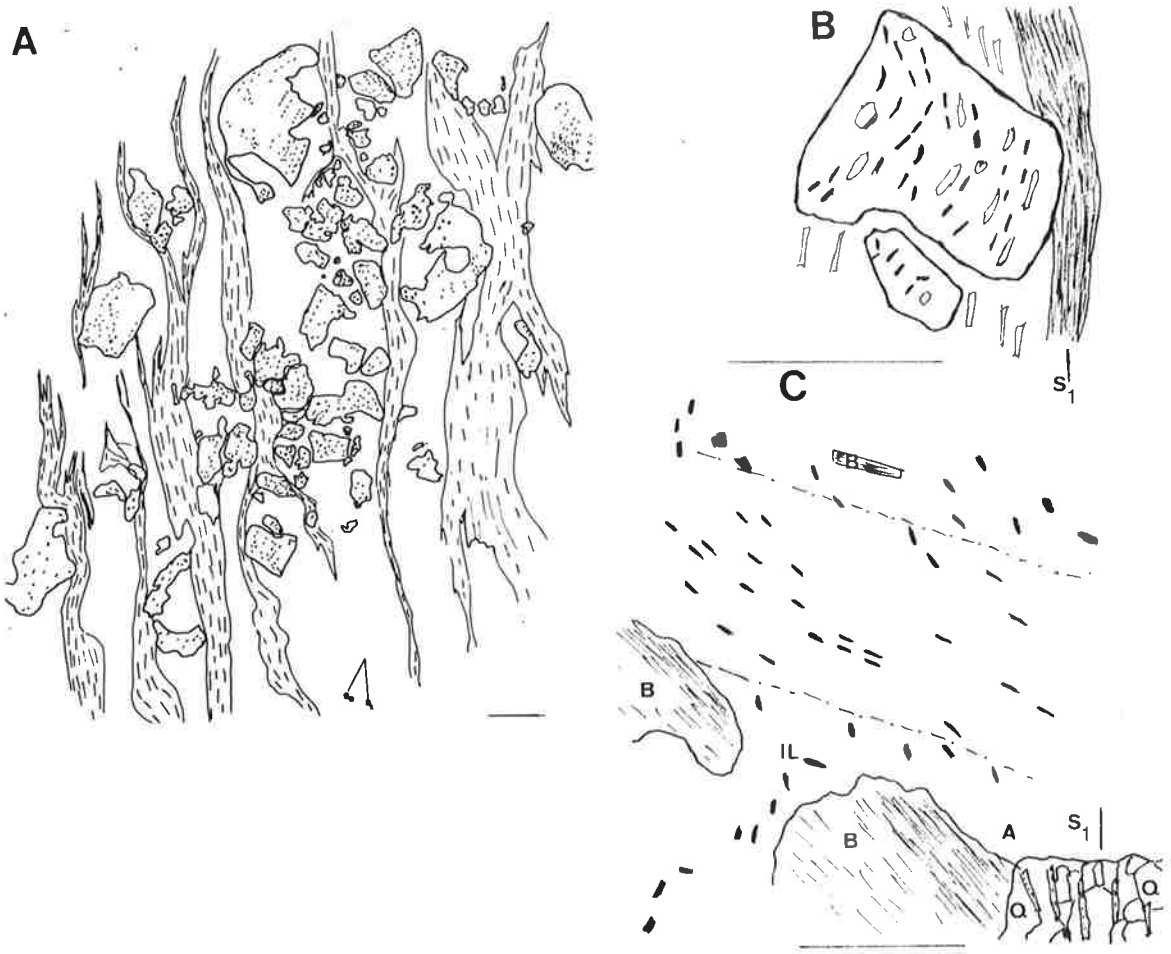
A
B
S_1
C
B
IL
B
A
S_1
a
a

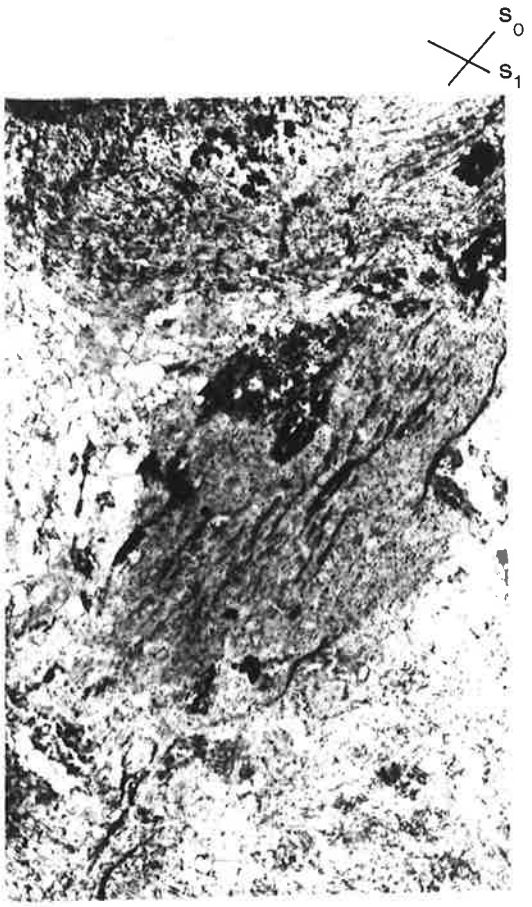
S_0
S_1

Fig. 4.10a Cracked and extended andalusite with S_1 muscovite growing in crack. Robe andalusite schist.
Specimen 1667, normal to S_1.
Sketched from photo. Bar scale 1 mm.

Fig. 4.10b Apollyon chiastolite schist. Internal biotite fabric preserved within retrograde andalusites. Note parallelism of orientation between adjacent porphyroblasts.
Specimen 843, normal to S_1.
Sketched from photo. Bar scale 1 mm.

Fig. 4.10c Apollyon chiastolite schist. Biotite fabric preserved within retrogressed chiastolite.
Specimen 843, normal to S_1.
PPL, base 2.7 mm.

Fig. 4.10d Biotite laths defining an early pre-S_1 fabric preserved in QM domain of S_1 fabric. M domains consist of biotite kink aggregates and muscovite.
Specimen 563, normal to S_1.
Sketched from photo. Bar scale 0.5 mm.

Fig. 4.10e Graphite trains define a bedding lamination. S_1 refracted across lamination and crenulates early sericite fabric. Apollyon chiastolite schist.
Specimen 843, normal to S_1.
Sketched from photo. Bar scale 1 mm.

Fig. 4.10f Pre-S_1 white micas marginal to black biotite and kinked about S_1. Apollyon chiastolite schist.
Specimen 843, normal to S_1.
XN, base 0.6 mm.

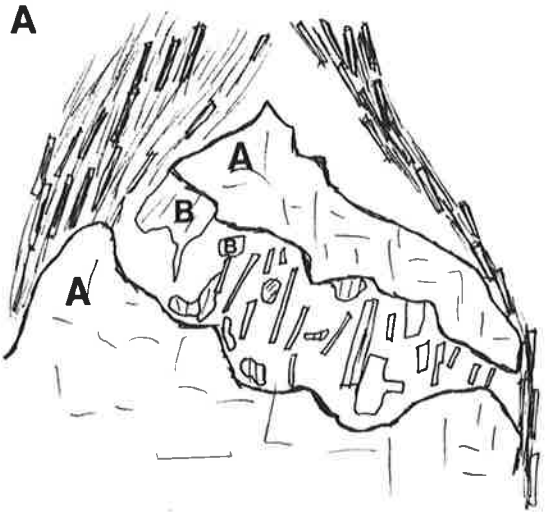
A
A
B
B
A

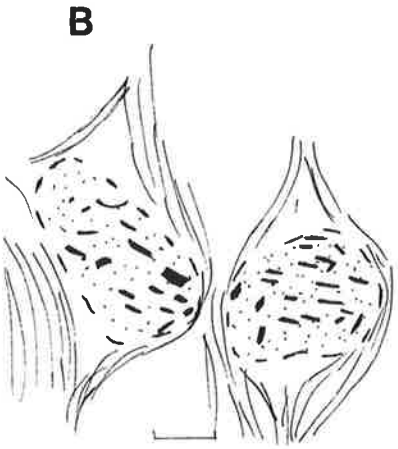
B

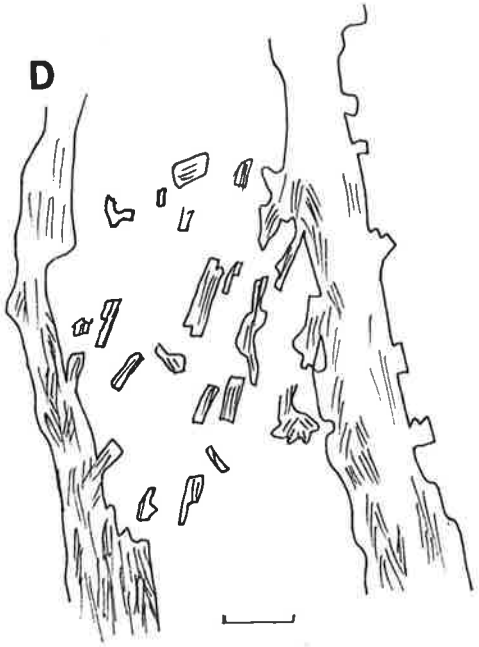
D

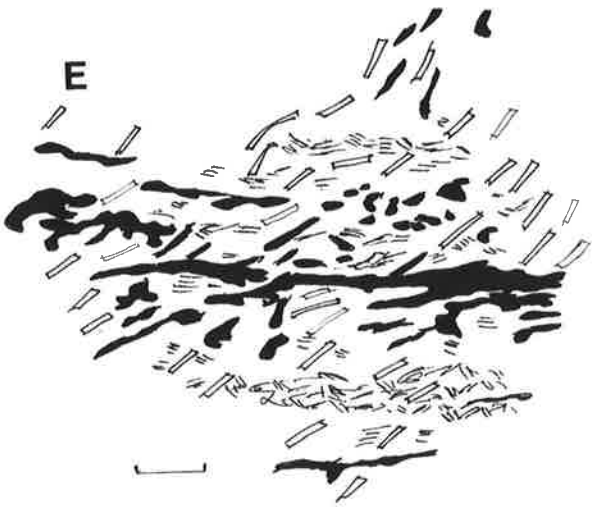
E

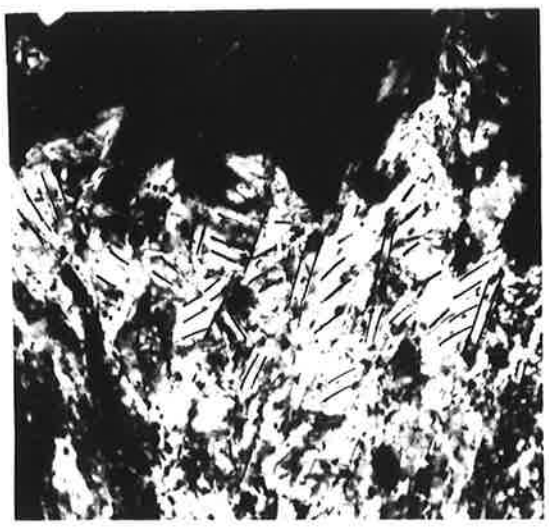

PRE-D_1 BIOTITES

Fig. 4.9 (left) Planar biotite lamination (parallel to S_0) showing random cleavage traces (outlined in white).
Specimen 817, normal to S_1.
PPL, length of side 7.5 mm.

Fig. 4.11 (right) Shadowmaster sketch of folded biotite laminations and detail of F_1 kinks in biotite.
Specimen 3911, normal to F_1.
bar scale 1 mm.

Fig. 4.12a (left) Biotite aggregates defining a pre-S_1 fabric in QM layer. This orientation lies at an angle to S_1, defined by biotite bands, and is crenulated about S_1.
Specimen 563, normal to S_1.
PPL, base 2.5 mm.

Fig. 4.12b (right) Stack of kinked and annealed biotite grains with muscovite laths lying in axial surface position.
Specimen 2012, normal to F_1.
PPL, length of side 1 mm.

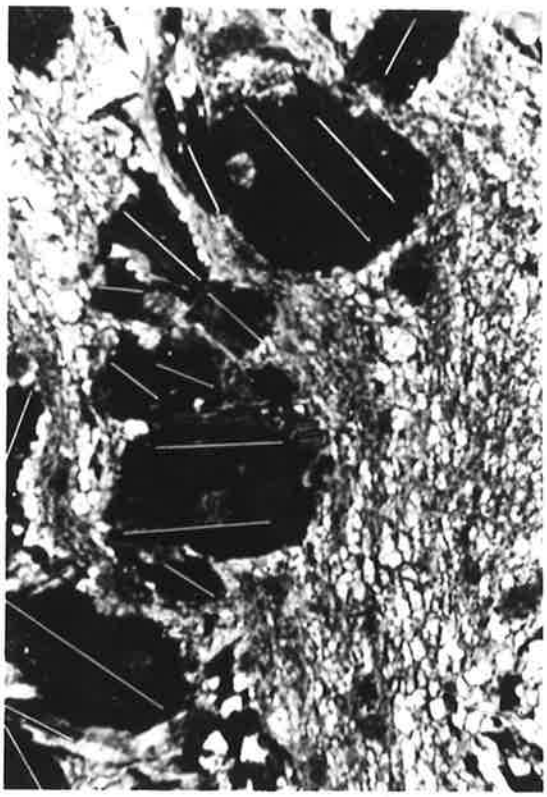

S_1

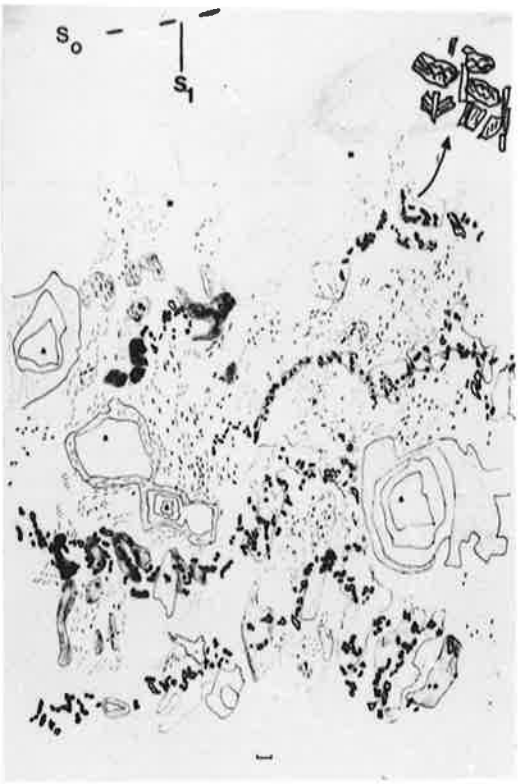

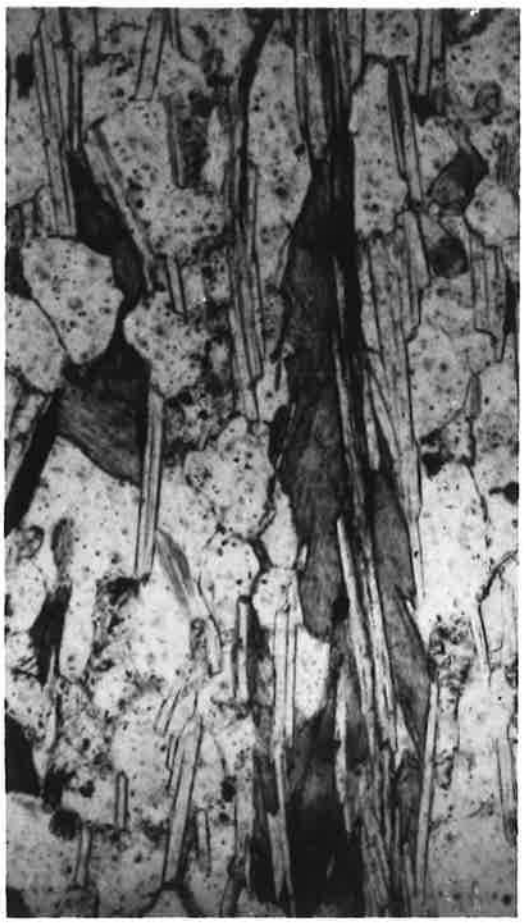

PRE-S_1 MINERAL PREFERRED ORIENTATION IN S_{1P} ROCKS

Fig. 4.13 (left) The vertical mica rich band defining S_1 here consists of biotites with crossing cleavage traces. These are interpreted as kinked pre-S_1 biotites which have sufferred kink boundary migration.
Specimen 4177.
PPL, base 2.5 mm.

Fig. 4.14 (right) Retrogressed andalusite and adjacent QM domain. Although the andalusite has altered to sericite, the internal biotite fabric is still preserved and lies at an angle to S_1, defined by biotites in the groundmass.
Specimen 4175.
PPL, base 2.5 mm.

Fig. 4.15 (left) M and QM domains in S_1. M domains consist of white mica and biotite; QM domains consist of quartz, biotite and retrogressed feldspar. In area A, biotites define an early preferred orientation and have been kinked about S_1 and annealed.
Specimen 3109.
PPL, base 2.5 mm.

Fig. 4.16 (right) Part of fibrolite clot showing interpreted F_1 folds.
Specimen 3140.
XN, base 2.5 mm.


S1

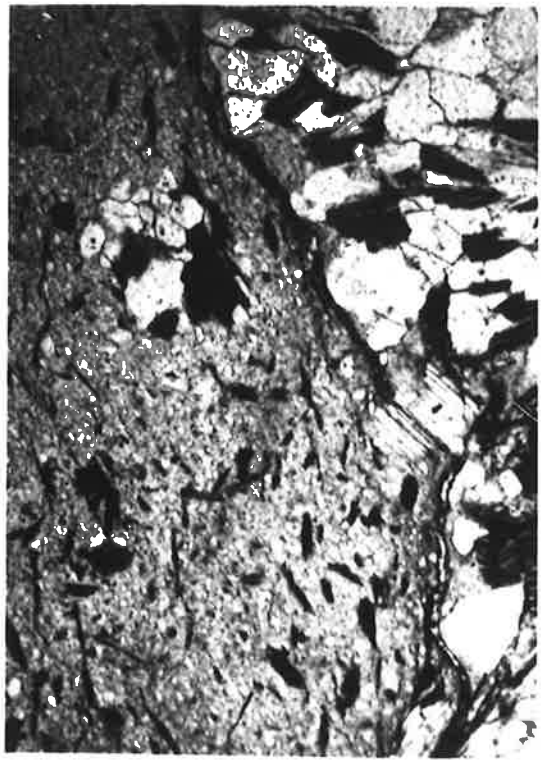
S1

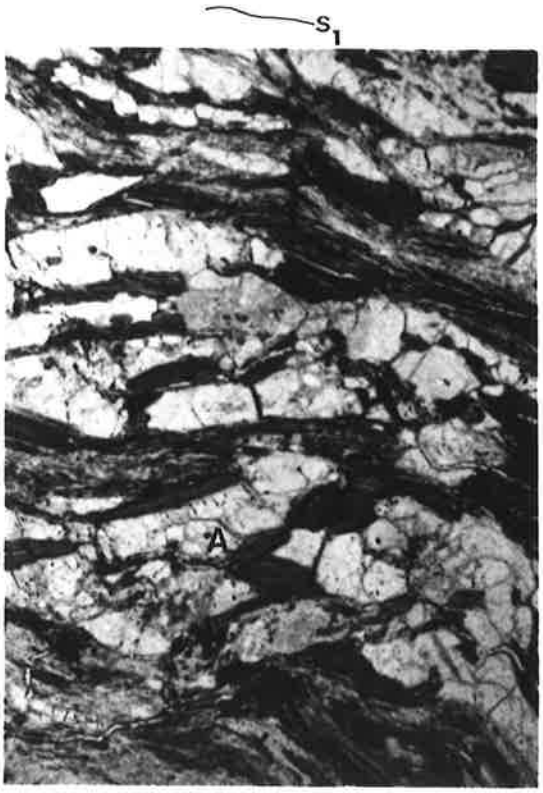
S1
A


S1

ANDALUSITE--SILLIMANITE TRANSITION

Figs. 4.17 - 4.19

Fig. 4.17 (left) Mineral clot of andalusite + sericite. Part of retrogressed andalusite with groundmass S_1 just visible in bottom left hand corner. Small squares of andalusite (A, dark mineral) surrounded by sericite occupy top of figure. Lower part of porphyroblast contains sericite (S) only.
Specimen 3061.
XN, base 7.5 mm.

Fig. 4.18 (right) Mineral clot of andalusite + sericite + fibrolitic sillimanite. Andalusite (A) surrounded by sericite occupies lower part of porphyroblast. Upper part is occupied by laths of sericite which surround a patch of fibrolite (F) elongate parallel to S_1.
Specimen 3061.
XN, base 3 mm.

Fig. 4.19 (left) Mineral clot of sericite + fibrolitic sillimanite. Sericite (S) totally surrounds a pod of fibrolite (F) within this clot. Fibrolite outlines a swirling pattern and is probably folded about S_1 with some fibrolite aligned parallel to S_1.
Specimen 3061.
XN, base 3 mm.

Fig. 4.20 (right) Aggregate of sillimanite needles in F_1 fold. Needles are bent in the hinge and some sillimanite lying parallel to S_1 in the centre of the fold (circled) has probably recrystallised from pre-S_1 sillimanite.
Specimen 4022.
XN, base 1.8 mm.

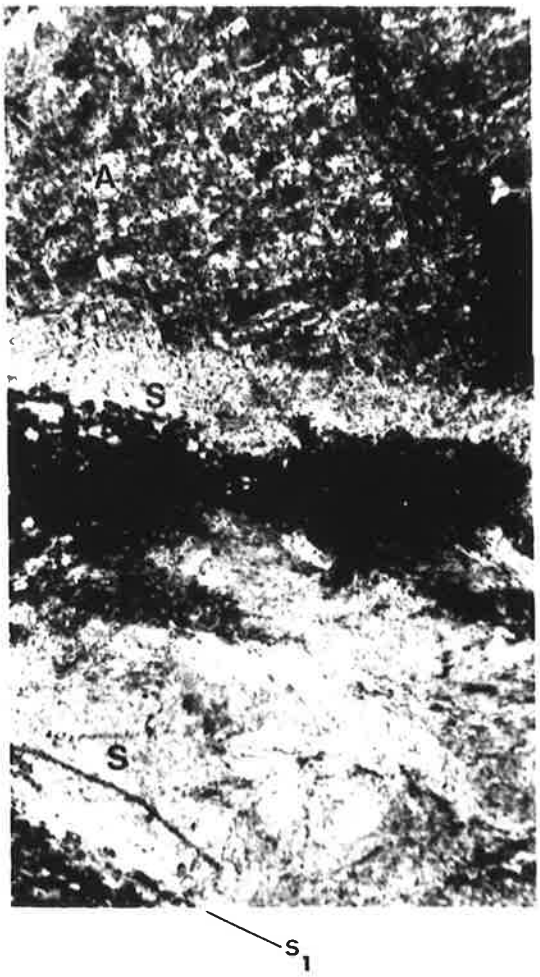
A
S
S
S1


F
A
S1


S1
F
S


S1

PRE-S_1 MINERAL PREFERRED ORIENTATION IN S_{1P} ROCKS

Fig. 4.21 (left) Kinked biotites and annealed kinks in pre-S_1 fabric folded about S_1. S_1 defined by laths of muscovite, opaques and slivers of biotite. Pre-S_1 fabric outlined by biotite and enhanced by some mimetic alteration to muscovite, resulting in light and dark striping.
Specimen 4175.
PPL, base 2.5 mm.

Fig. 4.22 (right) Early mineral preferred orientation preserved as short limb of F_1 microfold. The pre-S_1 fabric is defined by biotite and is seen in QM layer of S_1 fabric. M layer of S_1 fabric corresponds to high strain limb area of microfold and consists of tightly kinked and annealed biotites.
Specimen 3140.
PPL, base 2.2 mm.

Fig. 4.23 (left) Early mineral preferred orientation in S_1 QM layer is preserved by kinked and annealed biotites.
Specimen 4124.
PPL, base 2 mm.

Fig. 4.24 (right) Biotite inclusions within M_1 K feldspar (microcline) preserve an undeformed pre-S_1 mineral orientation at angles to S_1. Elsewhere, this evidence for early orientation is destroyed by D_1 rotation and corrosion of early biotites.
Specimen 4022.
XN, base 2 mm.

S_1

S_1

S_1

S_1

S_1 - LOW GRADE ROCKS

Fig. 4.25 S_1 oriented diagonally across figure is statistically defined by poor alignment of irregular shaped muscovite laths and equant-elongate quartz grains. Apollyon quartz-mica schist.
Specimen 882, normal to S_1.
XN, length of side 1 mm.

Fig. 4.26 Domainal S_1 defined by irregular narrow iron stained mica domains, which alternate with quartz rich domains. Apollyon carbonaceous schist.
Specimen 3912.
PPL, length of side 0.8 mm.

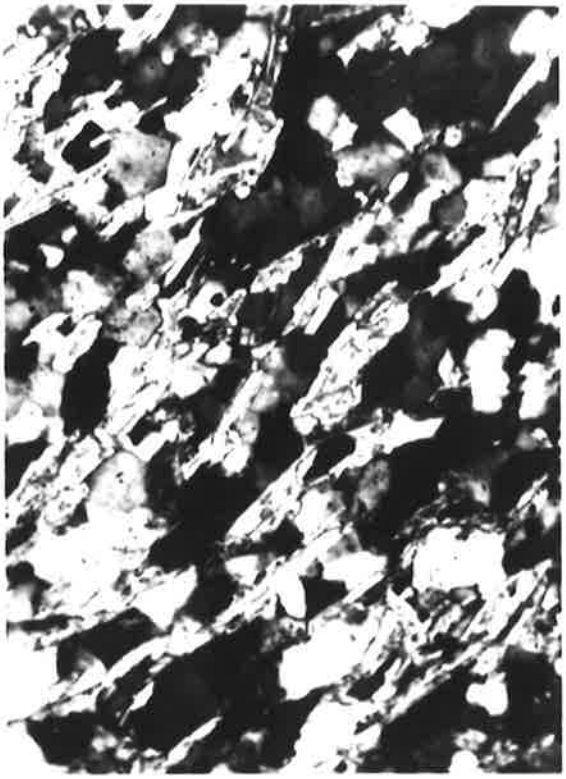

S_1 MICROFABRIC, APOLLYON CHIASTOLITE SCHIST (S_{1N})

Fig. 4.27 Negative print showing total S_1 microfabric in Apollyon chiastolite schist. S_1 is refracted across a central pelite defined by the concentration of andalusites (black) which are enveloped by biotite (white) and muscovite (white). Surrounding psammites contain biotites (white) and some andalusite spots.
Specimen 843, normal to F_1.
x $1\frac{1}{2}$.

Fig. 4.27a S_1 microfabric in pelite. Muscovite bands containing altered biotites (black) envelop sericitised andalusites elongate in S_1. Internal biotite structure still visible in andalusites.
Base 7.5 mm.

Fig. 4.27b Detail from above showing orientation of muscovite laths. Note orientation due to mimetic alteration of biotite (B). Graphite (G) present in S_1.
Bar scale 0.5 mm.

Fig. 4.27c Domain 1. Equant polygonal quartz grains with 120° triple point junctions.
XN, base 0.5 mm.

Fig. 4.27d Domain 2. Elongate, lozenge shape quartz and graphite defining S_1. Note the lack of intense quartz deformation.
XN, base 0.75 mm.

Fig. 4.27e Domain 3. Equant-elongate quartz + poorly oriented muscovite along quartz/quartz boundaries.
XN, base 0.75 mm.

Fig. 4.27f Rf/Ø plot for previous figure, showing scatter of points.

Fig. 4.27g Domain 4. Elongate quartz grains, with a well defined muscovite schistosity.
XN, base 0.75 mm.

Fig. 4.27h Rf/Ø plot for previous figure. Concentration of points much better than for domain 3.

Fig. 4.27i Domain 5, consisting of muscovite, some quartz and graphite. Note interleaving of muscovite laths.
XN, base 0.6 mm.

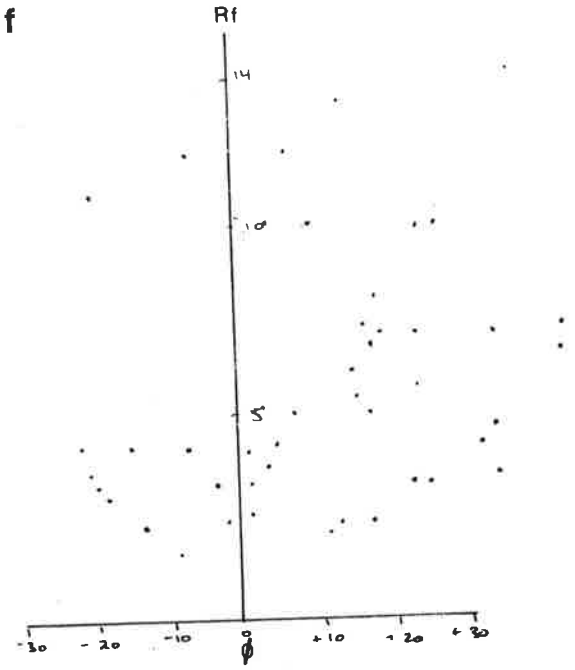
f
Rf
14
10
5
-30
-20
-10
0
+10
+20
+30
ϕ


g

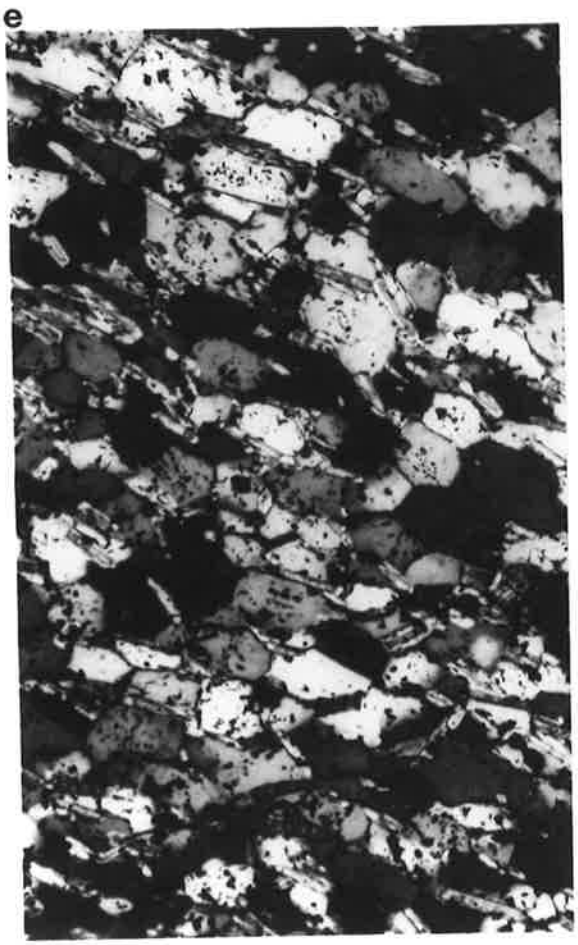
e

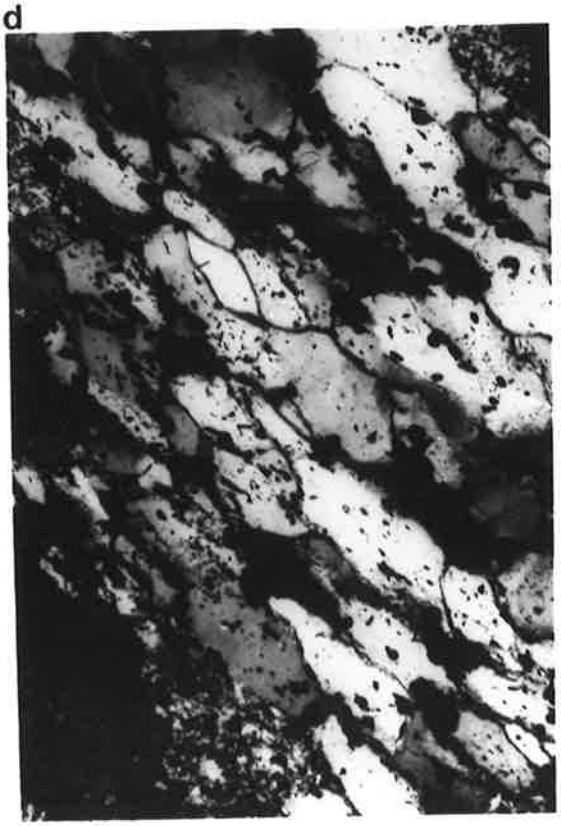
d

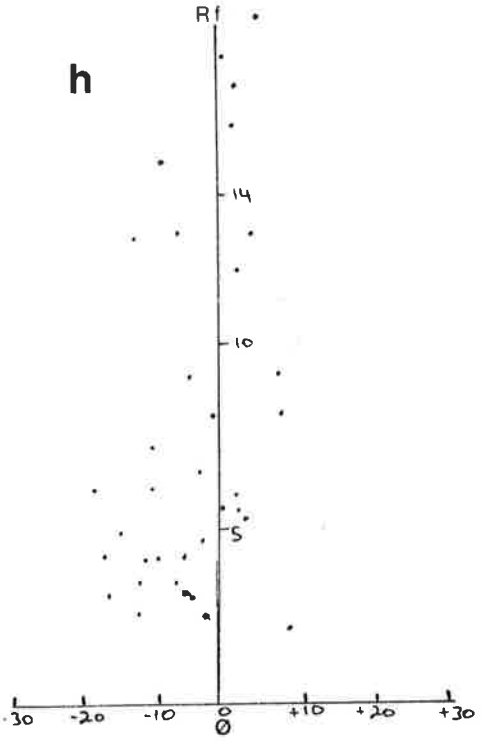
h
Rf
14
10
5
-30
-20
-10
0
Ø
+10
+20
+30

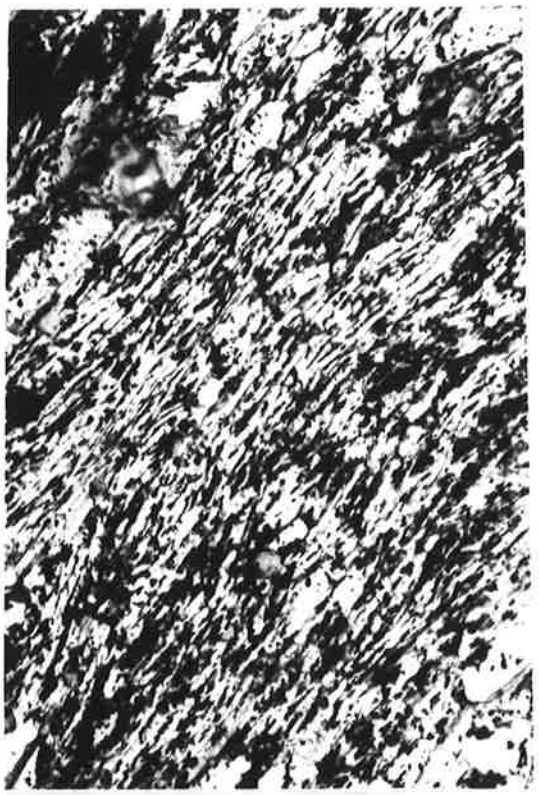
i


a

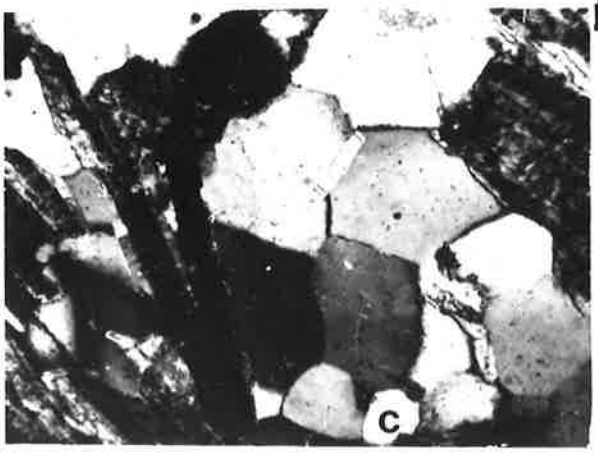
c

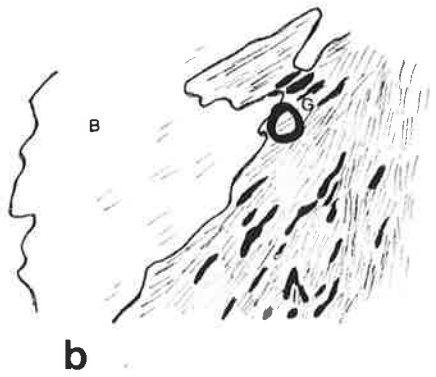
B
b

S_1 - MEDIUM GRADE ROCKS

Fig. 4.28 (left) Pseudomorphic alteration of biotite (black) by iron oxides, and formation of iron oxide tails in S_1. Surrounded by domain type 4.
Specimen 843, chiastolite schist.
PPL, base 1.5 mm.

Fig. 4.29 (right) Formation of segregated S_1 by alternation of domain 5 with domain 3. Note poor muscovite parallelism in domain 3 on right hand side, and equant quartz grains. Black object at top of figure is old biotite.
Specimen 811, chiastolite schist.
PPL, base 0.75 mm.

Fig. 4.30 (left) Folded biotite lamination (S_0) and axial planar S_1. Lamination consisted of continuous biotite grains, partly pseudomorphed to chlorite (light grey) in D_3 time. Note narrow bands of biotite elongate in S_1, and moulded on by muscovite.
Specimen 2012, andalusite schist.
PPL, base 7.5 mm.

Fig. 4.31 (right) Domainal S_1, defined by quartz + muscovite domains, and muscovite domains. In QM domain, muscovites lie along quartz-quartz boundaries. In left hand M domain, muscovites are moulded on biotite and iron oxides which are pseudomorphous after biotite.
Specimen 75.
PPL, base 0.75 mm.

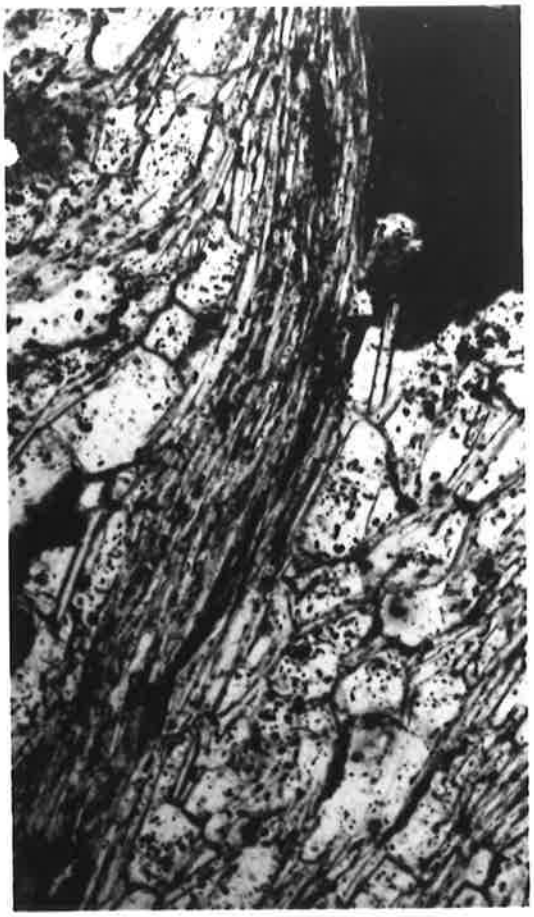

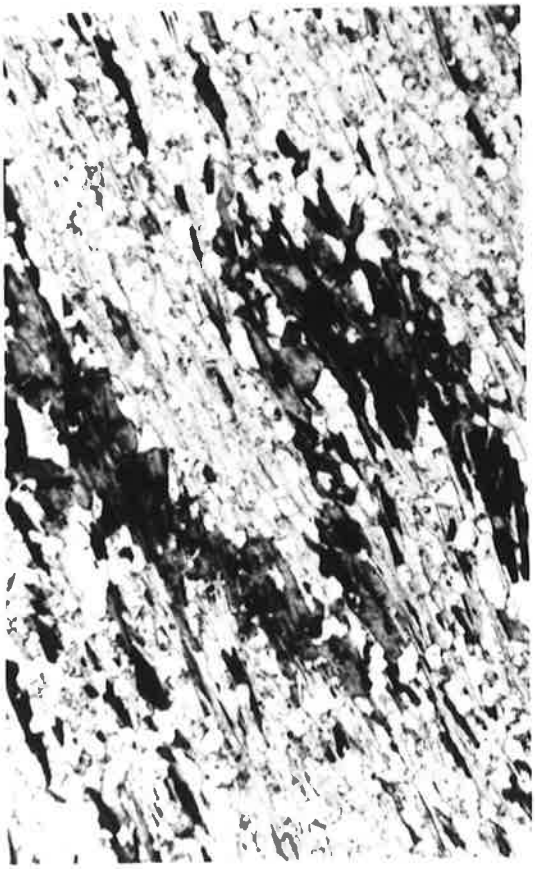

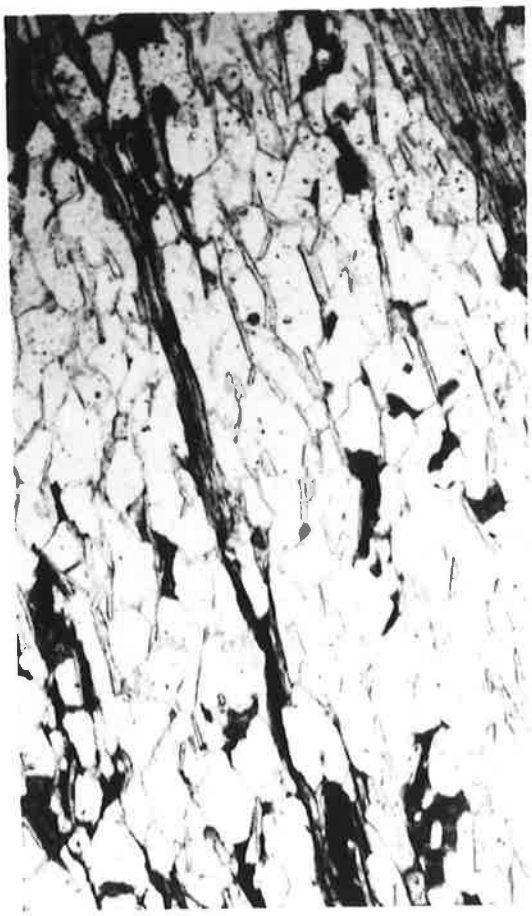

S_1 MICROFABRIC, ROBE ANDALUSITE SCHIST (S_{1N})

Fig. 4.32 Total microfabric, pelite (upper) and psammite (lower). The difference in S_1 orientation between beds here is due to F_3 rotation. S_0 dashed line.
Specimen 232, normal to F_3. PPL xI

Fig. 4.32a Homogeneous S_1, psammite.
Base 0.75 mm.

Fig. 4.32b Domainal S_1, psammite. Note change in shape of biotites between QM and M domains, and polygonal quartz aggregates in QM domain.
PPL, length of side 1 mm.

Fig. 4.32c Domainal S_1, psammite. M domains here dominated by biotite kinked aggregates with minimal muscovite.
PPL, base 1.8 mm.

Fig. 4.32d M domain in psammopelite showing elongate quartz grains (compare with quartz in Fig. 4.32f) and interleaved muscovites.
XN, length of side 1 mm.

Fig. 4.32e M domain in psammopelite showing ragged nature of biotites. These are elongate across (001).
PPL, length of side 1 mm.

Fig. 4.32f QM domain in psammopelite showing impersistent M layering and equant to elongate quartz. Biotite also present.
PPL, base 1.8 mm.

Fig. 4.32g QM domain in psammopelite. Change in shape and orientation of muscovites between mica bands and quartz rich areas is apparent.
Shadowmaster sketch.
Bar scale 1 mm.

f

g

e

d

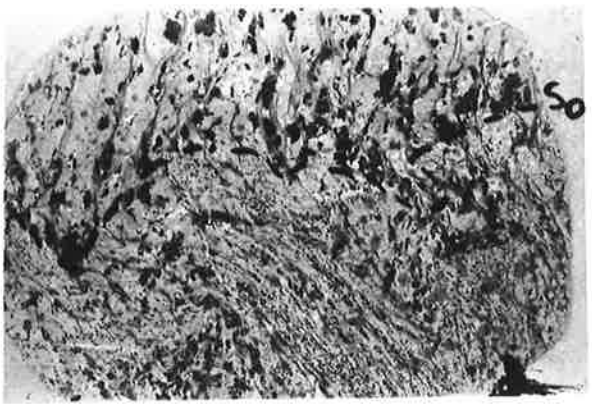
So

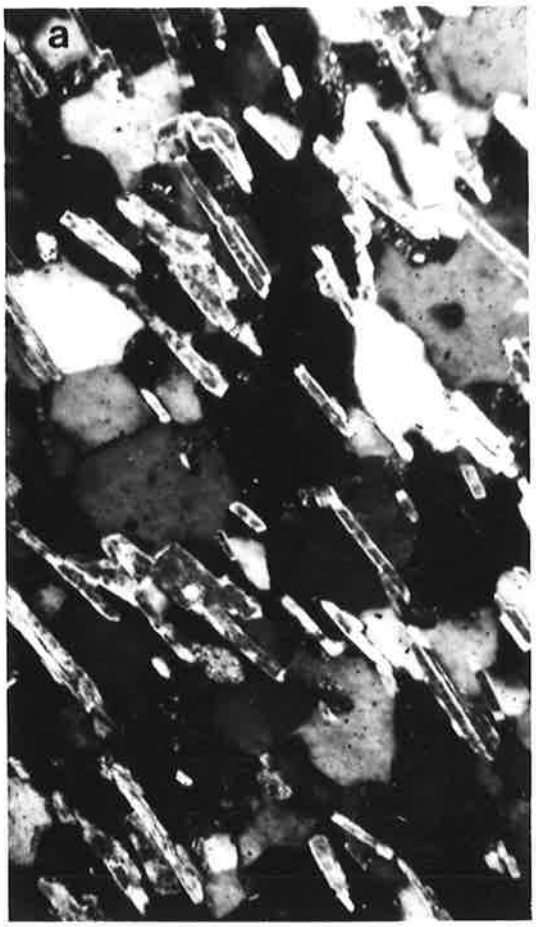
a

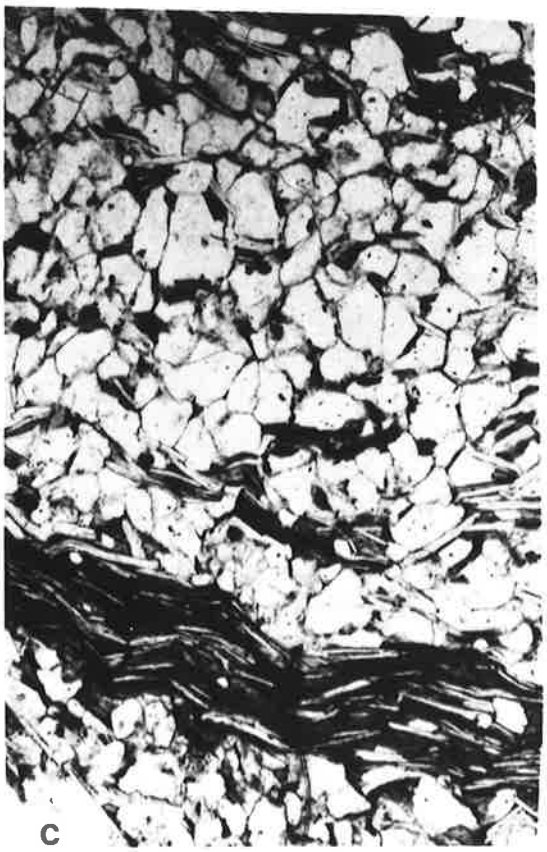
c


b

S_1 MICROFABRIC, ROBE ANDALUSITE SCHIST (S_{1P})

Fig. 4.33 Total microfabric showing S_1 in pelite (upper) and psammite (lower). Negative print so biotite occurs as white minerals in psammite where some laminations are cross bedded. White mica seen in pelite. Andalusite-sericite porphyroblasts in pelite are black with white biotite inclusions. F_3 folds clearly visible in pelite.
Specimen 4177, normal to F_3.
x 1.

Fig. 4.33a Domainal microfabric in psammite. M domains consist of kinked biotite aggregates, QM domains consist of biotite, quartz and sericite after feldspar.
PPL, length of side 3 mm.

Fig. 4.33b Enlargement of biotite aggregates in previous figure.
PPL, length of base 0.2 mm.

Fig. 4.33c Detail of muscovite band in pelite. Iron oxides have been cracked and pulled apart in S_1. Note that in biotite poor areas, M domains are muscovite rich.
PPL, length of base 0.5 mm.

Fig. 4.33d Detail of microfabric of sericite clot after andalusite. Sericite laths are aligned parallel to S_1 (top right to bottom left).
XN, base 1.8 mm.

Fig. 4.33 (inset) Microfabric in pelite. S_1 defined by muscovite laths, and the shape orientation of quartz and biotite.
Specimen 1614.
PPL, length of base 2 mm.

c

d

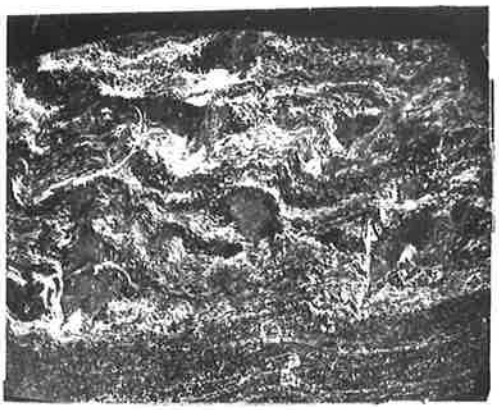

b

a

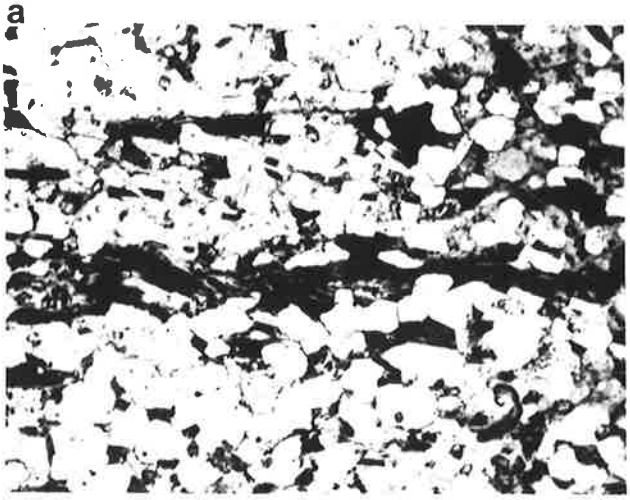

S_1 HIGH GRADE ROCKS

Fig. 4.34 (left) Shadowmaster sketch of S_1 microfabric in psammites defined by iron oxide stringers joining irregularly shaped biotite aggregates.
Specimen 3110, normal to S_1.
Bar scale 1 mm.

Fig. 4.35 (right) Pre-S_1 biotites oriented at high angle to S_1 (vertical) and overprinted by S_1 biotites.
Psammite, Robe Beds.
Specimen 3769, normal to S_1.
PPL, base 3 mm.

Fig. 4.36 (left) S_1 microfabric of psammopelite is domainal. M domains consist of biotite aggregates and minor muscovite; QM domains consist of variably oriented biotites (commonly sub parallel to S_1), quartz and sericite after feldspar.
Specimen 3061, normal to S_1.
PPL, base 3 mm.

Fig. 4.37 (right) S_1 horizontal. Randomly oriented aggregates of undeformed biotite laths.
Specimen 4022, normal to S_1.
XN, base 1.8 mm.

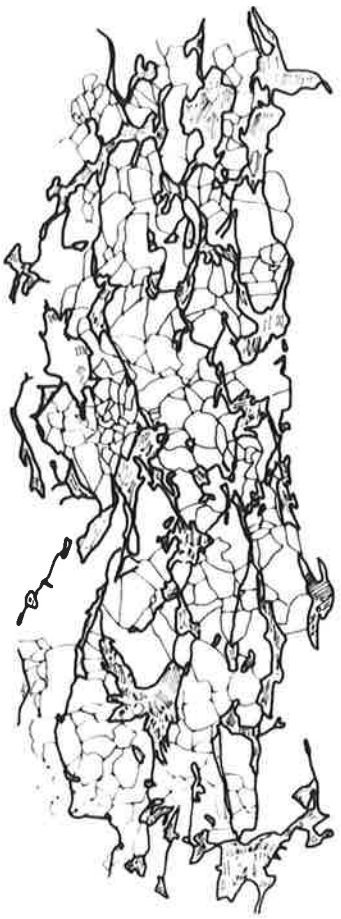

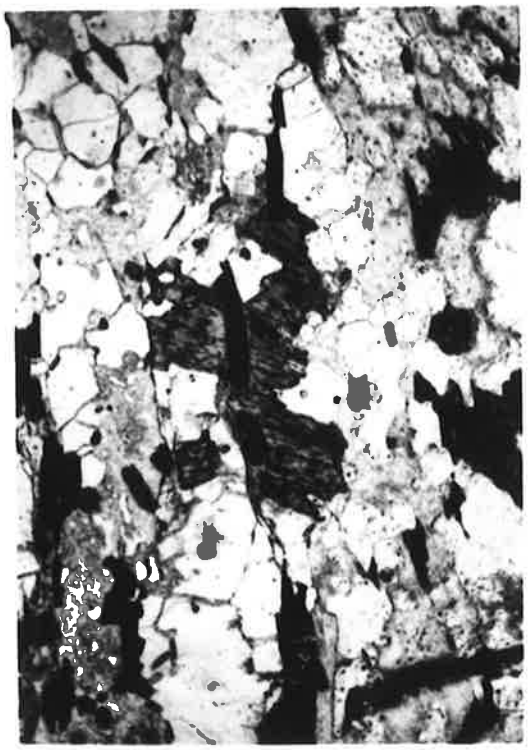

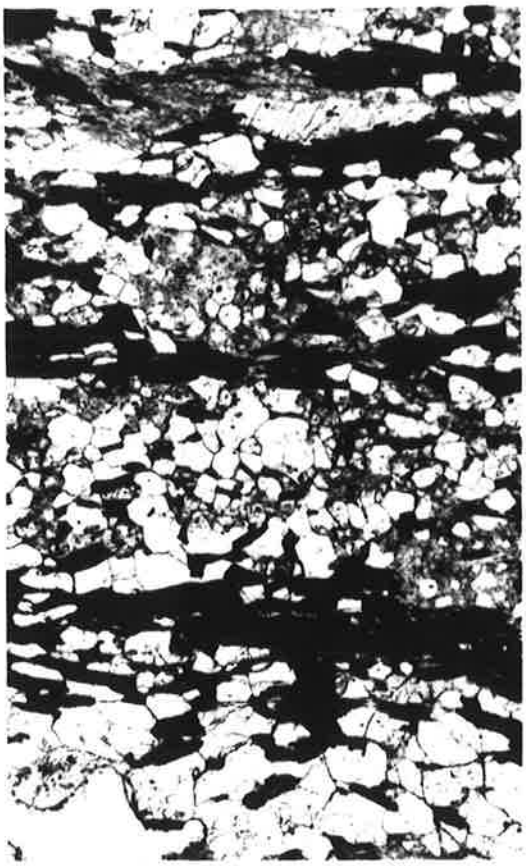

S_1 SILLIMANITE

Fig. 4.38a (left) S_1 defined by alternating bands of biotite kink aggregates and sillimanite needles. Needles themselves commonly fan about S_1.
Specimen 3140, normal to S_1.
PPL, base 0.75 mm.

Fig. 4.38b (right) Sillimanite - biotite relationships. Sillimanite needles lie parallel to S_1 except where associated with biotite grains.
Specimen 40221, normal to S_1.
PPL, base 0.6 mm.

Fig. 4.38c (left) Sillimanite needles in basal biotite. Two directions of sillimanite growth (parallel to black lines) lie at about equal angles to S_1 in the groundmass.
Specimen 4022, normal to S_1.
PPL, base of photo 0.3 mm.

Fig. 4.39 Fibrolite aggregates parallel to S_1 and overprinting early sericite laths crenulated about S_1.
Specimen 3061, normal to S_1.
XN, base 0.75 mm.


S_1


S_1


S_1


S_1

Fig. 4.40 Microperthite with inclusion trail of biotites aligned parallel to S_1 muscovites (subvertical - left side of figure).
Specimen 4022, normal to S_1.
XN, base 0.75 mm.

Fig. 4.41a S_1 showing both parallel and non parallel relations with S_0.
Specimen 3976-14, normal to F_3.
XN, x $1\frac{1}{2}$.

Fig. 4.41b Sketch of thin section showing both parallel and non parallel relations to F_3.
Specimen 3976-7, normal to F_3.
x 1.

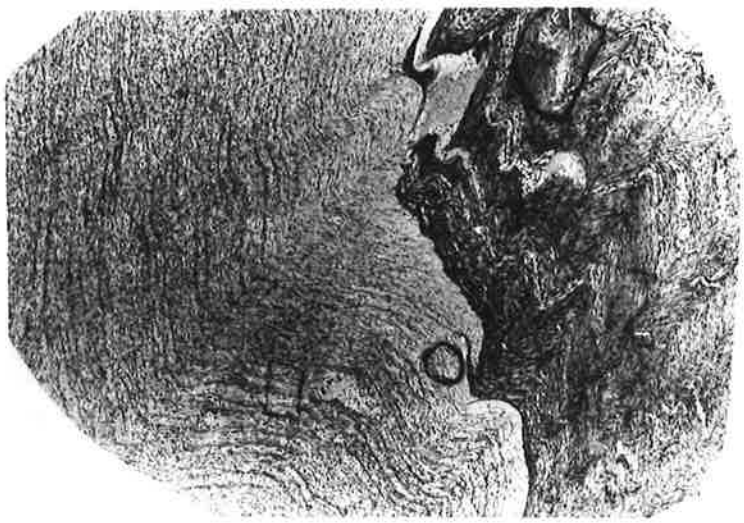

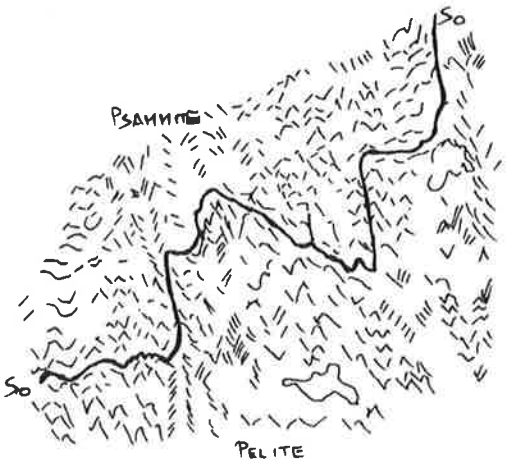
So
PSAMMITE
So
PELITE

DEFORMATION EFFECTS OF EARLY BIOTITES

Fig. 4.42 (left) Chemical alteration of biotite (dark) to muscovite (white) is accompanied by formation of spicules of magnetite along or near the interface.
Specimen 3384, Robe andalusite schist.
PPL, base 0.5 mm.

Fig. 4.43 (right) Type 1 biotite - kinked biotite. Note the irregular stepped axial surface, the undeformed nature of the limbs and the formation of S_1 muscovite parallel to the axial surface.
Specimen 94, Robe andalusite schist.
XN, base 0.75 mm.

Fig. 4.44 (left) Type 2 biotite - undeformed biotite. Biotite is elongate parallel to S_1 across (001) lying at high angles to S_1. Note strong concentration of opaques along margin of biotite.
Specimen 4204, Robe andalusite schist.
XN, base 1.8 mm.

Fig. 4.45 (right) Type 2 biotite - unkinked biotite. Biotite is elongate parallel to S_1 across (001) which is aligned at about 40° to S_1. Steps along biotite prism faces are interpreted as evidence for homogeneous glide. Biotite is partially pseudomorphed by iron oxides.
Specimen 811, Apollyon chiastolite schist.
PPL, base 0.5 mm.

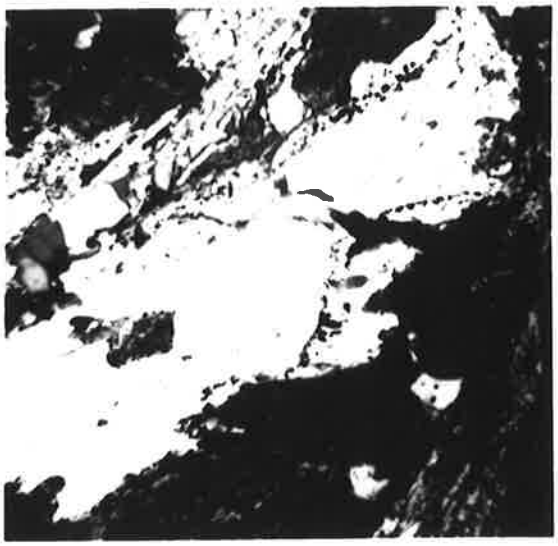

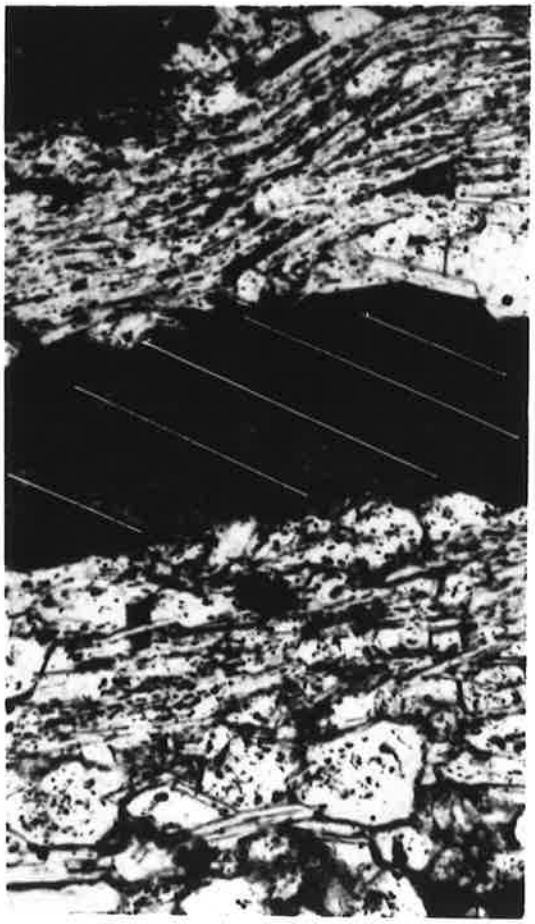

BIOTITE LAMINATIONS PARALLEL TO S_0 - APOLLYON ANDALUSITE SCHIST

Fig. 4.46

a Limb of F_1 fold. Basically planar to slightly irregular lamination. (001) traces suggest annealed kinks.

b Approaching hinge - irregularities in lamination reflect F_1 microfolds, with formation of projections into quartz rich layers. Well defined annealed kinks in left hand side.

c Transposed biotite lamination in hinge area, with formation of lenticles parallel to S_1.

d Short limb of F_1 fold partially transposed lamination, again suggesting annealed kinks.

Bar scale 1 mm.
Specimen 2012.


a

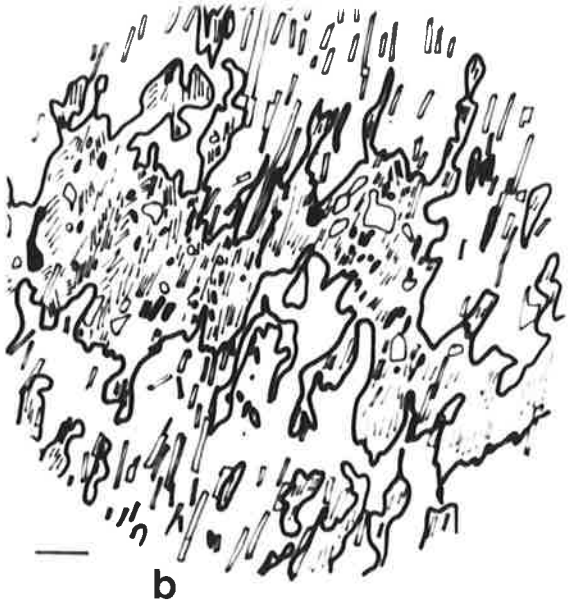
b


c


d

DISPLACEMENT OF BIOTITES

All Sections normal to F_1

Fig. 4.47 (left) Apparent continuity of biotite laths across M domain.
Specimen 94.
PPL, base 2.5 mm.

Fig. 4.48 (right) "Truncation" of biotite and its quartz inclusions by M domain. Continuity of biotite into M domain indicated by stringers of pseudomorphous opaques opposite quartz inclusions. Elongate stringers of biotite parallel to S_1 within M domain interpreted as relicts of large grain.
Specimen 94.
PPL, base 0.75 mm.

Fig. 4.49 (left) Boundary (dashed) between M domain and biotite grain (right of figure). Iron oxides outline relict biotite cleavage traces and show that biotite has been kinked marginal to, and within M domain. Relics of biotite within M domain form slivers parallel to S_1.
Specimen 75.
PPL, base 0.3 mm.

Fig. 4.50 (right) Thin section showing domainal S_1 (vertical) truncating bedding laminations defined by biotite aggregates (top right to bottom left).
Specimen 4202.
PPL x $1\frac{1}{4}$.

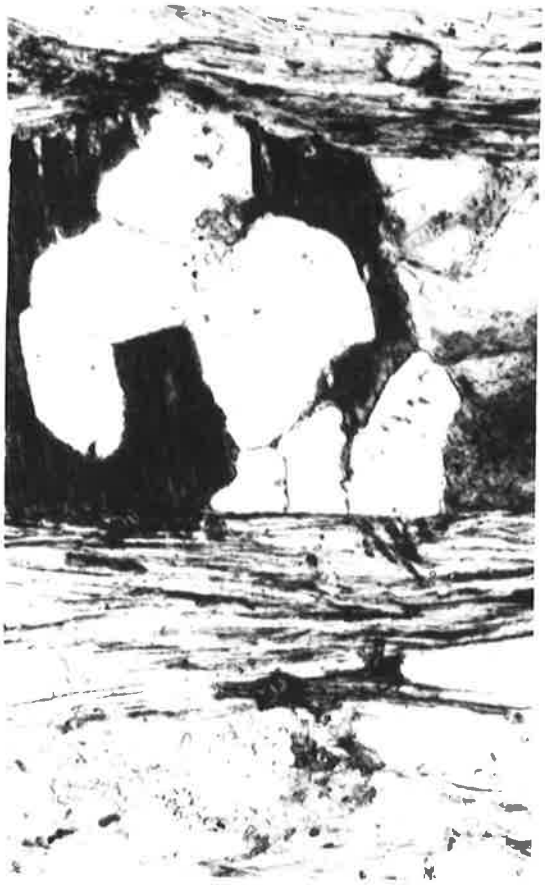

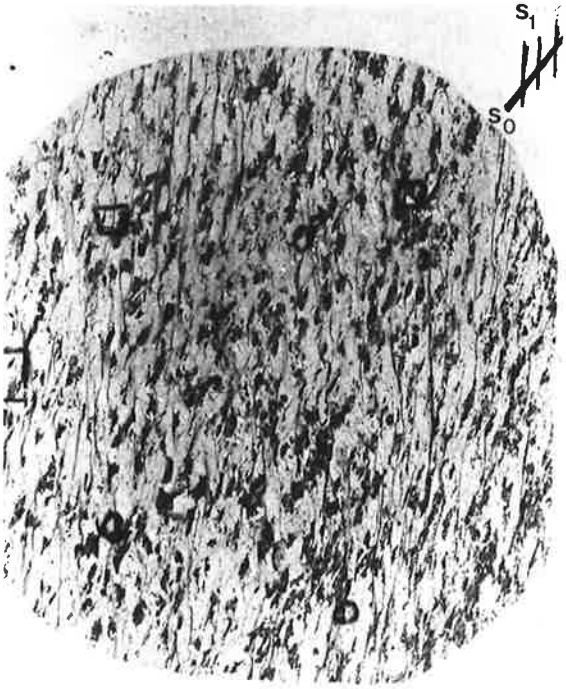
S1
S0

BIOTITES AND THE XY PLANE OF THE D_1 STRAIN ELLIPSOID

Fig. 4.51 (left) Apparent offset in biotite lamination (S_0) across mica rich band in S_1. Biotites here (and in Fig. 4.54) have been pseudomorphed by an iron oxide-quartz intergrowth.
Specimen 3659, Robe andalusite schist.
PPL, base 7.5 mm.

Fig. 4.52 (right) Shadowmaster sketch of Fig. 4.51. Note kinking of (001) traces adjacent to M domain.
Bar scale 1 mm.

Fig. 4.53 (left) Shadowmaster sketch showing offset of biotite lamination on M domain. No obvious kinking of (001). Sense of offset of this and above two figures is in same direction as dip of lamination.
Specimen 3659.
Bar scale 1 mm.

Fig. 4.54 (right) Offset of biotite in wrong sense for dip of lamination. Apparent displacement here is due to kinking of biotites, adjacent to M domain.
Specimen 4202.
PPL, base 0.5 mm.

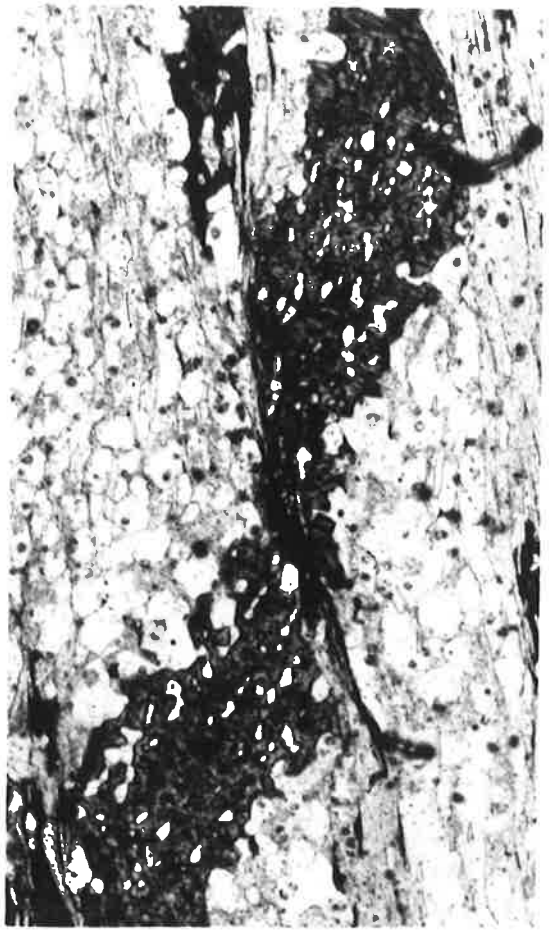

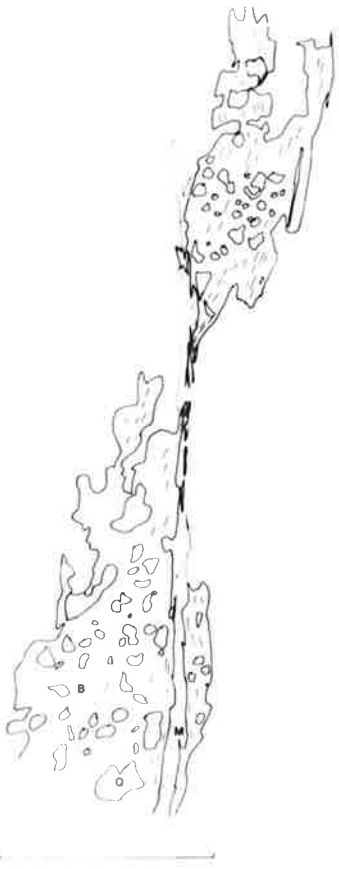
B
M

D_2 EFFECTS

Fig. 4.55a Shadowmaster sketch of F_2 microfold defined by rotation of biotite, sillimanite and quartz rich layers lying in S_1. Shape of fold varies from rounded to kink-like.
Specimen 3109, normal to F_2.
Bar scale 1 mm.

Fig. 4.55b Asymmetrical rotation of biotites resulting in formation of S_2 fabric. Opaque stringers (OP) also define S_2.
Specimen 3111, normal to F_2.
Sketch of thin section x 1.

Fig. 4.56 Kinked biotite aggregate with formation of axial plane biotite parallel to S_2.
Specimen 3109, normal to F_2.
Sketch from photo, bar scale 0.1 mm.

Fig. 4.57 Shadowmaster sketch of S_2 defined by alignment of sericite clot(s), and elongate biotite aggregates.
Specimen 3109, normal to F_2.
Bar scale 1 mm.

Fig. 4.58 S_2 defined by kink aggregates of biotite and sericite.
Specimen 3109, normal to F_2.
PPL, base of photo 3 mm.

Fig. 4.59 Deformed sillimanite aggregate with some recrystallisation to S_2.
Specimen 3109, normal to F_2.
Sketched from photo, bar scale 0.5 mm.

55 A

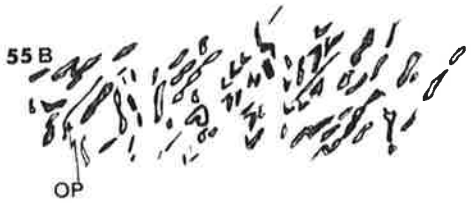

MORPHOLOGICAL VARIANTS OF S_3 (SCHEMATIC)

Fig. 4.60a (left) Formation of a segregated S_3 accompanied by asymmetrical or symmetrical microfolding.

Fig. 4.60b (right) Formation of S_3 by recrystallisation of muscovite, by "stylolite" formation, or by segregation in quartz rich rocks.

Fig. 4.60c (left) Formation of S_3 by rotation and corrosion of pre-S_1 biotites so that they possess a shape preferred orientation parallel to S_3.

Fig. 4.60d (right) Development of S_3 by the formation of asymmetrical crenulations and the formation of a long limb schistosity (S_3').

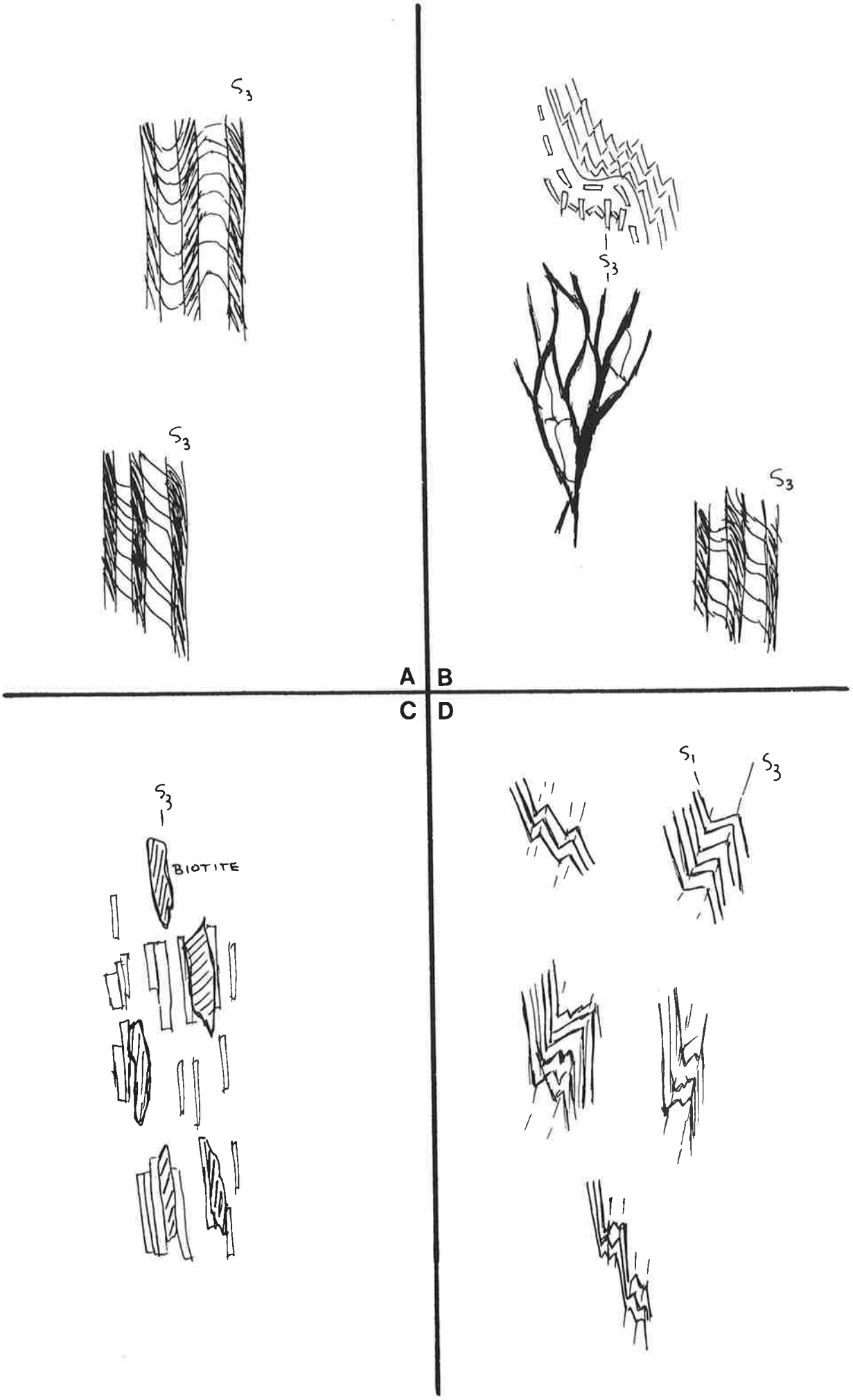
S3
S3
S3
S3
A
B
C
D
S3
BIOTITE
S1
S3

D_3 STRAIN IN QUARTZ

Fig. 4.61 (left) Lozenge and lenticular quartz grains defining an S_3 fabric.
Specimen 4977, normal to S_1.
Sketch from photo, bar scale 0.1 mm.

Fig. 4.62 (right) Grain boundary adjustment. Note irregularities along boundaries and formation of lobes of one grain into the other. Note strain in old grains.
Specimen 4275, normal to S_1.
XN, base 0.75 mm.

Fig. 4.63 (left) Development of bulges along quartz-quartz boundaries and formation of new grains by bulge nucleation.
Specimen 4275, normal to S_1.
XN, base 0.75 mm.

Fig. 4.64 (right) Host old grains surrounded by new quartz grains. Note strain in old grains.
Specimen 4275, normal to S_1.
XN, base 0.75 mm.

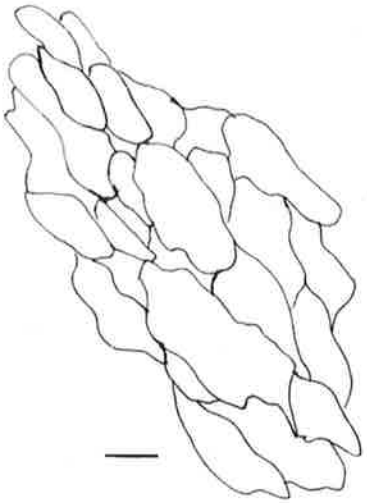

M_3 EFFECTS - ALTERED ANDALUSITE PORPHYROBLASTS

Fig. 4.65 (left) Part of sericite clot pseudomorphous after andalusite, with the alignment of sericite laths parallel to S_3.
Specimen 4202.
XN, length of base 0.75 mm.

Fig. 4.66 (right) Altered andalusite crystal, showing crenulation of sericite laths about S_3 (best seen as shape orientation of white minerals), crenulation and remobilisation of graphite into S_3 (horizontal) and ?rotation of ?ilmenite into S_3.
Specimen 815.
PPL, base 0.75 mm.

Fig. 4.67 (left) Edge of retrogressed andalusite showing rim of coarse grain muscovite plates at margin of porphyroblast and surrounding internal sericite mass.
Specimen 562.
PPL, base 3 mm.

Fig. 4.68 (right) Elongate crystals of chloritoid within sericite after andalusite. Chloritoid lies both parallel (aligned from top right to bottom left) and across S_3 which is defined by dark lines in sericite host. Round opaques are iron oxides. Margin of porphyroblast seen on left is sub parallel to S_3.
Specimen 280.
PPL, base 3 mm.

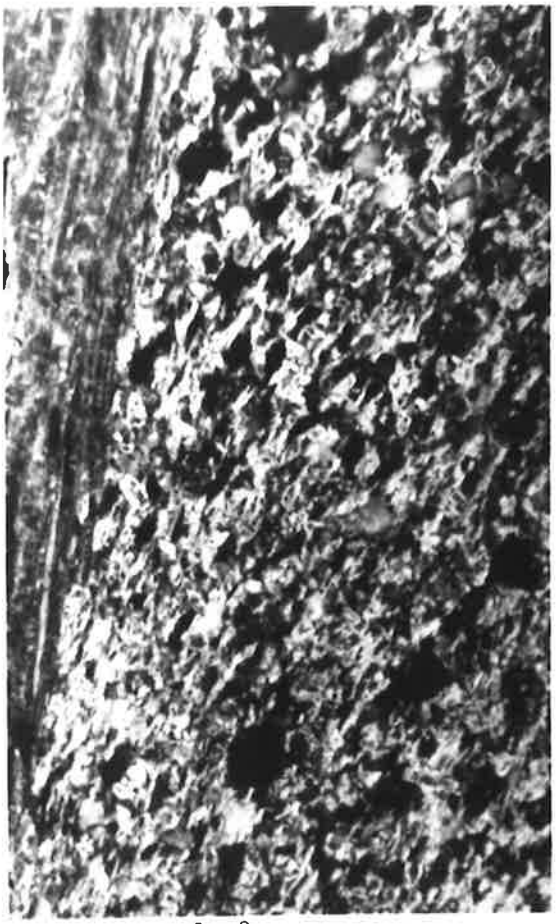
S_1
S_3

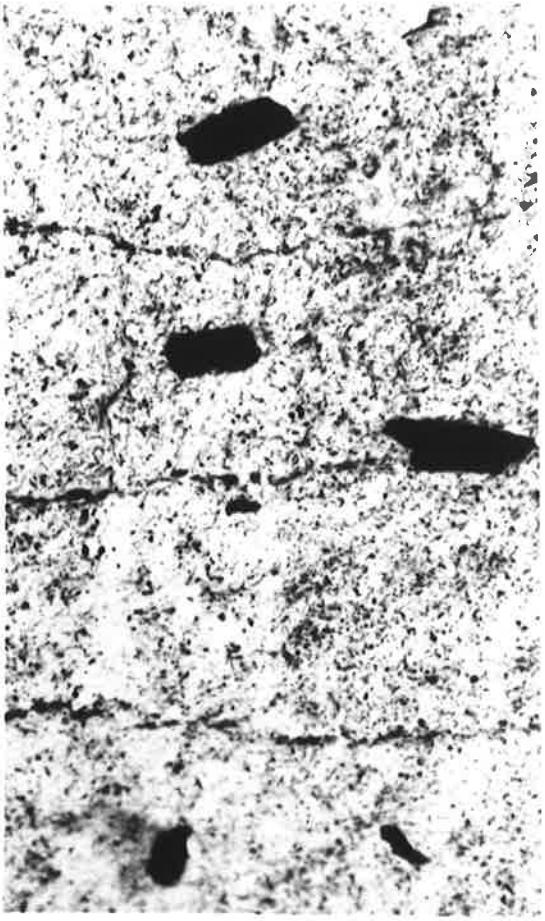


S_1

Fig. 4.69 (left) Alteration of biotite (B, striped) to chlorite (C, grey) which is aligned at small angles to S_3 (dashed, line). Muscovite layer (M) lies in S_3.
Specimen 280
PPL, base 0.5 mm.

Fig. 4.70 (right) F_3 kinks in biotite (B) with the formation of muscovite (M) parallel to S_3.
Specimen 231, normal to S_3.
PPL, base 0.75 mm.

Fig. 4.71 (left) Sketch of garnets cracked and extended in S_3.
Specimen 3386.
Bar scale 0.75 mm.

Fig. 4.72a (right) S_3 "eye" schistosity in Apollyon quartz-mica schists defined by the shape orientation of muscovite aggregates. S_3 in the groundmass defined by narrow laths of muscovite (bottom right).
Specimen 893,
XN, base 3 mm.

Fig. 4.72b (left) Staurolite crystal overgrowing open F_3 folds defined by ?ilmenite rods.
Specimen 3415, normal to S_3.
Sketch from thin section. Bar scale 0.75 mm.

71

72 b

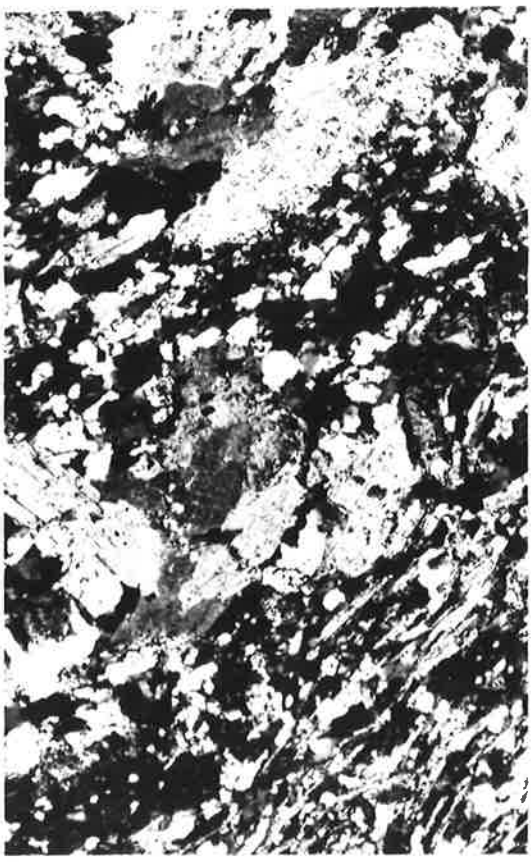

LOW STRAIN D_3 MICROFOLDS

Sections normal to F_3

Fig. 4.73 (left) Open microfold in muscovite rich layer. Note rounded hinge and strain (undulose extinction) in muscovites.
Specimen 3976-22.
XN, base 7.5 mm.

Fig. 4.74 (right) F_3 fold defined by sillimanite needles and biotite-sillimanite intergrowth (black). Shape of fold varies from rounded to kink-like.
Specimen 4022,
XN, base 1.8 mm.

Fig. 4.75 (left) F_3 kink fold in muscovite. Note stepping of axial surface because of pinning by muscovite prism faces. Minor curving only of (001) visible in limbs.
Specimen 3976-23
PPL, base 5 mm.

Fig. 4.76 (right) Open F_3 microfolds in psammopelite. Folds develop around porphyroblasts of altered andalusite and amplify deflection of S_1. Porphyroblasts now consist of sericite aligned in S_3.
Specimen 3976-22.
PPL, base 7.5 mm.

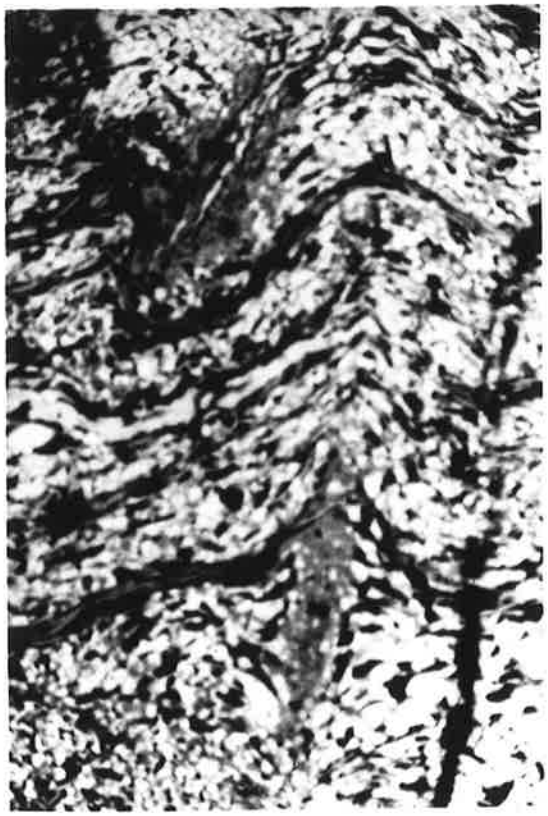

Fig. 4.77 (left) F_3 kink folds in a pelite of the Robe Beds. Note variation in tightness of folds along axial surfaces, and continuity of micas around the hinges.
Specimen 3976-14, normal to F_3.
PPL, base 3 mm.

Fig. 4.78 (right) F_3 fold in S_1 defined by shape of muscovite layer. Note the recrystallisation in the short limb and growth of sericite parallel to S_3.
Specimen 4471.
XN, base 3 mm.

Fig. 4.79 Shadowmaster sketch showing different development of F_3 folds in pelite (right) and psammite (left). Note especially kink geometry in the pelite and variable S_1/S_0 relations.
Specimen 3976-14, normal to F_3.
x 1.

Fig. 4.80 Measurement of kink angles in pelites of Fig. 4.79. Measurement of pairs of angles in both antiforms and synforms indicate that $\phi \sim \phi_K \sim 30^\circ$. See text.

ANTIFORMS

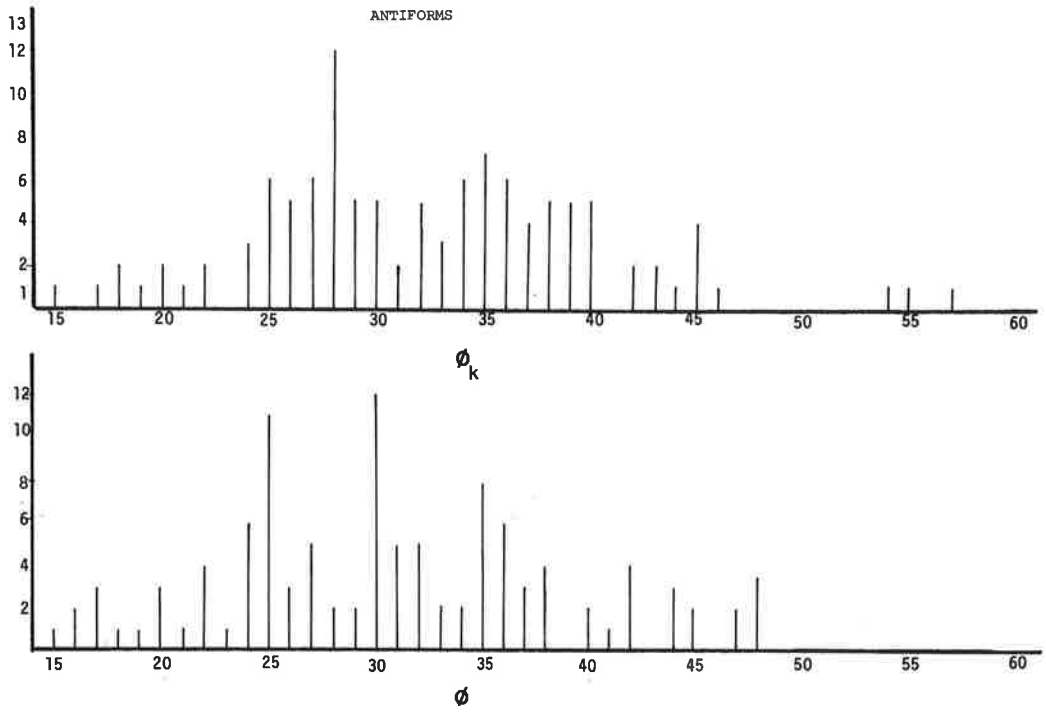

SYNFORMS

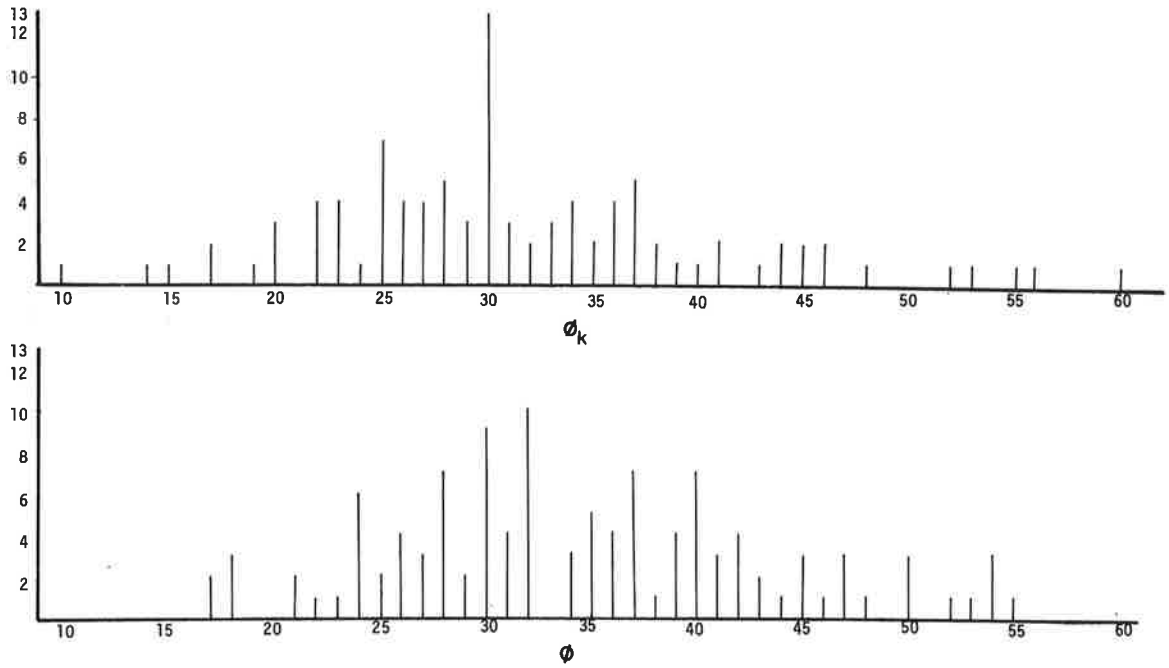

INTERMEDIATE STRAIN D_3 MICROFOLDS

Fig. 4.81 (left) Bulbous F_3 fold in S_1. Note overstepping of muscovite laths in hinge area and "thrusts" defined by muscovites. Note also change in shape of biotites between limb and hinge zones.
Specimen 3976, normal to F_3.
PPL, base 3 mm.

Fig. 4.82 (right) "Levering off" effects of muscovites in hinge zones. Note complex F_3 geometry, and change of shape of biotites between limb and hinge zones.
Specimen 4471, normal to F_3.
PPL, base 1.8 mm.

Fig. 4.83 (left) F_3 fold with formation of discontinuity along axial surface. Mismatch of limbs probably due to kink migration.
Specimen 753, normal to F_3.
PPL, base 0.75 mm.

Fig. 4.84 (right) F_3 fold with iron stained discontinuities along axial surfaces. Note preservation of biotites in hinge zone, and continuity of muscovite between hinge and limb except where discontinuity occurs.
Specimen 4257, normal to F_3.
PPL, base 0.75 mm.

Fig. 4.85 (left) S_3 defined by iron stained discontinuities wrapping around quartz grains.
Specimen 510, normal to S_3.
Sketch from photo, bar scale 0.05 mm.

Fig. 4.86 (right) S_3 "stylolites" seen in top left hand corner. Defined by iron oxides and graphite.
Specimen 689, normal to S_3.
PPL, base 0.6 mm.

Fig. 4.87 (left) Iron stained discontinuity developed parallel to S_3 along flexure in S_1 mica layer.
Specimen 4257, normal to S_3.
PPL, base 0.75 mm.

Fig. 4.88 (right) S_3(horizontal) defined by narrow zones of re-oriented muscovite.
Specimen 280, normal to S_3.
XN, base 1.8 mm.

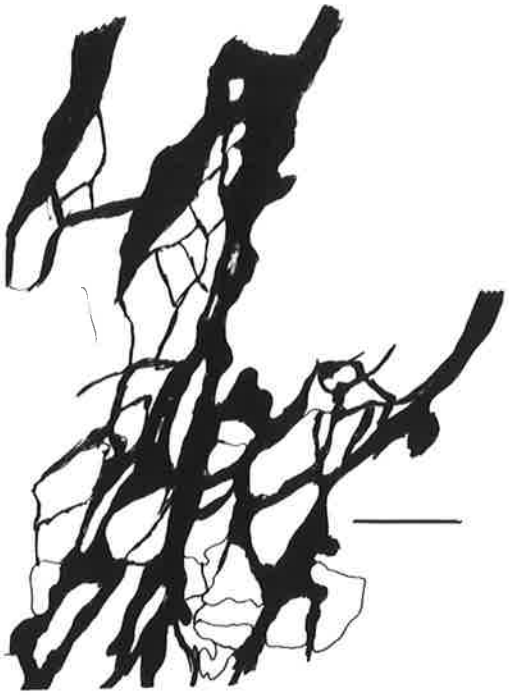

SEGREGATED S_3 SCHISTOSITY

Fig. 4.89 (left) Poorly delineated S_3 defined by the concentration of S_1 muscovite in a steep limb of an F_3 microfold. Muscovites in this M domain still lie within S_1.
Specimen 3976-19, normal to F_3.
XN, base 7.5 mm.

Fig. 4.90 (right) Segregated S_3 in Apollyon chiastolite schist. S_3 defined by the alternation of M and QM domains. M domains represent limbs of F_3 microfolds; QM zones represent hinge zones. Note equant quartz in QM domains and change in shape of quartz grains between domains.
Specimen 3, normal to F_3.
Tracing from thin section. Bar scale 1 cm.

Fig. 4.91 (left) Lozenge shaped quartz grains and anastomosing muscovites in QM domain, Apollyon chiastolite schist.
Specimen 19, normal to F_3.
PPL, base 0.3 mm.

Fig. 4.92 (right) M and QM domains in Apollyon chiastolite schist after general recrystallisation of muscovite but not quartz. Some relict S_1 orientations preserved.
Specimen 3, normal to F_3.
Tracing from photo. Bar scale 1 cm.

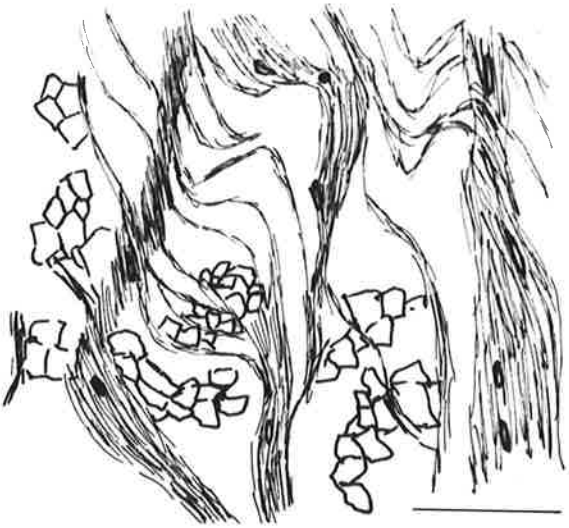

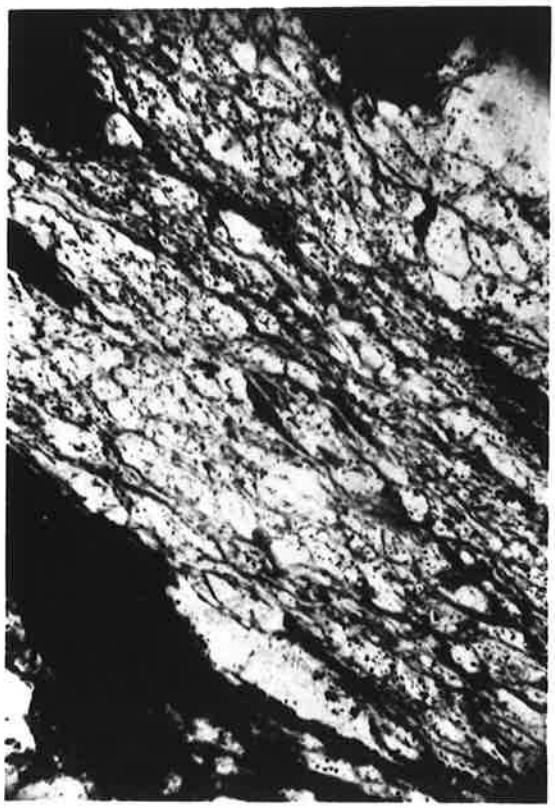

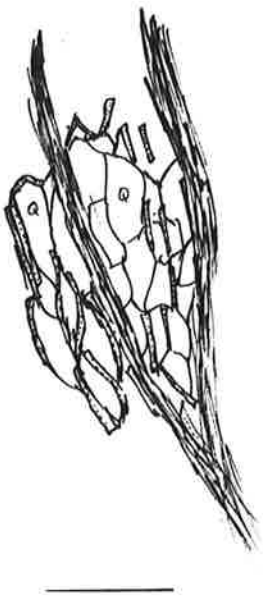

SEGREGATED S_3, SILLIMANITE SCHIST

Fig. 4.93 Segregated S_3 defined by M (biotite + sericite) and QM (quartz + biotite + sericite) domains, Robe Sillimanite schist. Note change in shape of quartz grains between QM and M domains, and width of domains; left hand M domain is of similar size to QM domain.
Specimen 4377, normal to F_3.
XN, base 7.5 mm.

Fig. 4.94 Enlargement of Fig. 4.93. Note rotation of biotites between domains and lack of axial plane discontinuities.
XN, base 3 mm.

SEGREGATED S_3 IN PELITE

Fig. 4.95 (left) Segregated S_3 defined by light and dark coloured bands. Dark coloured bands are M domains; light coloured bands are QM domains. Note impersistence of domains and relative widths; M domain on left is wider than many QM domains, other M domains same order as QM domain.
Specimen 753, normal to F_3.
PPL, base 7.5 mm.

Fig. 4.96 (right) Close-up of M and QM domains. Note:
1) continuity of muscovite across domain boundaries,
2) angles between muscovite (in S_1) and S_3 in both domains,
3) that M domains occupy steep limbs or even hinges of F_3 microfolds whereas QM domains occupy short limbs or hinge zones
4) change in shape between quartz and biotite (dark) between domains.

Speciman 753, normal to F_3.
XN, base 3 mm.

Fig. 4.97 (left) Boundary between M (left) and QM (right) domain. Note inclination of muscovite to domain boundary (S_3) which is defined by iron oxides. Change in muscovite orientation across domain interpreted as annealed kinks.
Specimen 753, normal to F_3.
PPL, base 0.75 mm.

Fig. 4.98 (right) Shadowmaster sketch of S_1 orientation across M and QM domains.
Specimen 753, normal to F_3.
Bar scale 1 mm.

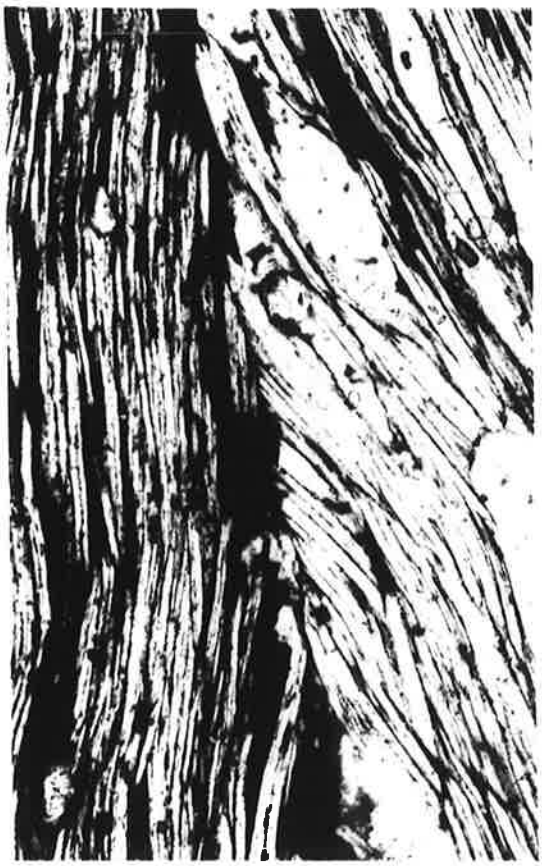

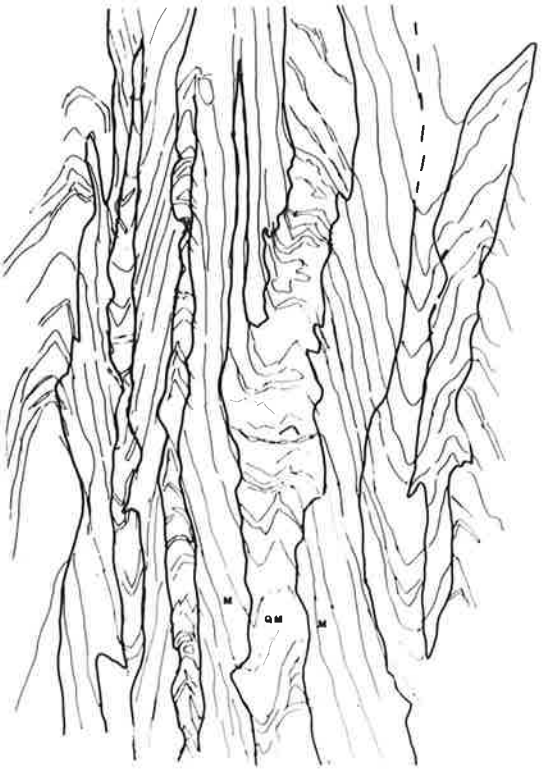

S_3 SEGREGATION SCHISTOSITY

Fig. 4.99 (left) Detail of M domain showing its relation to F_3 geometry. M domain has variable shape in detail and lies at variable angles to non planar S_3. M domain may even project into surrounding QM domain. Circled areas show continuity of micas between QM and M domains.
Specimen 753, normal to F_3.
Shadowmaster sketch, bar scale 1 mm.

Fig. 4.100 (right) Change of shape of quartz grains from equant in QM domain to elongate in S_1 in M domain.
Specimen 753, normal to F_3.
Shadowmaster sketch, bar scale 1 mm.

Fig. 4.101 (left) Change of shape of biotite grains from irregular in QM domains to elongate in S_1 in M domains.
Specimen 753, normal to F_3.
Shadowmaster sketch, bar scale 1 mm.

Fig. 4.102 (right) Change of shape of quartz grains from QM to M domains.
Specimen 753, parallel to F_3.
Shadowmaster sketch, bar scale 1 mm.

CHANGE of SHAPE of QUARTZ between M and QM DOMAINS

CHANGE of SHAPE of BIOTITES between M and QM DOMAINS

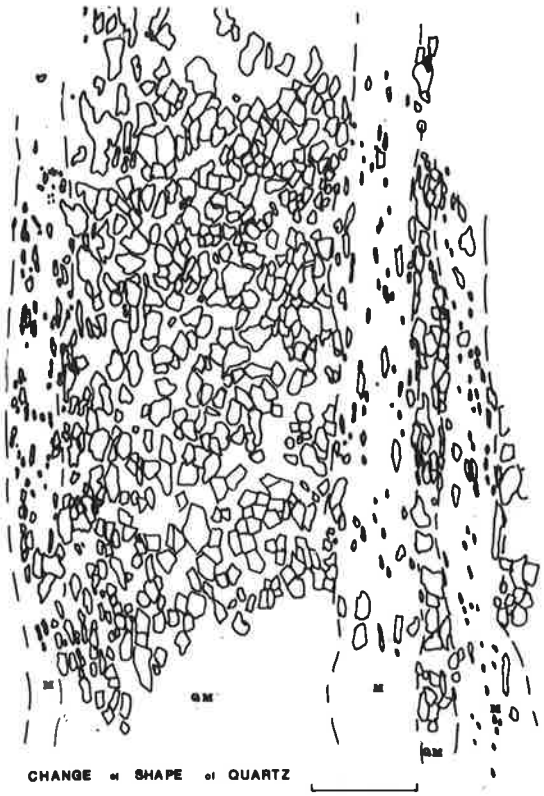

CHANGE of SHAPE of QUARTZ

Fig. 4.103 (left) Change in shape of biotites from ragged in QM domains to elongate in $S_1//S_3$ in M domains.
Specimen 753, parallel to F_3.
Bar scale 1 mm.

Fig. 4.104 (right) Bimodal muscovite orientation in psammite. Laths lie parallel to a folded S_1, and also S_3. In pelite, no S_3 is developed.
Specimen 232, normal to F_3.
Sketch from photo, bar scale 1 mm.

Fig. 4.105 (left) S_3 defined by hydrated iron oxides, psammite of Mt Franks facies. Quartz grains have been modified so that they are elongate in S_3.
Specimen 411, normal to S_3.
Sketch from photo, bar scale 1 mm.

Fig. 4.106 (right) F_3 effects in S_1Ps and S_1Pe. S_0 (dashed) lies parallel to S_3. Well developed kinks in S_1Pe contrast with lack of kinking in S_1Ps.
Specimen 3976-22, normal to F_3.
x 1.

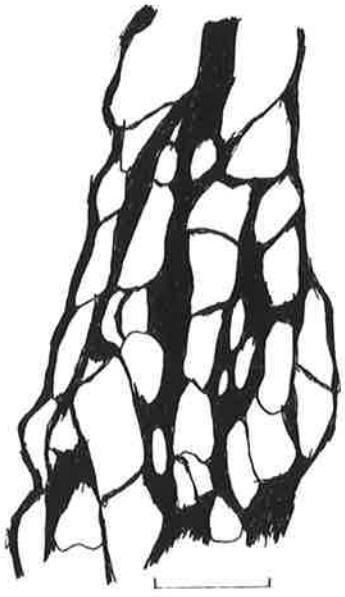

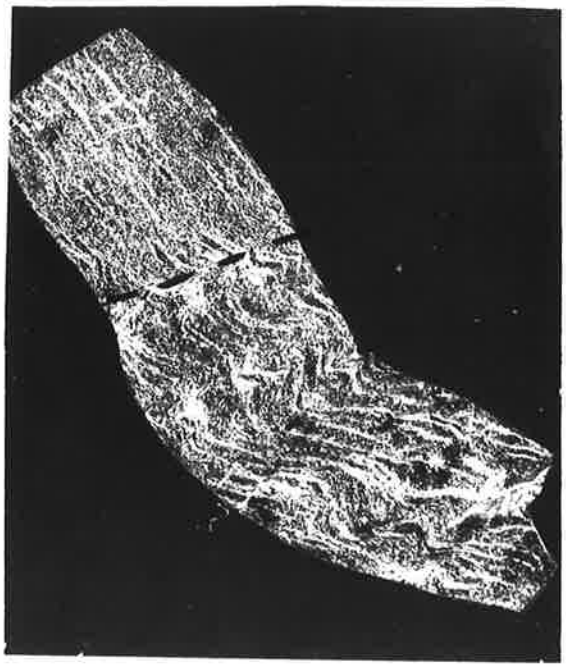

D_3 STRAIN IN BIOTITE LAMINATIONS

Fig. 4.107 (left) Open to tight F_3 folds in biotite laminations parallel to S_0. Vertical fabric is S_3. Biotite grains are white. Large porphyroblasts are partially retrogressed chiastolites.
Specimen 19, normal to F_3.
Negative print.

Fig. 4.108 (right) Disrupted biotite laminations with the resultant formation of a shape preferred orientation of biotites (white grains) parallel to S_3 (vertical).
Specimen 45, normal to S_3.
Negative print x 2.

Fig. 4.109 (left) Shadowmaster sketch of Fig. 4.108.
Bar scale 1 mm.

Fig. 4.110 (right) Enlargement of Fig. 4.109 showing remnants of biotite laminations and F_3 hinges. Relic S_1 also visible at lower right.
Bar scale 1 mm.

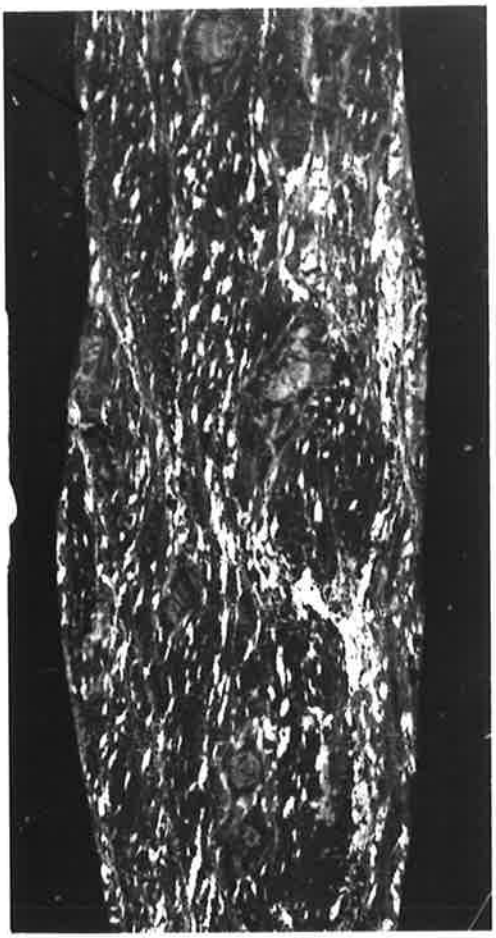

D_3 EFFECTS IN BIOTITE, APOLLYON CHIASTOLITE SCHIST

All sections normal to S_3, L_3

Fig. 4.111 (left) Stumpy biotites with stepped terminations. These are interpreted as annealed kinks, with the introduction of graphite and muscovite in the axial plane position. S_3 is E-W.
Specimen 817.
PPL, base 0.5 mm.

Fig. 4.112 (right) Step like terminations in biotite which is elongate sub parallel to S_3 across (001).
Specimen 15.
PPL, base 0.75 mm.

Fig. 4.113 (left) Elongate, unkinked biotite and stumpy, kinked biotite. Elongate biotite has (001) lying at a small angle to S_1; stumpy biotite has (001) lying at high angle to S_1. Elongate biotite may represent limb of F_3 kink. S_3 inclined to lower right.
Specimen 689.
PPL, base 0.6 mm.

Fig. 4.114 (right) Compound biotite grain, possibly representing an annealed kink. S_3 inclined to lower right. Relict S_1 preserved in bottom right hand corner.
Specimen 689.
PPL, base 0.5 mm.

LONG LIMB SCHISTOSITY

Figs. 4.115 - 122 - all shadowmaster sketches, normal to F_3.
M - mica layer; QM - quartz mica layer; C - sericite clot.

Fig. 4.115 (left) Low strain, open crenulation. S_3 from top right to lower left. Note asymmetrical crenulations at top left.
Bar scale 1 mm.
Specimen 280.

Fig. 4.116 (right) Asymmetrical F_3 crenulations with well defined long limbs. S_3 - top right to lower left. In areas A, B, short limbs are truncated by long limbs.
Bar scale 1 mm.
Specimen 246.

Fig. 4.117 (left) Similar amount of rotation as Fig. 4.116, but not accompanied by extensive recrystallisation of sericite. S_3 top right to lower left.
Bar scale 1 mm.
Specimen 107.

Fig. 4.118 (right) Development of good S_3' at an angle to S_3 defined by sericite laths in clots. Recrystallisation of muscovite to sericite clots results in truncation of M layers (e.g.A). Elsewhere (C,D) short limbs are still at a high angle to S_3.
Bar scale 1 mm.
Specimen 280.

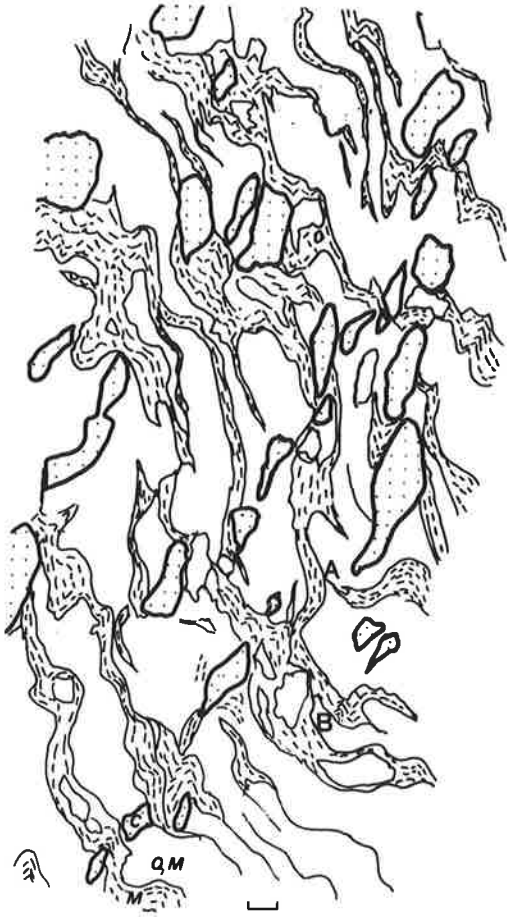
B
qM

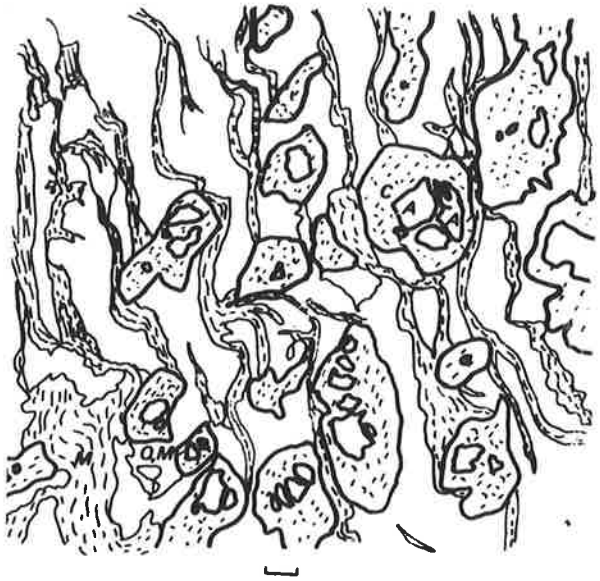
qM

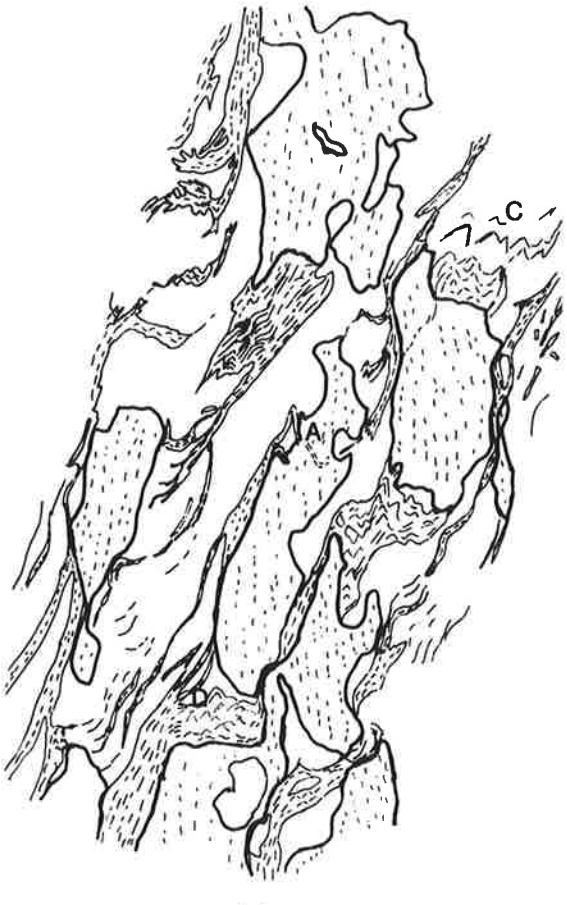
C
A

Fig. 4.119 (left) Relations between S_3' in psammopelite (Pe) and S_1 in psammite (Ps). Note the local parallelism of S_3' and S_3 (area A), the presence of open F_3 folds (area B) and the presence of tighter F_3 folds (areas C, D). Truncation of short limbs by long limbs shown in area E.
Bar scale 1 mm.
Specimen 411.

Fig. 4.120 (right) Multiple hinge effects, see text.
Bar scale 0.1 mm.
Specimen 233.

Fig. 4.121 (left) Maximum S_3' development at an angle to S_3. S_3 top right to lower left. Short limbs still present in areas A, B, C, D.
Bar scale 1 mm.
Specimen 4471.

Fig. 4.122 (right) $S_3' = S_3$, see text.
F_3 hinges preserved in areas A, B, C,D . Area D shows partial recrystallisation to sericite.
Bar scale 1 mm.
Specimen 589.


C
D
E
B
Ps
Pe

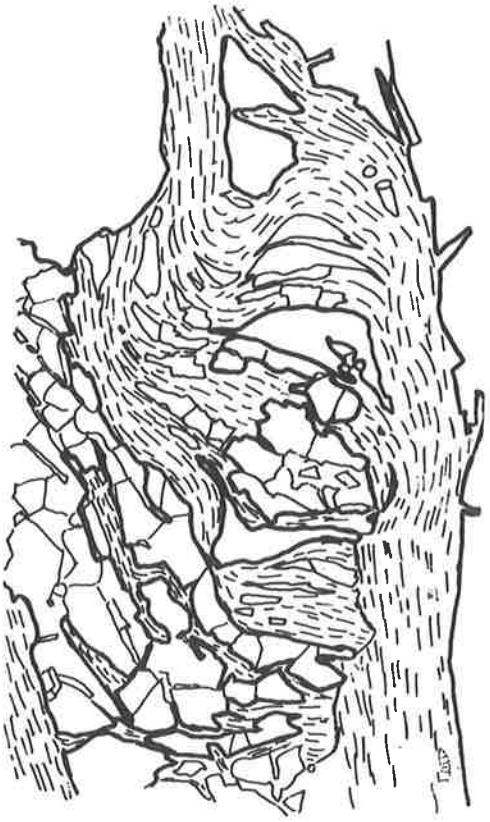

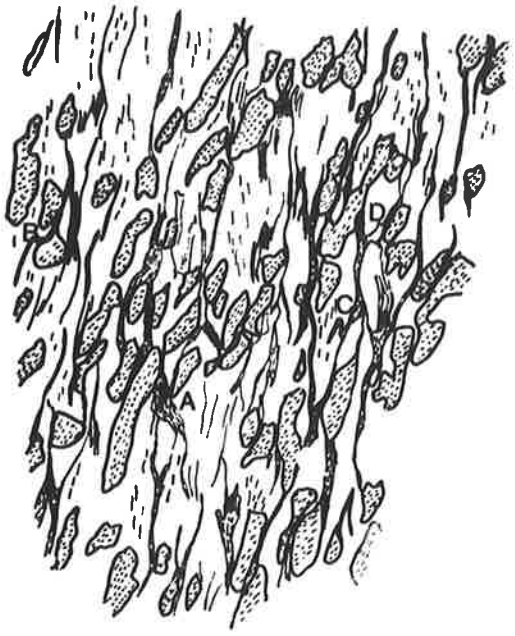
B
D
A


A
B
D
C

Fig. 4.123 (left) Hinge of F_3 fold partially disrupted by the recrystallisation of muscovite to sericite. S_3 dashed line.
Specimen 4471, normal to F_3.
XN, base 0.7 mm.

Fig. 4.124 (right) Disruption of limb of F_3 fold by sericite clot. S_3 dashed.
Specimen 4471, normal to F_3.
XN, base 1.5 mm.

Fig. 4.125 (left) Truncation of short limb by E-W trending long limb. A discontinuity generally separates two limbs so that there is mismatch of muscovites across this line.
Specimen 4471, normal to F_3.
XN, base 0.7 mm.

Fig. 4.126 (right) Multiple hinge effect, with truncation of short limb by long limb at A.
Specimen 233, normal to F_3.
XN, base 0.75 mm long.

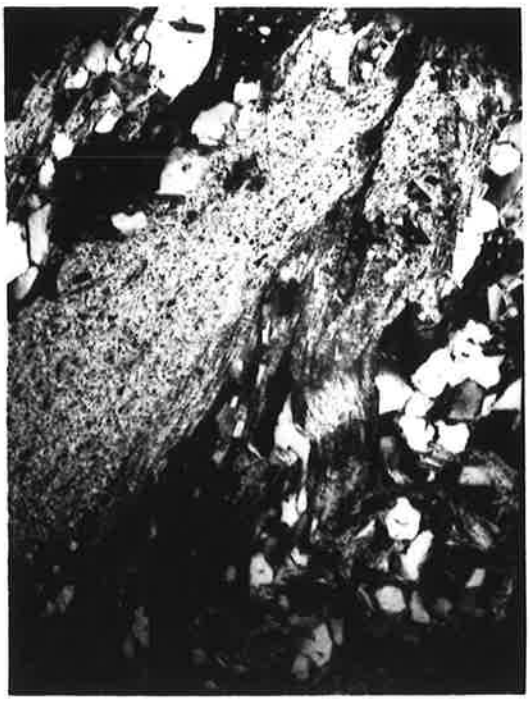


A

CHAPTER 5 METAMORPHIC RELATIONS

5.1 INTRODUCTION.

By using the microstructural criteria of the last chapter, it has been possible to categorise mineral growth into three metamorphic events; M_1, a high grade event which incorporates both pre-S_1 and syn-S_1 mineral growth, M_2 a lower grade event, and M_3 a retrograde event. These events are broadly correlable with D_1, D_2 and D_3. M_1 is a particularly significant event which results in the formation of the biotite, andalusite and sillimanite zones mapped in the field. The progressive nature of M_1 is represented not only by syn-S_1 mineral growth, but also by those minerals which ceased growth before final formation of S_1. M_2 is a simple, localised event. M_3 is more widespread, more complex and can possibly be divided into an early phase of localised staurolite formation and a later phase dominated by white mica growth.

This chapter proceeds by discussing each metamorphic event in turn - the field relations between index minerals, a description of mineral assemblages, a discussion of possible reaction mechanisms and mineral stability, and conditions of metamorphism.

Evidence for relative age relations between these minerals was discussed in the last chapter, and will not be repeated.

The results of the earlier metamorphic studies of Browne (1922), Binns (1963, 1964), and Anderson (1966, 1971) were discussed in Section 1.3.3.2.

5.2 METAMORPHISM M_1.

Metamorphism M_1 accompanies the first deformation (D_1) in what was probably a complex, progressive event. It was shown in Section 4.3.8 that three distinct phases of this event could be recognised on the basis of microstructural criteria:

1) a pre-S_1 schistosity defined by biotite, sericite, local sillimanite and white mica,

2) an interkinematic event represented by biotite, andalusite, sericite and local sillimanite, and

3) an S_1 schistosity defined by muscovite, sillimanite, local biotite and local andalusite.

Although the geometrical significance of the pre-S_1 schistosity is uncertain (Section 4.2.7.2) and the time of formation of this surface may be much earlier than S_1, the presence of biotite, muscovite and sillimanite as pre- and syn-S_1 minerals suggests a close time relation between pre- and syn-S_1 events. In such a situation, pre-S_1 minerals are envisaged as having ceased growth before final adjustment of S_1 minerals or before final modification of them.

5.2.1 Metamorphic Boundaries - Reflections of the M_1 Event

Three types of metamorphic boundaries can be distinguished in the field (Fig. 5.1). The first type is lithologically controlled and is manifested by the distribution of index minerals parallel to bedding and outlining distinct lithological units (for example, the boundary around the Mundi Mundi facies). The second type of boundary is structurally controlled and lies along retrograde schist zones. Included in this category is the boundary between the sillimanite schists east of the Apollyon Valley Retrograde Schist Zone, and the low grade biotite schists west of the Apollyon Valley Retrograde Schist Zone. The boundary between low grade rocks and medium grade rocks lies along the Mt Franks Retrograde Schist Zone and is also of this type: this boundary is defined by the change in index minerals in non carbonaceous rocks from biotite to biotite + andalusite + garnet passing from east to west across the zone. In carbonaceous rocks there is a change from biotite + local ?chiastolite + mineral aggregates in the low grade rocks to biotite + chiastolite + garnet in the medium grade rocks.

The third type of metamorphic boundary occur within a single lithological unit, and covers the low-?medium-high grade boundary in the southern part of the area between the Apollyon Valley and Mt Franks Retrograde Schist Zones

(central block), and the andalusite/sillimanite isograd in the Robe Beds.

The boundary in the southern part of the central block has not been precisely located by detailed thin section work. Definite sillimanite has been recorded in an area of F_1 folds just north of a cross-cutting pegmatite (Fig. 5.1, and Section 6.2.4) and may occur even further north in highly retrogressed schists. No definite andalusite has been recorded from this central area, although local chiastolite (now retrogressed) may be present in carbonaceous units. This metamorphic boundary cuts across bedding and S_1.

The andalusite/sillimanite isograd in the Robe Beds was defined by the first appearance of sillimanite in the field when mapping westwards from the Mt Franks Valley and refined by thin section work. The transition of andalusite to sillimanite is usually gradational over a distance of 50-80 m, and andalusite commonly occurs above the isograd throughout the sillimanite schists. In some areas, co-existing andalusite and sillimanite can be defined in the field as zones up to 150 m wide around the "boundary" (Map 1). Mesoscopically visible pockets of andalusite occur within the sillimanite schist, and Anderson (1966), Reynolds (1975) and Thomson (1976) mapped pockets of andalusite within sillimanite schist in the Mt Robe area to the north.

The andalusite/sillimanite isograd has been mapped for a distance of about 15 km and for much of this length it is parallel to both bedding and S_1. This parallelism is clearly demonstrated north of point A (Fig. 5.1), especially in the Black Prince Area where the isograd lies parallel to bedding in an F_3 fold, and also from point C to D, and from point E southwards where the isograd is partially folded around an F_3 fold. From A to B, and from D to E, the isograd transects both bedding and S_1. From B to C the isograd does not lie parallel to S_1, and must lie close to, or parallel to S_0 in orientation in an area of F_1 folding. In the south of the area, thin section studies have shown that the isograd cuts across S_1 in an area of F_1 folds, and must lie in part close to, or parallel to S_0 in orientation.

The mapped relation between the isograd, S_0 and S_1 could be due to three factors:

1) formation of sillimanite from andalusite in S_1 time with resultant isograd generally parallel to S_1,

2) formation of the isograd in a late stage event with its position controlled by a change in bulk composition so that it generally lies parallel to S_0 which is parallel to S_1 in most of the area,

3) formation of the isograd, generally parallel to bedding, before S_1 formation and F_1 folding.

Microstructural evidence from Sections 4.2.4 and 4.3.4 suggests that andalusite and some sillimanite predate S_1 and that some sillimanite lies in S_1. This data, coupled with inferred F_1 folding of the isograd between area B to C and in the south of the area favour the third possibility. Macroscopic evidence that the isograd predates F_3 folding is seen in the Black Prince Area (north of Area A). F_3 folds of the present study apparently correspond to the kink folds Binns (1963) related to his M_3 event and this finding thus throws doubt on Binns' view that andalusite growth occurred during this time.

The gradational nature of the isograd, the presence of scattered andalusites throughout the sillimanite schists and the presence of sillimanite in thin section just before its appearance in the field all suggest that the andalusite/sillimanite boundary is not localised along a structural discontinuity such as a thrust or slide.

5.2.2 Mineral Assemblages

M_1 assemblages in low, medium and high grade rocks are shown in Table 5.1, and AKF diagrams corresponding to these in Fig. 5.2. By using Winkler's (1967) metamorphic facies subdivision, it can be seen that the following conditions are approximated:

low grade: upper greenschist or lower cordierite-amphibolite facies

TABLE 5.1 - M_1 Assemblage

LOW GRADE ROCKS

carbonaceous schist - pre S_1: bio + q + gr + tour + op + white mica + aggregates $\pm$ chi

- syn S_1: musc + q $\pm$ bio + plag + op

non carbonaceous schist - pre S_1: bio + q + tour + op + aggregates $\pm$ white mica

- syn S_1: musc + q $\pm$ bio + plag + op

calc silicate : q + diop + plag (An_{25-35}) + sph + ?vesuv + ?amph

MEDIUM GRADE ROCKS

carbonaceous schist - pre S_1: bio + q + gr + tour + op + white mica + chi + gn + zir

- syn S_1: musc + q + op

non carbonaceous schist -

pelite, psammopelite - pre S_1: bio + q + tour + op + white mica + and + zir + gn $\pm$ plag (An_{35-50})

- syn S_1: musc + q + op + ?gn $\pm$ K spar

psammite - pre S_1: bio + q + tour + op + white mica + zir $\pm$ gn $\pm$ and $\pm$ plag (An_{35-50})

- syn S_1: musc + q + op + ?gn

amphibolite : amph + q + plag (An_{30-70}) $\pm$ musc

MEDIUM-HIGH GRADE ROCKS

carbonaceous schist - pre S_1: b + q + gr + op + white mica $\pm$ gr $\pm$ sill $\pm$ chi

- syn S_1: musc + q + chi $\pm$ bio + sill

non carbonaceous schist - pre S_1: b + q + op + and + sill + white mica + zir $\pm$ gn $\pm$ plag (An_{30-50})

- syn S_1: musc + q + sill + op

TABLE 5.1 - M_1 Assemblage (cont.)

HIGH GRADE ROCKS

pelite, psammopelite	- pre S_1:	b + q + and + sill + white mica + op + zir $\pm$ Kspar $\pm$ gn
	- syn S_1:	musc + sill + q $\pm$ bio $\pm$ gn
psammite	- pre S_1:	b + q + op $\pm$ gn $\pm$ sill $\pm$ and $\pm$ white mica $\pm$ Kspar
	- syn S_1:	musc + sill + bio + q $\pm$ gn
calc silicate	:	diop + q + op + ap + zir
amphibolite	:	amph + q + plag (An_{35-70}) $\pm$ musc $\pm$ bio

---

Abbreviations: bio - biotite; q - quartz; gr - graphite; tour - tourmaline; chi - chiastolite; and - andalusite; sill - sillimanite (including fibrolite); plag - plagioclase; gn - garnet; op - opaques; zir - zircon; diop - diopside; ap - apatite; vesuv - vesuvianite; amph - amphibole; musc - muscovite; sph - sphene; Kspar - K feldspar.

medium grade: lower cordierite amphibolite facies

medium to high grade: middle cordierite amphibolite facies

high grade: upper cordierite amphibolite facies

Table 5.1 shows that peak M_1 conditions did not occur at the same time throughout the whole area. Peak conditions are represented by biotite growth (pre- and syn-S_1) in low grade rocks together with possible localised pre-S_1 chiastolite. Peak conditions in medium grade rocks are represented by pre-S_1 biotite and chiastolite (andalusite) whereas in high grade rocks, sillimanite + biotite growth occurred in both pre- and syn-S_1 time. Elongate sillimanite in S_1 in the Mundi Mundi carbonaceous facies indicate that peak metamorphic conditions in this unit were syn-S_1 in age. The relation between mineral growth and the D_1 event will be further summarised in Tables 5.2, 5.3.

5.2.3 Possible Mineral Reactions, Growth and Stability

5.2.3.1 Biotite

Biotite is present in all metamorphic zones and as a result, there is no direct information on its method of formation. Most authors (e.g. Winkler, 1974) suggest that upgrade biotite forms from chlorite and muscovite. M_1 biotite possesses variable microstructural relations to S_1 and this suggests complex relations between cessation of biotite growth and consolidation of S_1. In low grade rocks, pre-S_1 biotite occurs as porphyroblasts and within mineral aggregates. These biotites have similar absorption colours to biotites lying in S_1. In medium grade rocks, pre-S_1 biotite occurs as oriented grains in the groundmass, as oriented and random inclusions in andalusite, and as randomly oriented porphyroblasts, many of which have been rotated into S_1. High grade rocks contain pre-, syn- and locally random biotites, all with similar colours. Overall there is a tendency for the Y=Z absorption colour to change from brown (low grades) through red-brown (medium grade) to red-brown/olive brown (High grade). Biotites in carbonaceous

units are more iron rich than those in adjacent graphite free beds since they are more heavily pseudomorphed by iron oxides during subsequent alteration.

Biotite breakdown commences in S_1 time and continues in the M_2 and M_3 events. Products of this alteration are muscovite (or sericite) together with square shaped hydrous iron oxides which may have been magnetite* (Fig. 4.42). This reaction can be written as:

1) 3 biotite $\longrightarrow$ muscovite + 3 magnetite + $2K^+$ + 6 quartz

(A. Purvis, pers. comm., 1975).

5.2.3.2 Muscovite

The widespread formation of muscovite laths in S_1 is not believed to indicate a period of K metasomatism. Rather, it is suggested that this muscovite developed by (re)crystallisation from earlier white micas, constituting a pre-S_1 fabric, as well as from biotite breakdown (see above). The origin of the early pre-S_1 mica is unknown.

5.2.3.3 Aggregates - Low Grade Rocks

As mentioned in Section 4.3.1.1 the origin of large green aggregates consisting of biotite + muscovite + quartz $\pm$ plagioclase in the quartz mica schists is unknown. The minerals present do not accord with breakdown minerals of andalusite, cordierite or feldspar and thus it is suggested that they might represent original, now disrupted early assemblages. In the carbonaceous schists, however, the presence of relict feldspar in some quartz + sericite + graphite clots suggests that these clots may represent altered plagioclase. Other pre-S_1 mineral clots without feldspar may represent retrogressed chiastolite or cordierite, but no relict minerals were found. In equivalent rocks further north, Laing (1969) tentatively identified relict cordierite. W. D'Arcy (pers. comm., 1976) also suggested cordierite had occurred in similar mineral clots further north.

---

* if biotites were titanium rich, ilmenite would also constitute part of the opaque phase.

5.2.3.4 Andalusite (including Chiastolite)

Andalusite is both pre-S_1 and syn-S_1 in age. It is suggested that andalusite growth and S_1 formation are part of a single progressive event, and that pre-S_1 andalusite represents cessation of porphyroblast growth before cessation of growth of S_1 minerals.

There is no direct evidence for the formation of andalusite. However, two possibilities may be considered - that it forms from porphyroblast breakdown (e.g. cordierite) or that it forms from earlier matrix minerals. Schreyer and Yoder (1961) suggested that andalusite may form from the reaction:

2) cordierite ⟶ chlorite + muscovite + andalusite

whereas Seifert and Schreyer (1970) suggested the following reactions:

3) cordierite ⟶ andalusite + chlorite + quartz, and

4) cordierite ⟶ pyrophyllite + chlorite + andalusite.

These reactions are inapplicable in this area because there is no evidence for any conversion of cordierite to andalusite and if cordierite does exist as mineral spots in low grade rocks further north (see above), it has a similar pre-S_1 age to andalusite. These reactions are also discounted by the absence of any pre- or syn-S_1 chlorite.

A common reaction which can explain andalusite growth from matrix minerals is

5) pyrophyllite ⟶ andalusite + 3 quartz + H_2O

(e.g. Kerrick, 1968),

and this curve is used in P,T space to indicate a lower stability limit for andalusite. Turner (1968), however, noted that pyrophyllite is only rarely observed (although it could be easily confused with mica) and suggested that this might be due to its narrow stability range between reaction 4 and

6) kaolinite + 2 quartz ⟶ pyrophyllite + H_2O.

The presence of inclusions of quartz, biotite, ?ilmenite and local graphite in andalusites is strong evidence that andalusite growth took place

from matrix minerals rather than from altered porphyroblasts. These inclusions, some of which are oriented, might represent an early crystallising part of the high grade assemblage rather than a distinct earlier metamorphic event (cf. Vernon, 1977).

5.2.3.5 Garnet*

No direct mineralogical evidence for the formation of garnet has been found. The absence of garnet in low grade rocks, even in pelitic lithologies suggests that the incoming of garnet may be closely related to the incoming of andalusite. Petrological evidence shows that biotite is commonly moulded on garnet in the andalusite and sillimanite schists.

One of the almandine forming reactions cited by Winkler (1974) involves the formation of almandine, garnet and alumino-silicate by breakdown of chlorite, muscovite and quartz, viz.,

7) Fe chlorite + muscovite + quartz $\longrightarrow$ almandine rich garnet + biotite + $Al_2 SiO_5$ + H_2O

However, the <u>local</u> presence of garnet in carbonaceous chiastolite schist might suggest that andalusite forms independently of garnet (Section 5.3.2.3). Alternatively widespread growth of garnet in carbonaceous schists may be hindered by wrong bulk composition or by reduced proportion of H_2O in the fluid phase. It is equally as likely that garnet forms from the breakdown of chlorite + biotite + quartz or chlorite + muscovite + quartz (or epidote) (Winkler, 1974, p.210).

In one situation in the Parnell Beds (Section 4.3.4) the presence of biotite free zones around garnets may suggest that garnet and biotite formation may be competing reactions.

---

* believed to be almandine rich.

5.2.3.6 Mineral Aggregates - Medium Grade Rocks - Andalusite and Chiastolite Breakdown Products

Andalusite and chiastolite schists are characterised by the presence of mineral aggregates containing sericite, quartz, biotite, opaques and local chiastolite. The presence of square outlines of these aggregates and the presence of relict andalusite or chiastolite within them suggests that they represent altered andalusites and chiastolites.

Similar spots ('knotenschiefer') have been described by Tilley (1924) from the outermost zone of the Comrie Granite aureole, and by Harker (1939) from other aureoles. They both suggested that they represent incipient andalusite growth. Chinner (pers. comm., 1976) has re-examined the thin sections of Tilley and Harker which show these spots and has found that the minerals in these, which include various layer silicates, form from the breakdown of andalusite. A similar explanation is put forward to explain the spots in andalusite and chiastolite schist here. However, it is not possible to rule out a cordierite origin for small more rounded mica aggregates.

Quartz, biotite and opaques in these aggregates are regarded as inclusions within the original alumino-silicate. The significant feature of these aggregates is the formation of sericite as a breakdown product in pre- and syn-S_1 time. This suggests that there was an increase in a_{K+} and f_{H_2O} at this time, and this is also supported by the formation of muscovite defining S_1.

5.2.3.7 Formation of Sillimanite - I. From Andalusite

The andalusite/sillimanite isograd mapped in the field separates pre-S_1 andalusite from pre-S_1 and syn-S_1 sillimanite and fibrolite. This section examines one mode of occurrence of sillimanite - that occurring in mineral clots together with sericite, muscovite and with local andalusite. These clots represent the first upgrade appearance of sillimanite and commonly define laminations which lie parallel to bedding (Fig. 3.9). Microstructural evidence (Sections 4.2.4, 4.3.4) indicates that within

these clots, fibrolite together with sillimanite needles occur as:

1) tightly folded pre-S_1 minerals with axial plane fibrolite and sillimanite,

2) as swirling masses which may represent "pre-S_1" oriented or static growth but which now have a shape elongation parallel to S_1, and

3) as bundles and needles parallel to S_1.

It was also shown that sericite laths within these clots may be crenulated about S_1, may be oriented parallel to S_1 or may have a random orientation. It was also shown (Fig. 4.39) that fibrolite parallel to S_1 overprints crenulated sericite. (Late stage muscovite and sericite may also occur in these clots).

Minerals within these clots may be grouped into the following assemblages:

1) andalusite (with inclusions of quartz, biotite and opaques) and sericite,

2) sericite $\pm$ quartz $\pm$ biotite $\pm$ opaques,

3) andalusite + sericite + sillimanite $\pm$ quartz $\pm$ opaques $\pm$ biotite, $\pm$ muscovite,

4) sillimanite + sericite $\pm$ quartz $\pm$ opaques $\pm$ biotite $\pm$ muscovite,

5) sillimanite,

and these are interpreted as an alteration sequence of andalusite to sericite ($\pm$ muscovite) to sillimanite in pre- and syn-S_1 time.

The alteration of andalusite to sericite within clots is a common feature in andalusite as well as in sillimanite schists. It is only in sillimanite schists, though, that sillimanite occurs within the clot pseudomorphing andalusite, and it is suggested that formation of sillimanite from andalusite occurs via an intermediate stage involving the growth of white mica and does not result from direct nucleation of sillimanite from andalusite. The andalusite-white mica- sillimanite association in these rocks is typical of many parts of the world.

Browne (1922, p.306) reported that andalusite in the Mt Franks - Mt Robe area had partially altered to sericite and was generally surrounded by a ruff of muscovite. He also noted the association, in clots, of quartz, sillimanite and mica and that tufts of sillimanite were associated with plates of cross cutting muscovite. Binns (1964) reported that one mode of occurrence of sillimanite in the same area was as large pods of fibrolite associated with mica, and he suggested that these pods had formed by the inversion from kyanite, although he noted that the associated muscovite was probably a late stage mineral formed in his M_2 metasomatic event. In the Mt Robe area, Anderson (1966) noted that andalusite within sillimanite schists was surrounded by a partial or complete ruff of muscovite flakes, 1-2 mm in size, except where it was in contact with quartz rich laminae, and he said that "the ruff forms a complete shield between the andalusite and any nearby sillimanite" (Anderson, 1966, p.90). In another part of the Willyama Complex, in the Bijerkerno area, Tuckwell (1975) described his first schistosity wrapping around whorls of fibrolite and showed that there was an association between sillimanite and muscovite.

Pitcher and Read (1963) described the formation of andalusite and sillimanite as contact minerals in the Donegal Granite aureole. They figured several types of sillimanite; one type was fibrolite occurring with fine or coarse grain muscovite after andalusite. They ascribed the formation of this, and also the instances of fibrolite fringing andalusite, to fluid activity during a metasomatic event. Green (1963) discussed andalusite/sillimanite relations from Vermont, New Hampshire, and noted that within the sillimanite zone, andalusite is surrounded by a rim of coarse grain muscovite while sillimanite in the rock was unaltered. He explained the non alteration of sillimanite by suggesting that "the stability field of sillimanite was not entered until after both the production of andalusite and its partial muscovitisation. This would imply two somewhat distinct pulses of metamorphism separated by either lowering of temperature, or a rise in the

humidity and very probably an influx of potassium" (Green, 1963, p.1005). Similar features were described from Vermont by Woodland (1963), who had concluded that some andalusite had altered to white mica, fibrolite and sillimanite, and described clots of fine-grain muscovite, fibrolite (and sillimanite) which he suggested represented altered andalusites. Woodland (ibid) suggested that some andalusite partly inverted to sillimanite while the remainder altered to white mica and fibrolite. Pitcher (1965) summarised data on alumino-silicates and noted that the replacement of andalusite is frequently accompanied by the growth of muscovite and fibrolite.

Carmichael (1969) suggested different metamorphic histories to explain these features. He suggested that instances of direct inversion between polymorphs were rare, and he thought that reactions such as kyanite $\rightleftharpoons$ sillimanite did not take place by direct replacement. Rather, he considered that they could be represented by "half" reactions occurring in different areas of a thin section and which were summed to give the final net reaction by the transfer, via a fluid intergranular phase, of mobile ions between domains. Carmichael (ibid) thus envisaged a situation of restricted alumina mobility and the presence of an intergranular fluid phase which acted as both a source and a sink for mobile ions which took part in the reaction but which were not represented as products or reactants and which did not affect the conditions of equilibruim (i.e. catalysts).

Carmichael (ibid) discussed the reaction kyanite $\rightleftharpoons$ sillimanite proposed by Chinner (1961). He suggested that the occurrence of droplets of kyanite which were rimmed by muscovite containing needles of sillimanite suggested the following reaction:

8) 3 kyanite + 3 quartz + $2K^+$ + $3H_2O \rightleftharpoons$ 2 muscovite + $2H^+$

In another part of the rock he suggested the following equation to account for the replacement of embayed muscovite by quartz and sillimanite;

9) 2 muscovite + $2H^+ \rightleftharpoons$ 3 sillimanite + 3 quartz + $2K^+$ + $3H_2O$

(see Tozer, 1955).

He thus considered that the net reaction in the rock was the sum of these two half reactions, viz. kyanite $\rightleftharpoons$ sillimanite.

Carmichael (ibid) suggested that similar reactions could be written for the andalusite $\rightleftharpoons$ sillimanite transition, i.e.

10) 3 andalusite + 3 quartz + $2K^+$ + $3H_2O \rightleftharpoons$ 2 muscovite + $2H^+$

The mechanism of this type of metamorphic reaction proposed by Carmichael (ibid) accords well with the formation of sillimanite after andalusite in the Mt Franks - Mundi Mundi area.

The observations of Browne, Binns and Anderson of the association of andalusite-white mica-sillimanite accord well with the observations of this study. However, the coarse grain muscovite of these authors is generally undeformed and is here regarded as an M_3 mineral which formed from the recrystallisation of early sericite and S_1 muscovite. No evidence has been found to sustain Binns' view that sillimanite pods formed from inversion of kyanite; indeed the presence of relict andalusites within some of these clots renders this method of formation unlikely.

In attempting to apply a Carmichael type model to metamorphic and microstructural changes at the andalusite/sillimanite isograd, the following points must be made:

1) within mineral clots, andalusite, sericite and sillimanite are all pre-S_1 in age. Sillimanite is also syn-S_1 in age and later sericite crystallisation occurs in S_1 and S_3 time and muscovite "ruffs" probably formed in D_3 time.

2) alteration of andalusite to sericite occurs throughout the deformation history (pre-, syn-S_1, syn-S_3).

3) sillimanite undergoes late stage pseudomorphism by $2M_1$ muscovite which can be detected by X-ray powder diffraction. Chinner (1973) pointed out that this sort of replacement may commonly go undetected.

4) One of Carmichael's tenets is the relative immobility of alumina. Whilst there is convincing evidence for mobility of alumina in other cases

(see below) it does appear that there is little movement of alumina released by breakdown of the andalusite lattice. Thus sericite clots generally retain the characteristic outlines of andalusite, and partially altered andalusites maintain their size grading (Fig. 2.19).

5) Carmichael (ibid) envisaged two separate half reactions occurring in different parts of a thin section. Evidence from the Robe Beds suggests that the formation of sillimanite from andalusite takes place via an intermediate stage (sericite) which is in contact with the products and the reactants of the reaction. The two domains in this case, andalusite altering to sericite in one, and sericite altering to sillimanite in the other, are only tenths of millimetres apart.

6) The first half reaction, that of andalusite breakdown to sericite occurs on both sides of the andalusite/sillimanite isograd. The second half reaction, which leads to the formation of sillimanite only occurs in sillimanite schists. The recrystallisation of sericite to muscovite laths is generally restricted to the sillimanite schist but does occur to some extent in the western part of the andalusite schists. The complete formation of sillimanite from andalusite only occurs if both of the half reactions go to completion. But, as is apparent from earlier in this section, all stages in the andalusite-sericite-sillimanite transition are seen.

It is not necessary to invoke widespread introduction of K^+ and H_2O into the system for the formation of sericite in syn-S_1 time since they could be easily supplied by breakdown of the early white micas. Alternatively, K^+ might be made available from biotite breakdown in S_1 time according to Reaction 1:

3 biotite $\longrightarrow$ muscovite + 3 magnetite + $2K^+$ + 6 quartz*

This reaction results in the formation of sericite, muscovite and opaques

---

* if the biotite is Ti rich, ilmenite might constitute part of the opaque phase.

commonly remobilised into S_1. Half reactions can be coupled together (cf. Carmichael 1969) to result in

11) 3 biotite + 3 andalusite $\longrightarrow$ 3 muscovite + 3 magnetite + 3 quartz

This reaction is thus a summation of two half reactions proceeding in different parts of the thin section yet linked by a fluid phase and by the exchange of cations. Biotite breakdown releases K^+ into the system which is able to migrate to sites around andalusite porphyroblasts and results in an increase in a_{K^+} which may initiate the breakdown of andalusite.

With reference to Eugster (1970) it is possible to represent the reaction alumino-silicate $\rightleftharpoons$ muscovite as a thermal (reaction 12) or ionic (reaction 13) reaction:

12) andalusite + K feldspar + $H_2O \rightleftharpoons$ muscovite + quartz, and

13) 3 andalusite + 3 quartz + $2K^+ + 3H_2O \rightleftharpoons$ 2 muscovite + $2H^+$

By using ionic reactions, Eugster was able to show that reaction 13 depends not only upon temperature, but also upon f_{H_2O}, a_{K^+} and pH.

Using Eugster's (1970) Figure 9 (Fig. 5.3) it is possible to explain the sericitisation of andalusite (at constant pH) in terms of

(1) a decrease in temperature,

(2) an increase in f_{H_2O}, or

(3) an increase in a_{K^+}

(Fig. 5.3).

It is suggested that in the andalusite schists, sericitisation of andalusite is a response to an increase in f_{H_2O} or a_{K^+} (or both). It is further suggested that this reaction is reversed in the sillimanite schists by an increase in temperature represented by the stability of sillimanite over andalusite (see Section 5.2.3.11). This temperature increase reverses the sericitisation process, but results in the formation of sillimanite, rather than andalusite.

Thus it is suggested that relations at the andalusite/sillimanite isograd can be accounted for by a two stage reaction involving the intermediate stage

sericite. The formation of sericite from andalusite requires an increase of a_{K^+} and f_{H_2O} in the local system around andalusite porphyroblasts.

5.2.3.8 Formation of Sillimanite - II. Sillimanite Associated with Biotite

Sillimanite commonly occurs as needles and as bands associated with biotite rather than andalusite, and microstructural aspects of this association were discussed in Section 4.3.4. There it was shown that:

1. randomly oriented biotite was commonly associated with inclusions of thin needles of sillimanite parallel to S_1, or to (001) traces, or aligned in two directions 60° apart in basal biotites,

2. bands of fibrolite and sillimanite commonly contained biotite inclusions, and

3. sillimanite and fibrolite associated with biotite were "dirty" in colour.

The association of biotite with sillimanite is common in the literature. The relation between these two minerals has been described in (i) chemical and (ii) structural terms.

(i) Chemical. Proponents of this view suggest that biotite is breaking down and sillimanite forms from the breakdown products. Watson (1948) described biotite/sillimanite relations ranging from sillimanite tufts in biotite to vague pleochroic relics in fibrolite surrounded by iron ore and suggested the following reaction

14) biotite $\rightarrow$ fibrolite + Fe oxide + quartz + K_2O + MgO + H_2O.

He also suggested that fibrolite inclusions within quartz formed by this reaction.

Tozer (1955) described mats of fibrolite developed along biotite rich foliae often parallel to cleavage traces and showing indistinct boundaries with them. He noted that as the amount of fibrolite increased, the biotite became paler in colour and eventually disappeared although patches with

residual pleochroism frequently persisted in the interior of dense fibrolite aggregates. Tozer (ibid) suggested that K, Mg, Fe, F and (OH) were liberated in this reaction and some magnetite formed. He cited fibrolite needles in quartz and feldspar as evidence of diffusion. Tozer further noted a later metamorphic event which resulted in the growth of muscovite and growth of sillimanite and regeneration of biotite. Francis (1956) suggested that biotite breakdown occurred by a reaction:

15) Fe biotite + dissolved kyanite → K feldspar + sillimanite + Fe_3O_4 + H_2O

and cited as evidence the decolouration of biotite and the formation of magnetite.

Woodland (1963) favoured the chemical hypothesis to explain bleached biotite associated with sillimanite in Vermont. He noted the absence of any K feldspar (as reported by Francis, 1956) and suggested that biotite altered to either or both sillimanite + muscovite. Carmichael (1969) also favoured a chemical relationship between biotite and sillimanite. However, he suggested that sillimanite was not replacing biotite, but that the relationship between the two was one of contemporaneous formation by replacement of another mineral, in a fluid phase with Al^{3+} immobile but with the transfer of mobile ions. Thus in the overall reaction kyanite to sillimanite, he figured three half reactions

16) biotite + Na^+ + 6 H^+ → albite + K^+ + 3$(Mg, Fe)^{2+}$ + 4 H_2O

and in another part of the rock,

17) 3 kyanite + 3 quartz + $2K^+$ + 3 H_2O → 2 muscovite + 2 H^+

and to close the system, the reaction

18) 2 muscovite + albite + 3 $(Mg, Fe)^2$ + H_2O → biotite + 3 sillimanite + 3 quartz + K^+ + Na^+ + 4 H^+.

These reactions when summed resulted in

19) 3 kyanite → 3 sillimanite.

The key reaction is the formation of sillimanite + biotite from albite and is based on Tozer (1955).

(ii) Structural. Chinner (1961) described fibrolite/biotite intergrowths

with c axes of sillimanite lying parallel to mica cleavages and he observed that the biotite/fibrolite ratio varied from biotite zones lacking fibrolite to bundles of fibrolite showing traces of faint brown pleochroism. In basal biotite sections, Chinner (ibid) noted that fibrolites formed a triangular pattern, forming parallel to the zone axis (010) and to two pressure fringe directions at 60°. He suggested that biotite acted as a structural nucleating control rather than a chemical one: instead of biotite breaking down and contributing Si and Al which re-arranged themselves to form fibrolite, he envisaged oriented growth (epitaxis) with the "trigonally arranged octahedral and tetrahedral O in the alternate mica layers acting as nuclei for the growth of octahedral Al - O and tetrahedral (Al, Si) - O chains that constitute the sillimanite structure." (Chinner, 1961, p.312). Chinner (ibid) found that bleached biotites had the same Mg/Fe ratios as normal biotites and suggested that rather than biotite breakdown, this decolourisation was due to superposition of fibrolite on top of biotite, thus reducing the intensity of pleochroism. Chinner (ibid) considered that the Al and Si came from kyanite breakdown elsewhere in the rock and migrated in solution to the structurally attractive biotites. Chinner (ibid) also noted that the instability of biotite may have aided fibrolite nucleation. However, he pointed out that this instability was only temporary, and suggested (pers. comm., 1976) that dirty fibrolite or bleached biotite represent intergrowths of biotite and fibrolite. Binns (1964) favoured epitaxial rather than chemical control to explain fibrolite/biotite relations in sillimanite schists near Mt Franks in the Willyama Complex. Chenhall (1973) has recently discussed biotite/sillimanite relations in the Willyama Complex. He found that the chemical analysis of bleached biotites associated with sillimanite were similar to normal biotites and thus agreed with the epitaxial view of Chinner.

In the Mt Franks - Mundi Mundi Area, sillimanite/biotite relations are consistent with the epitaxial growth model of Chinner. The simultaneous growth mechanism of Carmichael in this instance is militated against by the different ages of most of the biotite and sillimanite.

5.2.3.9 Formation of Sillimanite - III. Sillimanite in Quartz

Needles of sillimanite with well defined crystal faces are common as inclusions within M_1 quartz grains, where they lie both parallel to, and at angles to, S_1. These sillimanite/quartz relations are similar to those described recently from other parts of the Willyama Complex by Vernon (1975), and coexist with coarser grained M_1 sillimanite lying in S_1. As suggested by Vernon (1975), these sillimanite needles are probably an equilibrium phase of the high grade assemblage.

Although Watson (1948) has suggested that quartz/sillimanite intergrowths may form from the breakdown of biotite, the relationship in this area is more in accord with the ideas of Carmichael (1969). He suggested that sillimanite and quartz are co-products of muscovite breakdown (Reaction 9).

5.2.3.10 Formation of Sillimanite - IV. Sillimanite in Muscovite

Previous workers in the Willyama Complex have described this association. Browne (1922) noted tufts of sillimanite needles within cross-cutting muscovites, and Binns (1964) suggested that these muscovites grew in his M_2 event (sillimanite represented M_1) and that "during its growth it has dissolved the smaller fibres of the fibrolite aggregate, leaving the larger needles as included relics in contorted trains" (Binns, 1964, p.305). Anderson (1966) regarded these muscovites as products of his M_4 event, and noted that fibres of sillimanite were commonly subparallel to S_1.

Various models have been put forward to explain the association of sillimanite and muscovite. Tozer (1955) attributed the association of coarsely crystalline sillimanite with flakes of mica, and late fibrolite in, or associated with, muscovite, to a growth of muscovite brought about by an influx of K^+, F^- and $(OH)^-$ from the neighbouring granite. He suggested that "this was associated with the destruction of part of the early sillimanite, growth of a new crop of sillimanite needles and formation of muscovite-sillimanite intergrowths" (Tozer, 1955, p.310). Green (1963) and Woodland (1963) both described sillimanite inclusions within muscovite.

Carmichael (1969) suggested that the observations of Tozer (1955) could be re-interpreted by considering muscovite and sillimanite as minerals of the same ages and produced from a reaction involving an earlier phase, i.e.

20) 2 muscovite + 2 $H^+ \longrightarrow$ 3 sillimanite + 3 quartz + 2 K^+ + 3 H_2O.

At the andalusite/sillimanite isograd, he regarded this reaction complementary to one involving andalusite breakdown occurring in another part of the slide and which when added together, resulted in

21) andalusite $\rightleftharpoons$ sillimanite.

In the Mt Franks - Mundi Mundi Area, most of the muscovite laths which contain sillimanite inclusions are regarded as late stage minerals (M_3 event). Because of the difference in age between most of these muscovites and sillimanite, these relations cannot be explained by a Carmichael type reaction. Rather, sillimanite needles in muscovites are regarded as inclusions representing an earlier phase of growth. Muscovite growth probably takes place either by (re)crystallisation of M_1 muscovite (sericite) or by pseudomorphic alteration from early biotites. The sillimanite inclusions are thus regarded as inherited from a sericite/sillimanite mixture, or from a biotite/sillimanite mixture.

5.2.3.11 Stability of Sillimanite

Experimental studies on solid-solid reactions in the Al_2SiO_5 system have produced many different results (for discussion see, for example Althaus, 1969; Zen, 1969; Holdaway, 1971). Because of the small changes in free energy involved during reactions, boundary fields between various phases are sensitive to among other things, nature and size of starting material and nature of experimental equipment. Most commonly quoted, however, appear to be the curves of Holdaway (1971), and the results of Wall and Essene's work (reported in Vernon, 1976, Fig. 4.5), agree with Holdaway's suggestions. These experimental results are applied to field relations in order to derive conditions of formations of various phases. This, however, assumes that

phases are in equilibrium and that P and T are the sole controls on stability fields. Although Chinner (1966) noted that zones separating andalusite from kyanite and sometimes andalusite from sillimanite are generally well defined, he also noted that sillimanite tended to co-exist with andalusite or kyanite over vast areas.

This could be due to

1) divariance due to metal content constituting an additional component

2) the fact that direct inversion between phases is rare

3) the possibility of metastability in an overprinting situation.

1) Although Pitcher (1965) suggested that there may be a compositional control on development of Al_2SiO_5 species, Albee and Chodos (1969) and Chinner et al. (1969) suggested there was no real solid solution effect.

2) Although kyanite/andalusite inversions in nature have been described (see Chinner, 1966), sillimanite generally does not grow on andalusite or kyanite (see above). In these situations, there may be no direct applicability of experimental results.

3) Chinner (1966) suggested that evidence of metastability is hard to obtain. However, he suggested that some evidence of stability is the alteration of andalusite while co-existing sillimanite is unaltered.

In the Mt Lofty Ranges, Fleming (1973) considered that fibrolite lying within the andalusite/staurolite zone (distinct from the sillimanite zone) is metastable on the basis of Mg-Fe distribution between garnet and biotite.

4) Most authors (e.g. Pitcher, 1965; Chinner, 1966) suggest that most examples of co-existing alumino-silicates may be due to overprinting.

In the absence of any chemical studies of phase relations or whole rock analyses it is believed that sillimanite in the Mt Franks - Mundi Mundi area is a stable phase which formed within the P, T field of sillimanite.

This view is based on:

1. the general restriction of andalusite bearing schists and sillimanite

bearing schists to separate areas,

2. the fact that where later faulting has not occurred a narrow zone of andalusite/sillimanite co-existence can be drawn between andalusite schist and sillimanite schist, and

3. the fact that the sillimanite grade zone coincides with areas of migmatisation during D_1, indicating higher P, T conditions than in the andalusite zone.

5.2.3.12 Stability of Fibrolitic Sillimanite

Various workers such as Zen (1969) and Holdaway (1971) raised the possibility that fibrolite is disordered or non stoichiometric sillimanite. Holdaway (1971) considered fibrolite to be a disequilibrium phase, its high reactivity due to (1) fine grain size, (2) strain energy of bent fibres, (3) Al-Si disorder (4) other lattice defects, and (5) unstable composition.

Cameron and Ashworth (1972, p.135), however, reported that fibrolite "does not differ in its ordering scheme or composition from coarser grained sillimanites."

They noted that isobaric displacements of the andalusite/sillimanite line to the extent of 160°C towards high temperatures as reported by Richardson et al (1969) and 200°C towards high temperatures as reported by Holdaway (1971), if real, were probably caused by an increase in surface free energy due to fine grain size. However, in contrast to Cameron and Ashworth (1969), Bell and Nord (1973) found that the fibrolite used in the experimental work of Richardson et al (1968) consisted of finely intergrown sillimanite and quartz.

In the Mt Franks - Mundi Mundi area it is possible that fibrolite may be an intermediate phase in the formation of sillimanite from andalusite (cf. Holdaway who suggested that andalusite-fibrolite reaction was unlikely) and was possibly favoured by: a) lower temperature than that needed to form sillimanite,

b) high a_{K^+}, or

c) higher f_{H_2O}

because of its large surface area. Laing (1977) reported the alteration of M_1 sillimanite into M_2 fibrolite and associated sericite, and he suggested that the formation of fibrolite may have been favoured by higher water pressures.

The formation of sillimanite via a Carmichael type reaction rather than by polymorphic inversion is presumably favoured by energy considerations. Under normal conditions the reaction initiated will be that with the lowest activation energy. In the writer's area, the reaction andalusite-sericite-sillimanite appears more energetically favourable than direct conversion which requires nucleation with growth of sillimanite from andalusite. In this environment, fibrolite is a stable phase.

5.2.3.13 Sillimanite + K feldspar

Muscovite-free, biotite-rich rocks in the Robe sillimanite schist are marked by the presence of sillimanite + K feldspar + biotite. K feldspar occurs as equant or elongate grains parallel to S_1 containing inclusion trails of biotites outlining a pre-S_1 as well as an S_1 orientation, and sillimanite occurs as needles or in layers aligned parallel to S_1. Both these minerals are thus thought to be of similar age, and in equilibrium. The absence of muscovite may be due to

1) lack of biotite breakdown,

2) compositional control, or

3) may suggest formation of the pair sillimanite + K feldspar from the reaction

22) muscovite + quartz → sillimanite + K feldspar + vapour

(Evans, 1965; Kerrick, 1972).

Distribution of sillimanite + K feldspar pairs observed in thin section (Fig. 5.1) indicates the local development of this assemblage in the Robe sillimanite schists. This patchiness might be a reflection of local

variations in P_{H_2O} or in the proportion of H_2O in the fluid phase (see Kerrick's (1972) curves in Fig. 5.4.).

In the Parnell Beds, limited sampling suggests the pair sillimanite + K feldspar becomes dominant to the east away from the Apollyon Valley Retrograde Schist Zone, and the second sillimanite isograd has tentatively been drawn parallel to S_1 in this area (Fig. 5.1).

Some equant K feldspar is inferred to be present in the western part of the Robe andalusite schists. Strong retrogression prevents absolute determination of this mineral, or of its age with respect to S_1. Its presence here in a biotite rich area may be due to high K^+ content and poor P_{H_2O} so that muscovite is absent and suggests that not all K feldspar formed from Reaction 22.

5.2.4 Partial Melting in M_1

The presence of D_1 and M_1 migmatites and granitoids in sillimanite schists of the Mt Franks - Mundi Mundi area was established in Section 2.4.2 and Section 3.3.3. Although several theories for the origin of these banded rocks have been discussed in the literature (see Winkler, 1974) the presence of M_1 migmatites within sillimanite schists in this area is consistent with their formation as by-products of partial melt reactions.

Phillips (1975) has suggested six possible melt reactions which are relevant in the Willyama Complex:

23) quartz + K feldspar + plagioclase + H_2O $\longrightarrow$
plagioclase + melt $\pm$ quartz $\pm$ feldspar

24) muscovite + quartz $\pm$ plagioclase $\longrightarrow$ sillimanite + melt $\pm$ K feldspar

25) biotite + sillimanite + plagioclase $\longrightarrow$ K feldspar + garnet + plagioclase + melt

26) biotite + K feldspar + garnet + plagioclase + quartz
$\longrightarrow$ plagioclase + garnet + biotite + melt

27) hornblende + plagioclase + quartz $\longrightarrow$ o/pyroxene + c/pyroxene + plagioclase + ilmenite + melt

28) or → o/pyroxene + c/pyroxene + plagioclase + ilmenite + biotite.

Reaction 24 is the most likely to have occurred in this area since it does not involve destruction of K feldspar, biotite or the formation of pyroxenes and suggests that partial melting is able to supply the necessary melt for migmatite formation. The presence of migmatites in the sillimanite + muscovite zone suggests that most of the K^+ released by Reaction 24 may have migrated into the leucosome phase rather than appearing as K feldspar.

Similar relations were described by Lundgren (1966) who noted the predominence of migmatites in the sillimanite + muscovite zone in Connecticut, and suggested that they formed partly by the elimination of muscovite to form sillimanite + K feldspar + melt with the release of some K^+ into the leucocratic components of the migmatites. He also suggested that melts in the lower temperature part of the sillimanite + K feldspar zone must have also been controlled by the amount of H_2O released by muscovite breakdown, while melting in the higher temperature part could have formed by biotite breakdown reactions.

The formation of non migmatitic granitoid sheets with sharply defined boundaries in low and medium grade rocks during the D_1 event (Section 2.4.2) cannot be explained by partial melting in situ. However, they may be derived by the upward movement of melt generated in underlying sillimanite grade schists.

5.2.5 Conditions of Metamorphism during M_1

5.2.5.1 The Presence of a Fluid Phase and the Role of Graphite in Influencing its Composition

The treatment of S_1 fabric forming mechanisms in Section 4.3.7 suggested that a fluid phase was an integral part of the rock system during M_1. Further evidence for the existence of such a phase is provided by the success of ionic reactions in explaining petrological observations of the last section. Despite these two lines of approach, there is, however, no direct evidence for the existence of a fluid phase and Vernon (1976, p.53 et seq.)

has discussed aspects of this general problem.

The fluid phase in non carbonaceous rocks would be dominated by H_2O ($X_{H_2O} \sim 1$) and the extensive (re)crystallisation of muscovite in S_1 suggests that, at this stage of M_1, $P_{H_2O} \rightarrow P_T$. In carbonaceous rocks, however, the fluid phase would consist not only of H_2O, but also of CO, CO_2, and CH_4 liberated during the metamorphism of graphite. As a result, $P_{H_2O} < P$ fluid. As in the non carbonaceous schists, the presence of hydration reactions in M_1 would ensure that $P_{fluid} \rightarrow P_T$.

Various workers have discussed the composition of a fluid phase in carbonaceous rocks. Miyashiro (1964) showed that graphite exerted a strong reducing effect on its surrounding system, since it acts as a buffer maintaining constant f_{O_2} and, in so doing, is itself oxidised. Miyashiro (ibid) also suggested that f_{O_2} increases with increasing temperature. Miyashiro (ibid) also pointed out that in an interlayered graphite rich and graphite free unit (for example the Mundi Mundi facies) hydrogen could move from the graphite-bearing rocks into the adjacent layers thus causing some reduction in the graphite free layers. French (1966) also suggested that since graphite buffers f_{O_2}, variations in f_{O_2} may reflect original variations in the distribution of graphite. French (1966) further suggested that in the system graphite plus a C-O-H gas phase, cannot exist with a fluid phase consisting of greater than 85% water. He also found that the effect of CH_4 appears negligible above about 600°C. (Eugster and Skippen (1967) and Black (1976) suggested a figure of 400°C for this effect).

Eugster and Skippen (1967) investigated the composition of a C-O-H gas at 2 Kb in the presence of graphite and showed that at 500-600°C (the most likely temperatures in the thesis area at this pressure - see Fig. 5.4) the gas phase contained between 50 and 30% H_2O (NNO,OH buffer) and between 80 and 70% H_2O (QFM, OH buffer). Kerrick (1972) interpreted Eugster and Skippen's (1967) results by suggesting that in graphitic rocks, the maximum $P_{H_2O}/P_{fluid} = 0.85$ at $P_f = 2$ Kb and suggested that the muscovite and quartz out reaction at $X_{H_2O} = 0.8$ represents a maximum temperature for

assemblages at this isograd.

The presence of graphite, and the reduced H_2O component in the fluid phase of carbonaceous rocks in the Mt Franks - Mundi Mundi area is capable of explaining four major differences in mineralogical aspects between carbonaceous and non carbonaceous schists. These are now discussed.

1. Both the Mundi Mundi facies and part of the Apollyon chiastolite schist lie within the sillimanite grade zone as defined in non carbonaceous schists. In both these rock types, chiastolite persists as large crystals and is metastable.* Similar persistence of andalusite in other carbonaceous schists has been noted by A. Heitanen, V. Wall, R. Vernon and H. Zwart (all pers. comm., 1976). The slowing down of the andalusite to sillimanite transition can be readily explained in terms of the andalusite/sillimanite reaction discussed in Section 5.3.2.6. This reaction proceeds via an intermediate sericite phase, the formation of which is dependent upon increase in a_{K^+} and f_{H_2O}. Since X_{H_2O} is reduced in the fluid phase within carbonaceous schists, there is a consequent slowing down of the reaction and andalusite thus persists metastably into the sillimanite zone.

2. Where the Apollyon chiastolite schist crosses the sillimanite isograd, metastable chiastolite persists as described above, and there is a gradual bleaching of the rock which is caused by a decrease in graphite content. The loss of graphite in this area may be due to oxidation in buffering the system to a constant f_{O_2} during the breakdown of biotite and formation of muscovite + magnetite (Section 5.2.3.1).

3. The grain size of quartz in Apollyon chiastolite schist is generally smaller than in the adjacent andalusite schist, and this point was first noted by Anderson (1966). The smaller grain size in the carbonaceous unit is probably due to the physical presence of graphite spicules along

---

* andalusite crystals in these lithologies are larger than those in the surrounding non carbonaceous schist.

quartz/quartz, quartz/mica and also mica/mica grain boundaries which pin down grain boundaries and prevent grain enlargement. They thus act in much the same way as grains of mica which pin quartz boundaries and result in smaller quartz grains in quartz/mica assemblages than in pure quartz assemblages (e.g. Wilson, 1973).

4. Pre-S_1 assemblages are better preserved in carbonaceous schist than in non carbonaceous schist. This again is probably due to a slowing down of reactions and is caused either by the chemical effect of hydrocarbons in the fluid phase, or by the physical presence of graphite. Suess (1970) suggested that organic carbon is adsorbed onto layers on calcite grains and can produce physical isolation of grain surfaces from sea water and reduce or inhibit reaction rates. He suggested that if the free energy of adsorption is greater than the free energy of the reaction, the precipitation and dissolution of carbonate would cease unless there were "holes" in the carbon coating. Robinson (1971) studied the contact metamorphic effects of the Whin Sill on carbonaceous limestones, and suggested that the mantle of carbon prevented new calcite growth (recrystallisation) by inhibiting grain boundary movement.

5.2.5.2 Progressive Metamorphism and a Geothermal Gradient

The low, medium and high grade metamorphic zones in the area are products of the M_1 event and represent a progressive metamorphic series. Table 5.2 indicates that relicts of the low and medium grade zones persist up into the high grade zone. The subdivision of M_1 minerals on microstructural evidence into those lying in S_1, and those which predate S_1 (Table 5.3) is marked by overlap between pre- and syn-S_1 minerals. This then suggests that pre- and syn-S_1 minerals represent phases of the one event which is marked by progressive mineral growth.

An approximate geothermal gradient for the M_1 event is shown in Fig. 5.4. This gradient is controlled by several features:

1. On the high pressure side by the absence of kyanite.

TABLE 5.2

DISTRIBUTION OF INDEX MINERALS, M_1 EVENT

	LOW GRADES	MEDIUM GRADES	HIGH GRADES
muscovite	✓	✓	✓
biotite	✓	✓	✓
andalusite	(local in carbonaceous rocks)	✓	✓
garnet		✓	✓
sillimanite			✓

TABLE 5.3

MINERAL GROWTH/DEFORMATION RELATIONS, D_1 EVENT

	pre-S_1 event (preferred mineral orientation)	pre-S_1 event (interkinematic pophyroblasts)	syn-S_1 event
white mica			
biotite	m, h	l	
andalusite	m, h (l)		
mineral clots			
garnet		m, h	
sillimanite	h		
K feldspar		h (m)	
plagioclase		?	
quartz	?		
ilmenite	m, h		
graphite	l, m h		

l = low grade rocks, m = medium grade rocks, h = high grade rocks

2. On the low temperature side by the formation of biotite (Curve 3) from components. No evidence for the formation of biotite has been found in the Mt Franks - Mundi Mundi area. Curve 3 is the best available guess; but it is not fully satisfactory since it appears on the upgrade side of the andalusite forming reaction (Curve 2) whereas low grade rocks are characterised by the formation of biotite without andalusite. Both curves 3 and 2 are characterised by steep slopes and it is highly probable that overstepping may occur.

3. The position of quartz + muscovite $\rightleftharpoons$ sillimanite + K feldspar curves on the high temperature side. Kerrick's (1972) curves are used both for non carbonaceous schists ($X_{H_2O} = 1$) and for carbonaceous schists ($X_{H_2O} = .8$). The limited development of sillimanite + K feldspar rocks in non carbonaceous schists indicates that this line is just crossed.

4. The presence in the carbonaceous Mundi Mundi facies of K feldspar, sillimanite, andalusite, muscovite, graphite and quartz.

5. The presence of migmatites in sillimanite + muscovite rocks. This indicates that the geothermal gradient must lie above the intersection of the granite melt curve ($X_{H_2O} = 1$) with the quartz + muscovite out curve ($X_{H_2O} = 1$). It is significant that the field of high grade metamorphism reported by Laing (1977) in the Mine area contains essential cordierite and is shown in Fig. 5.4. The P,T conditions reported by him are regarded as occupying the maximum P,P conditions reached in the M_1* event in the Willyama Complex.

A significant feature of M_1 is the absence of chloritoid and staurolite, even though both of these minerals form in the retrograde M_3 event (Section 4.5.1.4 and Section 4.5.1.9). Both of these minerals require special bulk rock compositions for their formation which may be unavailable in M_1 time. Alternatively, the M_1 geothermal gradient may be outside the staurolite and chloritoid

---

* Correlation of structural/metamorphic events between the two areas is discussed in Section 7.3.

stability fields. V. Wall (pers. comm.,1978) has suggested that the staurolite curves in Fig. 5.4 should be raised by $1\frac{1}{2}$ - 2 Kb in the presence of muscovite, thus making them consistent with the inferred gradient.

5.3 METAMORPHISM M_2.

5.3.1 Mineral Assemblage

The M_2 event is very localised in the Mt Franks - Mundi Mundi area, and M_2 assemblages were only observed in the hinge zones of F_2 folds in the Shepherd's Hut Area (Map 1). Although S_2 in these rocks is dominated by rotated M_1 minerals, the following assemblage is indicated:

muscovite + sericite + quartz $\pm$ sillimanite $\pm$ biotite + opaques

5.3.2 Possible Mineral Reactions, Growth and Stability

The presence of local sillimanite needles aligned parallel to S_2 within folded bands of S_1 sillimanite suggests that M_2 sillimanite formed from the recrystallisation of M_1 sillimanite. Similarly, scattered M_2 biotite laths are associated with layers of folded M_1 biotite. But in contrast to M_1 biotite, M_2 biotites are free from quartz inclusions and vary in colour from pale yellow to yellow brown. The presence of opaque spicules within M_2 biotites might suggest they are less iron rich than M_1 biotites.

The main component of the M_2 assemblage is sericite which occurs in bands parallel to, and defining, S_2. Formation of sericite probably occurred by recrystallisation of M_1 muscovite, as well as by breakdown of M_1 plagioclase, K feldspar and some biotite. Other sericite may have formed by local reversal of Reaction 22

quartz + muscovite $\rightleftharpoons$ sillimanite + K feldspar + H_2O

Formation of sericite during M_2 indicates a high a_{K^+}, and a high P_{H_2O} at this time. M_2 is thus of lower grade than M_1, although sillimanite is locally stable as is biotite.

5.3.3 P-T-X Conditions

P-T-X conditions for the M_2 event are shown in Fig. 5.5. Formation of

sericite, breakdown of K feldspar and local breakdown of sillimanite suggests that the field of M_2 lies just to the left of the curve

muscovite + quartz $\rightleftharpoons$ K feldspar + sillimanite + H_2O

The large amount of sericite formed in S_2 suggests that $X_{H_2O} \sim 1$ for this reaction.

5.4 METAMORPHISM M_3.

In contrast to M_1 and M_2, M_3 is a retrograde event which is broadly correlated with the D_3 deformation. M_3 results in the formation of randomly oriented porphyroblasts of staurolite, muscovite, chloritoid and chlorite, as well as the formation of quartz, muscovite, chloritoid, iron oxides and sericite aligned parallel to S_3.

5.4.1 Mineral Assemblages

M_3 assemblages in low, medium and high grade rocks are shown in Table 5.4. AKF diagrams corresponding to these are shown in Fig. 5.6. Both chloritoid and staurolite have restricted distribution: chloritoid in sericite clots in andalusite schists, and staurolite in the Parnell Beds. The presence of identical minerals both in S_3 and as random porphyroblasts (e.g. muscovite, sericite, chloritoid) indicates that an S_3 phase and a phase of random growth are closely related in time and are part of an M_3 event.

5.4.2 Possible Mineral Reactions, Growth and Stability

5.4.2.1 Quartz

Microstructural evidence (Section 4.5.1.1) has clearly shown that most of the M_3 quartz develops by the recrystallisation of M_1 quartz. Quartz/muscovite M_3 associations are discussed below.

5.4.2.2 Muscovite and Sericite

Muscovite occurs as discrete syn-S_3 laths lying parallel to F_3 axial planes, or within S_3, and also as randomly oriented more equidimensional laths which cut across S_3 and F_3 hinges and which may overprint graphite

TABLE 5.4 - M_3 Assemblage

LOW GRADE ROCKS		
carbonaceous schist	- syn S_3:	q $\pm$ musc + ser + iron oxides $\pm$ ch
	- random:	musc $\pm$ ch
non carbonaceous schist	- syn S_3:	q $\pm$ musc + iron oxides $\pm$ ch
	- random:	musc $\pm$ ch
calc silicates	:	trem + ep + ch + cz $\pm$ carb
MEDIUM GRADE ROCKS		
carbonaceous schist	- syn S_3:	ser + q + musc + iron oxides $\pm$ ch $\pm$ bio
	- random:	m $\pm$ ch
non carbonaceous schist	- syn S_3:	ser $\pm$ bio $\pm$ q + m $\pm$ chd $\pm$ ch
	- random:	chd + musc $\pm$ ch + iron oxides
calc silicates	:	ser + ep + cz + tr
MEDIUM HIGH TO HIGH GRADE ROCKS		
psammites, pelites, psammopelites	- syn S_3:	q + musc + ser + iron oxides $\pm$ ch
	- random:	q + musc + ch + iron oxides $\pm$ staur $\pm$ gn
amphibolite	:	q + op + amph
calc silicates	:	ep + cz + ser + tr

---

abbreviations - as per Table 5.1 plus -
ep - epidote; ch - chlorite; cz - clinozoisite; chd - chloritoid; stau - staurolite; tr - tremolite; carb - carbonate.

spicules oriented in S_3. This latter group of muscovite corresponds to the M_2 event of Binns (1963). Most of the M_3 muscovite has formed by recrystallisation of M_1 muscovite and sericite. Other muscovite occurs together with chlorite as products of biotite breakdown.

A particular M_3 feature occurring in M_1 sillimanite + K feldspar rocks is the presence of muscovite quartz intergrowths (Fig. 5.7). Quartz within muscovite laths occurs as:

1) rods 0.1 mm long with bulbous or cuspate heads which may lie parallel to, or at high angles to the muscovite cleavage traces.

2) irregularly shaped lobes of quartz with an average length of 0.04 mm occurring along a particular horizon within muscovite.

3) irregularly shaped fingers of quartz emanating from a thin band of quartz within a muscovite grain.

4) lobes of quartz lying at high angles to, and emanating from the border of muscovite, and K feldspar near sillimanite.

These quartz/muscovite intergrowths imply simultaneous crystallisation. Their proximity to K feldspar and sillimanite suggests that they might form by reversal of reaction

muscovite + quartz $\rightleftharpoons$ K feldspar + sillimanite + H_2O

in response to falling P,T conditions, or to increasing a_{K^+} or P_{H_2O} or to all three. These intergrowths are different to the muscovite + plagioclase + quartz (myrmekite) intergrowths described from Broken Hill by Phillips et al (1972).

Fine grained muscovite (sericite) occurs as individual laths parallel to S_3, in bands parallel to S_3, and also as alteration products from sericite. In the first two cases, it is suggested that sericite forms by recrystallisation of coarse grained M_1 muscovite laths and this has been illustrated in Section 4.5.2.4. In the third case, sericite formation is a response to muscovitisation of andalusite as discussed in Sections 4.5.1.2 and 5.2.3.7. Pseudomorphism of sillimanite by sericite (Section 4.5.1.2)

may also be in part an M_3 feature. Other sericite probably forms by breakdown of feldspar - this also occurs in amphibolites.

5.4.2.3 Biotite

Biotite is generally unstable during M_3 and alters to chlorite, either parallel to S_3 or pseudomorphing biotite, or to chlorite + muscovite. However, biotite is locally stable in chiastolite schist during M_3 where it undergoes rotation into S_3, probably adjusting chemically from M_1 to M_3 conditions. Despite this, M_3 conditions are probably just below the limit of biotite stability.

5.4.2.4 Iron Oxides and Graphite

These two minerals undergo remobilisation during M_3, and form bands parallel to S_3.

5.4.2.5 Chlorite

Straw-yellow to pale green chlorite pseudomorphs biotite and also occurs as laths parallel to and cutting across S_3.

5.4.2.6 Chloritoid

Chloritoid laths cut across, and also lie parallel to, S_3 (Section 4.5.1.4). They are restricted to sericite clots after andalusite where they occur as polysynthetically twinned grains with iron oxide inclusions. They may be commonly moulded on biotite or iron oxide. The association of chloritoid with andalusite, sericite and biotite was first noted by Browne (1922, pp.304-305) who suggested that chloritoid formed from the alteration of biotite and andalusite in his M_2 event. Tilley (1925) noted a similar association in the Mt Robe area and suggested the following reactions may have been applicable:

andalusite + iron hydroxide $\longrightarrow$ chloritoid, and

2 K feldspar + 3 iron hydroxide $\longrightarrow$ 3 chloritoid + 3 quartz + 2 KOH + H_2O

Misar (1968) examined chloritoid from several localities in the Willyama

Complex, including Mt Franks and Mt Robe. He also noted a close association between sericite, andalusite and chloritoid from these areas and suggested chloritoid and andalusite formed by the reaction:

chloritoid + andalusite $\longrightarrow$ staurolite + quartz + water

Results from the present study are in conflict with those of Misar (1968) and are more in line with those of Tilley (1925). It is suggested that chloritoid in the Mt Franks - Mundi Mundi area does not form directly from andalusite, but forms from sericite after andalusite with the addition of iron oxides. These oxides are supplied by iron oxide occurring as inclusions and in contact with chloritoid.

5.4.2.7 Staurolite and Garnet

Staurolite has only been found in restricted areas of the Parnell Beds (Fig. 5.1). It occurs as idioblastic pale-golden yellow grains overprinting inclusion trails of ?ilmenite, quartz and biotite which outline F_3 folds (Section 4.5.1.9). Staurolites themselves show some signs of marginal sericitisation and it is suggested that they represent an M_3 mineral formed at higher P, T conditions than the common muscovite + chlorite + quartz assemblage.

Local small garnet porphyroblasts in the Parnell Beds are regarded as retrograde and M_3 in age. This association of garnet and staurolite has been previously reported by Browne (1922, pp.307-308) and Vernon and Ransom (1971) who described them from retrograde schist zones. Browne noted that staurolites locally included corroded biotite and sillimanite and it is suggested that the formation of staurolite + garnet represents reversal of

staurolite + garnet $\rightleftharpoons$ sillimanite + biotite

(Kwak, 1974)

5.4.2.8 Tremolite, Epidote, Clinozoisite and Carbonate

Retrogression of diopside, plagioclase and hornblende during the M_3 event in calc silicates and amphibolites have resulted in the formation of

tremolite, epidote, clinozoisite and minor carbonate. One reaction which may be important during this event is

5 diopside + $3CO_2$ + H_2O $\longrightarrow$ 1 tremolite + 3 calcite + 2 quartz

(Winkler, 1974, p.112)

5.4.3 P-T-X Conditions during M_3

Two stability fields in P T space can be established for the M_3 event (Fig. 5.8). The first is based on the co-existence of staurolite and garnet, and is determined by ingoing and outgoing curves of staurolite (Richardson, 1968 ; Winkler, 1974 after Hoschek, 1967, 1969). The second field is based on the predominance of the assemblage muscovite + chlorite + quartz and the instability of biotite. This field is locally crossed on the high temperature side where biotite is stable. The high temperature boundary of this field is based on the reaction used by Winkler (1974, Fig. 14.1) to denote the incoming of biotite, viz.,

stilpnomelane + muscovite $\rightleftharpoons$ biotite + muscovite

Although no reaction curves are known in P,T space for the formation of chloritoid, chloritoid is stable within this lower field.

The staurolite stability field is regarded as intermediate in the retrogression of high grade M_1 and M_2 assemblages to low grade quartz + muscovite + chlorite M_3 assemblages.

The large amounts of sericite, muscovite and chlorite in the non calc silicate, non carbonaceous assemblages suggest that $P_{H_2O} \sim P_T$ in these rocks. The amount of H_2O in the fluid phase in other rocks would be reduced by the equivalent component of hydrocarbons generated both in carbonaceous schists and in calc silicates.

The lack of partial melting during M_3 (Fig. 5.8) means that granitoids formed in D_3 time and which crystallised in syn or post D_3 time must have either formed by partial melting at greater depths, or have been remobilised from M_1 granitoids. Granitoids formed at this time lie in F_3 axial planes (e.g. Fig. 3.28) and are volumetrically minor compared to M_1

granitoids. These D_3 granitoids are surrounded by strongly retrogressed (M_3 event) metasediments.

Fig. 5.1 Distribution of Index Minerals and Isograds

B - biotite

M_1 event

A - andalusite

S - sillimanite

AS - relict andalusite + sillimanite

low grade zone - vertical ruling

medium grade zone - horizontal ruling

high grade zone - blank

M_3 event

C - chloritoid

ST - staurolite

Lithology - as per Fig. 2.1.

for discussion, see text.

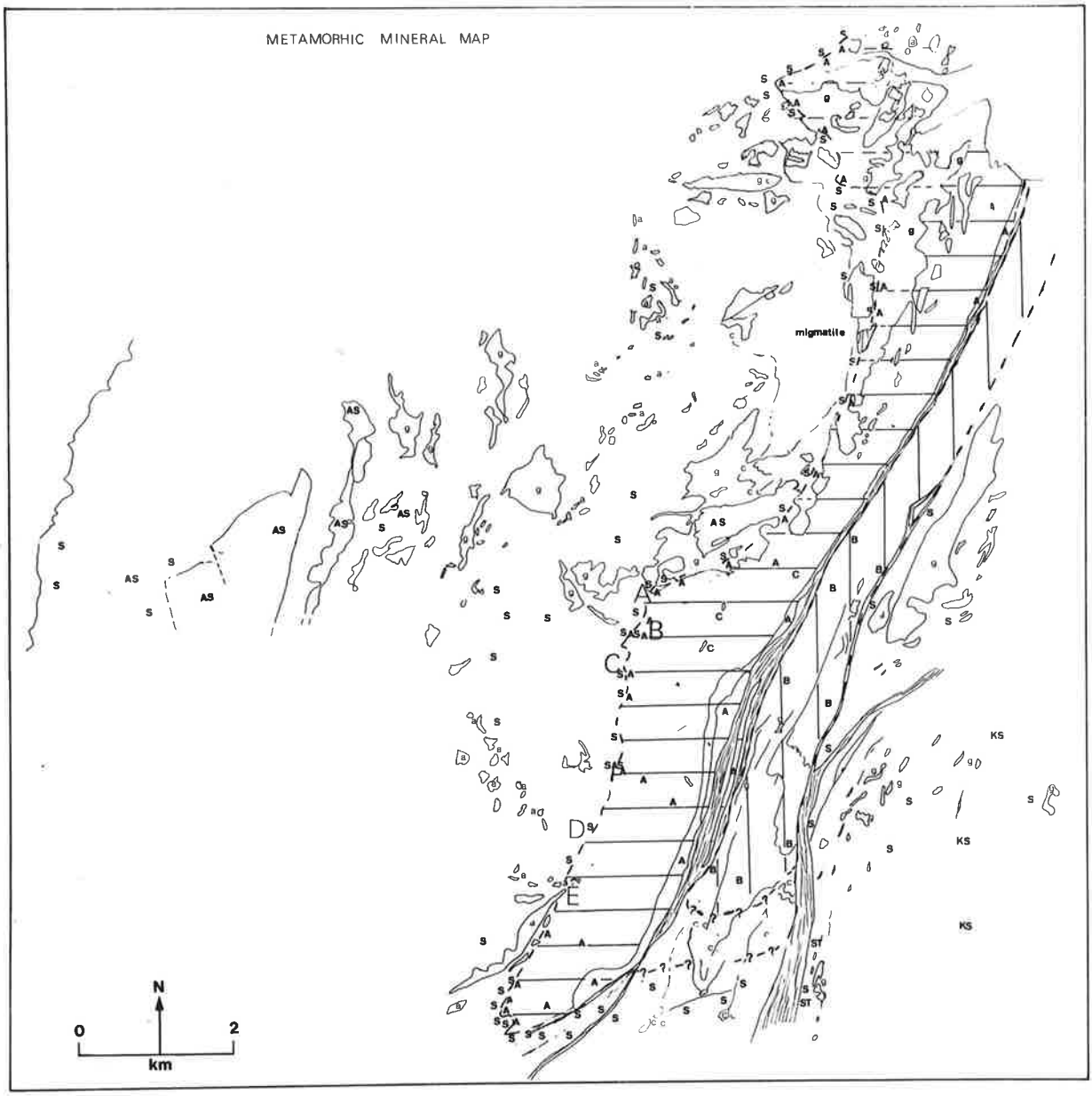
METAMORHIC MINERAL MAP
migmatite
A
B
C
D
E
AS
KS
ST
N
0
2
km

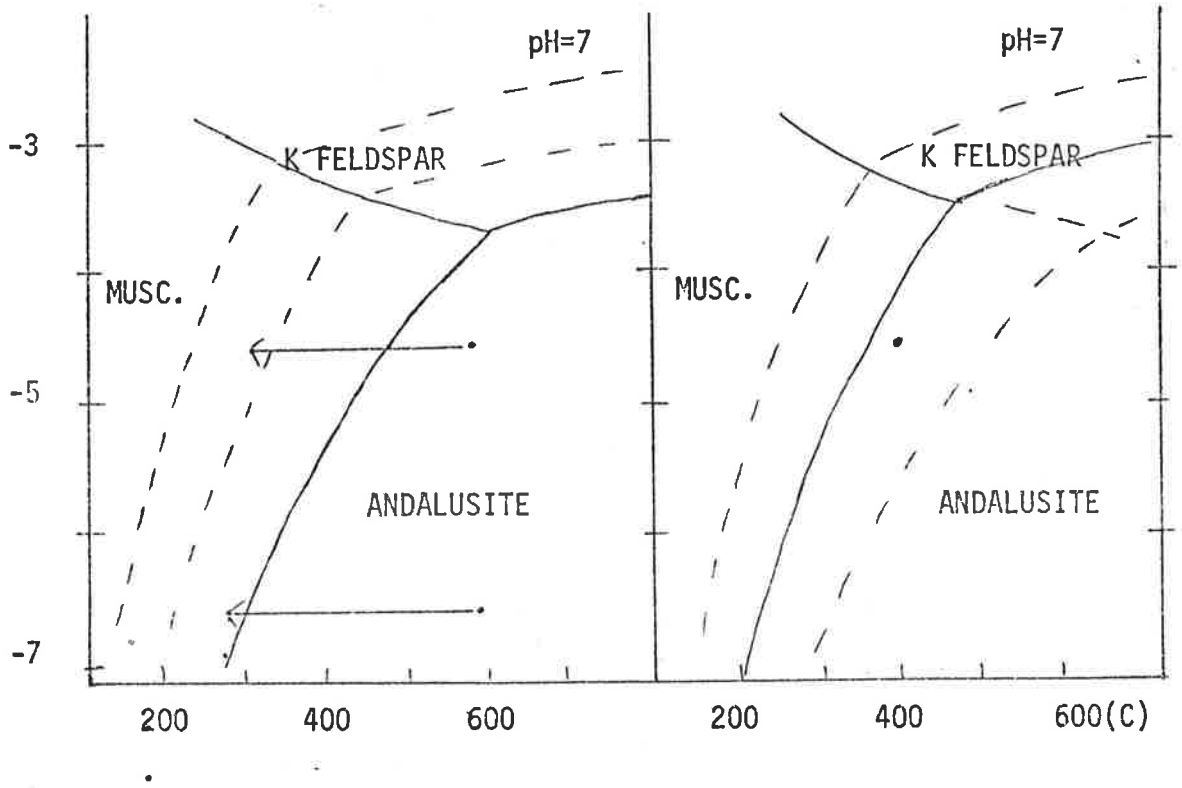

Fig. 5.3 Figure 9 from Eugster(1970). This figure shows how muscovitisation of andalusite can occur by raising the activity of K^+, or the partial pressure of H_2O. Reversal of this process at higher temperature may result in the formation of alumino silicate again, but sillimanite may be the stable phase.

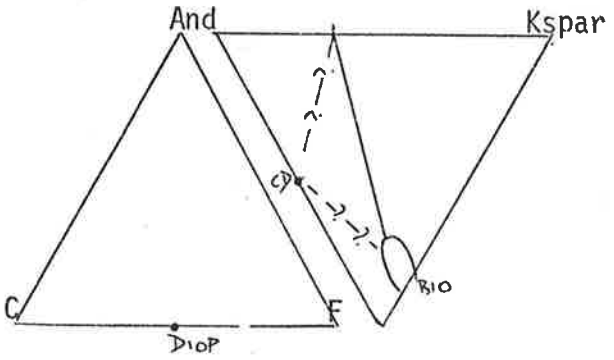

LOW GRADE ROCKS

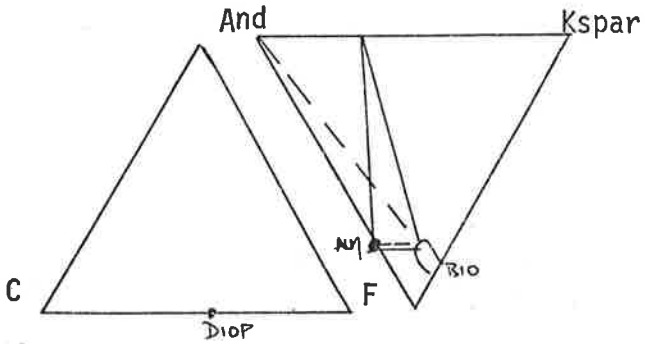

MEDIUM GRADE ROCKS

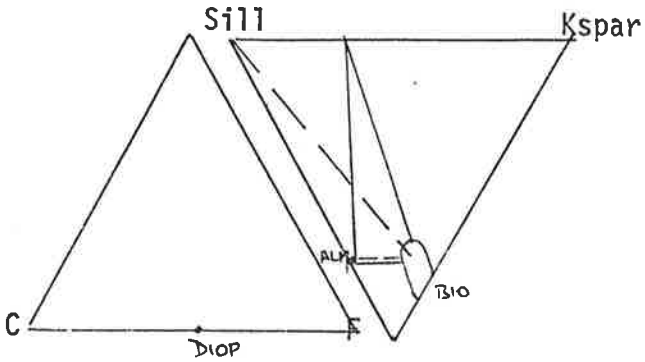

HIGH GRADE ROCKS

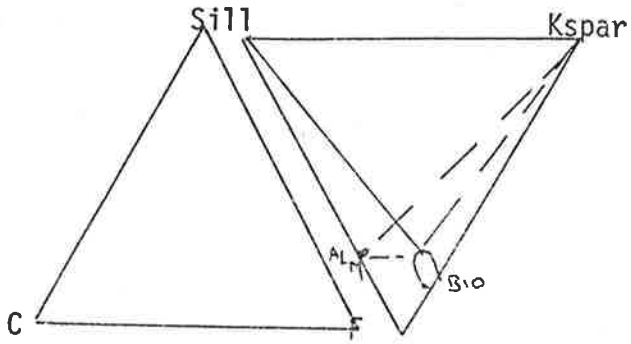

HIGH GRADE ROCKS with
K feldspar and sillimanite

FIG. 5.2.

Fig. 5.4 Approximate Geothermal Gradient in P-T field for M_1 Event

Relevant Curves:

1. alumino silicate curves, (Holdaway, 1971)
2. pyrophyllite $\rightleftharpoons$ Al_2SiO_5 + 3 qtz + H_2O (Kerrick, 1968).
3. Stilp + ph + act $\rightleftharpoons$ bio + ch + ep.
   biotite - in curve of Winkler (1973).
4. Chlorite + py $\rightleftharpoons$ cordierite + qtz + vapour
   (Seifert and Schreyer, 1970).
5, 6, 7. musc + qtz $\rightleftharpoons$ Al_2SiO_5 + Kspar + vapour
   at X_{H_2O} = 0.5 (5), 0.8 (6), 1 (7).
   (Kerrick, 1972).
8, 9, 10. granite melt curves at X_{H_2O} = 1 (8),
   0.8 (9), 0.5 (10) (Kerrick, 1972).
11. Chloritoid + Al_2SiO_5 $\rightleftharpoons$ staurolite + qtz
   (Richardson, 1968).
12. staurolite + qtz $\rightleftharpoons$ cordierite + Al_2SiO_5
   (Richardson, 1968).
13. staurolite + qtz $\rightleftharpoons$ almandine + Al_2SiO_5
   (Richardson, 1968).
   Curves 11, 12, 13 d fine maximum position for
   Fe staurolite.

hachured area-- M_I field of Laing(I977).

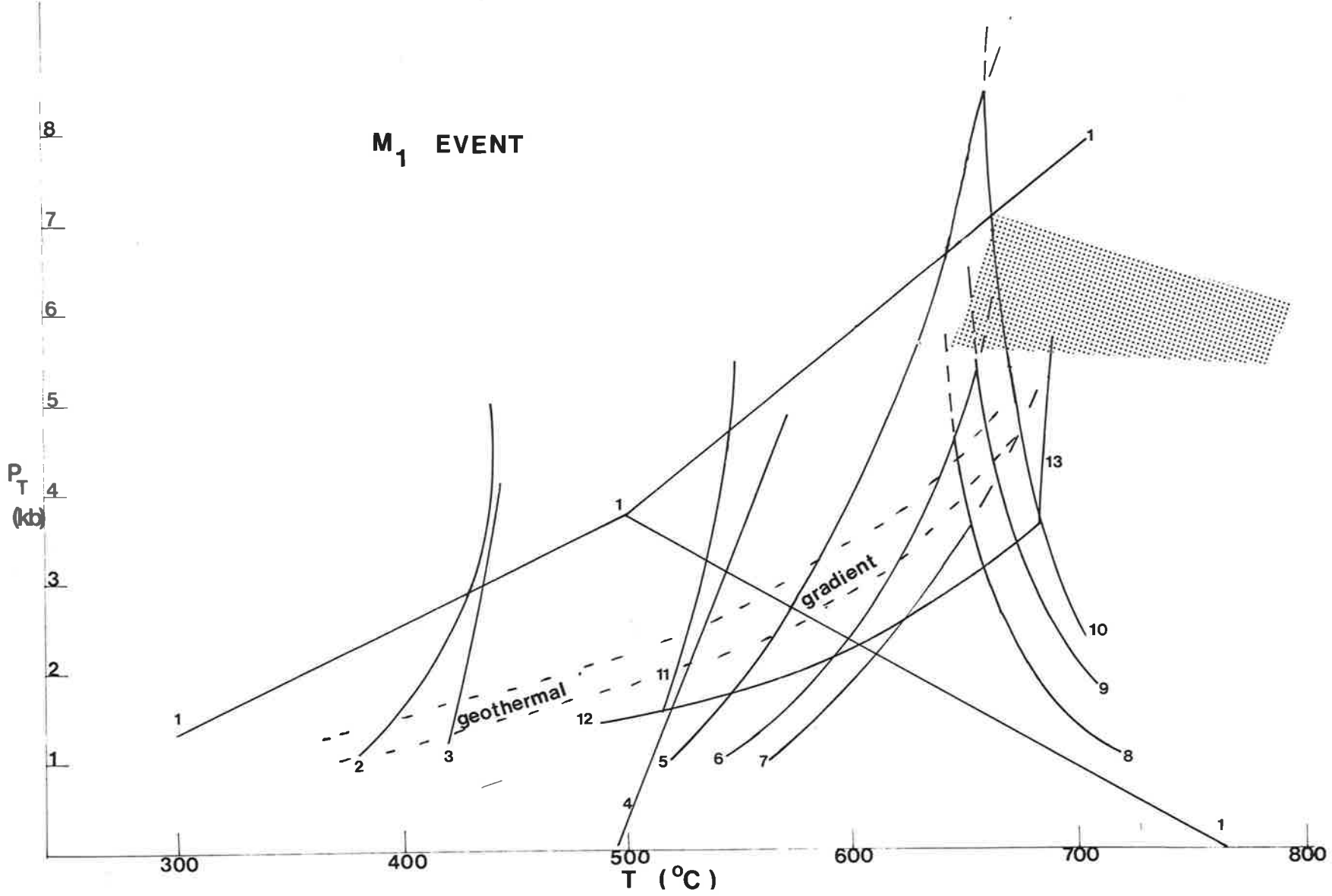
M1 EVENT
P_T (kb)
8
7
6
5
4
3
2
1
300
400
500
600
700
800
T (°C)
geothermal gradient
1
2
3
4
5
6
7
8
9
10
11
12
13

Fig. 5.5 Relevant Reaction Curves and possible P-T conditions for M_2 event.

Stability field constrained by

1) large amount of sericite, implying $P_{H_2O} \sim 1$
2) local sillimanite
3) general breakdown of sillimanite + K feldspar.

Field may be extended much further into low temperature areas; maximum temperatures shown only.

Curves as per Fig. 5.4.

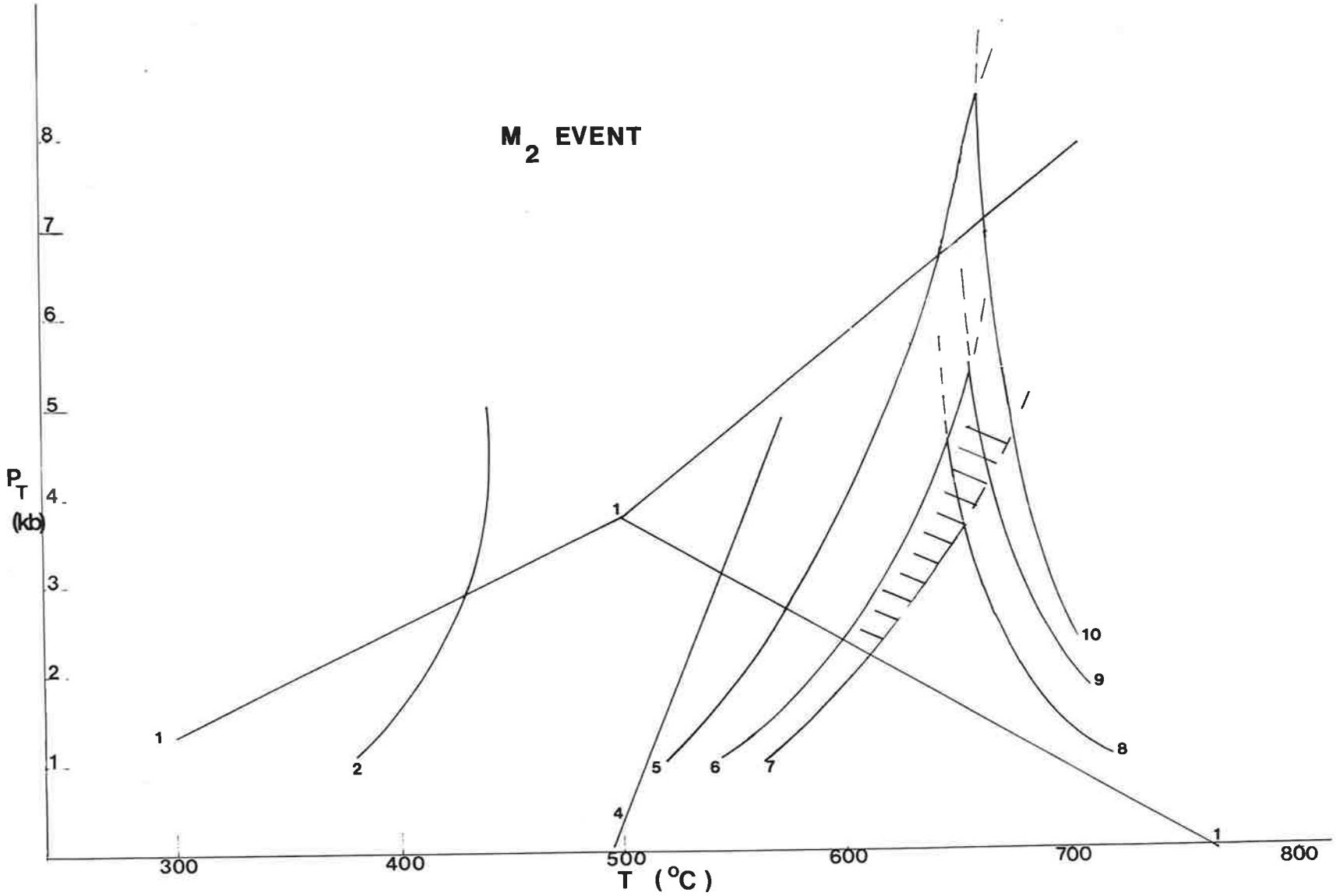
M2 EVENT
PT (kb)
8
7
6
5
4
3
2
1
300
400
500
600
700
800
T (°C)
1
2
4
5
6
7
8
9
10

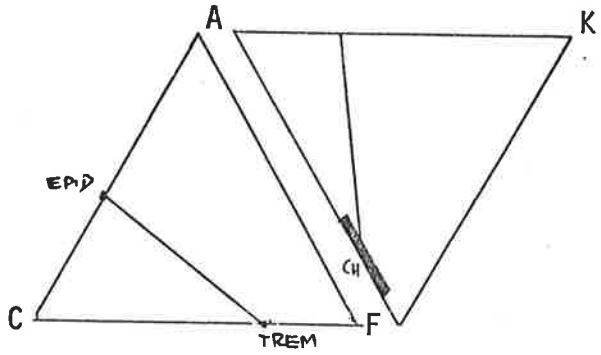

LOW GRADE ROCKS

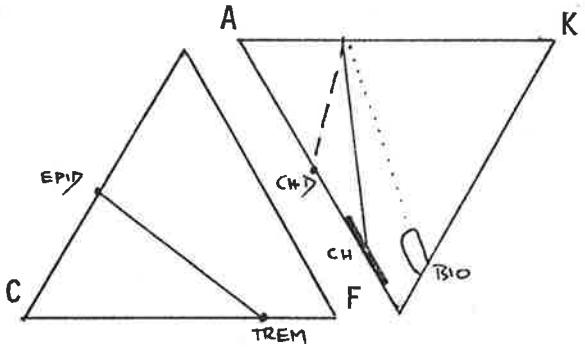

MEDIUM GRADE ROCKS

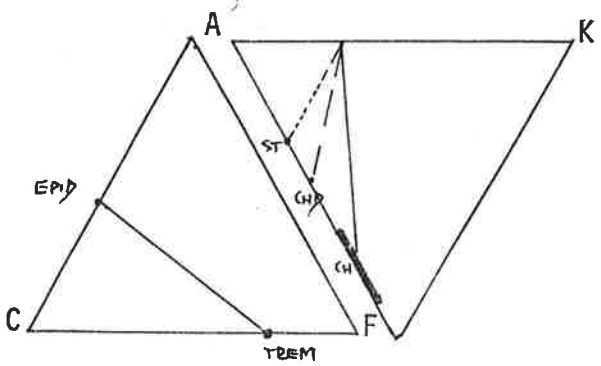

HIGH GRADE ROCKS

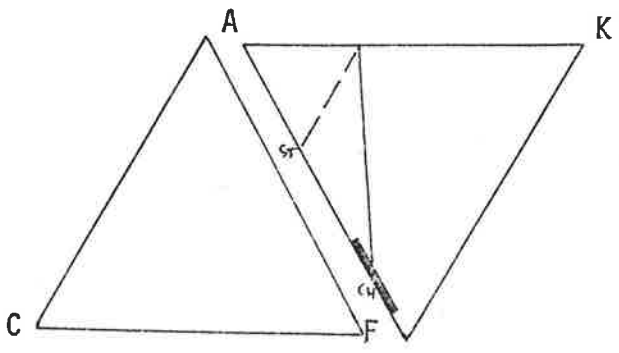

HIGH GRADE ROCKS with
K feldspar + sillimanite

FIG. 5.6.

Fig. 5.7a Myrmekitic quartz/muscovite relationship developed in M_3 event. Muscovite fringes M_1 sillimanite at bottom of figure.
Specimen 4022, normal to S_1.
Length of side 0.75 mm.

Fig. 5.7b Myrmekitic quartz/muscovite relationship developed in Robe sillimanite schist. Needles of relict M_1 sillimanite running E-W and NW-SE visible in right hand side of figure. Large grain at bottom of figure is M_1 microperthite with biotite inclusions (outlined). S_1 orientation: E-W.
Specimen 4022, normal to S_1.
Length of side 0.75 mm.

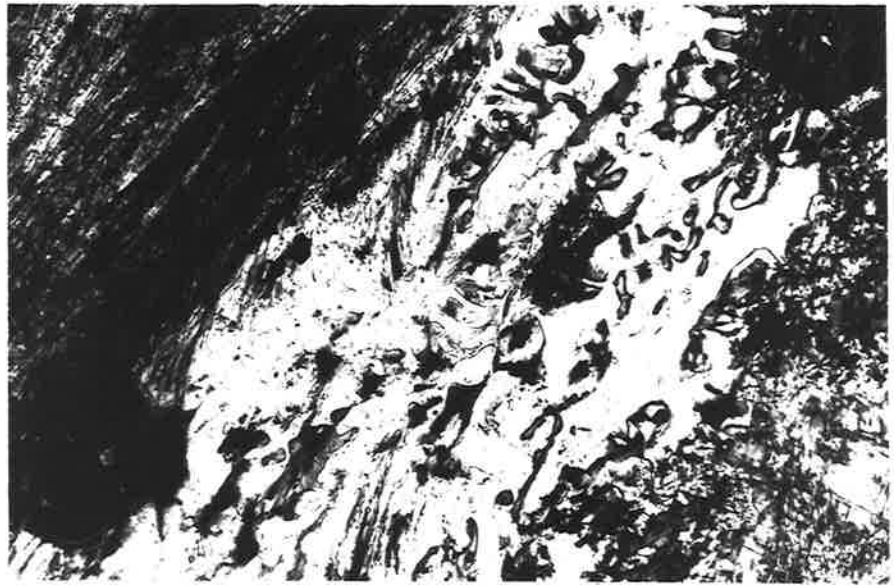

Fig. 5.8 Relevant Reaction Curves and Possible P-T field for M_3 Event. The two fields of horizontal ruling define

a) staurolite stability field limit; and

b) field of biotite instability.

Curve 14 (from Winkler, 1973 after Hosheck, 1969) is used to limit field a because P,T conditions in M_2 event lie below Curve 13 (staurolite stability of Richardson, 1968).

Stability field for M_3 event can lie anywhere on the low temperature side of curve 14, provided biotite is stable above curve 3.

There is no restriction on the M_3 event, being associated by a water influx, resulting in temperature drop without pressure drop. In this case, stability field may lie in the kyanite stability field.
Other curves as per Fig. 5.4.

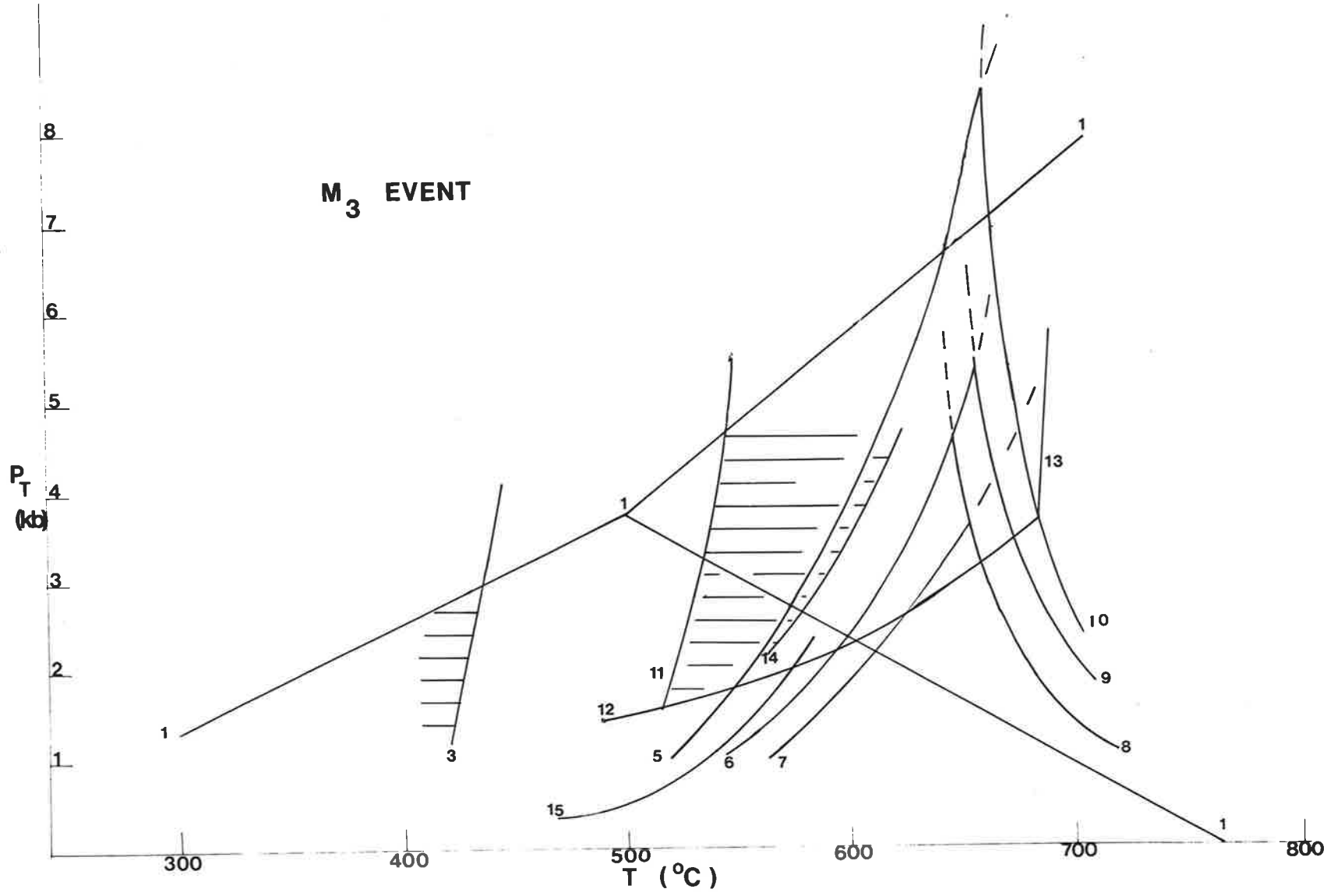
M3 EVENT
PT (kb)
8
7
6
5
4
3
2
1
300
400
500
600
700
800
T (°C)
1
3
5
6
7
8
9
10
11
12
13
14
15